Papers presented to the

FIFTEENTH SYMPOSIUM

ON ANTARCTIC METEORITES

May 30 – June 1, 1990

NATIONAL INSTITUTE OF POLAR RESEARCH,
TOKYO

国立極地研究所

Papers presented to the

FIFTEENTH SYMPOSIUM

ON ANTARCTIC METEORITES

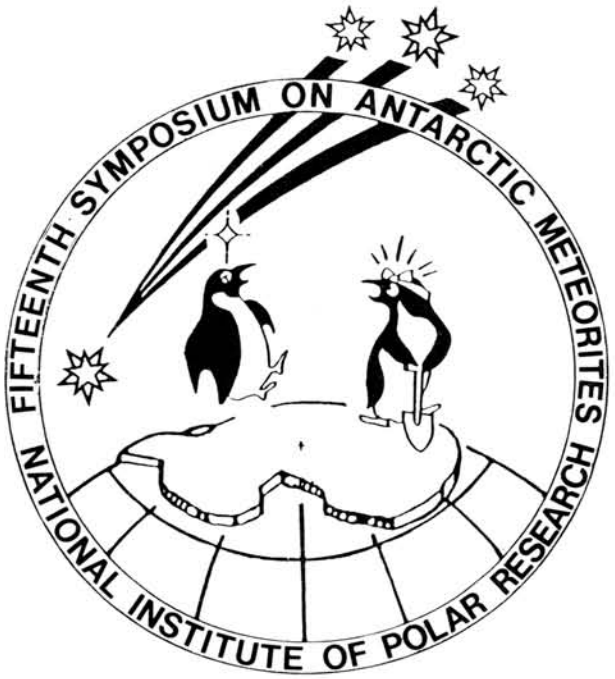

May 30 – June 1, 1990

NATIONAL INSTITUTE OF POLAR RESEARCH, 国立極地研究所
TOKYO

Wednesday, May 30, 1990

0900 - 1200 Registration Auditorium (6th Floor)

0930 - 0935 Opening Address **Takao Hoshiai**
Director-General
National Institute of
Polar Research

* Speaker

Chairmen: Akira Shimoyama and Hirokazu Fujimaki

1 0935 - 0950 **Fujita S.*, Naraoka H., Yanai K., Azuma N. and Mae S.**
Distribution of meteorites and strain in ice sheet in Nansenisen, Dronning Maud Land, Antarctica

2 0950 - 1005 **Naraoka H.*, Shimoyama A., Yanai K. and Harada K.**
Organic compounds in Asuka carbonaceous chondrites

3 1005 - 1020 **Komiya M.*, Shimoyama A., Naraoka H. and Harada K.**
Analyses of insoluble organic matter in some Antarctic carbonaceous chondrites by a DTA/TG-GC/MS method

4 1020 - 1035 **Murae T.* and Masuda A.**
Pyrolytic studies of carbonaceous matter in C3 carbonaceous chondrites

5 1035 - 1050 **Kimura M.*, Ikeda Y., Ebihara M. and Prinz M.**
Petrology and mineralogy of new enclaves from the Vaca Muerta mesosiderite

6 1050 - 1105 **Yamaguchi A.* and Takeda H.**
Mineralogical study of eucrites Yamato-793548 and Yamato-82202 with reference to impact histories on the HED parent body

7 1105 - 1120 **Saiki K.* and Takeda H.**
The chemical map analysis (CMA) study of mesostasis in some Antarctic eucrites

8 1120 - 1135 **Saito J.* and Takeda H.**
Mineralogical study of metallic grains in Antarctic ureilites

9 1135 - 1150 **Kimura M.*, El Goresy A. and Zinner E.**
Refractory inclusions in anomalous ALH85085 chondrite: Mineralogy, bulk chemistry and isotopic compositions

1150 - 1250 Lunch Time

Chairmen: Kosuke Onuma and Naoyuki Fujii

10 1250 - 1305 **Isobe H.*, Tsuchiyama A. and Kitamura M.**
Formation of pallasite and eucrite-diogenite parent magma by partial melting

11 1305 - 1320 **Matsunami S.*, Kino H., Nishimura H. and Takeshi H.**
Alteration texture of pyroxene in Allende chondrules and the formation of matrix materials

12 1320 - 1335 **Kojima H.* and Yanai K.**
Petrological study on evolution and alteration of CM chondrites

13 1335 - 1350 **Nakamura T.*, Tomeoka K. and Takeda H.**
Deformation effects in the Leoville CV carbonaceous chondrite

14 1350 - 1405 **Noguchi T.**
Relationship between grain size and chemical composition of augite in ordinary chondrites

15 1405 - 1420 **Kitamura M.*, Okamoto Y. and Watanabe S.**
Preferred orientation of olivine crystals in an inclusion of ALH-764 (LL3)

16 1420 - 1435 **Kitamura M.* and Tsuchiyama A.**
Comet-like grand parent body of chondrites

17 1435 - 1450 **Imae N.* and Tsuchiyama A.**
An experimental study on the reaction kinetics of forsterite-SiO gas

18 1450 - 1505 **Tsuchiyama A.**
Fo-En-Gas equilibrium and Mg/Si ratios of chondritic meteorites

1505 - 1530 Tea Time

19	1530 - 1545	**Miura Y.*, Imai M., Alvaretz W. and Izett G.** Mineralogical direct evidences of impact from shocked quartz grains in K/T boundary
20	1545 - 1600	**Miono S.*, Ono H., Nakanishi A., Nakayama Y. and Shoji M.** PIXE analysis of magnetic spherules in the Paleozoic-Mesozoic bedded chert
21	1600 - 1615	**Iwahashi J.*, Yoshida M. and Miono S.** Magnetic microspherules in Permian and Triassic bedded chert in Southwest Japan
22	1615 - 1630	**Tazawa Y.* and Fukuoka T.** Origin and characteristics of dust particles in Antarctic Ice/Snow and other terrestrial environments
23	1630 - 1645	**Nakai I.* and Tsuchiyama A.** Two dimensional chemical state analysis of meteorites by X-ray fluorescence analysis
24	1645 - 1700	**Nagata T.*, Funaki M. and Kojima H.** Magnetic properties and natural remanent magnetization of carbonaceous chondrites containing pyrrhotite
25	1700 - 1715	**Nagata T.*, Kaito C., Saito Y. and Funaki M.** Tetrataenite in chondrites and experimental demonstration of formation of tetrataenite fine grains
26	1715 - 1730	**Fujii N.*, Tashiro K. and Kanamaru T.** Shock effects in chondrites -(I) From dislocations and grain shapes
27	1730 - 1745	**Mizutani H.*, Yamamoto T., Kozasa T. and Honda R.** Formation of chondrules by collisions between planetesimals
28	1745 - 1805	**Sears D.*, Batchelor J., Lu Jie. and Keck B.** Metamorphism of CO and CO-like chondrites and comparisons with type 3 ordinary chondrites
	1810 - 2000	**Reception Lecture Room (2F)**

Thursday, May 31, 1990

Chairmen: Takaaki Fukuoka and Yukio Ikeda

29 0900 - 0915 **Takahashi K.* and Masuda A.**
REE abundances and cosmochronology of several ureilites

30 0915 - 0930 **Yoneda S.*, Shinotsuka K., Mihara H., Nagai H. and Honda M.**
REE and Y abundances in Allende group II inclusions

31 0930 - 0950 **Floss C. and Crozaz G. (Walker R. M.*)**
Antarctic weathering and REE remobilization in Antarctic eucrites

32 0950 - 1010 **Geiger T.* and Bischoff A.**
The metamorphosed carbonaceous chondrites - A new meteorites group?

Special Session (I): CI Chondrites

33 1010 - 1025 **Ikeda Y.**
Mineralogy of clasts in the Y-82162 chondrite (C1)

34 1025 - 1040 **Tomeoka K.**
The origin of phyllosilicates in the Yamato-82162 CI carbonaceous chondrite

35 1040 - 1055 **Akai J.**
Thermal metamorphism in four Antarctic carbonaceous chondrites and its temperature scale estimated by T-T-T diagram

36 1055 - 1110 **Matsunami S.*, Nishimura H. and Takeshi H.**
Compositional heterogeneity of alteration products in Yamato-86720 chondrite

37 1110 - 1125 **Miyamoto M.**
Midinfrared diffuse reflectance spectra of some Antarctic carbonaceous chondrites

Special Session (II): Unique Meteorites

38 1125 - 1140 **Nagahara H.*, Fukuoka T., Kaneoka I., Kimura M., Kojima H., Kushiro I., Takeda H., Tsuchiyama A. and Yanai K.**
Petrology of unique meteorites, Y-74063, Y-74357, Y-75261, Y-75274, Y-75300, Y-75305, A-77081, A-78230, and Y-8002

39 1130 - 1155 **Yanai K.* and Kojima H.**
Y-74063: Unique meteorite classified between E and H chondrite

40 1155 - 1210 **Yamamoto K.*, Nakamura N., Misawa K., Yanai K. and Matsumoto Y.**
Lithophile trace element abundances in Antarctic unique meteorites and in unique clasts from L6 chondrites

1210 - 1300 Lunch Time

Chairmen: Hiroshi Takeda and Noboru Nakamura

41 1300 - 1315 **Fukuoka T.* and Kimura M.**
Chemistry of Y-74063, -74357 and ALH-78230 unique meteorites

42 1315 - 1330 **Takaoka N.* and Yoshida Y.**
Noble gases in unique meteorite Y-74063

43 1330 - 1345 **Hiroi T. and Takeda H.***
Reflectance spectroscopy and mineralogy of primitive achondrites - Lodranites

Special Session: Lunar Meteorites

44 1345 - 1400 **Premo W. R. and Tatsumoto M.***
A step toward the primary lunar Pb composition: U-Pb isotope systematics of lunar norite 78235

45 1400 - 1415 **Takeda H.*, Saito J., Mori H., Yanai K. and Kojima H.**
Consortium reports of lunar meteorites Y-793274 and Y-86032

46 1415 - 1430 **Mori H.*, Saito J. and Takeda H.**
Mineralogy of lunar meteorites, Y-86032, Y-793274 and MAC88105

47 1430 - 1450 **Lindstrom M. and Martinez R. (Score R.*)**
Lunar meteorites Y793274: A second basaltic breccia

Friday, June 1, 1990

Chairmen: Mitsuru Ebihara and Hiroshi Shimizu

58 0900 - 0915 **Kagi H.*, Takahashi K., Shimizu H., Kitajima F. and Masuda A.**
In-situ micro-Raman observation on some differentiated meteorites: Graphitic materials in Antarctic ureilites

59 0915 - 0930 **Ebihara M.* and Ozaki H.**
Chemical composition of Antarctic meteorites (1) - Ordinary chondrites

60 0930 - 0945 **Fukunaga K.* and Matsuda J.**
Noble gas composition in the vapour growth diamond

61 0945 - 1000 **Matsuda J.*, Yajima H., Kusaba K. and Syono Y.**
Noble gas studies in shock-produced diamonds

62 1000 - 1015 **Nakamura N.*, Matsuda H., Yokoyama S., Shimoda H., Shimaoka T. and Yamamoto K.**
Fractionated alkali metal abundances in Allende BO chondrules: A clue to melting processes

63 1015 - 1030 **Shimaoka T.* and Nakamura N.**
Volatilization studies of alkali metals on a chondritic material (V) - an effect of total pressure -

64 1030 - 1045 **Matsubara K.* and Matsuda J.**
Ne enrichment in tektites and experiment of Ne diffusion into silica glass

65 1045 - 1100 **Fukuoka T.**
Pairing of five Yamato-79 achondrites by the chemical compositions

Chairmen: Nobuo Takaoka and Jun-ichi Matsuda

66 1100 - 1115 **Tazawa Y. and Sasaki T.***
Alteration in ordinary chondrite fusion crust and their relation to chemical and mineral compositions of spherules

67 1115 - 1130 **Miura Y.*, Beukens R. and Rucklidge J.**
Carbon-14 terrestrial, exposed and glacial ages of Antarctic meteorites

68 1130 - 1145 **Ninagawa K.*, Kubo H., Fujimura S., Yamamoto I., Wada T., Matsunami S. and Nishimura H.**
Thermoluminescence study of ordinary chondrites by TL spatial distribution readout system-II

69 1145 - 1200 **Hashizume K.* and Sugiura N.**
Nitrogen isotope anomaly in ordinary chondrites

1200 - 1300 Lunch Time

70 1300 - 1315 **Sugiura N.* and Hashizume K.**
Anomalous nitrogen in Y74191 (L3) chondrite

71 1315 - 1330 **Misawa K.* and Nakamura N.**
Mg isotopic composition of chondrules from the Allende meteorite

72 1330 - 1345 **Misawa K.* and Tsuchiyama A.**
Mg isotope composition of silicates produced from gas-condensation furnance

73 1345 - 1400 **Uyeda C.* and Tsuchiyama A.**
Mass fractions of minerals produced from gas-condensation process

74 1400 - 1415 **Nakamura Y.*, Ogata A. and Nagao K.**
An attempt to measure cosmogenic ^{81}Kr in ordinary chondrites

75 1415 - 1430 **Nagai H.*, Honda M., Kobayashi I., Imamura M. and Kobayashi K.**
Be-10 and Al-26 in Antarctic meteorites

Chairman: Akimasa Masuda

-- Special Lecture --

76 1430 - 1545 **Anders E. (Invited Speaker, Professor, Enrico Fermi Institute, University of Chicago)**

Title: Interstellar diamond, graphite, and SiC in meteorites

Abstract only

77 **Bischoff A. and Metzler K.**
Petrogaphy and chemistry of the three carbonaceous chondrites Y-86720, Y-82162, and B-7904

78 **Eugster O.**
Lunar meteorite Yamato-793274: Cosmic-ray produced and solar wind noble gases. Relation with Allan Hills A81005?

79 **Kimura M.**
Antarctic two new winonaites, Y-74025 and Y-75305: Mineralogy and classification.

80 **Kitamura M. and Miyamoto M.**
A possible effect of ^{26}Al heating to the formation of CAI's

81 **Kurat G., Brandstätter F. and Koeberl C.**
Lunar meteorite Yamato-793274: A lunar Highland sample possibly rich in mare minerals

82 **Mayeda T. K. and Clayton R. N.**
Oxygen isotopic compositions of B-7904, Y-82162, and Y-86720

83 **Metzler K. and Bischoff A.**
Petrography and chemistry of accretionary dust mantles in the CM-chondrites Y-791198, Y-793321, Y-74662 and ALHA83100 - Indications for nebula processes

84 **Miura Y.**
Mafic contents and densities of meteoritic plagioclase-estimation of impact sites

85 **Nayak V. K.**
The Chiang Khan meteorite shower, Loei province, Thailand

86 **Nomura K., Tomeoka K. and Takeda H.**
Electron microscope observations of Ca-Al-rich inclusions in the Yamato-791717 CO carbonaceous chondrite

87 **Vogt S., Aylmer D. and Herzog G. F.**
Cosmic ray exposure history of the lunar meteorites Yamato 791197 and Yamato 86032

88 **Zbik M.**
Links between structural features and physical properties in stony meteorites

Wednesday, May 30, 1990

0900-1200	*Registration, 6th Floor*
0930-0935	*Opening address, Auditorium*
0935-1805	*Symposium, Auditorium*
1810-2000	*Reception, Lecture Room, 2nd Floor*

DISTRIBUTION OF METEORITES AND STRAIN IN ICE SHEET IN NANSENISEN, DRONNING MAUD LAND, ANTARCTICA

*) **) ***) *) *)
Fujita, S., Naraoka, H., Yanai, K., Azuma, N. and Mae S.

*)Department of Applied Physics, Faculty of Engineering, Hokkaido University, Sapporo 060. **)Department of Chemistry, University of Tsukuba, Tsukuba, Ibaraki 305. ***)National Institute of Polar Research, Itabashi-ku, Tokyo 173.

From January 1988 to January 1989, more than 2000 specimens of meteorite were found on the bare ice surface around the Sør Rondane Mountains, by the Asuka winter party of the Japanese Antarctic Research Expedition (JARE 29th)(1). Then most of them, i.e. more than 1600 specimens, were found in Nansenisen which is in up-stream area of the Sør Rondane. During search for meteorites, distribution of meteorites were investigated by counting total finds of specimens in each region in Nansenisen. In addition, glaciological survey was carried out to investigate the flow condition there.

Glaciological survey contains strain-grid measurements for measuring surface strain rate, sampling of surface ice for investigating strain history by analyzing preferred orientation of c-axes, and installing snow stakes for measuring ablation rate. Strain-grid and snow stakes were installed in 1988 by JARE 29th, and re-surveyed after one year period in 1989 by JARE 30th. Structural analyses of ice samples were carried out in Hokkaido University. Ice fabrics, cracks, and crystals in the samples were investigated. We report preliminary results of these investigations.

The average concentration of meteorites was 5.3 (specimens per km^2) in Nansenisen. However distribution of the meteorites wasn't uniform. High concentration was observed roughly in three regions which apart by more than 10 km from each other. Around such regions concentration was higher than average value by factor of 2 or 3. Moreover, high concentration of morainic deposits were also observed on the same regions with no exceptions. Since there is not any exposed nunataks in up-stream side of the Sør Rondane, the only possible origin of the moraines is bedrock under ice sheet.

The analysis of ice samples showed that ice fabric pattern i.e. preferred orientation of c-axes, was so called "horizontal great circle girdle pattern"(2,3) in such regions. According to previous study of ice fabric(4), such pattern is formed when ice is compressed horizontally and extended in the vertical axis. Thus the configuration of cumulative strain in bare ice in such regions is compression in horizontal plane and extension in the vertical axis in ice sheet. Moreover, strain condition measured by strain grid was similar. There is compression in horizontal plane, and strain

rate is in the order of 10^{-5}(per year). This fact shows that cumulative strain in ice corresponds with in situ strain condition. On the other hand, in regions where concentration of meteorite was relatively low and no moraine was found, the different fabric pattern was observed(2,3). This fact means strain condition is different there.

These facts suggest that distribution of the meteorites is determined by the local strain in ice sheet. The observed strain condition in regions where high concentration is observed is suitable for meteorite concentration. Because, vertical extension cause the upward flow, and horizontal compression concentrate meteorites and moraines into limited area.

(1)Yanai,K. and the JARE-29 Asuka Party. (1989) Papers presented to the fourteenth symposium on Antarctic meteorites. pp.1
(2)Fujita,S. and Mae,S. (In press) Proc. NIPR Symposium on Polar Meteorol. and Glaciol. No.4
(3)Fujita,S. in preparation
(4)Fujita,S., Nakawo,M. and Mae,s.(1987) Proc. NIPR Symposium on Polar Meteorol. and Glaciol. No.1, 122-131

ORGANIC COMPOUNDS IN ASUKA CARBONACEOUS CHONDRITES.

Naraoka,H., Shimoyama,A., Yanai,K.*, and Harada,K.

Department of Chemistry, University of Tsukuba, Tsukuba, Ibaraki 305, *National Institute of Polar Research, 9-10, Kaga 1-chome, Itabashi-ku, Tokyo 173.

A systematic search for Antarctic meteorites was carried out by the Asuka winter party of the 29th JARE on the bare ice fields around the Sør Rondane Mountains during 1987-88 and 1988-89 field seasons. As a result, more than 2000 specimens of meteorite have been collected as individuals or fragments. Preliminary classification indicate that they contain about 30 carbonaceous chondrites.

In this study, two Asuka carbonaceous chondrites were analyzed for amino acids. Both samples, Asuka(A)-2 and A-14 (tentative names), were classified as CM2 type petrographically. Their carbon and nitrogen contents we determined were 2.49%C and 0.12%N for A-2, and 1.59%C and 0.08%N for A-14. These contents reassured that these chondrites belong to C2 type.

For amino acid analysis, one gram each of the powdered samples was extracted with water by refluxing in a degassed-sealed glass tube. The extract was divided into two fractions, one for the unhydrolyzed, the other for the hydrolyzed with 6M hydrochloric acid. Portions of the two fractions were analyzed quantitatively by an amino acid analyzer. Rests of fractions were converted to N-(trifluoroacetyl)-amino acid isopropyl esters and analyzed by GC-MS with a chiral capillary column in order to separate the D,L-enantiomers.

Figure 1 shows the amino acid chromatograms of the hydrolyzed fractions of A-14 and A-2 chondrites, together with that of the procedural blank. In the hydrolyzed fraction of A-14, eighteen peaks were identified. Of these, 14 peaks are attributed to amino acids including proteineous and non-proteineous ones. It was found that amino acids were increased in kind and amount by hydrolysis. For example, the amount of glycine in the hydrolyzed fraction was 2.7 times more than that in the unhydrolyzed fraction. This indicates that some portions of amino acids detected were converted from the precursors. The total amounts of amino acids were estimated about 60 nmol/g. α-amino-i-butyric acid was the most abundant in both fractions. The other four peaks are compounds containing an amino group such as methylamine and ethylamine. The selected mass fragment analysis by GC-MS showed that amino acids were present as racemic mixtures. Based on these results, amino acids found from A-14 were abiotic origin, not from terrestrial biological contamination.

On the other hand, the amino acid chromatographic pattern of

A-2 in the unhydrolyzed and hydrolyzed fractions did not differ considerably from those of the procedural blanks. These results indicate that A-2 contains no detectable amounts (above 0.3 nmol/g) of amino acids in both fractions, although the contents of carbon and nitrogen in A-2 were higher than those in A-14. Perhaps this chondrite lost organic compounds by aqueous alteration on the chondritic parent body. So far, analyses for amino acids of Antarctic CM2 chondrites have been carried out with 5 specimens. Of these, three contained various types of amino acids [1]-[3], and the other two are devoid [4]. Our present finding of amino acids from A-14 and no finding from A-2 support those previous analyses of Antarctic carbonaceous chondrites.

REFERENCES:
[1]A.Shimoyama et al,(1979) Nature, 282, 394, [2]J.R.Cronin et al, (1979) Science, 206, 335, [3]A.Shimoyama et al,(1985) Chem. Lett., 1985, 1183, [4]A.Shimoyama and K.Harada,(1984) Geochem. J., 18, 281.

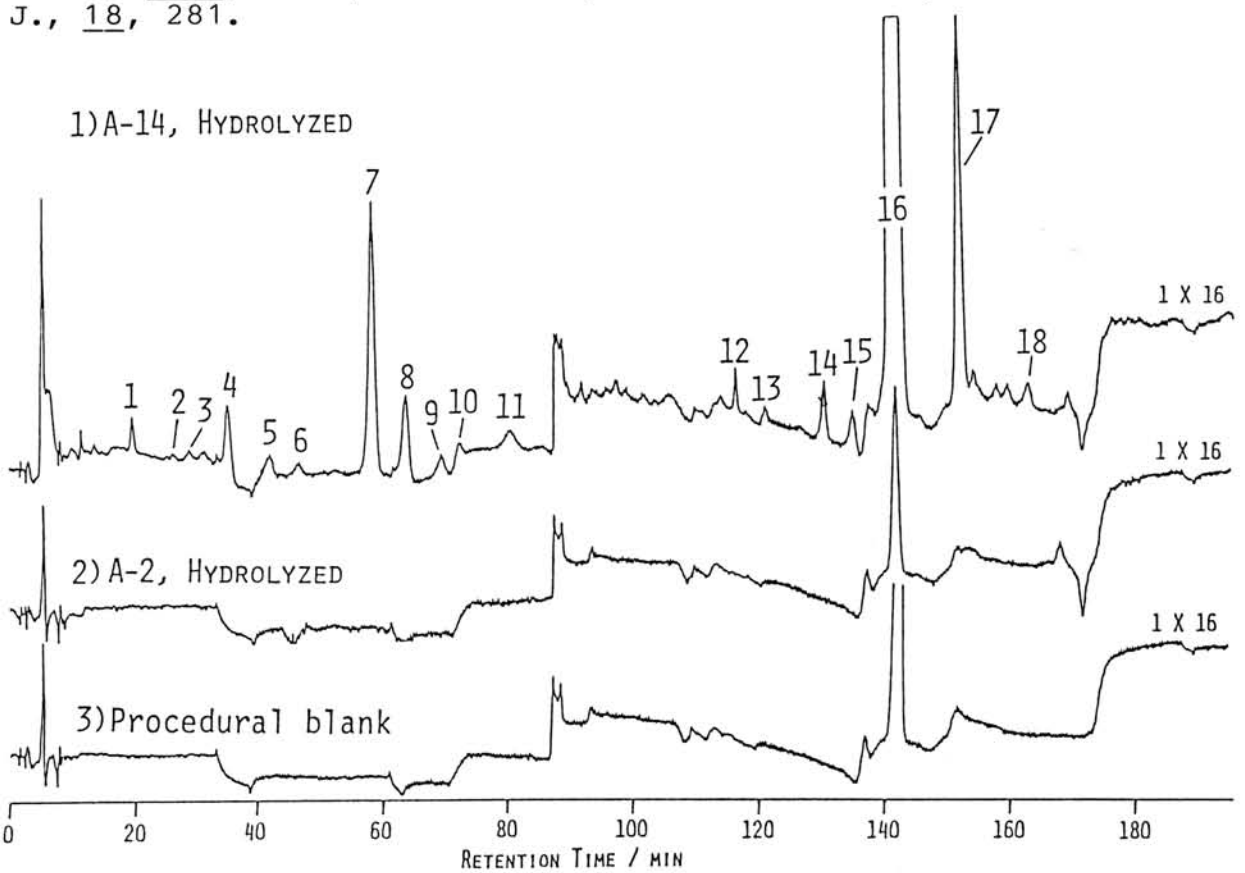

Fig. 1. Amino acid chromatograms of the hydrolyzed fraction from 1)A-14, 2)A-2 and 3)Procedural blank.

Peak no. 1, aspartic acid; 2, threonine, 3, serine; 4, glutamic acid; 5, sarcosine; 6, α-aminoadipic acid; 7, glycine; 8, alanine; 9, α-amino-i-butyric acid; 10, α-amino-n-butyric acid; 11, valine; 12, β-alanine; 13, β-amino-i-butyric acid; 14, γ-aminobutyric acid; 15, ethanolamine; 16, ammonia; 17, methylamine; 18, ethylamine.

ANALYSES OF INSOLUBLE ORGANIC MATTER IN SOME ANTARCTIC CARBONACEOUS CHONDRITES BY A DTA/TG-GC/MS METHOD.

Komiya, M., Shimoyama, A., Naraoka, H., and Harada, K.

Department of Chemistry, University of Tsukuba, Tsukuba, 305

We have found various amino acids, carboxylic acids, and hydrocarbons in the Yamato-791198 carbonaceous chondrite[1)2)3)]. However, we could not detect these organic compounds in the Belgica-7904 carbonaceous chondrite[4)], although its carbon content is similar to that of Yamato-791198. Most of the organic compounds in these two chondrites are probably present as insoluble macromolecular organic matter. Therefore, in this study, we examined the insoluble organic matter in the two chondrites by a DTA/TG-GC/MS method.

The Yamato-791198 sample, pre-extracted with a mixture of benzene and methanol, was treated with HF/HCl in order to demineralize and concentrate the insoluble organic matter which was then, washed with carbon disulfide, benzene, methanol, and water, successively, to remove inorganic sulfur compounds. The Belgica-7904 sample was directly treated with HF/HCl (because it does not have extractable organic compounds) and followed the same washes as for Yamato-791198. The $\delta^{13}C$ of the insoluble organic matter was found to be -14.6‰ for Yamato-791198 and -13.6 ‰ for Belgica-7904, both of which are very similar.

The insoluble organic matter were heated under a helium flow in a DTA/TG instrument from room temperature to 800°C at the increasing rate of 10°C/min. As compounds were released, they were directly introduced into a mass spectrometer(direct-MS method), and continuous temperature profiles of compounds released were obtained. For identification of compounds released, those released from the Yamato-791198 sample pre-extracted with the mixture of benzene and methanol were introduced into GC/MS by a cold trap(trap-GC/MS method). For comparison, the bulk samples of the Belgica-7904 without any treatment were also examined by the direct-MS method.

The insoluble organic matter in Yamato-791198 released aromatic and aliphatic hydrocarbons(Figs. 1 and 2, respectively). Each aromatic hydrocarbon shows a similar release pattern, starting at 200-300°C, and ending at 500-600°C with maximum at 440°C. But benzene shows another release peak with maximum at 260°C and shows large release below 200°C. However, most of these benzene released at low temperature, particularly below 200°C, probably come from remaining benzene which was used in the wash. Aliphatic hydrocarbons show the similar release patterns to those of aromatic ones. They were also released with maxima at 440°C, although their release were occurred at a rather wide

temperature range. The Yamato-791198 sample pre-extracted with the mixture of benzene and methanol released over 20 compounds as identified by the trap-GC/MS method. This supports the identities of those compounds released from the insoluble organic matter. Among those compounds, unsaturated hydrocarbons are most abundant followed by aromatic and saturated hydrocarbons. Nitriles and aldehydes are also present.

Thermal analyses of Yamato-791198 treated with HF/HCl showed no prominent peak related with the release of organic compounds on the DTA curve. The TG curve indicates continuous weight loss from room temperature to 800°C. However, between 200 to 500°C, the slope of the TG curve is slightly steep in comparison with those of before and after its temperature range. Therefore, this region may correspond with the release of the organic compounds such as hydrocarbons. The total weight loss of this sample is 31%.

The direct-MS analysis of insoluble organic matter in Belgica-7904 shows the release of benzene, but does not shows any other compounds. The result of the Belgica-7904 fresh bulk sample indicates the releases of compounds are very small. These data suggest that insoluble organic matter in Belgica-7904 is more graphitic than that in Yamato-791198.

Furthermore, we measured the IR spectra of the insoluble organic matter in the two chondrites. The Yamato-791198 sample before heating shows broad absorptions with medium intensity, at the range of 1800-1500cm^{-1} and 1500-1000cm^{-1}. But after heating, these absorption peaks became very weak. The Belgica-7904 sample before heating also has absorptions at the similar range, but their intensity is rather weak. After heating, it shows very weak absorptions similar to the Yamato-791198 sample after heating. These IR data confirm the difference of insoluble macromolecular organic matter between Yamato-791198 and Belgica-7904.

References

1) Shimoyama, A., Harada, K., and Yanai, K. (1985) Chem. Lett., 1985, 1183.
2) Shimoyama, A., Naraoka, H., Yamamoto, H., and Harada, K. (1986) Chem. Lett., 1986, 1561.
3) Naraoka, H., Shimoyama, A., Komiya, M., Yamamoto, H., and Harada, K. (1988) Chem. Lett., 1988, 831.
4) Shimoyama, A., and Harada, K. (1984) Geochem. J., 18, 281.

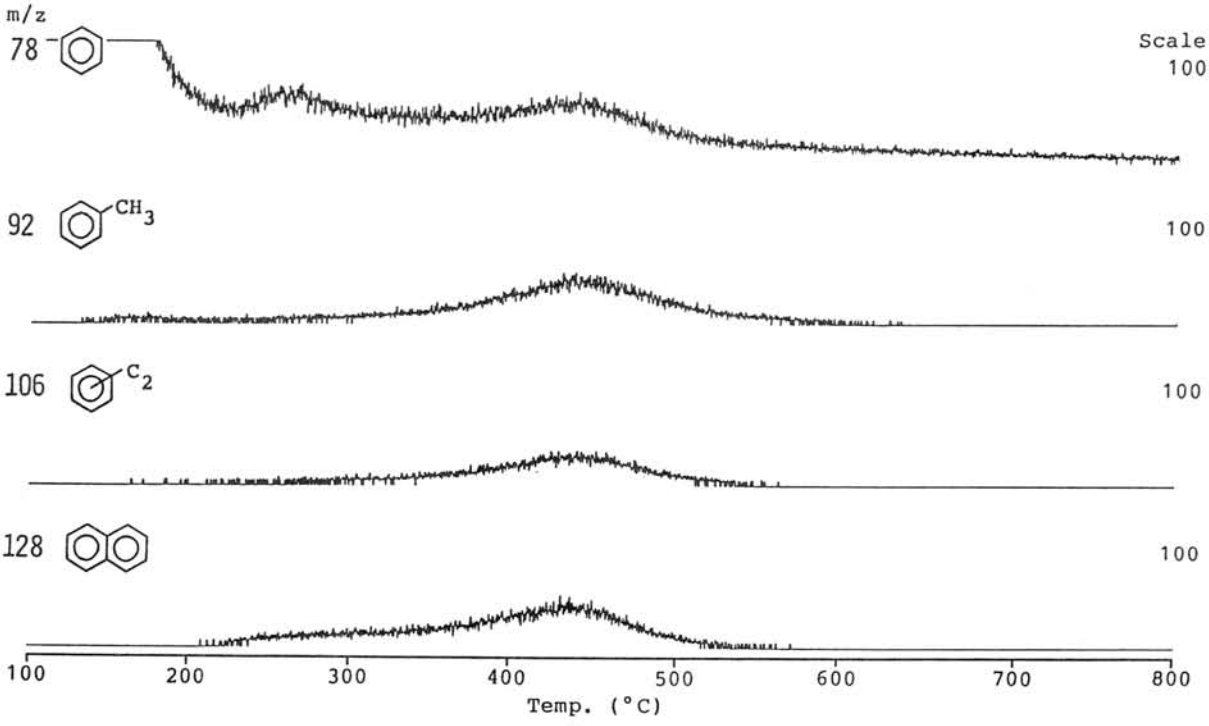

Fig.1 Thermal release patterns of ions for components released from Yamato-791198 sample treated with HF/HCl

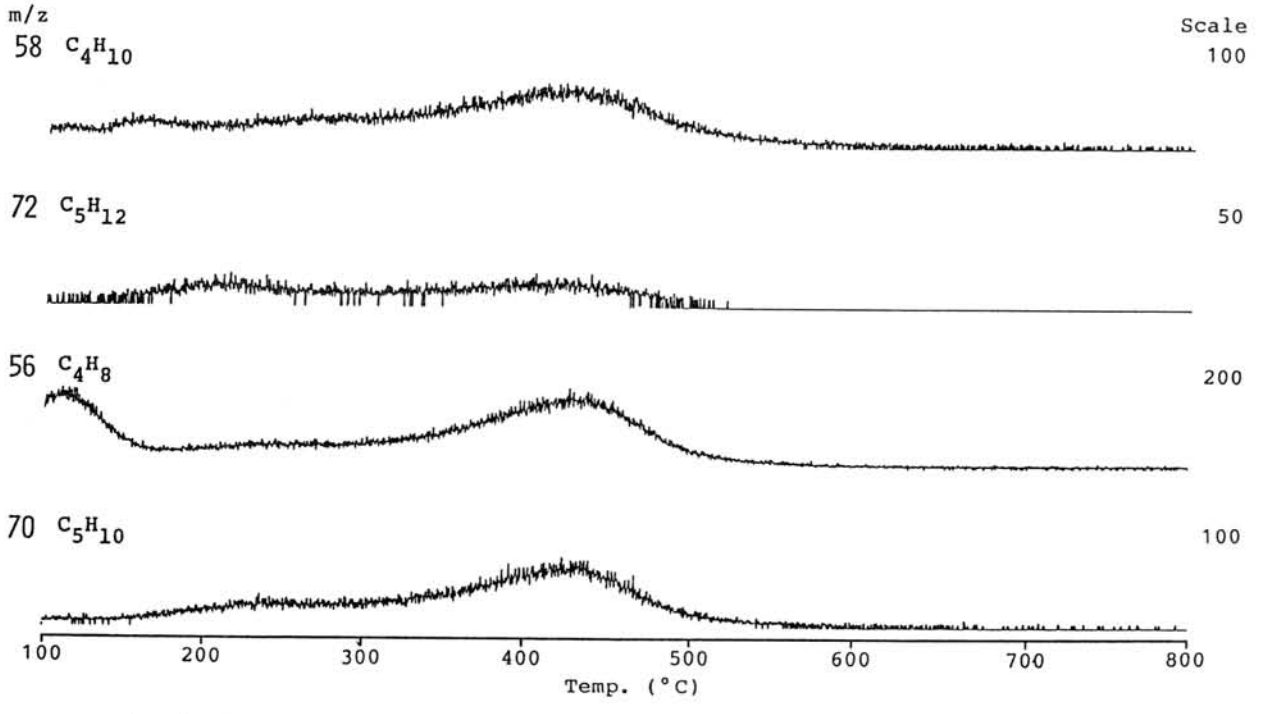

Fig.2 Thermal release patterns of ions for components released from Yamato-791198 sample treated with HF/HCl

PYROLYTIC STUDIES OF CARBONACEOUS MATTER IN C3 CARBONACEOUS CHONDRITES

Tatsushi Murae and Akimasa Masuda

Department of Chemistry, Faculty of Science, The University of Tokyo, Hongo, Bunkyo-ku, Tokyo 113

Major carbonaceous matters in carbonaceous chondrites are present as solvent-unextractable high-molecular organic compounds. A highly condensed polycyclic aromatic structure bearing edge defects has been proposed for the compounds by the authors [1]. The number of the edge defects is considered to reflect the formation processes of the organic polymer (high molecular organic compound) and the history (mainly thermal history) of the meteorite which contains the polymer. Gas chromatogram of the pyrolysis products of the polymer clearly indicates the characters of the edge defects of the polymer [1]. We have found that C2 carbonaceous chondrites could be classified into three sub groups according to the components of the products of the pyrolysis of the organic polymer [2].

In this investigation, we have pyrolysed carbonaceous matter in three Antarctic C3 carbonaceous chondrites, ALH-77003, Y-81020, and Y-790992. The pyrograms of previously analysed C3 chondrites, Allende, ALH-77307, and Y-791717 are shown in Fig. 1, and those of the current analyses are shown in Fig. 2. The carbon contents of these chondrites are listed in Table 1.

On the assumption that the structures of organic polymers were mainly modified during the alteration of the chondrites, we presumed the following:

1) The pyrograms of the meteorites examined in this investigation are very different each other (Fig. 2). This fact suggests that these meteorites probably have different histories of alterations.

2) Although Y-81020 contains carbon as much as C2 chondrites, no specific pyrolysis product (such as naphthalene) was observed (Fig. 2: F). This fact suggests that Y-81020 is probably thermally altered seriously and most of the organic polymer in this meteorite may have been converted into nearly complete graphite.

3) Pyrogram of Y-790992 (Fig. 2: E) has some resemblance to those of ALH-77307 (Fig. 1: B) and Y-791717 (Fig. 1: C). The thermal histories of these three meteorites may be similar each other.

4) The carbon content of ALH-77003 is the same level as that of usual C3 carbonaceous chondrites, and the pyrogram of ALH-77003 (Fig. 2: D) and that of Allende (Fig. 1: A) resemble each other. But the amount of the pyrolysis products from ALH-77003 is much more than that of any other C3 chondrites. This fact suggests that the thermal history and the alteration degree of this meteorite may be similar to those of typical CM2 chondrites such as Murchison and Y-74662.

References: [1] Murae, T., Masuda, A., and Takahashi, T. (1987), ***Mem. Natl Inst. Polar Res., Spec. Issue*, 46**, 196. [2] Murae, T., Masuda, A. and Takahashi, T. (1985), ***Abst. 10th Symp. Antarct. Meteor.***, 50.

Fig. 1. Gas chromatograms of the products yielded in pyrolysis at 740 ℃ for 3 s for **A**: Allende (15 mg), B: ALH-77307 (15 mg), and C: Y-791717 (16 mg). Column: OV-101 wall coated fused silica capillary (25m x 0.25 mm i.d., 0.4 μm), Detector: FID. Attenuation: 16 for A, 8 for B and C, Temperature: 4 ℃/min from 60 to 260 ℃ after 16 min at 60 ℃.

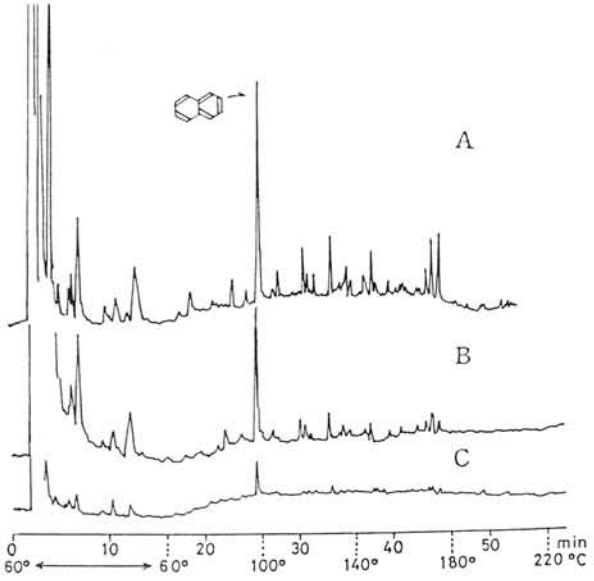

Fig. 2. Gas chromatograms of the products yielded in pyrolysis at 740℃ for 3 s for D: ALH-77003 (12.6 mg), E: Y-790992 (12.2 mg), and F (12.9 mg). Column: silicon OV-1 chemically bonded fused silica capillary (25m x 0.25 mm i.d., 1.5 μm), Detector: FID. Attenuation: 64 for D, 8 for E and F.

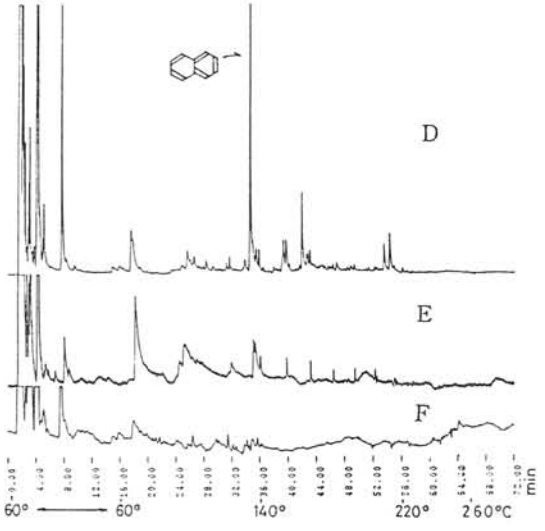

Table 1. Carbon contents: determined by combustion methods.

Chondrite	Content (%)	Chondrite	Content (%)
Y-81020	0.96	ALH-77307	0.74
ALH-77003	0.28	Allende	0.23
Y-790992	0.25	Y-791717	0.12

PETROLOGY AND MINERALOGY OF NEW ENCLAVES FROM THE VACA MUERTA MESOSIDERITE

Kimura M.[1], Ikeda Y.[1], Ebihara M.[2] and Prinz M.[3]
1)Ibaraki Univ., 2)Tokyo Metropolitan Univ., and 3)Amer. Mus. Nat. His.

Thirty eight new enclaves from the Vaca Muerta mesosiderite have been petrologicaly and mineralogicaly studied, in order to clarify the genetic relationships between mesosiderite and HED meteorite. Especially, detailed SEM-petrography was made for fourteen enclaves. Table 1 shows their texture, mineral assemblage and the average chemical composition of major pyroxene. There are two coarse-grained gabbroic enclaves consisting mainly of pigeonite and plagioclase. They look to be cumulate rocks. Eight fine- to medium-grained enclaves show ophitic to granular texture, and four enclaves are breccia. The most important is the presence of diogenitic monomict breccia (No.4659) and diogenite-dunite polymict breccia (No.4670). The former consists of orthopyroxene with abundant phosphate and opaque minerals including ilmenite and rutile which are never observed in diogenites. The dunitic clasts in an enclave (No.4670) consisting mainly of olivine of Fo_{73-71} also include abundant phosphate. These two breccias and another very fine-grained breccia (No.4689) include MgO-rich orthopyroxene (En_{74-65}). Pigeonites from cumulative enclaves are more enriched in MgO (En_{56-49}), in comparison with those from fine-grained enclaves (En_{49-36}).

The reduction-induced orthopyroxenes commonly surround pigeonite grains in cumulative enclaves, and rarely occur in fine-grained enclaves. In addition to microscopic exsolution lamellae well noticed in pigeonites of cumulative enclaves, SEM observation shows that pigeonites always include very thin lamellae of (001) direction, thinner than 2 microns in width. Reduced orthopyroxenes in cumulative enclaves usually show the lamellae of (100) direction, suggesting the slow cooling after the reduction. These orthopyroxenes have nearly equilibrium compositions with coexisting pigeonites. However, orthopyroxenes in fine-grained enclaves and a cumulative enclave do not have (100) lamella well developed and their compositions are much more enriched in MgO. They were not equilibrated with coexisting pigeonites.

Ilmenite and rutile occur in fine-grained FeO-rich enclaves and a diogenitic enclave. Coexisting pyroxenes are more enriched in TiO_2 (0.20-0.51%), in comparison with those from cumulative and dunitic enclaves (<0.29%). The various subsolidus reaction texture of chromite, ilmenite and probably pre-existing pseudobrookite are encountered.

We found two kinds of Zr-bearing minerals, zircon and baddeleyite. The latter is the first discovery from mesosiderites. FeO-rich fine-grained enclaves (En_{40}>) always include a small amount of baddeleyite, up to 30 microns across. They occur mostly associated with ilmenite, and rarely with pigeonite, troilite and SiO_2. Zircon occurs only in a

polymict breccia enclave (No.4687). The abundant occurrence of ZrO_2-bearing phases is never observed in HED meteorite.

Fig. 1 shows the plagioclase and pyroxene compositions from thirty eight enclaves. Compared with HED meteorites, these enclaves are slightly depleted in Na_2O. In addition, the enrichment of TiO_2 and P_2O_5 in MgO-rich enclaves, and the abundant occurrence of ZrO_2-minerals, suggest that the parent body and parental magma of enclaves of mesosiderite were evidently different from those of HED meteorites.

Fig.1 Anorthite (mole %) of plagioclase plotted against enstatite (mole %) of pigeonite or orthopyroxene. Trends A, B and C are alkali-poor, alkali-rich and cumulate-eucrite trends of HED meteorites, respectively (Ikeda and Takeda, 1985).

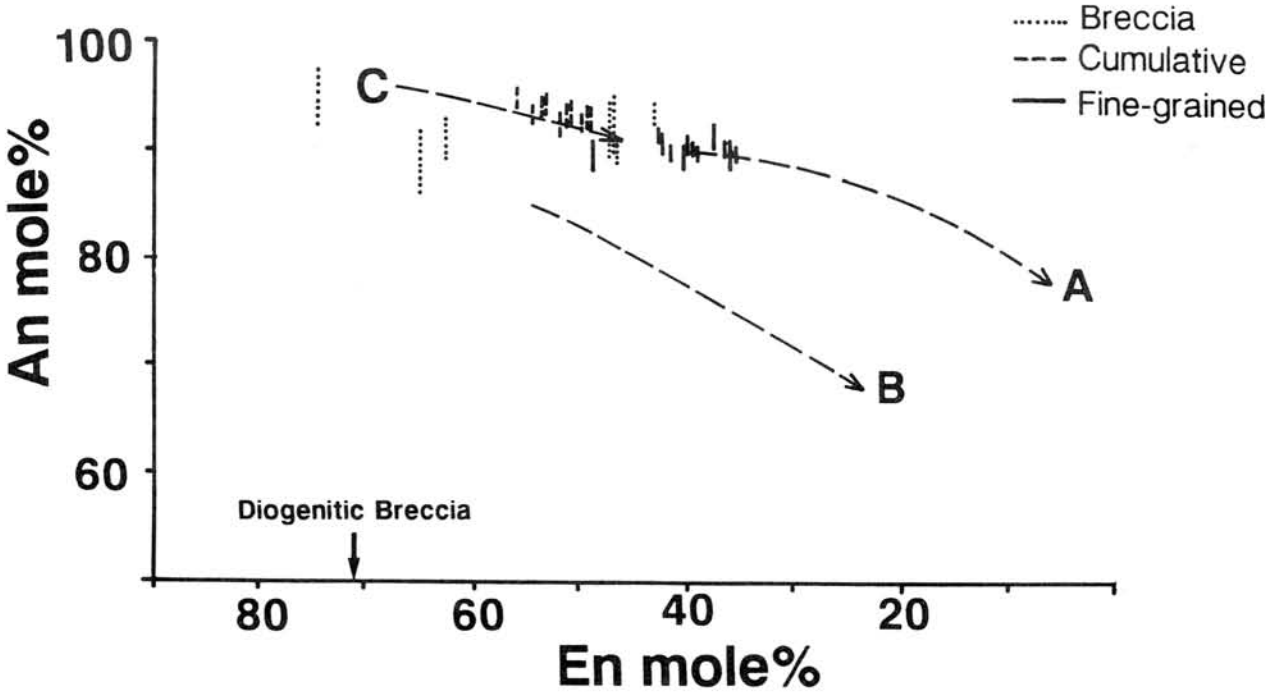

Table 1. List of samples and the mineralogy

No.	Texture	Pig	Red.	Opx	Aug	Ol	Pl	SiO2	Phos	Met	Tro	Chr	Ilm	Rut	Zir	Bad
4657	op-gr	36		-	+		+	+	+	+	+	+	+	+		+
4659	breccia	-		71					+	+	+	+	+	+		
4669	gb-gr	49		-	+		+	+	+	+	+	+				
4670	breccia	-		74	+	+	+	+	+	+	+	+				
4671	op	36		-	+		+	+	+	+	+	+	+	+		+
4672	gb	56	++	+	+		+	+	+	+	+	+				
4674	gb	54	++	+	+		+	+	+	+	+	+				
4677	op	49		-	+		+	+	+	+	+	+	+	+		+
4678	gb-gr	39	+	+	+		+	+	+	+	+	+	+	+		+
4679	op	38		-	+		+	+	+	+	+	+	+	+		+
4683	gb-op	40		-	+		+	+	+	+	+	+	+	+		+
4687	breccia	47		+	+		+	+	+	+	+	+	+	+	+	
4689	breccia	-		65	+		+	+	+	+	+	+	+	+		
4695	op	40	+	+	+		+	+	+	+	+	+	+	+		+

op:ophitic, gb:gabbroic, gr:granular / Number means average En mole.% of major pyroxene.
Reduction ++:remarkable, +:weak
Pig:pigeonite, Opx:orthopyroxene, Aug:augite, Ol:olivine, Pl:plagioclase, Met:Fe-Ni metal, Tro:troilite, Chr:chromite, Ilm:Ilmenite, Rut:rutile, Zir:zircon, Bad:baddeleyite
"Phos" means both apatite and/or whitlockite.

MINERALOGICAL STUDY OF EUCRITES YAMATO-793548 AND YAMATO-82202 WITH REFERENCE TO IMPACT HISTORIES ON THE HED PARENT BODY

Yamaguchi, A. and Takeda, H.
Mineralogical Inst., Faculty of Science, Univ. of Tokyo, Hongo, Tokyo 113

Introduction

Yamato(Y)-793548 and Y-82202 are eucrites characterized by shock textures. The clasts of these specimens are mainly composed of the surface eucrites [1]. To gain better understanding of the impact histories of the shallow layer of the HED (Howardite-Eucrite-Diogenite) parent body, we investigated the polished thin sections (PTS) of these specimens by optical microscope, scanning electron microscope (SEM) equipped with energy dispersive spectrometer (EDS), and electron probe microanalyser (EPMA).

Results and Discussions

Y-793548

This eucrite composed of four types of dominant clast and fine-grained matrix. (a) Clasts of variolitic to subophitic rocks with slightly zoned pyroxene and plagioclase [Fig.1]. These are most common clasts. (b) Coarse-grained clast with plagioclases and pyroxene. This clast has pigeonites with Fe-Ca-Mg zoning from core to rim. (c) Clasts of dendritic crystals of pyroxene and plagioclase. (d) Fine-grained (partially glassy) clasts. One of them has elongated shape. Most of the above four clasts have sub-spherical shape.

The matrix is composed of fine-grained plagioclase, pyroxene, and glassy material, and minor minerals such as ilmenite, troilite, silica. The glassy matrix is irregular in shape, and it seems to intrude into the fine grained-matrix. The matrix is partially fractured and recrystallized by intense shock. There are melt-pockets-like mesostasis, which contain droplet-shaped troilites and fragments of Ca-phosphate in glassy silica.

Most of the plagioclase crystals display wavy extinction when viewed under cross polarizer. A degree of wavy extinction is more severe in matrix. The matrix is fractured, recrystallized, and includes melt-pocket-like mesostasis.

Y-82202

The dominant clast of Y-82202 is ophitic one with lath shaped pyroxene. Fine-grained clasts and glassy clasts are not common. The large ophitic clasts contain zoned pyroxene. This pyroxene exhibits the Pasamonte-type zoning trend [2]. There is olivine (2 microns width) intruded into grain boundaries of pyroxenes. The minor minerals include ilmenite, chromite, and troilite.

The characteristic texture of Y-82202 is a shock melt vein with swirly glass texture produced by impact (19% modal) into fracture (Fig.2). The fractures and veins form net-work like texture in the PTS. The boundary between the vein and the host is very sharp. The fragments less than about 100 microns in diameter in the vein are of sub-spherical shape. The fragments

in the vein consists of various kinds of minerals and lithic clasts which composed of the host materials. Particularly, many fragments less than 50 microns are troilite, ilmenite, chromites. An ellipsoidal clast in the glassy vein consists of olivine (Fa_{88}), plagioclase (An_{90}), and Fe-rich low-Ca clinopyroxene, minor ilmenite and silica. The vein has also many vesicles (less than 400 microns). The veins are not totally glassy, and partially it contains dendrites which are located parallel to edges of the host. The compositions of all glassy veins are very homogenous in this PTS. The compositions of glass and dendrites are nearly the same.

In spite of the presence of swirly glass, the host of Y-82202 does not show a intense shock texture. It only shows weak wavy extinction. This may represent different shock pressure [3]. The glass compositions are plotted near the peritectic point in the silica-olivine-anorthite pseudoternary system [4] (Fig.3). Judging from the rounded shape of fragments in the vein and their uniform composition, we interpreted that there may be total melting of the eucrite at another place and rapidly injected into this area.

Conclusions

Dominant clasts in Y-793548 have rapidly cooled textures. Grain sizes of minerals are very fine in comparison with other Antarctic eucrites [2]. Some clasts show dendritic textures of pyroxene and plagioclase. There may be the original rock which must have been cooled rapidly on the surface. Those surface rocks were brecciated and mixed by impacts.

In spite of the presence of the swirly glass vein of impact melt, the host of Y-82202 does not keep records of the intense shock. It may be ejected out from the ground after impact melt had been injected into the specimen and quenched on the surface. A similar texture of such vein has been reported in the Cachari eucrite [5].

The fact that rocks with impact melt coexisting with quickly cooled surface rocks, suggest that Y-82202 and Y-793548 kept recording of events took place near surface of this parent body. Further study is required to determine their ^{36}Ar-^{38}Ar ages of these surface materials to relate these events to their history.

We thank the National Institute of Polar Research for the meteorites specimens, and Mr. O. Tachikawa and Mr. H. Yoshida for technical assistance for the SEM-EDS and EPMA studies.

Reference

[1] Takeda, H. (1979) Icarus, 40, 455-470
[2] Delany, J. et al. (1984) Proc. Lunar Planet. Sci. Conf. 15th, in J. Geophys. Res., 89, C251-C258.
[3] Stoffler, D. et al. (1988) in "Meteorites and the Early Solar System" ed. by Kerridge, F. and Matterws, M. S., The Univ. of Arizona Press, 165-202
[4] Stolper, E. (1977) Geochim. Cosmochim. Acta, 41, 587-611
[5] Fredriksson, K. and Kraut, F (1964) Geochim. Cosmochim. Acta, 31, 1701-1704

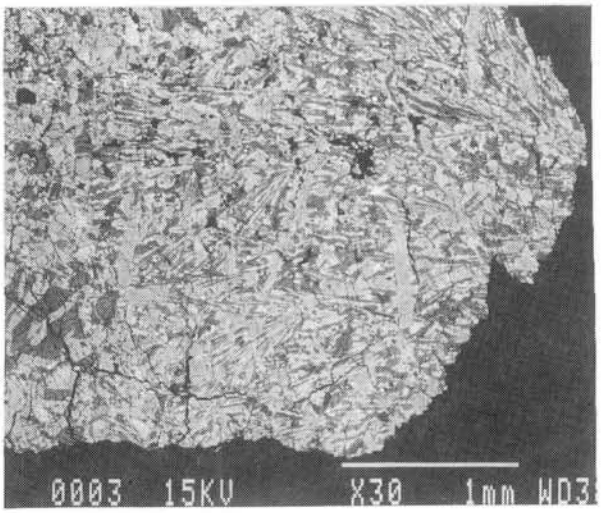

Fig.1 Backscattered electron image (BEI) of the variolitic clast of fine-grained texture in Y-793548.
Black crystals : plagioclase.
White crystals : pyroxene.

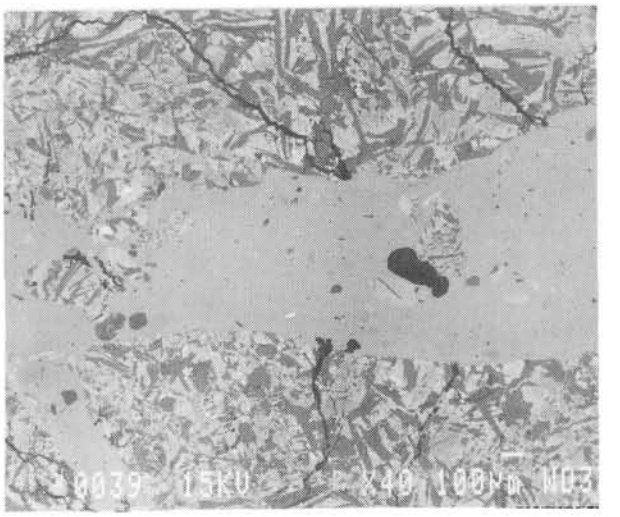

Fig.2 BEI of the shock melt vein of swirly glass in Y-82202.
Black crystals : plagioclase.
White crystals : pyroxene.
Gray area in the middle : shock melt vein.

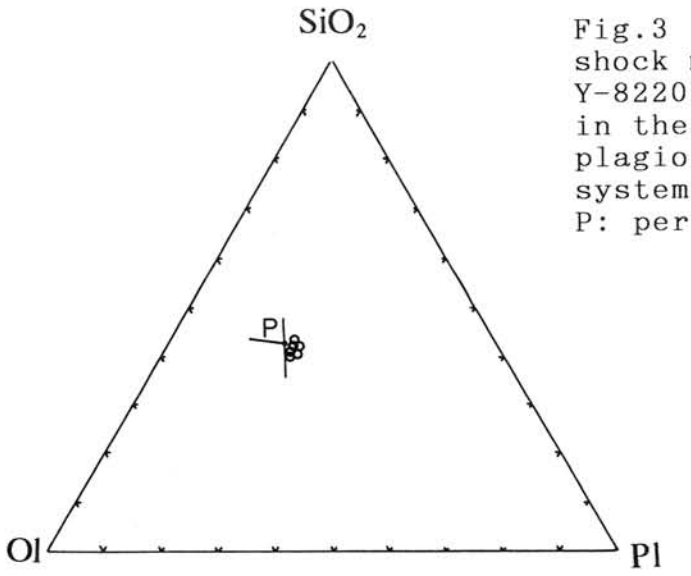

Fig.3 Composition of the shock melt glasses from Y-82202 (open circle) plotted in the silica-olivine-plagioclase pseudoternary system [4].
P: peritectic point.

THE CHEMICAL MAP ANALYSIS (CMA) STUDY OF MESOSTASIS IN SOME ANTARCTIC EUCRITES.

Saiki Kazuto and Takeda Hiroshi.
Mineralogical Inst., Faculty of Science, Univ. of Tokyo, Hongo, Tokyo 113.

To study the behavior of some refractory elements in eucrites, we investigated mainly Y-791438, which contains zircon, by SEM (JEOL 840A) equipped with EDS and by X-ray chemical map analysis (CMA) utilities of Kevex. Other refractory element rich eucrites Y-75011(84C) and Stannern were compared with Y-791438.

Y-791438 is one of the rare crystalline eucrites found in Antarctica. It is composed mainly of pyroxene and plagioclase (36 vol. %). This meteorite has both ordinary eucritic and cumulate eucritic characters. The ordinary eucritic characters are summarized as follows : (a) The original texture was ophitic or subophitic. (b) The pyroxenes have thin exsolution lamellae. (c) The host pyroxene was homogenized in mg number (Mgx100/(Mg+Fe)). The cumulate eucritic characters are: (a) Y-791438 ptroxene has Mg-rich bulk chemical composition ($Ca_8Mg_{50}Fe_{42}$). (b) The plagioclase crystals are Ca-rich (An=90-95) and are slightly zoned. (c) Rare earth element (REE) pattern shows cumulate eucritic pattern (1,2,3,4). All these characters make this eucrite unique. Y-75011 is a polymict eucrite that contains several coarse-grained mesostasis-rich basaltic clasts with subophitic texture (5). Clast Y-75011,84 is one of those clasts. It represents the oldest pristine, unambigously basaltic lava as yet recovered from a solar system object (5). Extensive Mg-Fe chemical zoning in pyroxenes is preserved (5). Stannern is a monomict eucrite, and contains mesostasis-rich basaltic clast with subophitic texture, but their mg number of the host pyroxene is constant and the mesostasis is recrystallized.

One zircon grain about 30 microns has been found on the PTS of Y-791438 at the interstices of plagioclase and pyroxene together with chromite, ilmenite, troilite and Ca phosphate (4). The CMA work suggests that this portion is a mesostasis portion. A characteristic feature observed on this portion (Fig.1) is a presence of calcium phosphate region. Micron-sized pyroxene and silica sticks are found by CMA study. They seem to have crystallized at the last stage of solidification. Ca and Nd have been detected in this Ca phosphate. From the fact that this region is adjacent to zircon and that the size of zircon is fairly large with respect to the that of mesostasis, it may be concluded that the zircon nucleated at an earlier stage, grown in a residual liquid and solidified as a part of mesostasis. A typical mesostasis region was found on the other portion of Y-791438 (Fig.2). SiO_2-rich residue was solidified at this portion. Similar regions are observed on a larger scale in Y-75011 (84C) and Stannern.

There is another interesting portion in Y-791438, which has a very different appearance. There are some characteristics indicating the secondary shock texture. This portion might have been produced by a secondary shock event. About a half of the pyroxene grain boundaries are covered with fuzzy glassy materials with chemical compositions intermediate between augite and plagioclase (Fig.3). Globules of FeS ranging from 0.5 to 1 microns in diameter (up to 4 microns) often observed in such areas, where chromite, ilmenite and troilite are abundant. The texture indicates that these glassy materials with FeS gloubules might have been produced by rapid cooling of shock partial melt. In the pyroxenes of Y-75011(84C) Fe-rich bands are observed. It is questionable whether these two textures have the same kind of origin or not, but it can be stated that both textures have not undergone severe thermal metamorphism since their formation as was proposed for Stannern (5).

A possible hypothesis for the origin of Y-791438, in addition to

those what have been proposed to the origin of eucrites, may be that Y-791438 crystallized in a shallow magma. In a shallow magma, initial crystallization takes place at a shallow place and forms a magnesian non-cumulate eucrite. SiO_2-rich residues of Y-791438 are much smaller in scale than that of Y-75011(84C) and Stannern, but in Juvinas and Serra de Magé, such residues could not be found. This fact may suggest that the cumulate process was not so severe in case of Y-791438 because of the shallowness of magma. However, the presence of zircon cannot be explained. Even in the refractory-element-rich clast Y-75011(84C), we found one ZrO_2 only 4-5 microns, but Y-791438 has 30 microns zircon grain. There is a possibility that the shallowness of magma did not make the concentration of Zr efficiently. If once zircon was nucleated, it continued to grow until the later stage and incorporated in the mesostasis. The exsistence of one relatively large zircon in small mesostasis may be due to the low nucleation density of zircon. Owing to a lack of the knowledge of zircon, a definite conclusion must be reserved.

We thank the N.I.P.R. and Dr. M.Prinz, Amer. Museum of Natural History for providing us with the meteorite samples. We are much indebted to Mr. Osamu Tachikawa for his assistance during the CMA work.

References:(1) Yanai K. and Kojima H. (1987) Photo. Catalog of the Antarctic Meteorites, 298p. (2) Takeda H. and Tagai T. (1989) Lunar and Planetary Science XX. 1101-1102. (3) Takeda H., Saiki K. and Tagai T. (1989) Abstr. NIPR Symp. Antarct. Meteorites, 13th, p64-66. (4) Saiki K., Takeda H., Toyoda K. and Tagai T. (1990) Lunar and Planetary Science XXI. 1061-1062. (5) Nyquist L.E., Takda H., Bansal B.M., Shih C.Y., Wiesmann H. and Wooden J.L. (1986) Journal of Geophysical Research, Vol.91, No.B8, p.8137-8150.

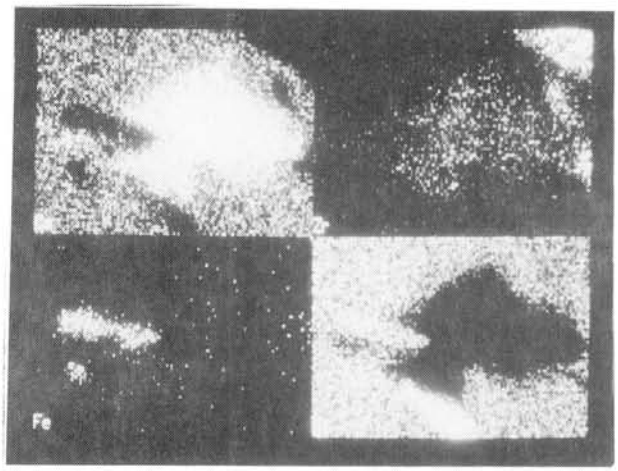

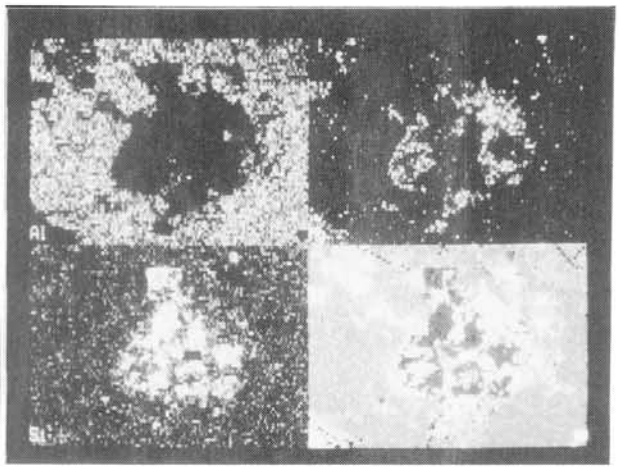

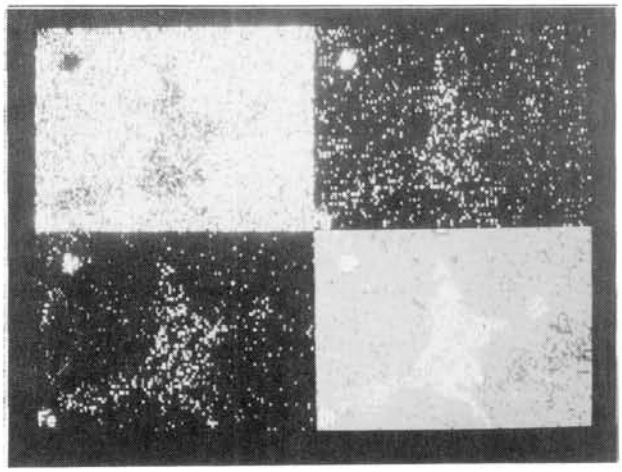

Fig.1

Ca	Zr
Fe	Si

20μm

Fig.2

Al	Mg
Si	BEI

270μm

Fig.3

Al	Mg
Fe	BEI

50μm

Fig 1-3. CMA outputs of (1) Ca phosphate region; (2) a SiO_2-rich mesostasis; and (3) fuzzy glassy part around a pyroxene.
Every figure is composed of 4 different element frames of the same portion, given above.
Each scale bar represents the width of one element frame.

MINERALOGICAL STUDY OF METALLIC GRAINS IN ANTARCTIC UREILITES

Jun saito and Hiroshi Takeda
Mineralogical Institute, Faculty of Science, University of Tokyo, Hongo, Tokyo 113, Japan

Ureilite is an olivine-pyroxene achondrite with carbonaceous vein materials, and it also contains the Fe-Ni metal and sulfides as minor phases. Many researchers suggested that ureilites are related to carbonaceous chondrites because of their high amounts of carbon and oxygen isotope ratios similar to carbonaceous chondrites (e.g. Clayton and Mayeda, 1988; Vdoykin, 1970). Among many models about ureilite origin presented up to date, a process to remove Ca,Al-rich and Fe-Ni-S components out of the ureilite source materials without changing their oxygen isotope ratios too much has been subject of debate. To investigate the process of removing Fe-Ni-S components, we studied ureilitic metals at grain boundaries by electron probe microanalyser (EPMA) and scanning electron microscope (SEM). The results are interpreted on the basis of a planetesimal-scale collision (PSC) model (3,4).

Samples used in this study (Y-74130, Y-82100, Y-74123, MET-78008, ALH81101, ALH78019, LEW85328) were supplied from National Institute of Polar Research (NIPR) and Meteorite Working Group (MWG) in the U. S. Electron probe microanalysis has been performed at Geol. Inst., Univ. of Tokyo, using JEOL 733 mk II superprobe, and scanning electron microscopy was performed by using JEOL 840A SEM and Kevex Super 8000 Energy Dispersive System (EDS) equipped with digital beam controller for acquiring the two dimensional X-ray mapping and backscattered electron images (BEI).

A plot Ni versus Co of the ureilitic metals revealed that the metallic grains in relatively weakly shocked ureilites (ALH78019 and Y-82100) show fairly uniform chemical compositions (Fig. 1.). It is thought that these metals in ALH78019 and Y-82100 keep their original chemical compositions, without detectable disturbance of shock events. The chemical compositions of several ureilites tend to scatter in Ni and minor element contents (Fig. 2). These scattering are discussed below. More Ni-poor metal compositions of heavily shocked ureilite (ALH81101) than those of weakly shocked ureilites suggest that the Ni content of pre-existing metals in ALH81101 may have been diluted by reduced metals produced by the shock event during the breakup of the parent body.

In General, Co contents of ureilitic metals tend to decrease as their Ni contents decrease (Fig. 1,2.), and the ureilitic metals may be classified into three types of Ni vs. Co distribution patterns: (a) the chemical compositions of metals show very slight variations as shown by Y-82100 and ALH78019 (Fig. 1); (b) the Ni contents of metals show relatively lower (1~2.8 wt %) as shown by ALH81101 (Fig. 1); (c) Ni vs. Co plots fall in very wide range of Ni and Co contents, as shown by Y-74123, LEW85328, MET-78008, and Y-74130 (Fig. 2).

The chemical compositions of metals in ureilites with interstitial materials (Y-74123 and LEW85328) show very wide variations in their Ni and minor element contents. However, observations of BEI of Y-74123 shows numerous reduced metals. This suggests that the Ni contents of pre-existing metals in Y-74123 may have been diluted by reduced metal produced at the time of parent body

breakup, as discussed for the ALH81101 metals.

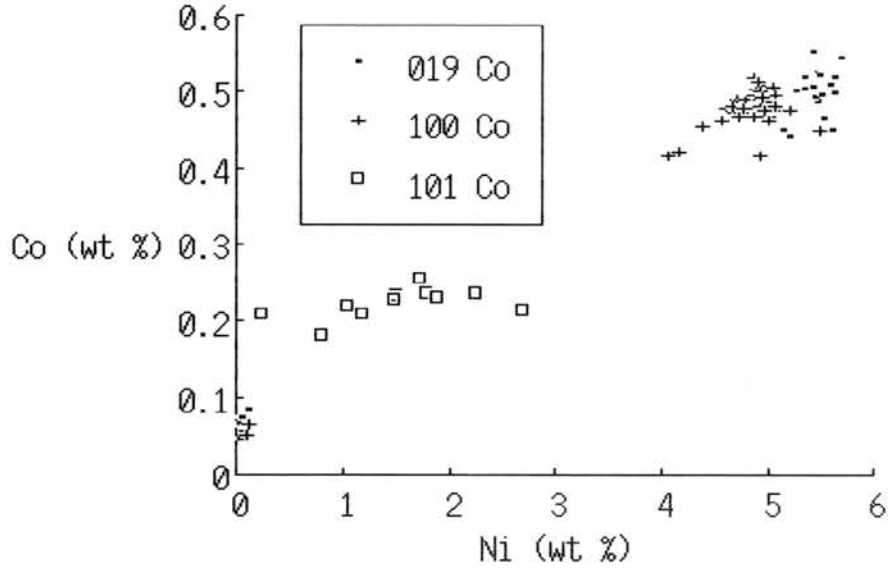

Fig. 1. Co vs Ni plot of A78019, Y-82100, and A81101 metals. Note that the A81101 metals show less Ni contents than others. The numbers in the figure represent last three digits of sample numbers.

LEW85328 shows heavily shocked features such as cloudy pigeonites, and these shock features exist in some portions but not in the entire specimen as described by Saito and Takeda (5). They also suggested two possibilities to interpret the shock features in LEW85328: (a) LEW85328 had experienced the shock event which resulted in the parent-body breakup, but this shock effect was so heterogeneous; (b) LEW85328 had been heavily shocked prior to the parent body breakup, but the shock texture of pigeonite was annealed by the residual heat. In both cases, the fact that the shock effect produced by the latest shock event of parent body breakup is relatively weak, and that the BEI of LEW85328 shows less amounts of reduced metals than Y-74123, suggest that LEW85328 had been less affected by latest shock event of breakup than Y-74123.

Ogata et al. (6) proposed that the interstitial materials were formed from melts produced by the shock event prior to the parent-body breakup. Because the amounts of reduced metals of LEW85328 seem to be smaller than the case of Y-74123, and the dilution of Ni contents of the metals in LEW85328 may be weaker than Y-74123, the scattering of chemical compositions of LEW85328 metals may be formed from the metallic melts accompanied by the shock melts that formed interstitial materials.

The metal grains of augite-bearing ureilites, MET78008 and Y-74130, also show the scattering of their chemical compositions (Fig. 2). The recent studies of ureilites (7) proposed that these ureilites were produced by the Ca-rich shock melts formed by the shock event prior to the breakup. The above scatterings may be due to the mixing of such shock melts, but these specimens show relatively heavily shocked features and prolonged annealing, and a large amount of reduced metals in BEI. It is still unknown whether

these scatterings had been formed by the shock event prior to the breakup or not.

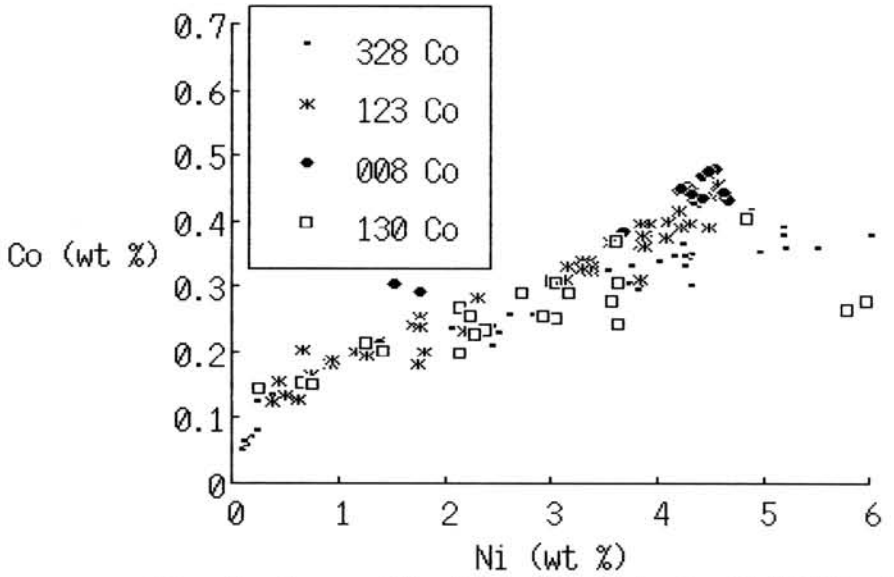

Fig. 2. Co vs Ni plot of metals in Y-74123, LEW85328, MET-78008 and Y-74130. Note that the chemical compos itions of these metals scattered in very wide range.

In summary, the chemical compositions of ureilitic metals are divided into three types. The metals in weakly shocked ureilites has very narrow range of chemical compositions, since these metals had not been disturbed by any shock events. The metals in heavily shocked ureilite (ALH81101) shows relatively Ni poor, and the Ni content of pre-existing metals may have been diluted by reduced metals produced by the shock event of the parent-body breakup. The scattered chemical compositions of metals found in augite-bearing ureilites and ureilites with interstitial materials suggest that these scatterings may have been produced by the shock melts prior to the parent-body breakup.

We thank National Institute of Polar Research and Meteorite Working Group for meteorite samples, and Mr. O. Tachikawa and H. Yoshida for technical assistance of SEM-EDS and EPMA studies.

REFERENCES:

(1) Clayton, R. N. and Mayeda, T. K. (1988) Geochim. Cosmochim. Acta. 52, 1313-1318
(2) Vdoykin, G.P. (1970) Space Sci. Rev. 10, 483-510
(3)Takeda, H. (1987) Earth. Planet. Sci. Lett., 81,358-370
(4)Takeda, H. et al. (1988) Proc. NIPR Symp. Antarct. Meteorites, 1, 145-172,
(5)Saito, J. and Takeda, H. (1988) Lunar and Planetary Science XX, 938,
(6) Ogata, H. et al. (1988) 13th Symp. on Antarctic Meteorites, No.62 (Abstract)
(7) Takeda, H. (1989) Meteoritics, 24, 73-81.

Refractory inclusions in anomalous ALH85085 chondrite: Mineralogy, bulk chemistry and isotopic compositions

Makoto Kimura[1], Ahmed El Goresy[2], and Ernst Zinner[3]
1)Department of Earth Sciences, Ibaraki University, Mito 310.
2)Max-Planck-Institut fuer Kernphysik, D-6900 Heidelberg, F.R.G.
3)McDonnell Center for the Space Sciences and Physics Department, Washington University, U.S.A.

We report the mineralogy, bulk chemistry and isotopic compositions of refractory inclusions from anomalous ALH85085 carbonaceous chondrite. This chondrite is significantly different from other carbonaceous chondrite in mineralogy [1,2] and inclusions [3].

We found at least 47 inclusions and related fragments. In spite of their small sizes (5-70 microns), the refractory inclusions look to be not fragments from pre-existing coarse inclusions. They did not suffer the secondary alteration. However, noble-metal-bearing nuggets are not encountered, which is consistent with the depletion of refractory siderophile elements. The abundant occurrences of Calcium-dialuminate $CaAl_4O_7$ (CA2), almost never found in other inclusions, also characterize refractory inclusions in ALH85085.

Refractory inclusions in ALH85085 are classified into 4 groups: (1)hibonite-bearing inclusions consisting of Ti- and Mg-poor hibonite with gehlenitic melilite, perovskite, spinel and Ca-rich pyroxene, (2)spinel-rich inclusions with melilite, perovskite, pyroxene and rare glass, (3)CA2-bearing inclusions consisting of pure stoichiometric CA2 with melilite, spinel, perovskite and pyroxene. One inclusion contains Mg- and Ti-rich hibonite on the surface of CA2. In addition to these inclusions, there are many fragments from pre-existing inclusions. We found a complete petrographic suite covering intermediate characters between these types of inclusions. The textural observation shows that the formation sequence of minerals are (hibonite, perovskite, CA2) - spinel - melilite - pyroxene. Pyroxenes have variable contents of Al_2O_3 (2.4-46.0 wt.%).

We measured the bulk chemical compositions of these inclusions using defocused beam of electron microprobe. They are enriched in Al and Ca, and depleted in Si. Most of inclusions continuously distribute between the region of spinel-hibonite and type A inclusions in the other carbonaceous chondrites (Fig.1). CA2-bearing inclusions can not be distinguished from the others. Two inclusions distributes near to the region of type B inclusions.

The isotopic compositions and trace elements were measured by ion microprobe. Two inclusions have excess ^{48}Ca (Table 1). The ^{26}Mg excesses in these inclusions correspond to the "canonical" $(^{26}Al/^{27}Al)_0$ ratio,

whereas the other inclusions have lower ratios. All Ti isotopic ratios (δ^{50}Ti) are normal. There is no relationship between REE patterns and other properties. A remakable feature is the fractionation in the LREE to Sm in some inclusions. The lack of large isotopic fractionation indicates that the inclusions did not experience much distillation during their formation.

References: [1]Kimura M. and El Goresy A. (1989) Meteoritics, 24, 286. [2]Grossman J.N. et al. (1988) EPSL, 91, 33. [3]MacPherson G.J. et al. (1989) Meteoritics, 24, 297.

Table 1. Isotopic and REE patterns of inclusions

Inclusions	Type	δ^{48}Ca	REE patterns
174	Hib	-3.4±3.3	volatile enriched Group II
181	Hib	7.4±2.9	Group III
50.2	CA2	2.3±4.5	Group II
76	CA2	-4.1±7.8	
138	CA2	0.6±4.5	
143	CA2	4.7±5.6	LREE fractionated group III
163	CA2	3.6±4.9	
185	CA2	11.7±3.8	volatile enriched Group II
216	CA2	-2.4±2.0	Group II
80	CA2	-7.0±8.5	

Fig. 1 Bulk chemical compositions of inclusions on the atomic plot of (Al+Ti)-Ca-Si.

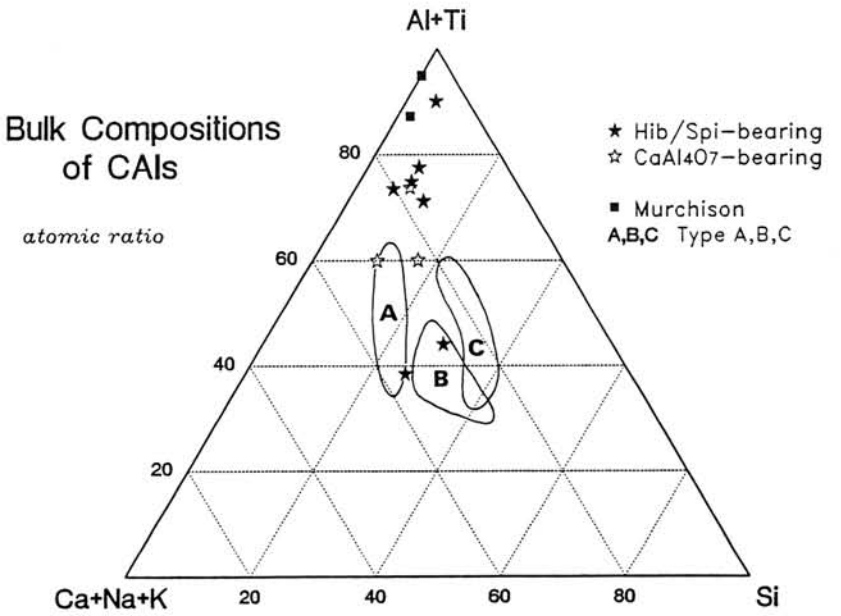

FORMATION OF PALLASITE AND EUCRITE-DIOGENITE PARENT MAGMA BY PARTIAL MELTING

Hiroshi ISOBE, Akira TSUCHIYAMA[1] and Masao KITAMURA[2]
Dept. of Environ. Safety Res., Japan Atomic Energy Res. Inst., Tokai, Ibaraki, 319-11
[1]College of General Education, Osaka Univ., Toyonaka, Osaka, 560
[2]Dept. of Geol. and Mineral., Fac. of Sci., Kyoto Univ., Sakyo, Kyoto, 606

According to the results of the partial melting experiments of a chondritic material [1], where Mg# (Mg/(Mg+Fe)*100 in mol ratio) of silicate portion in the starting material is around 79, olivine of Fo_{87} can coexist with the melt of eucrite-diogenite mixture with Mg# of 65 at around 1400℃ in equilibrium. This olivine composition is equal to that of pallasite olivine. Fe-Ni metal in pallasites can coexist with the olivine and the melt in equilibrium in the HED (howardite-eucrite-diogenite) parent body. Then, pallasite can be easily explained by the separation of the olivine (and metallic Fe) from the coexisting melt in equilibrium. Furthermore, the melt obtained in this condition can produce eucrite and diogenite.

Maximum fractionation process can also separate olivine in pallasite from the chondritic material. The chemical composition of olivine crystallized in the maximum fractionation process can be calculated based on the experimental results. The olivine crystals have a wide variation in the composition (Fo_{93-81}), and the average composition is Fo_{88}, which is almost the same as those of pallasitic olivine (Fo_{87}). However, the fractionated melt becomes more rich in Fe (Mg#=55) than the equilibrium melt (Mg#=65) (Fig. 1). Eucrite and diogenite can not be produced from this Fe-rich melt. Therefore, pallasite and the parent magma of eucrite-diogenite can not be explained by the maximum fractionation process from the chondritic material.

On the other hand, maximum fractionation of olivine to produce a dunite layer instead of pallasite in the parent body model is proposed [2] based on the study of olivine fragments in a howardite. Further discussion [3] on a fractionation trend from a chondritic material was done with the bulk composition of the HED parent body [4]. The melt produced in this process has the Mg# of 63, and will produce the eucrite-diogenite association (Fig. 1). Therefore, the maximum fractionation is possible as long as the hypothetical dunite layer is the member of the parent body of HED meteorites. However, pallasitic olivine can not be formed in his model, because olivine crystallized changes its composition from Fo_{93} to Fo_{85} with the average of Fo_{90}, which is richer in Mg than the pallasitic olivine (Fo_{87}).

Gravitational separation should be taken into considerations in discussions on solid-liquid separation in igneous processes on planets. Solid-liquid separation process of magmatic systems must be controlled mainly by density difference between crystals and partial melt, and viscosity of melt, as well as degree of the partial melting. On the other hand, in a case of solid-liquid separation by crystallization, the process should be discussed based on

data of sinking velocities of crystals and behavior of natural convection in a magma ocean. In the partial melting experiments [1], metallic Fe-Ni phase were excluded from the system. In the present study, physical parameters to describe an effect of gravity to the solid-liquid separation on the HED parent body including metallic phase were calculated using the results of the partial melting experiments from a chondritic material.

There are two typical cases for differentiation processes of the magma; (1) the solid-liquid separation during cooling process of total melt, and (2) that during partial melting by heating of starting material.

In the first case, the magma of a chondritic composition should be once heated above liquidus temperature of Fe-Ni metal, because liquidus temperature of olivine in the present system is above 1600℃ and Fe-Ni metal is solid below 1500℃. If not, the case is almost similar to the second case. Then, Fe-metal coexisting with silicate melt must be small bubbles of metallic melt due to the immiscibility between metallic and silicate melts. The metallic bubbles can adhere each other and grow rapidly. Thus, until the temperature of the solid-liquid separation (1400℃), Fe-metal must be separated from silicate portion and form metallic core.

The critical size, in which sinking velocity of crystals is equal to velocity of convective flow, of olivine at 1400℃ is about 0.15 mm, which is significantly larger than that of Fe-metal (about 0.05 mm) (Fig. 2). This process of the solid-liquid separation results in the formation of not pallasite but layers of dunite and metallic iron. Therefore, it is hardly suggested that pallasite was formed during the cooling of magma.

The second case is that pallasite was formed as a residue from a partial melt during heating process of a chondritic material. At the temperature of the separation of pallasite (1400℃), the volume ratio of crystals (olivine and Fe-metal) and melt is about unity. This ratio can allow to form a network of melt in a chondritic material. The density difference between crystals and the partial melt at 1400° is about 0.45 g/cm^3.

In the partial melting process, the change of melt composition and volume fraction of solid suggest that viscosity of the melt drastically decreases at above 1350℃. While the segregation process of the partial melt is not understood, the density difference and the decreasing of the viscosity must allow the segregation of the partial melt after the formation of the network of the melt even in a small planet. Therefore, as a conclusion of the solid-liquid separation, the partial melting process is suggested.

References: [1] Isobe, H. *et al.*, (1988) Abstr. 19th Symp. Antarctic Meteorites, 65-67, NIPR. [2] Ikeda, Y and Takeda, H. (1985) Proc. 15th Lunar Planet. Sci. Conf., JGR, **90**, C649-663 [3] Ikeda, Y (1989) Abstr. 28th Intnl. Geol. Cong., Washington, 2, 92-93 [4] Dreibus and Wanke (1980) Z. Naturfosch. **35a**, 204-216

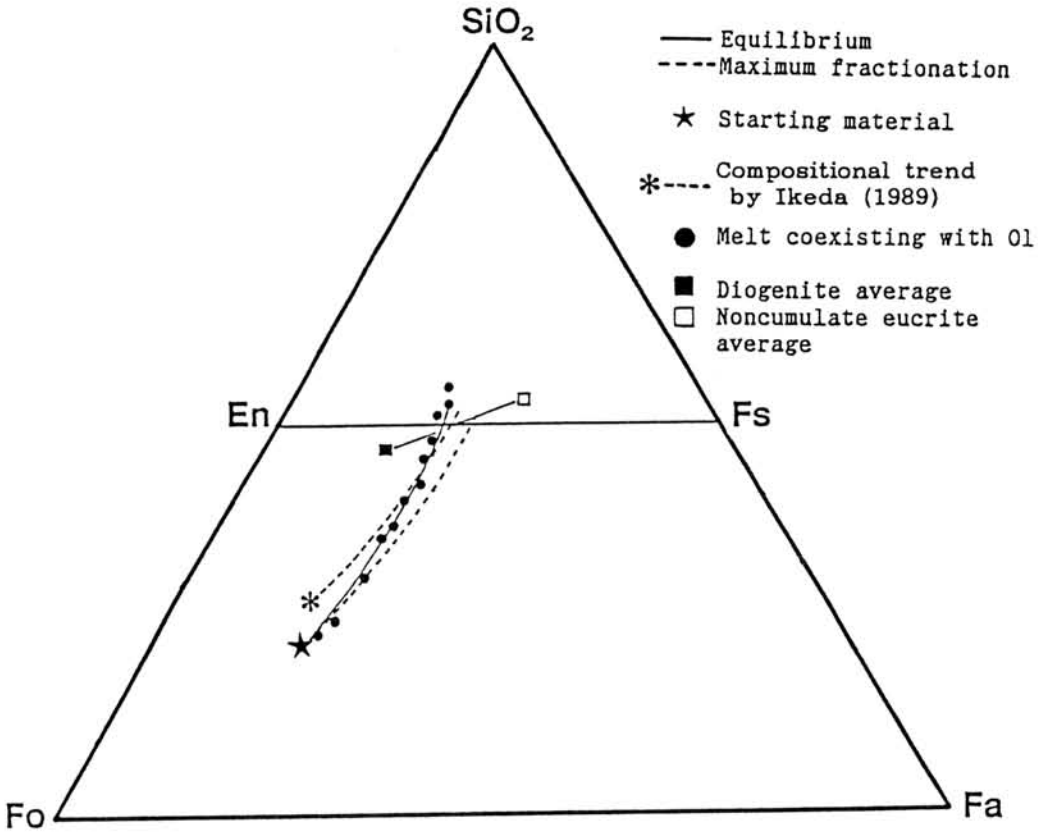

Figure 1
Calculations on the equilibrium crystallization and the maximum fractionation from a chondritic material. Calculated values and the melts with olivine produced in experiments [1] are plotted on the SiO_2-Fo-Fa system. Fe-Mg partition coefficient between Ol and melt used in the calculations is 0.3. The compositional trend by Ikeda [4] is also shown.

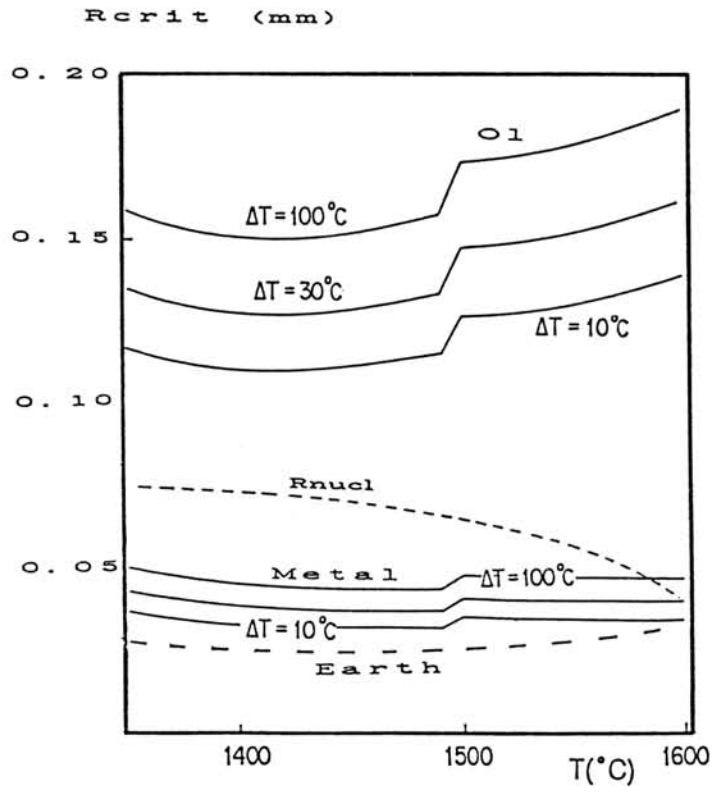

Figure 2
Calcurated critical radii of olivine, metal and pyroxenes. Grains which is smaller than these values cannot separate from the melt by the motion of convection. From smaller gravity than the Earth, on the HED parent body, larger crystals can float in melts than on the Earth.

ALTERATION TEXTURE OF PYROXENE IN ALLENDE CHONDRULES AND THE FORMATION OF MATRIX MATERIALS

S. MATSUNAMI, H. KINO, H. NISHIMURA AND H. TAKESHI: NARUTO UNIVERSITY OF EDUCATION, NARUTO, TOKUSHIMA 772, JAPAN.

Ferrous olivine is the most abundant and ubiquitous mineral in the matrix of the Allende carbonaceous chondrite (CV3) (Peck, 1983; Kornacki and Wood, 1984). Formation of matrix ferrous olivine in primitive unequilibrated ordinary chondrites (UOCs) and several CV3 chondrites seems to be records of non-equilibrium condensation processes in the early solar nebula (Nagahara, 1984; Kornacki and Wood, 1984; Palme and Fegley, 1989; Matsunami et al., 1989, 1990). They may give clues to understanding of exact formation processes of primitive chondritic materials in the early solar system.

As already suggested by many investigators, enstatite phenocrysts in some Allende chondrules appear to be altered to form ferrous olivine around them (Housley and Cirlin, 1983). Housley and Cirlin (1983) considered that the formation of ferrous olivine observed in several enstatite-bearing chondrules may be the results of alteration due to solid-solid reaction between enstatite and metallic iron during the metamorphism in the parent body and that matrix ferrous olivines were derived as comminuted fragments of altered chondrules through brecciation due to impact processes on the parent body. However, detailed features of alteration of enstatite phenocrysts in Allende chondrules are poorly known. In this study, mode of occurrence of altered enstatites in eight Allende chondrules (7 porphyritic ol-px chondrules and 1 poikilitic ol-px chondrule) was observed with SEM in detail. Next, chemical compositions of ferrous olivine on enstatite crystals ("alteration olivine" hereafter), which were analized with EPMA, are compared in detail with those of matrix ferrous olivine. We finally discuss the implications for the formation of matrix ferrous olivine and origin of the alteration textures of enstatite phenocrysts in Allende.

Alteration of enstatite in Allende chondrule are mainly observed along the margin of individual chondrule. It is revealed that alteration olivine frequently occurs along the periphery of enstatite phenocryst and along the minor cracks of enstatite.

Fig. 1 shows histograms of Fa contents of magnesian olivine phenocrysts and olivine inclusions in enstatete phenocrysts, matrix olivine and alteration olivine. Fa mole % of alteration olivine and matrix olivine are ranging from Fa_{28} to Fa_{48} (alt. ol.) and from Fa_{37} to Fa_{51} (m. ol.), respectively. Although Fe/Mg ratios of alteration olivine largely overlap those of matrix olivine, the mean Fa mole % of the former is different from that of the latter. Fig. 2 illustrates the MnO and FeO contents of alteration olivine and matrix olivine. It is shown that there exists a strong positive correlation of MnO with FeO. It seems that they form a trend on the diagram, suggesting that they are genetically related. Fig. 3 shows a comparison of the Al_2O_3 and Cr_2O_3 contents between alteration olivine and matrix olivine. Although the Al_2O_3 and Cr_2O_3 contents of alteration olivine are widely scattered on the diagram, those of matrix olivine are concentrated near the origin of the diagram. It is shown that matrix ferrous olivines are not regarded as comminuted fragments of alteration olivines and that they were formed through a different process.

Fig. 2 also shows the comparison of the MnO and FeO contents of enstatite phenocrysts (one of reactants) with those of alteration olivine (product). The MnO content of enstatite is mostly below 0.2 wt %. As shown in this figure, it is difficult to form alteration olivine (>0.1 wt % MnO) only through the reaction between enstatite (<0.2 wt % MnO) and Mn-free metallic iron. Therefore, it is concluded that alteration textures of enstatite phenocrysts in Allende chondrules were not formed through solid-solid reaction between enstatite and metallic iron.

An alternative explanation of the alteration textures is solid-gas reaction between chondrule enstatite and Fe,Mn-rich nebular gas during chondrule formation. It is possible that gaseous Fe and Mn atoms stick onto the surface of enstatite-bearing chondrules and diffuse into the inner parts to react with enstatite phenocryst to form

alteration olivine during chondurle formation. Hua et al. (1988) have also shown that Fe diffusion to form fayalite-rich rims, veins and halos around and in forsteritic olivines is a wide-spread phenomenon in chondrules and CAIs of Allende. Matrix ferrous olivine would have formed through a different formation mechanism to that of alteration olivine, although they seem to be genetically related. It is suggested that matrix ferrous olivine were formed through non-equilibrium vapour → solid condensation in cooling nebular gas (Kornacki and Wood, 1984; Palme and Fegley, 1989; Matsunami et al., 1989, 1990).

References: Housley and Cirlin (1983): In "Chondurles and Their origins", pp. 145-161./ Hua, Adam, Palme and El Goresy (1988): GCA, **52**, 1389-1408./ Kornacki and Wood (1984): GCA, **48**, 1663-1676./ Matsunami, Nishimura and Takeshi (1989): Submitted to EPSL./ Matsunami, Nishimura and Takeshi (1990): Proc. 14th Symposium on Antarctic Meteorites, in press./ Nagahara (1984): GCA, **48**, 2581-2595. / Palme and Fegley (1989): Submitted to EPSL./ Peck (1983): Meteoritics, **18**, 373-374.

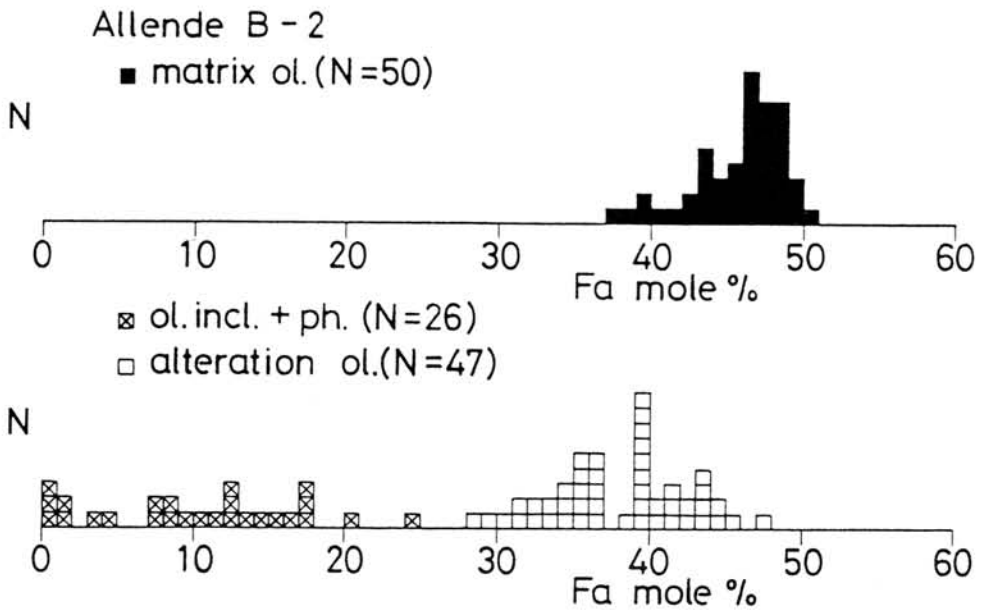

Figure 1. Frequency diagrams of Fayalite mole % of matrix olivine, alteration olivine and olivine inclusion and phenocryst in 8 Allende chondrules, investigated in this study.

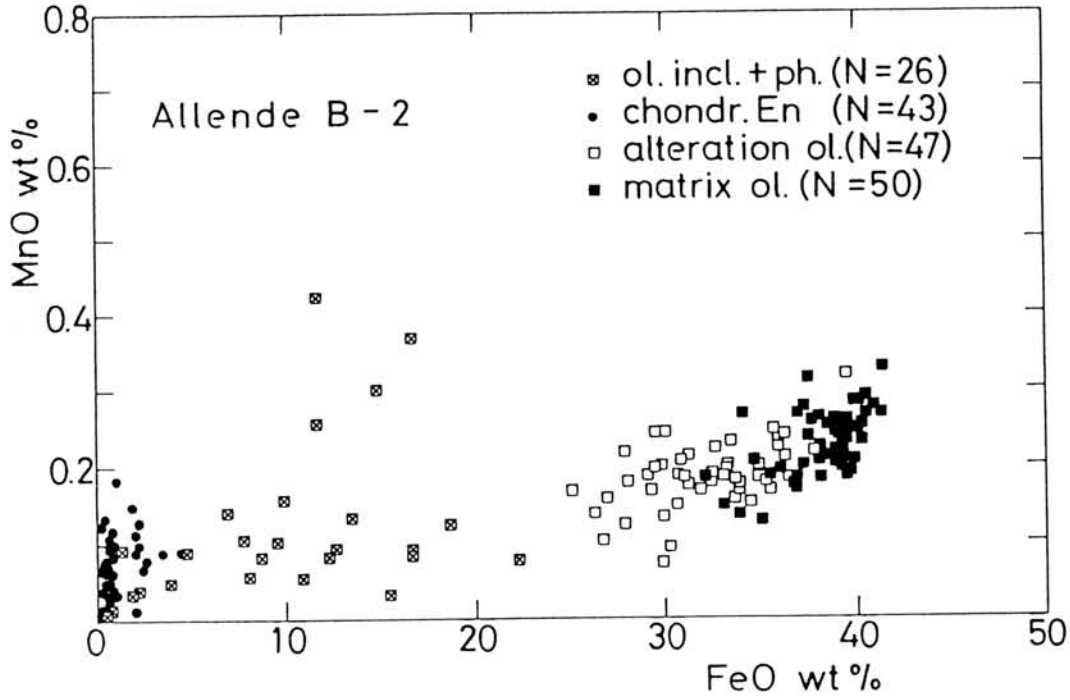

Figure 2. MnO vs. FeO variations in matrix olivine, alteration olivine, olivine phenocryst and inclusion, and enstatite phenocryst in Allende.

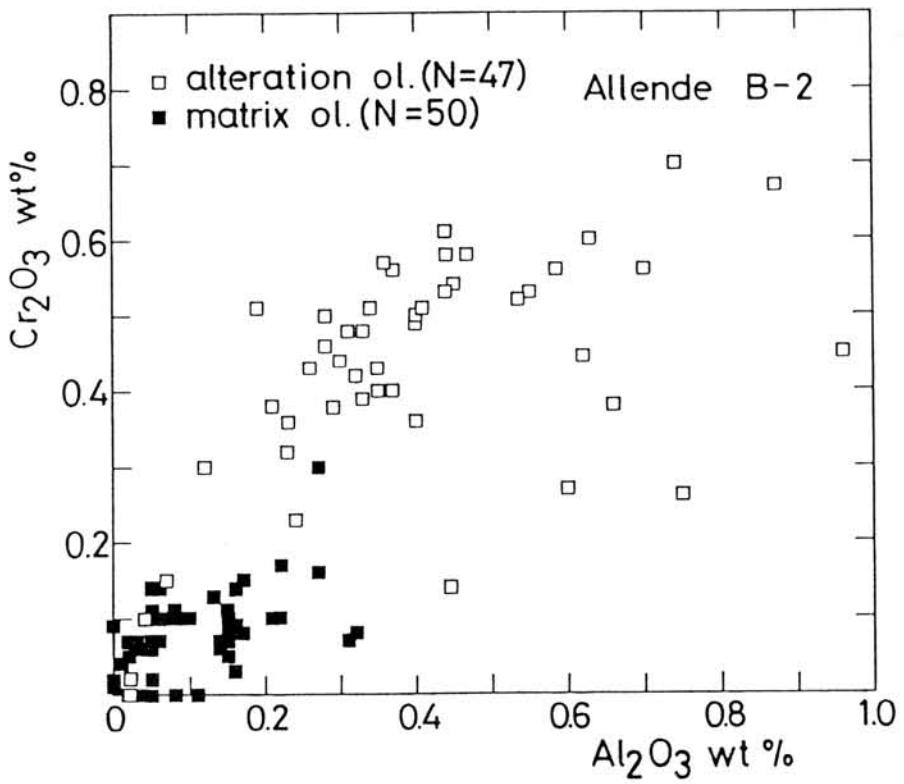

Figure 3. Al_2O_3 vs. Cr_2O_3 variations of matrix ferrous olivine and alteration olivine in Allende.

PETROLOGICAL STUDY ON EVOLUTION AND ALTERATION OF CM CHONDRITES

Hideyasu Kojima and Keizo Yanai
Department of Meteorites, National Institute of Polar Research
9-10, Kaga 1-chome, Itabashi-ku, Tokyo 173, Japan

Mighei group carbonaceous (CM) chondrites from Antarctica have been investigated petrologically in order to clarify their evolution and alteration process. The samples studied are 14 CM chondrites: Y-74642, Y-74662, Y-75293, ALH-77306, Y-790003, Y-790032, Y-790123, Y-791190, Y-791198, Y-791824, Y-7793321, B-7904, Y-82042, Y-86720.

Among 14 samples, well-developed concentric texture has been revealed in four samples; Y-74662, Y-791198, Y-791824, Y-82042. Chondrules, inclusions and their fragments occupied the core, with rims of several hundreds μm thick outside of the core, and with PCP (poorly characterized phase) along the outermost rim. The concentric texture was considered to be primary, because it has been rarely seen in brecciated CM chondrites formed through gardening on the parent body. Therefore it was thought that PCP situated outside of the rims had not been altered products derived from Fe-Ni metals and sulphides in chondrules, inclusions, their fragments and rims, however PCP had accreted on rims prior to parent body formation (Kojima and Yanai, 1989).

The CM chondrite had been altered in various degrees probably with in the parent body. Microscopic observations revealed the order of the alteration of chondrules as follow; the first stage alteration changed the fresh glass into phyllosilicates with high FeO contents, the second stage altered the phyllosilicates and low-Ca pyroxene into Fe-Mg serpentine, and the final stage altered olivine into Fe-Mg serpentine(Ikeda, 1983; Kojima et al, 1984).

PCP in the low-altered CM chondrites consist of tochilinite and cronstedtite in various proportions. On the other hand, PCP in the highly altered CM chondrites show chemical compositions between Fe-Mg serpentine and the mixture of 75% cronstedtite and 25% tochilinite.

The matrices of CM chondrites are classified into three groups as follows (Fig.1): Group A which are primitive matrix of CM chondrites, showing chemical compositions between B and C; group B composed mainly of Fe-rich phyllosilicate which have formed by gardening (brecciation); group C composed of Fe-Mg serpentine which have formed by aqueous alteration (Fig.1). These facts indicate two mode of chemical changes of the primitive matrix. One is Fe-increasing trend (group A group B) which is the result of mechanical mixture of primitive rim and cronstedtite by gardening on the surface of the parent body. The other is Fe-decreasing trend (group A group C) which is the result of progressive aqueous alteration in the parent body.

On the basis of the textures and alteration process mentioned above, the authors propose the evolution model of CM chondrites in early solar system as follow.

1. Formation of chondrules and inclusions.
2. Fragmentation of chondrules and inclusions.
3. Rim accretion on chondrules, inclusions and their fragments.
4. PCP accretion.
5. Ice accretion on the PCP layer.
6. Accretion and formation of CM parent body.
7. Aqueous alteration within the parent body.

References:
Kojima H. and Yanai Y. (1989): Meteoritics **24**, 288.
Ikeda Y. (1983): Mem. Natl Inst. Polar Res., Spec. Issue, **30**, 93-108.
Kojima H., Ikeda Y. and Yanai K. (1984): Mem. Natl Inst. Polar Res., Spec. Issue, **35**, 184-199.

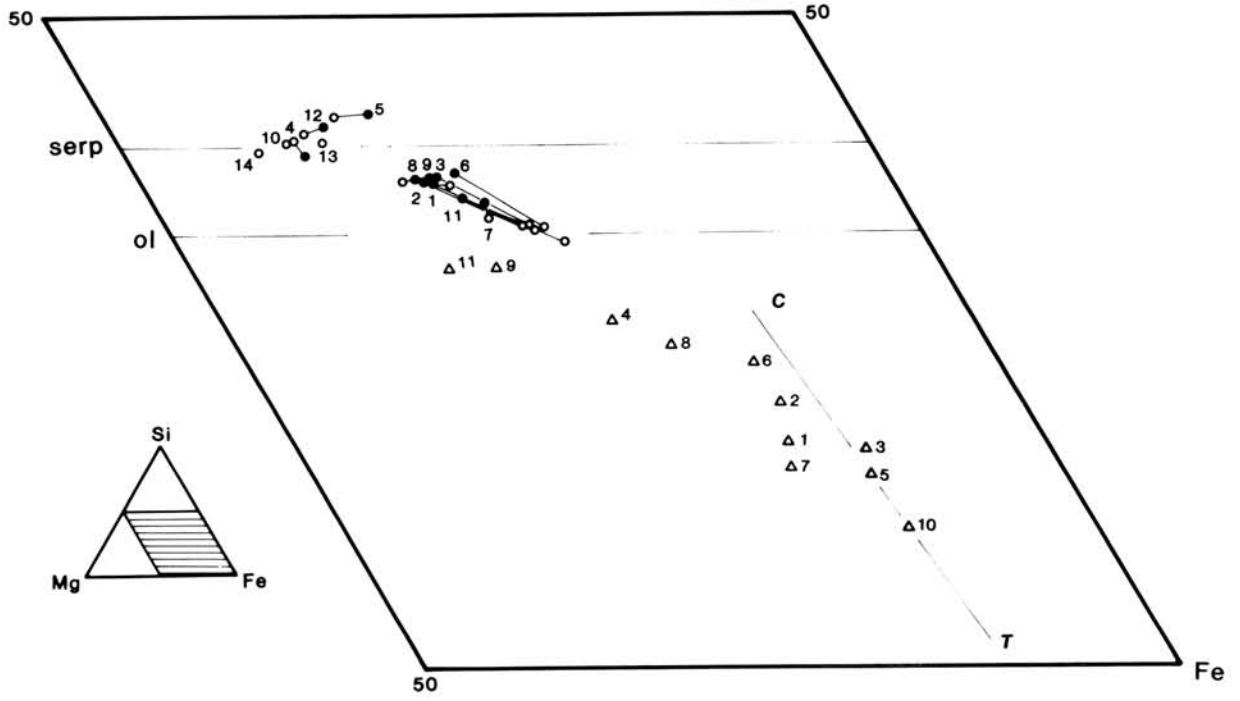

Fig.1: Average compositions of rims(●), matrices(O) and PCP(△).
T: tochilinite C: cronstedtite

DEFORMATION EFFECTS IN THE LEOVILLE CV CARBONACEOUS CHONDRITE

Tomoki Nakamura, Kazushige Tomeoka and Hiroshi Takeda

Mineralogical Institute, Faculty of Science, University of Tokyo, Hongo, Tokyo, 113

Leoville is a unique CV carbonaceous chondrite that shows foliation defined by alignment of elongated chondrules and inclusions with high aspect ratios. The texture is strongly suggestive of deformation. Leoville contains CM-chondrite-like clasts that display the same foliation as the Leoville host, indicating that the deformation took place after accretion [1]. However, whether the deformation resulted from shock-induced pressure or static compaction due to overburden remains inconclusive. We have studied mineralogy and petrology of chondrules and matrix in Leoville by using a petrographic microscope, a scanning electron microscope (SEM), an electron-probe microanalyzer (EPMA) and a transmission electron microscope (TEM). Our goals are to understand how the deformation of Leoville affected its texture and mineralogy and to find out what caused its deformation.

Chondrules in Leoville consist mostly of olivine, pyroxene, opaque minerals (kamacite, taenite and troilite) and mesostasis glass. Most chondrules are elongated with axial ratios from 1.4 to 2.7. There is an apparent tendency that chondrules containing larger amounts of opaque minerals have higher axial ratios. Olivine and pyroxene grains in chondrules show fine fractures in high density, when they are observed by an optical microscope; fracture domains range in size from 10 to 50 μm. Nearly 80 % of chondrules that we observed display wavy or mozaic extinction. Many large olivine grains show subparallel fractures with spacings of 10-30 μm in orientations oblique to the elongation axis of deformation.

Matrix in Leoville consists mainly of olivine (Fo40-55) and minor kamacite and troilite. Many kamacite and troilite grains are elongated along chondrules. TEM observations reveal that olivine grains in the matrix range in size from 1 to 3 μm and they are commonly subdivided into small domains ($\sim$0.1 μm in diameter). Amorphous material fills interstices of these domains. Most olivine grains show complex strain contrast and fine subparallel fractures with a spacing of $\sim$50 A.

Our study reveals that many olivine grains in Leoville chondrules show wavy or mozaic extinction and fine subparallel fractures. These textures are characteristic of shock-induced deformation. Reimold et. al.[4] conducted shock experiments of olivine and reported that fine planar fractures with a spacing of $\sim$50 μm were produced by shock pressures approximately 15-30 Gpa. Some olivine grains in different chondrules in Leoville display subparallel fractures in the same orientations oblique to the elongation axis of deformation, suggesting that those fractures were produced simultaneously after accretion. In addition, olivine grains in matrix show subparallel fractures similar to those in chondrule olivines, although the spacings between the fractures are much smaller.

Although more extensive observations as well as experimental studies

would be required to determine precisely the nature of deformation, our observations suggest that the deformation of Leoville resulted from shock-induced pressure rather than static compaction.

REFERENCES

[1] A. Kracher, K. Keil, G.W. Kallemeyn, J.T. Wasson, R.N. Clayton, and G.I. Huss (1985) Proc. Lunar Planet. Sci. Conf. 16th, in J. Geophys. Res., 90, D123-135.
[2] P.M. Cain, and H.Y. McSween (1984) Lunar Planet. Sci. XV,116-117.
[3] J.T. Wasson (1985) in Meteorites, 164-165 (Springer-Verlag).
[4] W.U. Reimold and D. Stoffler (1978) Proc. Lunar Planet. Sci. Conf. 9th, 2805-2824.

Relationship between grain size and chemical composition of augite in ordinary chondrites

T. Noguchi (Geological Institute, University of Tokyo, Hongo 7-3-1, Tokyo, Japan)

Petrographic variations among ordinary chondrites have been regarded as a scale of "metamorphism". Petrologic types as a scale for "metamorphism" was quantitatively assessed by compositional variation of pyroxenes and relationship between grain size and chemical composition of augite in 61 (24 H3-6, 31 L3-6, 6 LL3) chondrites.

Average and standard deviation of pyroxenes in chondrules exhibit large variation among petrologic types from 3 to 6 (e. g. Kitamura et al., 1986; Noguchi, 1987 and 1989), in contrast to the case of olivine. Standard deviation of pyroxenes is used as indicators of the compositional variation of pyroxene, two parameters are selected: parameter 1, standard deviation of Mg number of low-Ca pyroxenes or that of augite; parameter 2, standard deviation of Wo content of low-Ca pyroxenes or that of augite. The relationship between these two parameters in augite for investigated chondrites are plotted in Fig. 1. This figure shows that petrologic types are insufficient as a quantitative scale for "metamorphism". Petrologic types are often inconsistent with the heterogeneity of pyroxene composition within a same chemical group. In addition, heterogeneity of pyroxene composition in H chondrites are different from that in L chondrites with same petrologic types, the fact which is remarkable among H4 and L4 chondrites. Relationship between these parameters in low-Ca pyroxenes is similar to that of augite.

The data plotted in Fig. 1 are divided into two segments in terms of the distribution pattern. The first part shows that parameter 1 decrease remarkably but parameter 2 do not change. Type 3 and some L4 chondrites belong to this part. Although some of relatively "metamorphosed" type 3 and some L4 chondrites have pyroxenes as heterogeneous as the least "metamorphosed" type 3 chondrites, though heterogeneity of Mg value of olivine is different between these two sets. The second segment exhibits positive correlation between parameters 1 and 2. This correlation results from linear distributions of augite composition on pyroxene quadrilateral diagrams for chondrites in this segment.

As increasing petrologic types, matrices of chondrites become transparent and outline of chondrules become blurred. This textural change reflects on grain size of groundmass augite in chondrules. It can be used as a indicator of degree of recrystallization. Augite in chondrules shows basically the same occurrences among chondrites from type 3 to 6 and often occurs as rims on low-Ca pyroxenes and as a groundmass mineral in chondrules. Size of augite in both occurrences is related to the heterogeneity of pyroxene composition. Fig. 2 shows the relationship between parameter 2 of augite and average grain size of groundmass augite. Among chondrites of

the former part of Fig. 1, grain size and standard deviation of Wo content (parameter 2) do not change remarkably though standard deviations of Mg number of olivine and pyroxenes and even averages and standard deviations of minor elements such as Al in pyroxenes decrease. The size of augite of both occurrences increases conspicuously among chondrites of the second segment of Fig. 1 (chondrites with fairly homogeneous pyroxenes). It was observed that grain size of secondary feldspar also increases among those chondrites.

If various petrographic variations of ordinary chondrites formed by "metamorphism", Fig. 2 can be interpreted that augite composition changes its composition without remarkable increase of its grain size in weakly "metamorphosed" chondrites and that the growth rate of augite abruptly accerelated when standard deviation of Wo content in pyroxenes started to decrease. In those chondrites, minor elements such as Al in augite are also decrease and become homogeneous. This interpretation suggests that diffusion rate of Al as well as Ca in augite was fast enough to change augite composition and that diffusion rate of Ca in secondary feldspar was fast enough for the growth of augite because of sufficient residential time at high temperatures.

However, TEM studies of microstuctures of pigeonite (e. g. Ashworth and Barber, 1977; Watanabe et al., 1985) suggest that cooling rates, several ^{o}C/hr from 1100 to 800 ^{o}C. Exsolution lamellae is not observed in chondrites with homogeneous pyroxenes by SEM. Ashworth and Barber (1977) reported that exsolution lamellae was not observed by TEM. Nucleation of low-Ca pyroxene in augite, therefore, seems to have prohibited because of rapid cooling, which is inconsistent with the slow cooling inferred strongly "metamorphosed" on the basis of homogeneities of Ca and Al in chondrites. The variation of Al and Ca contents in augite in ordinary chondrites with various petrographic variations may have formed through difference in growth rate of augite from chondrule melt. In other words, thermal history from the time of chondrule formation may have played a role to determine composition and grain size of augite showing wide petrographic diversities.

References: Ashworth and Barber (1977): Philos. Trans. R. Soc. Lond., Ser. A286, 493-506; Kitamura et al. (1986): papers presented to the 11th symposium on antarctic meteorites, 71-73; Noguchi (1987): papers presented to the 12th symposium on antarctic meteorites, 48-50; Noguchi (1989): papers presented to the 14th symposium on anterctic meteorites, 54-55; Watanabe et al. (1985): Earth Planet. Sci. Lett., 72, 87-98.

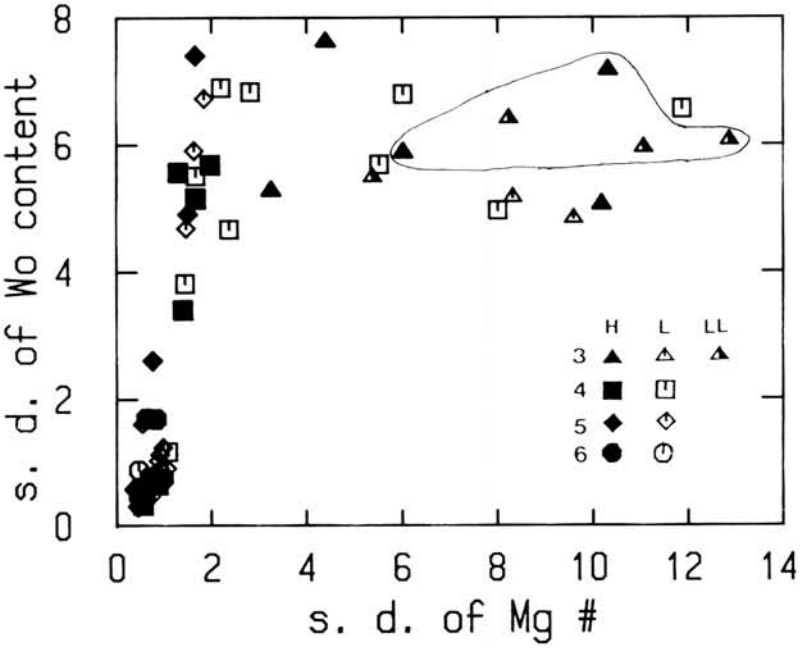

Fig. 1 Relationship between standard deviation of Mg number and standard deviation of Wo content in augite. The least metamorphosed ordinary chondrites (Semarkona, Krymka, Chainpur, Sharps and Tieschitz) are encircled.

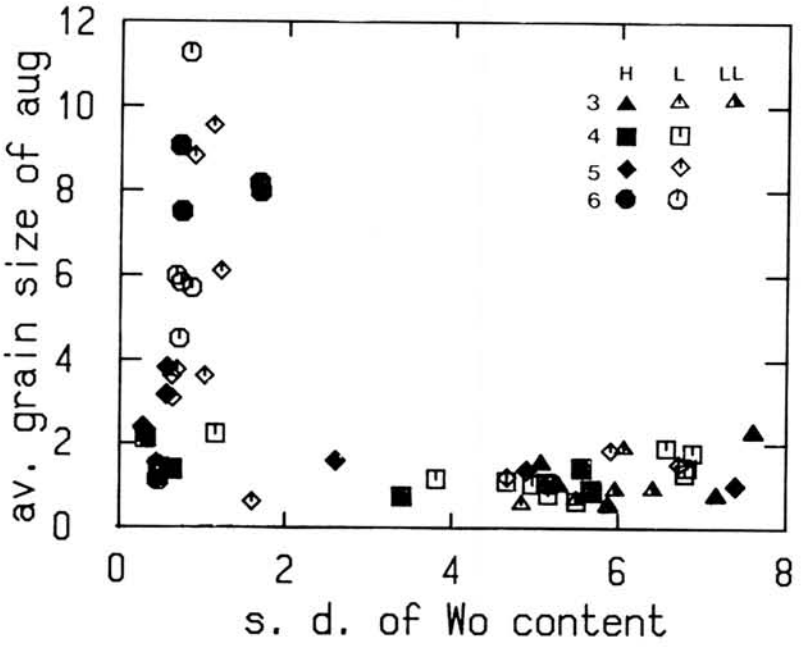

Fig. 2 Relationship between standard deviation of Wo content in augite and average grain size of groundmass augite in chondrules.

PREFERRED ORIENTATION OF OLIVINE CRYSTALS IN AN INCLUSION OF ALH-764(LL3)

Masao KITAMURA, Yasuhiro OKAMOTO and Seiko WATANABE
Department of Geology and Mineralogy, Faculty of Science, Kyoto University, Sakyo, Kyoto 606, Japan

A unique inclusion with preferred orientation of olivine crystals was found in ALH-764 (LL3). This inclusion (3mm x 2mm) has an equigranular texture, and consists mainly of olivine, orthopyroxene, augite and plagioclase (Fig. 1). The inclusion contains several veins of opaque mineral (probably graphite).

The constituent minerals in the inclusion are not homogeneous and show chemical zonings in back-scattered electron images. Olivine has the compositional range from Fo_{95} (core) to Fo_{93} (rim). Orthopyroxene is heterogeneous in a back-scattered electron image, but no significant compositional changes around $En_{93}Fs_4Wo_3$ were detected by EDX analysis. The composition of cores of augite is $En_{56}Fs_3Wo_{41}$ and that of rims around $En_{55}Fs_3Wo_{42}$. Plagioclase is also heterogeneous and has the compositional range of Ab_{100} to $Ab_{80}An_{20}$.

These compositional change from cores to rims of crystals suggests that the inclusion is a fragment of a slowly cooled igneous rock. The temperature estimated from the composition of rims of orthopyroxene and augite is about 1100°C.

This mineral assemblage and mineral compositions of the inclusion is rather similar to, but essentially different from those of achondrites such as ureilites and "lodranite".

A petrofabric analysis of olivine grains in the inclusion was carried out. The fabric of the olivines is characterized by a strong maximum of Z(a) axes and girdles of X(b) axes (Figs. 2a, b, and c). Orientation of Y(c) axes is relatively random.

Concentrations of Y(c) axes were observed in ureilite (e.g., Berkley et al., 1980) and "lodranite" (Nagahara and Ozawa, 1986). On the other hand, the present type of petrofabric of olivine crystals is common in terrestrial rocks, but is first found in chondrites.

Preferred orientation of olivine crystals was not observed in chondrules of this chondrite. Therefore, the petrofabric of the inclusion must be formed by deformation before the chondrule formation of ALH-764. Even if the inclusion suffered partial melting during the chondrule formation, degree of partial melting should be small enough to maintain the petrofabric of olivine crystals. It is not clear whether the fabric was formed by shock or static deformation. However, since the characteristic wavy extinction of olivine by shock deformation was not observed in the inclusion, the static deformation in a parent body of the inclusion is preferred.

Characteristics of the inclusion suggest that the inclusion was formed in its parent body or the grand parent body of the

chondrite, and that some parts of the body must be differentiated by an igneous process, deformed and then brecciated before the accretion of ALH-764.

References

Berkley,J.L., Taylor,G.J. and Keil,K. (1980) Geochim. Cosmochim. Acta, 44, 1579-1597.

Nagahara,H. and Ozawa,K. (1986) Proc. 10th Symp. Antarc. Meteo. 181-205.

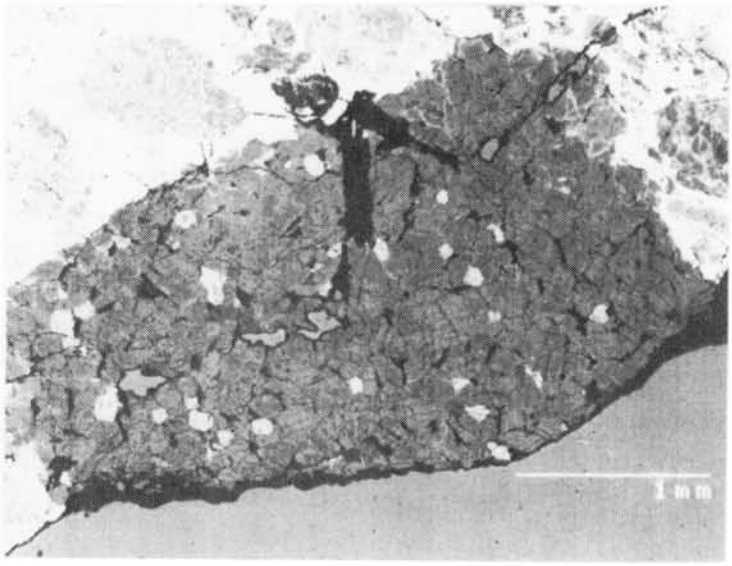

Figure 1. Back-scattered electronimageofan inclusion of ALH-764(LL3).

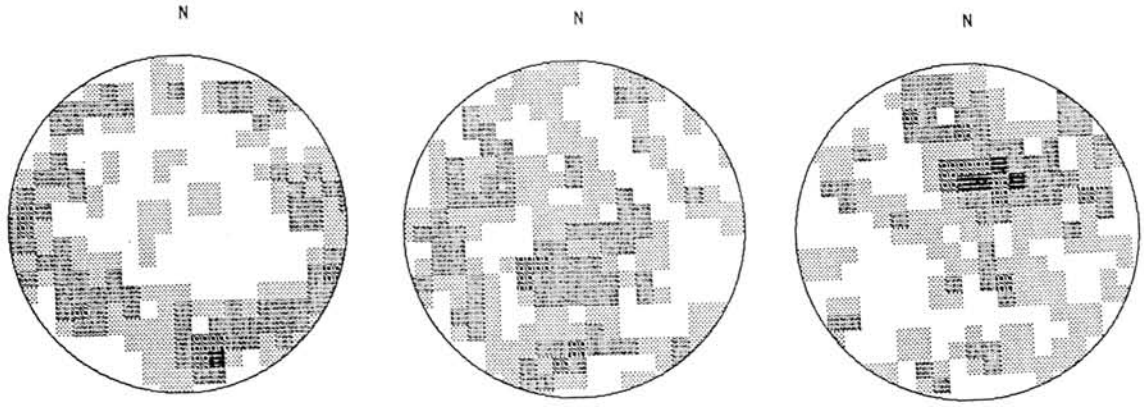

Figure 2. Equal-area projection of olivine indicatrix axes. Measurements on 100 grains.

COMET-LIKE GRAND PARENT BODY OF CHONDRITES

Masao KITAMURA and Akira TSUCHIYAMA*
Department of Geology and Petrology, Faculty of Science, Kyoto University, Sakyo, Kyoto 606, Japan
* present address : Collage of General Education, Osaka University, Machikaneya, Toyonaka 560, Japan

Shock origin of ordinary chondrites has been suggested by the facts that relict minerals in chondrules have high dislocation density (Kitamura and Watanabe, 1989), and that shock melt and fine grained aggregates produced by shock melting experiments of porous starting materials have similar compositional variation to natural chondrules and fine grained aggregates (Kitamura et al., 1989). Constituent minerals in matrix in chondrites were explained to be fine fragments and condensates from vapor produced by the shock event.

These facts indicate that precursor materials formed porous grand parent bodies. In the present study, a possible model of the porous grand parent body will be presented.

Following four conditions which are related with the shock origin were considered here.

1) When a solid rock was shocked and brecciated, the brecciated fragments should have a wide variation in size. On the other hand, the constituents of chondrites such as chondrules do not show such a wide variation. This suggests that shock wave in the grand-parent body propagated rather homogeneously in a wide range, like in a case of vapor explosion. Then, the grand parent body should consist of a mixture of highly volatile solids, silicates, metal, sulfides and others.

2) The shock experiments show that starting materials should be more porous than a chondrite to produce abundant shock melt. Thus, the grand parent body should be more "porous" than chondrites or the parent body. However, when a body is reconstructed by shock event and the following accretion, its porosity should decrease in general. This discrepancy can be solved if the grand parent body consists of a mixture of highly volatile solids (e.g. ice), silicates and others, because the highly volatile solids can act as "pores" during the shock deformation.

3) Mg numbers of silicates in chondrules are different from those in matrix. This difference can be explained as that oxygen fugacity in the formation of matrix minerals was controlled by vapor produced by the shock event from the highly volatile solids in the grand parent body.

4) Chondrites generally have no melt pockets by shock events, indicating no significant shock events after the formation of chondrites. However, probability of collision of small planets to the body should not change significantly before and after the formation of chondrites. Therefore, the shock event of the chondrite formation must occur only once under

specific conditions which are characteristic not of the parent body but of the grand parent body. These conditions are considered to be (1) the grand parent body contains highly volatile solids, and (2) large amount of vapor produced by the shock event from the solids escapes before the accretion.

As described above, when the grand parent body contains highly volatile solids (e.g. H_2O and CO_2), the characteristics of chondrites can be explained well. A simple calculation shows that when two bodies composed of H_2O ice collide head-on with each other with a speed of 10^4m/sec, most of the ice can evaporate. This calculation supports the above discussions.

In conclusion, we suggest that the grand parent body contained highly volatile solids, and then was a comet-like.

References

Kitamura,M. and Watanabe,S. (1989) 14th Symposium on Antarctic meteorites (abstract) pp.73-74

Kitamura,M., Tsuchiyama,A., Watanabe,S., Syono,Y. and Fukuoka,K. (1989) 14the Symposium on Antarctic meteorites (abstract) pp.75-77

AN EXPERIMENTAL STUDY ON THE REACTION KINETICS OF FORSTERITE-SiO GAS

Imae, N.[1] and Tsuchiyama, A.[2]

[1] Department of Geology and Mineralogy, Faculty of Science, Kyoto University, Kyoto 606, JAPAN

[2] Department of Earth and Planetary Sciences, College of General Education, Osaka University, Toyonaka 560, JAPAN

According to the equilibrium condensation theory [1] which is based on chemical equilibrium calculations, forsterite reacts with Si-rich gas to form enstatite. This reaction is very important when we think fractionations of Mg/Si in the solar nebula because Mg and Si are the most abundant refractory elements in the solar system. In the present study, experiments on the forsterite-gas reaction were carried out to investigate kinetics of the reaction, such as reaction rates and textures including effects of crystallographic orientation. Furthermore, we applied the results to the reaction in the primordial solar nebula.

A "double capsule method" was newly designed for the present experiments. Figure 1 shows the assembly of a experimental charge, in which inner and outer capsules of molybdenum are used. In the inner capsule, a single crystal of synthetic forsterite ($5 \times 1.25 \times 1 mm^3$ along a, b, and c, axis, respectively) is placed. The powders of cristobalite (SiO_2) are filled in the outer capsule. The capsules are heated in a vacuum furnace at about 3×10^{-5} Torr. During the heating Si-rich gas in equilibrium with crystobalite (mainly SiO, O_2) will be formed inside of the outer capsule because the outer capsule behaves as a Knudsen cell (the diameter of the orifice is 0.1mm). Enstatite will be formed by the reaction between the forsterite crystal and the Si-rich gas.

The experiments were carried out at temperatures ranging from 1450°C to 1610°C and for durations ranging from 5 to 100 hrs. The temperature was measured by a $W_{95}Re_5$-$W_{74}Re_{26}$ placed near the capsule. Run products were mounted in an epoxy, and polished thin sections were made. They were observed with an optical microscope (OM) and a scanning electron microscope (SEM).

In the experiments, a layer of enstatite surrounding the forsterite crystal was formed (Fig. 2) except for a run at 1610°C. The width of enstatite is almost constant in a single run (about a few - a few tens μm) irrespective of the crystallograptic orientation. Polysynthetic twins were observed in the enstatite layer. This shows that protoenstatite was formed at high temperatures during the experiments, and transformed to clinoenstatite during cooling. Observation of the charges under OM and a back Laue photograph of a charge show that a single crystal of protoenstatite was not formed, but a small number of the crystals were formed with preferred orientation on the forsterite substrata. In a run at 1610°C, the charge was melted probably due to melting of enstatite. The melting was

not observed in runs at 1575°C although the melting point of enstatite is 1557°C. This is probably because the temperature of the thermocouple was higher than the temperature in the capsule. The calibration of the temperature was not done.

The width of the enstatite layer increases with increasing the temperature or run duration. It was found that the square of the width, x^2, is proportional to time, t, at a constant temperature (Fig 3);

$$x^2 = kt,$$

where k is the reaction rate. This x-t relation strongly suggests that the reaction is controlled by diffusion in elements in the enstatite layer. Arrhenius plot of the reaction rate, k (Fig. 4) shows that the activation energy and pre-exponent term of k, are about 100.2 kcal/mol and 2.6 cm^2/sec, respectively although the data are scattered to some extent. The value of the activation energy is not inconsistent with activation energies of the diffusion (usually 30 kcal/mol) because the partial pressures of SiO and O_2 are changed with the temperature.

The reaction rate and its activation energy obtained in the present experiments were applied to the reaction in the solar nebula. Hasegawa [2] theoretically estimated the final width of the reaction layer, d, in a cooled nebula, as follows;

$$d^2 = k(Te)(RTe/E)\tau_{cool}$$

where Te is the equiliblium temperature of enstatite, about 1375K [1], R is the gas constant, E is the activation erergy of the reactoin rate, and τ_{cool} is the cooling time scale of the nebula [3]. The values of k in this case should be smaller than those obtained in the experiments, because the partial pressure of SiO in the nebula was smaller than that in the experiments, where the gas is in equiliblium with cristobalite. Accordingly, if the values obtained in the experiments are used in the equation, the values of d are overestimated. Thus, the maximum value of d is roughly estimated to be about 5.0×10^{-2} Å - 5.0×10^{-3} Å for typical values of, τ_{cool}, 10^8-10^{10} sec. This result indicates that the reaction that forsterite reacts with SiO gas to form enstatite would not occur, but a maximum fractionation would take place during cooling in the solar nebula.

References:

[1] Grossman, L., and Larimer, J. W. (1974) Rev. Geophys. Space Phys.,**12**, pp71-101,

[2] Hasegawa, H., (1984) in 'Modern Solar Sciences', eds. H. Hasegawa and T. Obayashi (in Japanese), pp17-47.

[3] Yamamoto, T., and Hasegawa, H. (1977) Prog. Theor. Phys., **58**, pp816-828,

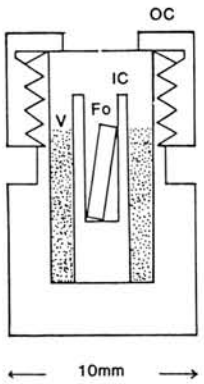

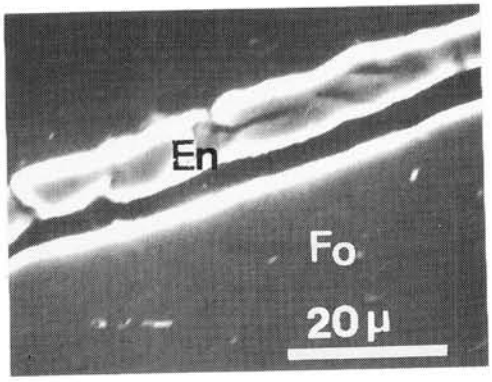

Fig. 1 An assembly of a charge of a 'double capsule method'.
OC: outer capsule (Mo), IC: inner capsule (Mo),
Fo: sigle crystal of forsterite,
V: vapour source (cristobalite powder),

Fig. 2 A layer of enstatite(En) formed by the reaction between forsterite(Fo) and Si-rich gas at 1575°C and for 21hrs (SEM image).

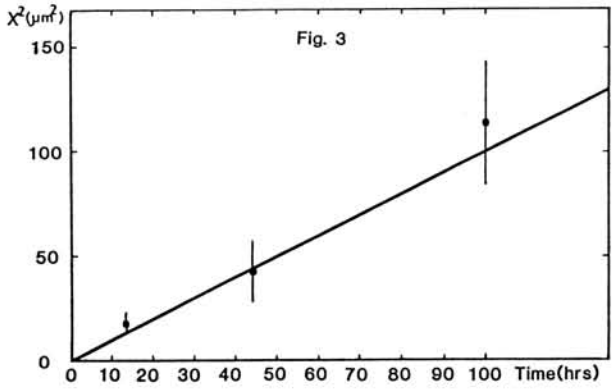

Fig. 3 A relation between time and the square of the width of the enstatite layer, x^2 at 1575°C.

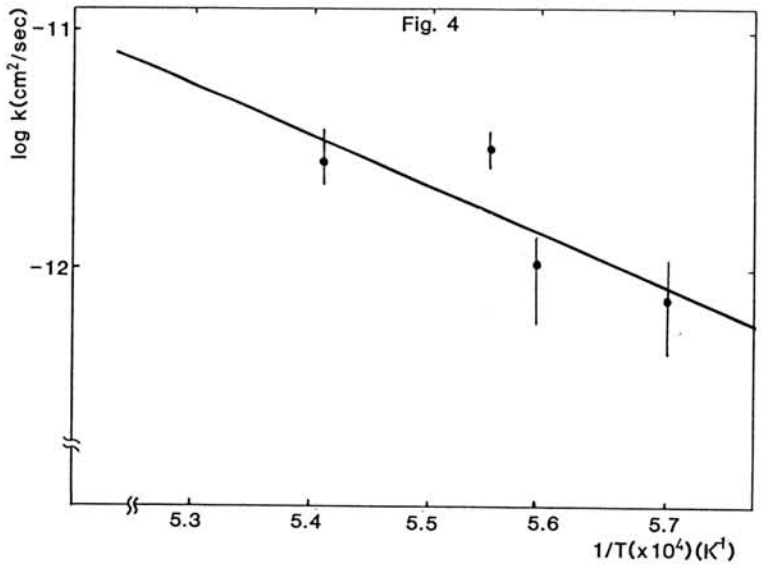

Fig.4 Arrhenius plot of the reaction rate, k.

Fo-En-GAS EQUILIBRIUM AND Mg/Si RATIOS OF CHONDRITIC METEORITES.

Tsuchiyama, A.
Dept. Earth and Planet. Sci., Coll. General Education,
Osaka University, Toyonaka, Osaka 560, JAPAN.

Si and Mg are the most abundant refractory elements which construct silicates in the primary solar nebula. In the present paper, fractionation of Mg/Si are discussed by considering equilibria between Mg-Si minerals and gas. Based on the results, the Mg/Si ratios of meteorites are discussed.

When we consider forsterite-enstatite-gas equilibrium as an example, the following equation can be written;

$$2Mg_2SiO_4(s) + SiO(g) \rightleftharpoons 3MgSiO_3(s) + Mg(g).$$

The equilibrium constant of the above equation, K, is as follows;

$$K = a_{En}^3 p_{Mg} / a_{Fo}^2 p_{SiO} = p_{Mg}/p_{SiO},$$

where a_{En} and a_{Fo} are activities of enstatite and forsterite, respectively, and p_{Mg} and p_{SiO} are partial pressures of the Mg and SiO molecules, respectively.

If gas species of Mg and Si are exclusively Mg and SiO molecules, respectively, the p_{Mg}/p_{SiO} ratio is equal to the Mg/Si ratio of the gas. This condition is almost held in high temperature gas with the cosmic abundance. In this case, the Mg/Si ratio of gas in equilibrium with forsterite-enstatite is determined by the equilibrium constant alone, and independent from other gas species (*e.g.*, O_2 or H_2O), total pressure and concentrations (*e.g.*, Si/H). In other words, the ratio is determined only by temperature. In similar ways, the Mg/Si ratios of gas in equilibrium with periclase-forsterite and enstatite-silica can be determined as a function of temperature (Fig.1) Figure 1 can be regarded as a phase diagram, and is verified by condensation experiments from gas with Mg/Si=2 [1] and Mg/Si<1 [2]. It should be noted that the condensation temperature depends on other gas species, total pressure and concentrations.

Changes of the Mg/Si ratios of gas and solid(s) during condensation and vaporization of a material with the cosmic abundance are obtained by using the phase diagram (Figs.2-4). In the case of equilibrium condensation (or vaporization), forsterite condenses first at normal pressures ($p_{tot}=10^{-3}$-10^{-5} bar) (c in Fig.2) and is followed by enstatite (d). At low pressures (p_{tot} is at least less than 10^{-7} bar), enstatite is a primary phase (a), and followed by forsterite (b). Reaction experiments of forsterite and Si-rich gas prefer the fractional condensation rather than equilibrium condensation in the nebula [3]. In this case, gas passes through the reaction line of the forsterite-enstatite boundary (d in Fig.3) and reaches the enstatite-silica boundary (e). In the case of fractional vaporization, rapid or moderate heating produces similar path to the equilibrium one (f,g to h in Fig.4), while very slow heating produces enstatite residue (b-c).

The Mg/Si ratios of some chondrites [4], Halley's Comet

dusts [5] and Earth [6] are also shown in the phase diagram (Figs.1-4). The fractionation paths of the Mg/Si ratios by the condensation and vaporization indicate that condensation at low pressures cannot explain Si-rich materials, Earth of [6] contains a solid fraction, and the chondrites and Halley's Comet dusts contain gas fractions if the Mg/Si ratios of these materials were determined by separation of solid and gas in the nebula.

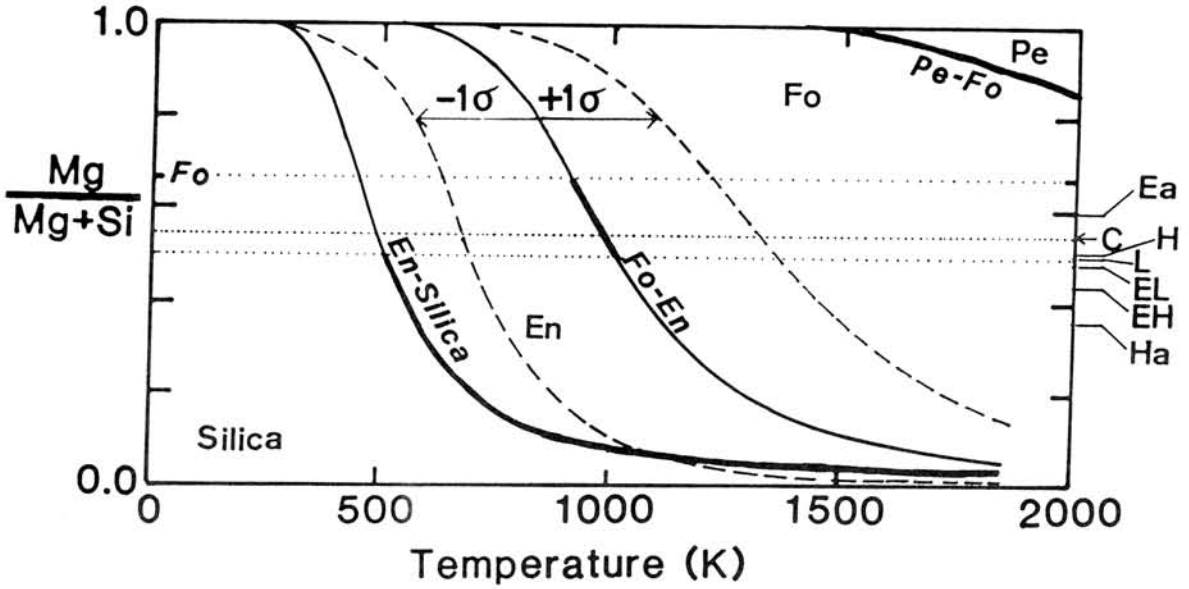

Figure 1. A phase diagram showing periclase (Pe), forsterite (Fo), enstatite (En) and silica fields. Bold lines are cotectic lines (others are reaction lines). Errors of the Fo-En boundary are shown as dashed lines. The Mg/(Mg+Si) ratios of Earth (Ea), Cosmic abundance (C), H- (H), L- and LL-(L), EL- (EL) and EH-chondrites (EH), and Halley's Comet dusts (Ha) are also shown.

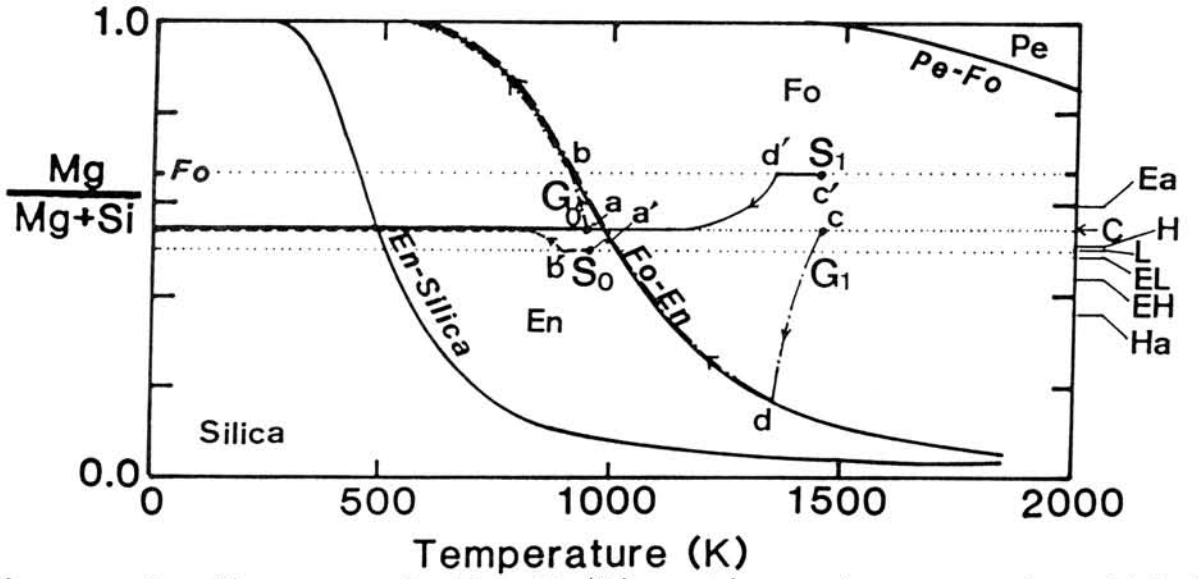

Figure. 2. Changes of the Mg/Si ratios of gas and solid by equilibrium condensation. At low pressures (at least less than 10^{-7}bar) gas changes from a to b while solid from a' to b'. At normal pressures (10^{-3}-10^{-5}bar) gas changes form c to d while solid c' to d'.

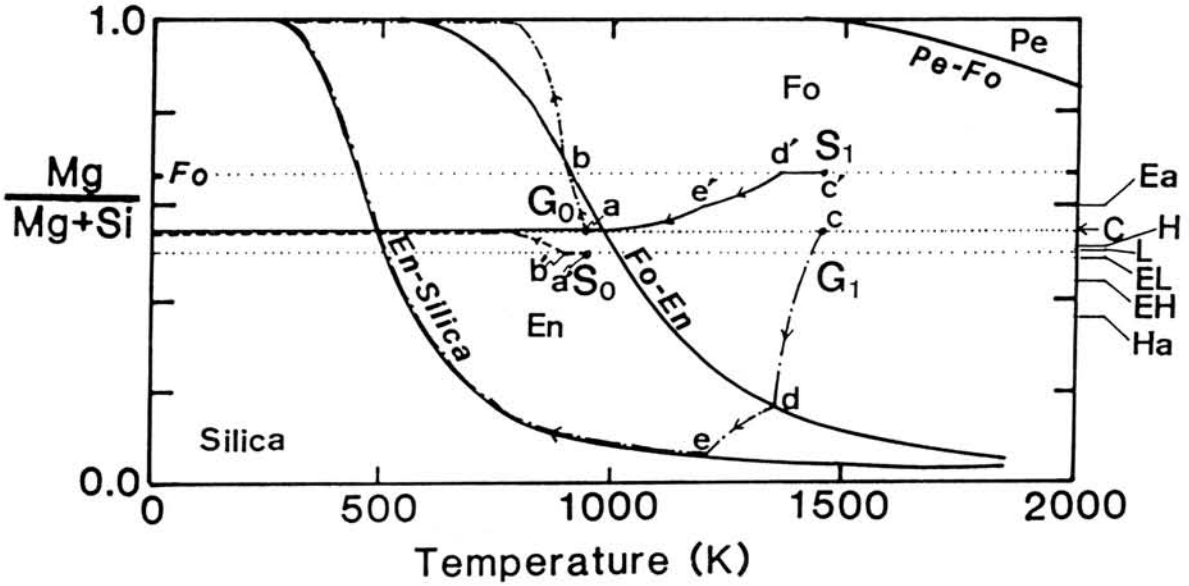

Figure. 3. Changes of the Mg/Si ratios of gas and average solid by fractional condensation. At low pressures (at least less than 10^{-7}bar) gas changes from a to b while solid from a' to b'. At normal pressures (10^{-3}-10^{-5}bar) gas changes form c to e while solid c' to e'.

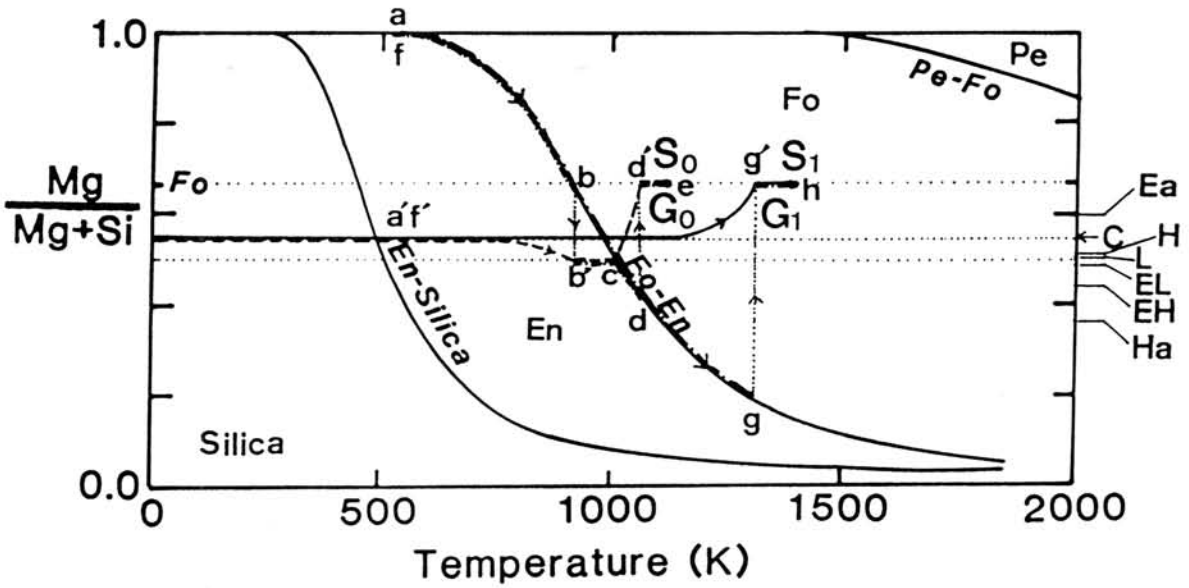

Figure. 4. Changes of the Mg/Si ratios of gas and solid by fractional vaporization. By very slow heating solid changes along a'-b'-c-d'-e while gas a-b-b'-c-d-d'-e. By moderate or rapid heating solid changes along f'-g'-h while gas f-g-g'-h.

References: [1] Tsuchiyama (1989) *Lunar Planet. Sci.*, **XX**, 1136. [2] Tsuchiyama *et al.* (1988) *Proc. NIPR Symp. Antarc. Met.*, **1**, 185. [3] Imae & Tsuchiyama (1990) this volume. [4] Wasson & Kallemeyn (1988) *Phil. Trans. R. Soc. Lond.*, A**325**, 535. [5] Anders & Grevesse (1989) *Geochim. Cosmochim. Acta*, **53**, 197. [6] Sun (1982) *Geochim. Cosmochim. Acta*, **46**, 179.

MINERALOGICAL DIRECT EVIDENCES OF IMPACT FROM SHOCKED QUARTZ GRAINS IN K/T BOUNDARY

[1]Yasunori MIURA, [1]Masashi IMAI, [2]Walter ALVARETZ AND [3]Glen IZETT.

[1] Dept.Min. Sci. & Geol., Yamaguchi University, Yamaguchi, 753 Japan.
[2] Dept. Geol. & Geophysics, Univ. California at Berkeley, Berkeley, California, 94720, U.S.A.
[3] U.S. Geological Survey, Denver, Colorado, 80225, U.S.A.

1. Introduction

The Cretaceous-Tertiary (K/T) boundary samples have been discussed from archaeological, mineralogical and geochemical data by many scientists [cf.1-7]. Quartz minerals show shocked texture and wide pressure-dependent region (~30kbar) in the low-temperature quartz [8].

The purpose of the present study is to present the direct evidence of impact shocked data of shocked quartz grains with multiple lamelle from K-T boundary sample of Clear Creek North (CCN), Colorado, U.S.A. [7], compared with those of the Barringer meteorite crater and five terrestrial metamorphic, volcanic and plutonic rocks, tectonic complex, and acid-rain experimental data [9,10].

2. Identification of CCN quartz grains

From cell-parameters (as hexagonal-cell), calculated density and shocked lamelle, the CCN quartz grains are classified as follows (Table 1 and Fig. 1 [9,10]):

(1) Type Q:
Quartz grains (20%) are similar to standard quartz crystals which are obtained from Gifu rock-crystal and Yamaguchi granite.

(2) Type I:
Metamorphic type quartz grains (ca. 20%) are similar to the those of Sangun pressure-type metamorphic quartz. This type quartz includes almost all K/T boundary quartz samples from Italy, Japan, Denmark, Austria and Tunisia of sea-sedimental samples.

(3) Type II:
Direct impact type quartz grains (ca.20%) showing typical multiple shocked lamellae are the same as those of the Barringer meteorite crater with higher density. This is the direct evidence of impact metamorphism in the K/T boundary phenomena, though the type II quartz has been observed only in large single quartz grains of the CCN-type sedimental sample.

(4) Type III:
Low-shocked quartz grains (ca.40%) with a few sets of lamellae are easily obtained and similar to those of Nagato tectonic orthogneiss, Rhyoke metamorphic schist, Kanmon rhyolitic tuff, Manicouagan impact melt rock and acid-rain experimental samples.

Table 1. Classification of the CCN quartz grain data [9,10].

Type	a	c	ρ	P/T	Major Example	Sample No.	Shocked lamellae	Rock type
Q	-	-	-	-	Standard Q	Q1,Q3	No	Rock Crystal
I	↓	↑	↑	P	Metamorphic (Pressure)	Q2,Q4	(irreg.)	Met.quartz. High P meta.
II	↓	↓	↑	P	Barringer Crater	SQ2,SQ20	Multiple	Shocked quartz
III	↑	↓	↓	T	Acid rain (Tectonic)	SQ21,22 SQ1,12	A few sets	Quartzite Sed.,Melt, Plutonic
IV	↑	↑	↑	P	(Acid rain)	--	(irreg.)	Melt, Sed.

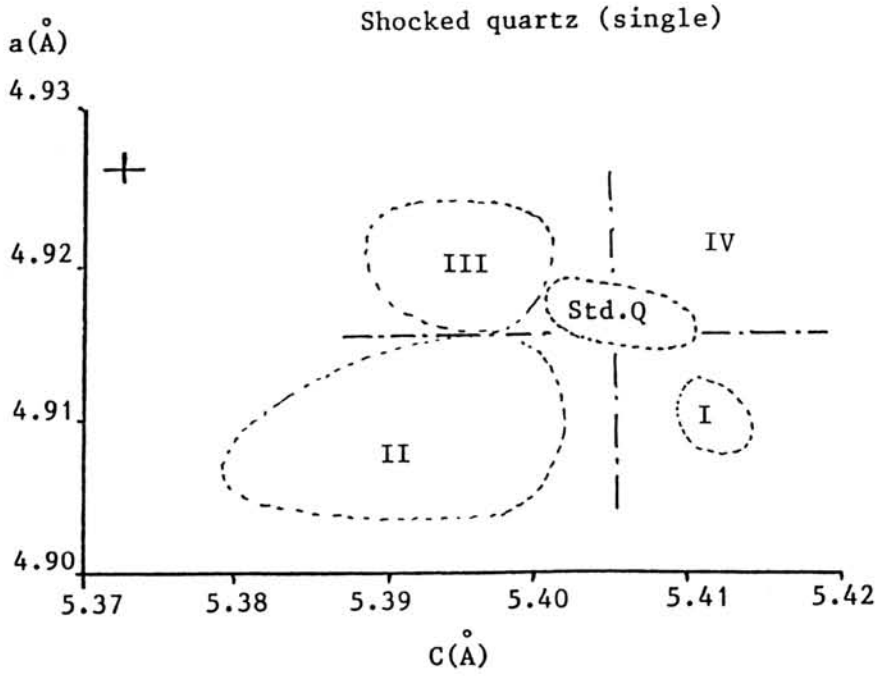

Fig. 1. Types 1 to IV quartz (cf. Table 1) from various type samples including the CCN shocked quartz grains in a and c axes of quartz (as in hexagonal cell).

(5) Type IV:
Unique high-pressure type quartz which is similar to some of Abu rhyolites, Manicouagan impact melt rock, and acid-rain samples could not be, however, obtained in the CCN-type quartz grain.

3. Formation processes of the CCN K-T boundary samples

The CCN K-T boundary quartz samples condidered to be mixed with various types of geological and impact processes as follows:

(1) K/T boundary samples of Western North America contain
unshocked quartz (ca.45%),
shocked quartz (ca.30%),
chert(ca.28%),
feldspar (ca.4%) and
chalcedony (ca.3%).

(2) Quartz crystal grains obtained in this study are classified as
unshocked normal quartz (type Q, ca .20%),
high-pressure type shocked quartz (type I, ca. 20%),
Barringer impact crater type shocked quartz with multiple lamellae (type II, ca. 20%),
tectonic type shocked quartz (type III, ca. 40%).

Therefore, it is found in this study that type II shocked quartz grains of Clear Creek North, Colorado, U.S.A. are surely the direct evidence of meteoritic impact process which could not explained by normal terrestrial geologic (i.e. volcanic and tectonic) processes.

But, even in the large shocked quartz grains of the CCN K/T boudary sample, the major quartz grains (ca. 80%) have relict data of normal terretrial geologic processes (including acid-rain type events), which have been produced various interpretations of the K/T boundary problem. In discussion of the K/T boundary problem, it is important to identify the types (Q, or I to IV) of quartz samples before final interpretation and conclusion.

References:

[1]Alvarez L. W. et al. (1980): Science, 208, 1095-1107.
[2]Bohor B. F. et al. (1986): Science, 224, 867-869.
[3]Miura Y.(1986): LPSC XVII, 555-556.
[4]Miura Y. et al.(1988): Global Catastrophes in Earth History, 124-125.
[5]Johnson, K.R. and Hickey L.J. (1988): Ibid, LPI Contrib. No.673, 87.
[6]Miura Y.(1989): 52th Meteoritical Soc.(Vienna), 163.(in Meteoritics).
[7]Izett, G. (1985): EOS, 66, 1149-1150; (1989): GSA Special Paper, 249.
[8]Mason B. and Moore C.(1982): Principles of Geochemistry, 4th Ed., 97.
[9]Miura Y. (1990): LPSC XXI (NASA-LPI),793-794.
[10]Miura Y. (1990): International Mineral. Asocciation (in press).

PIXE ANALYSIS OF MAGNETIC SPHERULES IN THE PALEOZOIC-MESOZOIC BEDDED CHERT

MIONO,S.[1], ONO,H.[1], NAKANISHI,A.[2], NAKAYAMA,Y.[3], SHOJI,M.[3]

1. Department of Physics, Osaka City university, Osaka 558
2. Shiga University of Medical Science, Shiga 520-21
3. Department of Physics, Ritsumeikan University, Kyoto 603

Particle Induced X-ray Emission (abbreviated PIXE) method is very useful elemental analysis of small specimens due to its high sensitivity.

In This report, magnetic spherules (about 100 μm in diameter) collected from the Paleozoic-Mesozoic bedded chert and magnetic components in meteorites and terrestrial materials were analyzed by this method. From the result obtained, comparing ratios Ti/Fe with Cr/Fe, terrestrial and extraterrestrial materials are differentiated clearly. And the spherules are grouped into the extraterrestrial part.

In order to measure such very small specimens as the spherules, a background must be decreased as possible. Since a charge up of backing materials makes the background increase, the backing should better be small and must have an electrical conduction. Therefore a carbon fiber is suitable for the backing.

Reference : H. Ohashi, et.al. Pro. 12. Int. Symposium of Hosei University Aplications Ion Beams in Materials Science

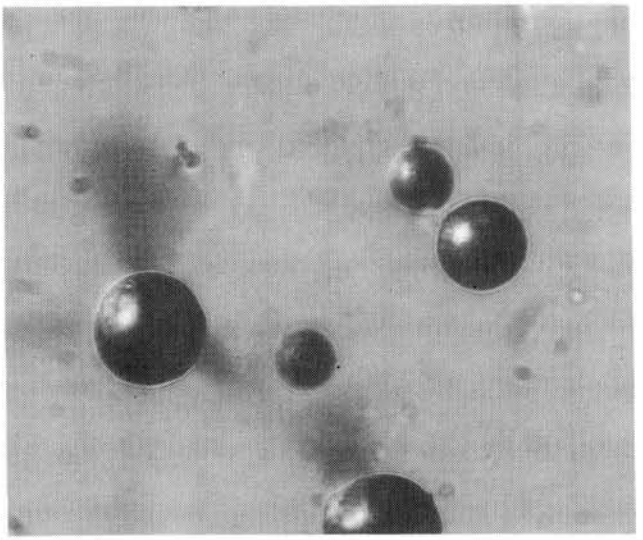

Fig 1 : The spherules in the Paleozoic-Mesozoic bedded chert.

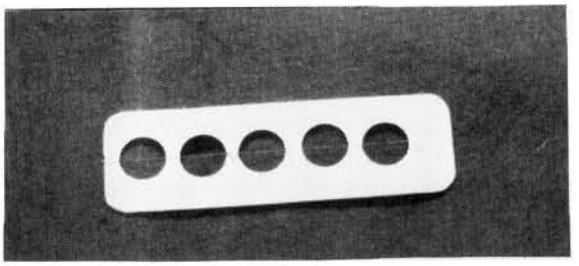

Fig 2 : The carbon fiber backing. Samples are fixed on it by collodion.

MAGNETIC MICROSPHERULES IN PERMIAN AND TRIASSIC BEDDED CHERT IN SOUTHWEST JAPAN

Iwahashi, J.[1], Yoshida, M.[2] and Miono, S.[2]
1: Geographical Survey Institute, Ministry of Construction, Tsukuba 305
2: Faculty of Science, Osaka City University, Osaka 558

A total of 810 magnetic microspherules including some semi-spherical graines was collected from 8 beds of the Permian and Triassic bedded chert in the Mino Belt, Southwest Japan. Through the collection procedure of the spherules from a group of specimens of a chert bed, almost all spherules which had been included in the specimen are considered to have been collected. The age of the sedimentation of the chert bed were determined by examining the radiorarian fossils following Yao et al.(1980, Jour. Geosci., Osaka City Univ., Vol. 23) and some other published works.

The surface structure of the spherules were observed under the electron scanning microscope. They are various, and are grouped into five types: geometrical mosaic, random mosaic, dendritic, scaly, and cracked. Trangitional type among some of these types are not rare, suggesting the gradational relationship among them, leading to an estimation that the variety of surface structure reflects the mode of the rapid quenching from an ironic liquidus hot pellet.

The size (diameter) of the spherules collected from each bed range from about 5 - 50 micrometers with a peak of 10 - 20 micrometers (an example is shown in Fig. 1), and $\log_{10}N$ (their numbers) are proportional to about -2.8logD (their diameter) for spherules larger than 10 - 20 micrometers. The chemical composition of 39 spherules was analysed mostly on the cross section using the electron microprobe analyser, resulting in the understanding that almost all the spherules are magnetite. The average chemical composition of 17 spherules , every spherule having the sum of all oxides amounting over 80%, is as follows . FeO:86.29%, SiO_2:0.57%, MnO:0.50%, Cr_2O_3:0.25%, Al_2O_3:0.17%, CaO:0.07%, NiO :0.05%, P_2O_5:0.05%, Na_2O:0.02%, K_2O:0.02%, TiO_2:0.01% (total iron oxide being calculated as FeO).

The size, surface structure and composition of these magnetic microspherules indicate that almost all of them are considered to be the cosmic spherules. The total weight of the cosmic spherules fell on the earth per day in each geological time when each bed of the bedded chert had accumulated are preliminarily obtained, provided with the assumption of several indefinite factors, calculating from the volume of the spherules in each bed collected, the amount of the chert samples used for extracting the spherules, the thickness of the bed of the chert, and the speed of the sedimentation of the chert of the corresponding age obtained from published works (0.75mm/1000y for the Permian chert and 2.8mm/y for the Triassic chert). The result indicates that the consmic dust fell on the earth about 1 ton/day during early-Middle, late-Middle and early-Late Permian and about 3 tons/day during late-Late Permian and Middle Triassic (Fig. 2).

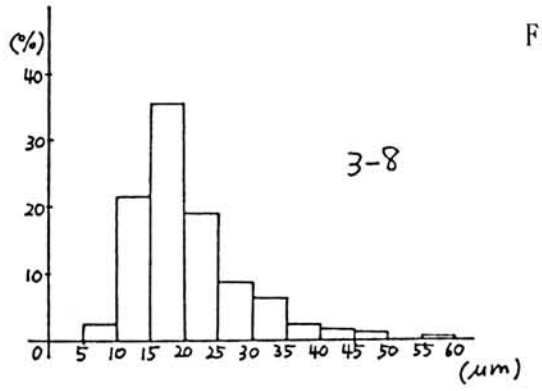

Figure 1. Size distribution of magnetitic microspherules collected from a bed of the Permian bedded

Figure 2. Estimates of the total weight of the cosmic spherules fell on the earth per one day in some time during Permian and Triassic.

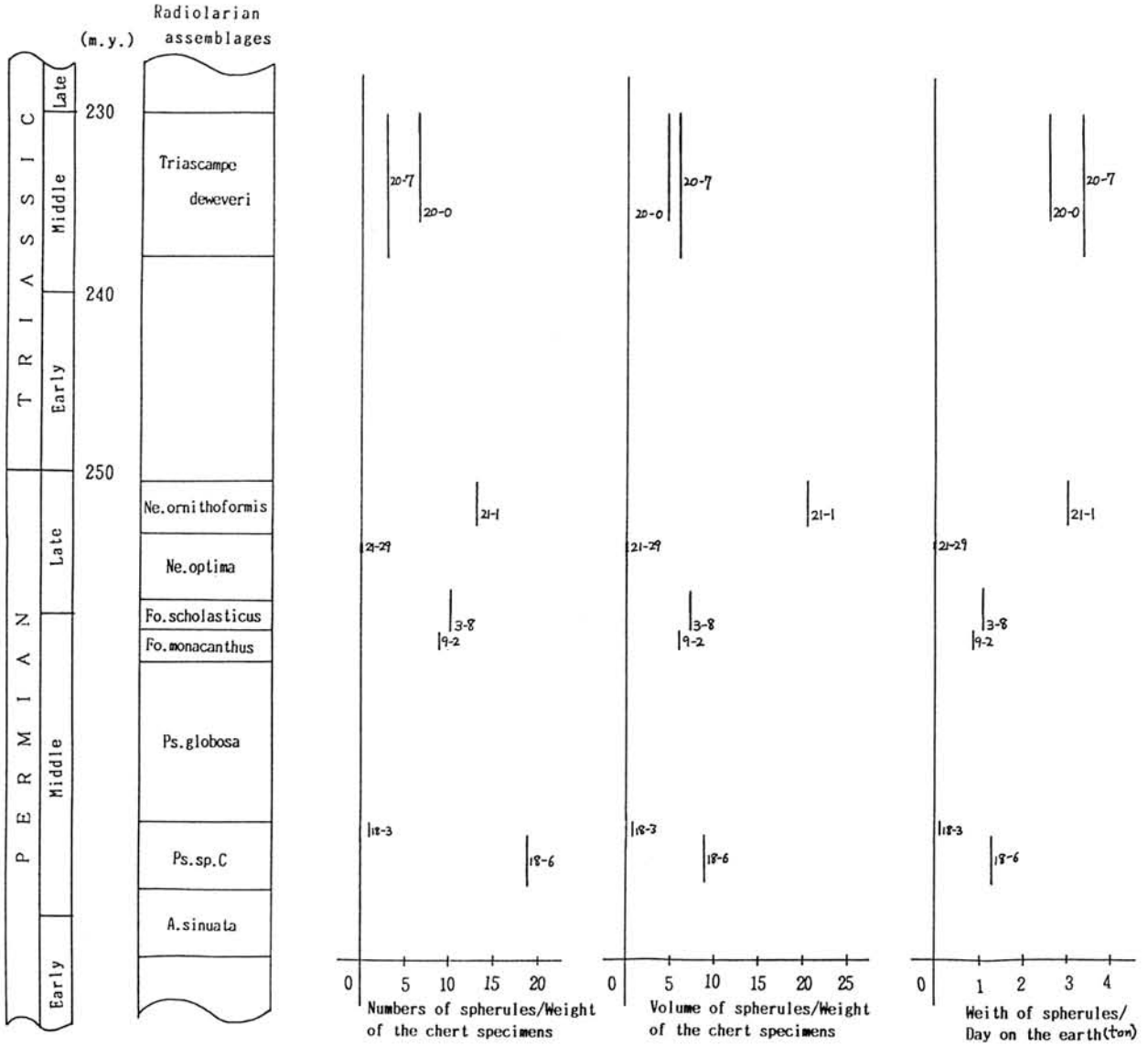

Origin and Characteristics of Dust Particles in Antarctic Ice/Snow and other Terrestrial Environments

Tazawa, Y.[1] and Fukuoka, T.[2]

1) Dept. Phys., Kyoto Univ., Sakyo, Kyoto 606.

2) Dept. Chem., Gakushuin Univ., Toshima, Tokyo 171.

The Earth's surface is full of dust particles a great majority of which are of terrestrial origin whether they are natural or artificial. More than 10^4 tons/yr of cosmic matter continuously fall on the Earth, however, mostly as dust particles smaller than 1 mm [1]. The particles are recovered from a wide range of terrestrial environments far from densely populated and/or arid continents, such as the deep-sea floor, the stratosphere and the Polar ice. Most of the particles larger than 10 um have a round shape suggestive of melting at the time of atmospheric entry [2] or at an event of a huge body impact [3].

More than a century ago, spherical microparticles (spherules) had been first recovered from the Polar (Greenland) ice cap [4] and the deep-sea floor [5]. Until the first particulates were collected from the Antarctic snow in the late 1950's [6], deep-sea spherules had been the only samples except meteorites for laboratory study of the cosmic materials. The particles are well preserved in the Polar ice/snow in order of accumulation age without serious disturbance and contamination, as well as in the deep-sea sediments, so that stratigraphic study of the particles will present a lot of information about a continuous history of the terrestrial accretion of cosmic debris and about isolated events, such as the terrestrial impact of a large body and a global scale volcanic eruption.

The most pristine dust particles are collected in the stratosphere. The stratospheric particles of proven extraterrestrial origin were first collected in 1970 using a balloon-borne collector [7] and successful collections using NASA U2 aircraft began in 1974 [8].

References:

[1] Hughes, D.W., Meteors, in Cosmic Dust, ed. J.A.M. McDonnell,pp. 123-186, John Wiley & Sons, New York, 1978.
[2] Blanchard, M.B. et al., Earth Planet. Sci.,Lett., 46, 178-190, 1980.
[3] Smit, J. & G. Klaver, Nature, 292, 47-49, 1981.
[4] Nordenskjold, N.A.E., Philos. Mag., 48(4), 546, 1874.
[5] Murray, J. & A.F. Renard, Proc. R. Soc. Edinburgh, 12, 474-495, 1883.
[6] Nishibori, E. & M. Ishizaki, Nankyoku shiryo (Antarct. Res), 7, 35-38,1959
[7] Brownlee, D.E. & P.W. Hodge, Space Res., 13,1139-1151,1973

TWO DIMENSIONAL CHEMICAL STATE ANALYSIS OF METEORITES BY X-RAY FLUORESCENCE ANALYSIS

Izumi Nakai and Akira Tsuchiyama,
Department of Chemistry, University of Tsukuba, Ibaraki, 305
College of General Education, Osaka University, Toyonaka-shi, Osaka 560

Introduction

Knowledge of chemical states of elements and distribution of trace elements in a meteorite is important to study origin and formation condition of the meteorite. Several spectroscopic methods such as Mössbauer spectroscopy, X-ray and optical absorption spectroscopy have been often used to examine the chemical states of elements. However, these methods do not provide two dimensional data. Recently, a new XRF (X-ray fluorescence analysis) technique based on the selective excitation of specific chemical species by tunable synchrotron radiation (SR) was developed[1]. This paper reports the first application of this technique to geological problems[2]. Advantage of the SR-XRF technique in trace element analysis is also examined in this study.

Experimental

SR-XRF measurement was made at BL-4A at Photon Factory, KEK, Tsukuba, utilizing an energy dispersive XRF system with Si(Li) detector. Schematic illustration of the measurement system is shown in Fig. 1. Monochromatic X-ray with desired energy and beam size was obtained with Si(111) double crystal monochromator and a set of vertical and horizontal slit system. Two dimensional analysis was carried out by scanning a sample on a computer controlled XZ stage normal to the orbital plane of SR.

Samples used are pseudomorph of goethite after pyrite and two chondrites: Allende and Murchison meteorites. Reference samples as standards for iron in various oxidation states include Fe metal, FeS_2, Fe_3O_4, FeOOH, Fe_2SiO_4, olivine and $YFeO_3$.

X-ray absorption spectra were measured by X-ray fluorescence detection. The intensity of the fluorescent X-rays was measured as a function of the incident energy. Figure 2 shows Fe K-edge absorption spectra of iron (Fe^0), pyrite (Fe^{2+}) and goethite(Fe^{3+}) indicating chemical shift of the absorption edge depending on their oxidation states. Accordingly, if a sample is excited at 7.1123keV, metallic iron is mainly excited, and at 7.1170 keV, both Fe^0 and Fe^{2+} are excited while at 7.5989keV, total iron should be excited. The pyrite/goethite sample was excited at the latter two energies and the meteorites were at the three energies. Two dimensional Fe image at each energy was measured. Experimental conditions are as follows: beam size ca. 0.2x0.2mm^2, 47x59 points, 0.2mm step, and 2s/point for pyrite/goethite; 0.13x0.13 mm^2, 0.1mm step, 2s/point and 57X40points for Allende and 39x50points for Murchison).

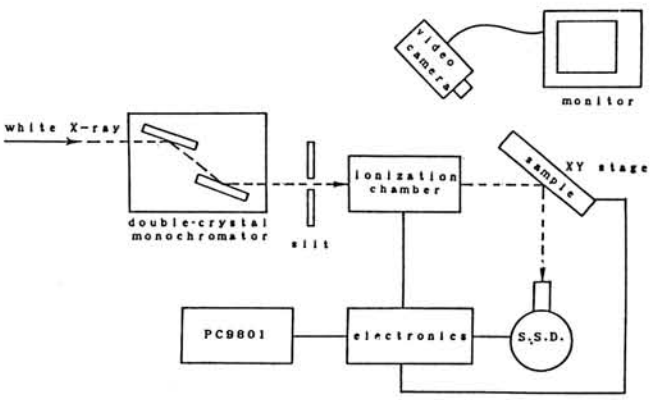

Fig. 1. Schematic illustration of the XRF measurement system at the Photon Factory.

Results and Discussion

An isolated image of each oxidation state of iron is obtained by a subtraction of two normalized data measured at different energy [1]. The results for the pyrite/goethite sample are shown in Fig. 3(a) and (b), where Fe concentration corresponds to 16 degree of darkness (black is the highest concentration). Fig.3(a) indicates distribution of divalent Fe, which corresponds well with pyrite, while Fig. 3(b) indicates trivalent iron corresponding to goethite, which was formed by the oxidation of pyrite. Figure 4 shows an example of the analysis of Allende meteorite indicating distribution of Fe^0 + Fe^{2+}. Two dimensional distribution of trace elements, Cu and Zn was also measured. A separate SEM-EDX analysis using the same sample showed that the chondrule is rich in Mg, Si, the inclusion is fine grained CAI and the matrix is rich in Fe and Si. The present analysis indicates that Cu and Cr are concentrated at the region rich in metallic Fe, while Zn is in the fine grained CAI.

This study has demonstrated the capability of the chemical state imaging and trace elements analysis of meteorite samples by the SR-XRF technique. This method is truly nondestructive and has therefore more advantage over electron microprobe because it does not require any pretreatment of sample such as carbon coating and is suitable for analysis of samples containing water. But the spatial resolution is around a few ten microns, which is much worse than that of the electron microprobe.

The authors thank Dr. A. Iida , Mr. S. Hayakawa and Mr. K. Imai for their kind help in the measurements.

1) K. Sakurai et al. Jap. J. Appl. Phys., **27**, L1768(1988).
2) I. Nakai et al. Photon Factory Activity Report #6, 141 (1988)

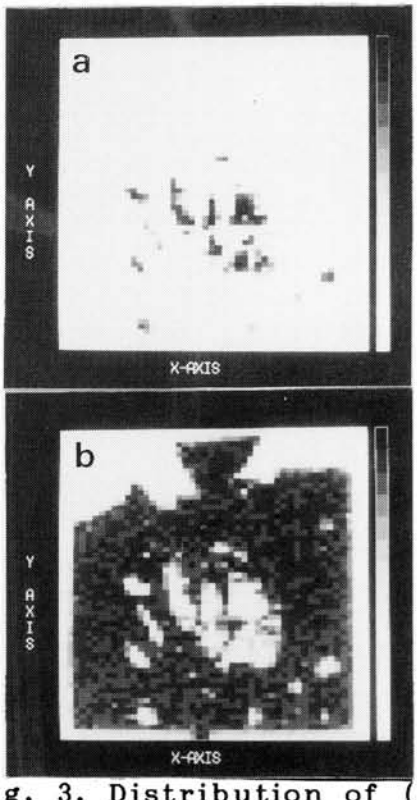

Fig. 3. Distribution of (a) Fe^{2+} and (b)Fe^{3+} in goethite after pyrite. Analyzed points 47x59, beam size ca. 0.2x0.2mm^2, 0.2mm step.

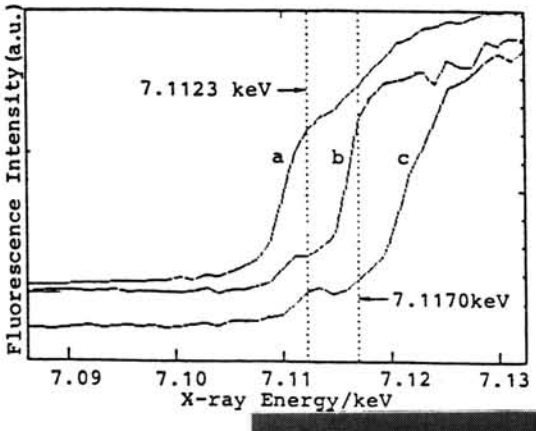

Fig. 2. X-ray absorption spectra of (a)iron, (b)pyrite and (c)goethite.

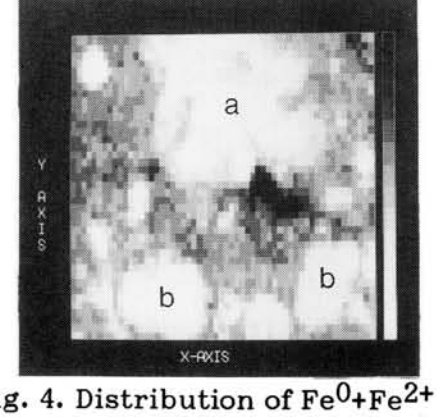

Fig. 4. Distribution of Fe^0+Fe^{2+} in allende meteorite. 57x40 points, 0.13x0.13mm^2 beam, 0.1mm step, 2sec/point. a:CAI, b:chondrule.

MAGNETIC PROPERTIES AND NATURAL REMANENT MAGNETIZATION OF CARBONACEOUS CHONDRITES CONTAINING PYRRHOTITE

NAGATA T., FUNAKI M. and KOJIMA H.
National Inst. Polar Research, Tokyo 173.

Magnetic minerals and magnetic properties of C-chondrites

Chemical and magnetic analyses of opaque minerals indicate that magnetic (ferro- or ferri-magnetic) minerals in C-chondrites are, in most cases, abundant in Fe_3O_4 (Magnetite), with Fe-Ni α (Kamacite), Fe-Ni γ (Taenite), or FeS_{1+x}(Pyrrhotite) as auxiliary components. Allende (CV3), Leoville(CV3), Y-74662(CM2) and Y-81020 (CO3) chondrites are petrographically, chemically and magnetically analyzed for the purpose of detecting their principal magnetic constituents responsible for their magnetic properties and NRM characteristics, results being summarized in Table 1.

As shown in Table 1, the major magnetic constituent is Fe_3O_4 except in Y-74662 in both petro-chemical and magnetic analyses. By EMPA analysis in some detail, however, pyrrhotite grains are detected in Y-74662 and Allende.

Table 1. Magnetic Mineralogy and Bulk Magnetic Properties.

Item	ALLENDE (CV3)	LEOVILLE (CV3)	Y-74662 (CM2)	Y-81020 (CO3)
Main Mag.Mineral	Fe_3O_4	Fe_3O_4	FeS_{1+x}	Fe_3O_4
AUX. Mag.Mineral	Fe-Ni γ	Fe-Ni α	Fe-Ni γ Fe-Ni α	Fe-Ni α
EMPA (FeS_{1+x})	◎		◎	◎
Maj. Mag. Trans. Temp. (°C)	590 Fe_3O_4 Fe-Ni γ	575(Fe_3O_4)	300(FeS_{1+x})	590(Fe_3O_4)
Min. Mag. Trans. Temp. (°C)		770(Fe-Ni α)	620(Fe-Ni γ) 750(Fe-Ni α)	780(Fe-Ni α)
Bulk Mag. Properties (RT)				
I_S (emu/g)	0.80 1.31	10.3	0.81～1.08	14.0
I_R (emu/g)	0.13 0.26	0.58	0.093～0.103	1.39
Hc (Oe)	179 174	34	118～170	170
H_{RC} (Oe)	592 527	225	660～855	503

NRM Characteristics

As shown in Table 2, however, the major portion (>60%) of NRM of all the four C-chondrites is thermally demagnetized at temperatures below 330°C, almost uniquely suggesting that major parts of NRM are possessed by magnetic pyrrhotite. In comparison of Table 2 with Table 1, the low temperature component of NRM can be identified to the remanent magnetization (RM) of magnetic pyrrhotite phase.

Table 2. NRM Characteristics.

Item	ALLENDE (CV3)	LEOVILLE (CV3)	Y-74662 (CM2)	Y-81020 (CO3)
NRM Intensity (emu/g)	(0.8～2.5) x10^{-4}	2.1x10^{-4}	5.9x10^{-4}	8.6x10^{-4}
Low Temp. Component	T≲330°C (>95%)	T<300°C (66%)	T≲300°C (86%)	T≲320°C (60%)
High Temp. Component	330<T≲700°C (<5%)	300<T≲470°C (19%)	300<T<700°C (13%)	320<T<640°C (36%)
Low Temp. Fp(Oe)	0.8～3.0	0.97	0.77	1.2
High Temp. Fp(Oe)	≲0.02	≲0.06	～0.01	～0.09

The paleointensity (Fp) of the chondrites is estimated on an assumption that the NRM was produced with TRM acquisition mechanism in an ambient magnetic field, Fp. A remarkable observed fact would be a distinctly large Fp value of the pyrrhotite phase NRM component, which ranges between 0.8 and 3.0 Oe, in comparison with much smaller Fp values of the high temperature component.

Some Critical Examinations of NRM Component of Pyrrhotite

(a) β- and γ-phase Structures of Magnetic Pyrrhotite

The magnetic pyrrhotite phase consists of β- and γ- phases, their transition temperature being 180～220°C, while Curie point of β-phase is about 310°C. Since the stable state of γ-phase below the transition temperature is antiferromagnetic, the formation processes of NRM in nature as well as TRM in laboratory depend on cooling or heating rate. Experimental comparisons of PTRM spectra between NRM and laboratory TRM demonstrate a roughly approximate agreement between the two RMs with respect to their PTRM spectra.

(b) Possible Crystal-Growth Effect of Magnetic Minerals.

If magnetic pyrrhotite grains were formed with the coalescence of Fe- and S- superfine particles in the solar nebula, there is a possibility that already magnetically oriented pyrrhotite particles continue to further grow up with the same magnetic orientation even in Non-magnetic space, resulting in an increase of remanent magnetization. A theoretical approach to evaluate the possible effect of crystal growth on Fp value shows that the expected increasing rate of apparent Fp value should be smaller than 30% regardless of the crystal-growth rate.

TETRATAENITE IN CHONDRITES AND EXPERIMENTAL DEMONSTRATION OF FORMATION OF TETRATAENITE FINE GRAINS

T. Nagata*, C. Kaito**, Y. Saito** and M. Funaki*
* National Institute of Polar Research, Tokyo 173.
** Kyoto Technical University, Physics Dt. Kyoto 606.

Tetrataenite in Antarctic Chondrites.

As already reported, Antarctic chondrites, metallic components of which are relatively rich in Ni content, often contain tetrataenite (FeNiγ") phase, which has a large crystalline anisotropy owing to its tetragonal crystal structure, so that its magnetic coercivity also is unusually large (i.e. magnetic coercive force (H_C)>10^3Oe). These Antarctic chondrites are, for example, Y-7301(H_4), Y-74647(H_5), Y-74191(L_3), Y-74354(L_6) and Y-74362(L_6).

Magnetic Analysis of Chondrites.

The magnetic analysis scheme for meteorites consists of (a) magnetic hysteresis cycle curve analysis dependent on temperature, and (b) thermomagnetic analysis of their original test samples and those which are subjected to various heat treatments, together with coordinated analyses of metallic constituents with the aid of EMPA images, Mössbauer spectra, electron diffraction patterns, X-ray spectra, etc. Results of the magnetic analysis of bulk samples of LL chondrites, which are particularly rich in FeNiγ" in their metals, in comparison with results of the Mössbauer analysis of the same chondrite samples are summarized in Table 1. The compositions of metallic phases determined by different methods for these FeNiγ" rich chondrites are in approximate agreement with each other.

Superfine Particles of Tetrataenite in Chondrites

Some chondrites contain superfine particles of tetrataenite metal.
(Example 1). Matrix of St. Séverin LL_6 Chondrite. The silicate rich matrix of this chondrite still contains fine metallic grains. Since the fine single-domain magnetic particles behave superparamagnetically at temperatures higher than their blocking temperature, which depends on their magnetic anisotropy energy as well as their volume, the magnetic analysis of their magnetization curve characteristics can lead to the volumetry to estimate their grain size spectrum. Fig.1 illustrates the bulk content in weight of FeNiγ" phase at temperatures between -269℃ and +25℃, where -200℃, -100℃ and 0℃ in temperature correspond to 4.4nm, 5.9nm and 6.8nm respectively in terms of mean diameter of FeNiγ" particles. The measured result given in Fig.1 indicates that the mean diameter of the majority of FeNiγ" fine particles is smaller than 4.4nm.
(Example 2). Tetrataenite grains in Tuxtuac LL_5 chondrite.

The Mössbauer spectral analysis shows that metallic grains of Tuxtuac LL_5 chondrite contains about 15wt% of FeNiγ" phase, whereas the magnetic analysis of the same sample at 25℃ shows that this chondrite contains no FeNiγ" phase at 25℃. As shown in Table 2, however, the magnetic analysis at -269℃ indicates that this chondrite contains 9wt% FeNiγ" phase (H_C=2160 Oe) together with FeNiγ phase of H_C=38 Oe. Since the magnetic analysis of this Tuxtuac chondrite after heat treatment at 800℃ shows that no FeNiγ" phase can be detected at both 25℃ and -269℃, it is certain that the high coercive ferromagnetic phase contained in the original sample before the heat treatment is FeNiγ". The grain size of the FeNiγ" particles is around 4～5nm, smaller than 7nm at most, in their mean diameter.

Table 1. Composition of Metallic Components in LL Chondrites

Chondrite	Mössbauer Analysis (wt%)			Magnetic Analysis (wt%)		
	α	γ	γ''	α	γ	γ''
Olivenza (LL6)	45	15	40	40	14	46
St. Séverin (LL6)	40	10	50	47	11	42
Appley Bridge (LL6)	～0	20～40	80～60	～0	57	43

(Remarks) α :Kamacite γ :Taenite γ'':Tetrataenite

Table 2. Composition of Metallic Grains of Tuxtuac LL5 Chondite

Analysis Method	α	γ	γ''
(Original)		(wt%)	
Mössbauer	～0	85	15
Magnetic (25℃)	～0	100	～0
Magnetic (-269℃)	～0	91	9
(After heat treatment			
Magnetic (25℃)	～0	100	～0
Magnetic (-269℃)	～0	100	～0

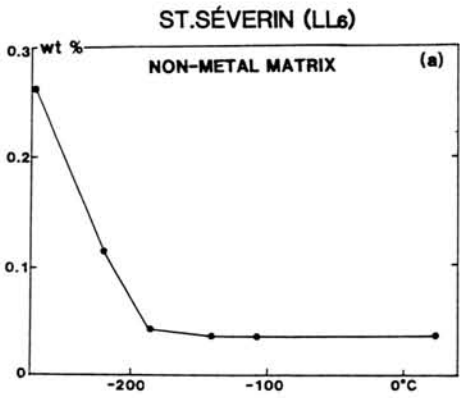

Fig. 1

Experimental Formation of FeNiγ'' and other Fe-Ni particles of Ordered Crystal Structure by Coalescence of Fe and Ni Smoke Streams.

The instrumentation system for producing FeNiγ'' and other Fe-Ni alloy particles of ordered crystal structure is schematically shown in Fig. 2. The whole system is operated in a glass cylindrical jar filled with Ar gas at 13 kPa in pressure. The upward stream of Fe smoke and that of Ni smoke evaporated from respective metallic pieces heated at 1700℃ in tungsten boats, emerge near the top of a guiding system composed of 2 glass plate roofs, further flowing upward through a heater system to the particle collector made of an electron microscope grid, which is located at Point Q in Fig. 2. The collected metallic particles are analyzed with the aid of electron microscope images, X-ray spectra and electron diffraction patterns.

When no heater is operated, temperature of the emerging smoke is lower than 80℃, and no Fe-Ni alloy particles is formed, only Fe and Ni metallic particles being detected. When the merging smoke temperature is raised by the heater system up to 200℃ or higher, the produced metallic particles obtained by the collector are identified to either one or their interacted combination of ordered FeNi(FeNiγ'', tetrataenite), ordered Fe_3Ni(Ordered Kamacite), ordered $FeNi_3$(FeNiγ', Awaruite) and disordered Fe-Ni alloy (Taenite). Fig. 3 shows an example of the X-ray spectrum of a part (about 10nm in diameter) indicated by an arrow in the attached EM image of a FeNiγ'' particle.

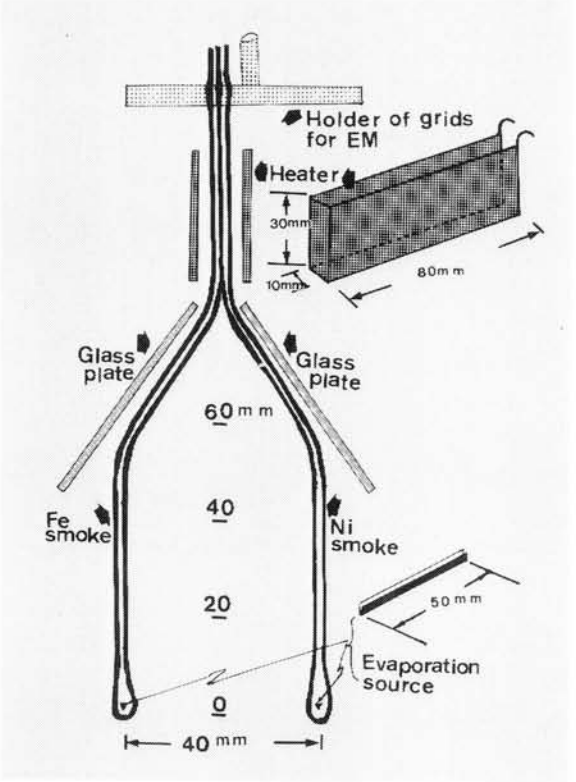

Fig. 2

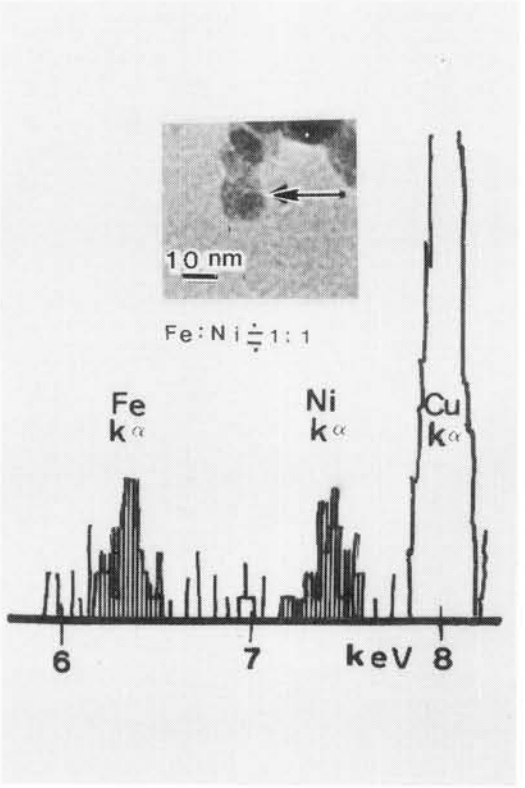

Fig. 3

Magnetic Properties of FeNi fine particles produced by the present Coalescence Method.

The FeNi γ" phase produced by the present coalescence technical procedure is very often with Fe-Ni alloy phases in individual single particles. For example, some single FeNi γ" microcrystal is fully enveloped by a Fe_3Ni layer. Such an interaction of 2 magnetic phases should result in a considerable reduction of the magnetic coercivity of the larger coercivity component.

Typical examples of the magnetic analysis and the following magnetic volumetry of the present Fe-Ni fine particles are given in Table 3. All the results of EM images, X-ray spectra, electron diffraction patterns together with magnetic analysis confirm presence of FeNi γ" metallic phase in the Fe-Ni fine particles produced by the present coalescence method.

Table 3. Composition of Fe-Ni Particles of Coalescence Products

Temperature	Sample #2 α	γ	γ"	Sample #3 α	γ	γ"
(Original)	(wt%)			(wt%)		
25℃	40		60	35		65
-150℃	38		62	-		-
-269℃	22		78	-		-
(After heat treatment) 25℃	100		～0	100		～0

SHOCK EFFECTS IN CHONDRITES
— (I) From Dislocations and Grain Shapes —

Naoyuki **FUJII**[1],[2], Kazuhiko **TASHIRO**[2] and Tsuyoshi **KANAMARU**[1],[3]

[1] *Dept. Earth Sci., Faculty of Sci. Kobe Univ., Nada, Kobe 657, Japan.*

[2] *Div. Environ. Sci., Grad. School Sci & Technol., Kobe Univ. Nada, Kobe 657, Japan.*

[3] Now at *Software Work., Hitachi Co., Totsuka, Yokohama 244, Japan.*

Shock effects recorded in meteorites are observed in a variety of features, *i.e.*, breccias, mineralogical and chemical effects, and melting [*Dodd*, 1981]. Shock intensity of the ordnary chondrites is classified by the petrographic deformation structures in olivine and plagioclase, based mainly on the shock experiments [*e.g. Reimond and Stöffler*, 1978; *Dodd and Jarosewich*, 1979]. It is, however, noted that the shock duration occurred among the planetary bodies would be more than a few to tens of seconds which could obviously be far longer than those (order of microseconds) in the shock experiments [*Jeanloz*, 1980].

Effects of transient deformation and recovery processes in the petrographic features should carefully be examined in the shock pressure estimation. Recovery and transient creep processes of dislocations in deformed terrestrial olivines have been investigated for low strain rates [*e.g. Toriumi and Karato*, 1978, 1984]. However, little attention has been paid for the recovery processes of shock-induced dislocation textures. In this paper, preliminary results from week shock experiments and some prospect are reported on dislocation structures in olivine grains.

Millimeter sized olivine grains from San Carlos (Fo_{92}) and Kilborn Hole (Fo_{90}), Arizona, were ground to disks with 1-2 mm thick. By using a newly designed week shock apparatus [*Fujii and Kanamaru*, 1989], a shock compression is applied to a 3 to 5 mm thich Pb disk in which several olivine disks are embedded, through the 30 mm long upper piston which is compressed by a freely falling steel cylinder of 10 or 20 kg. By using densities and elastic constants of Pb and steel, shock pressures are estimated to be 450 *MPa* for a 0.5 m free fall hight (H) of steel cylinder and 850 *MPa* for H = 2.0 m. No direct measurement of shock duration, pressure and temperature is made at present moment. It is, however, noted that the duration of shocked state in the sample may be order of 0.1 to several miliseconds if the elastic wave velocity and the deformation of the steel cylinder and pistons are considered.

Both of shocked at and unshocked olivins are decolated by the oxidation method [*Köhlstedt et al.*, 1976]. In Figure 1, some examples of dislocations are shown for (1a) unshocked and (1b) shocked at room temperature and 620 *MPa* of San Carlos olivines, and oriented olivines from Kilborn Hole of (1c) unshocked and (1d) shocked at room temperature and 750 *MPa*. Dislocations of unshocked San Carlos olivines are not cellular type unlike the observations of *Toriumi and Karato* [1978], instead almost straight dislocations are present nearby grain surfaces (Figure 1a) and almost free of dislocations inside grains. However, cellular type dislocations are observed in the shocked samples as shown in Figure 1b (shocked at 620

MPa), which may indicate the transient nature of shock deformation, though the dislocation density is low ($\sim 10^{10}$ m^{-2}). Figure 2 shows dislocation densities as a function of shock pressures for all olivines studied. Dislocation densities are within a range of $(1 \sim 20) \times 10^9$ m^{-2}.

A slight increase of dislocation densities of homogeneous part on the shock pressure may indicate the generation of dislocation-pairs and quenched during shocked state. Mobility of the pre-existed dislocations is small enough in the present experimental pressure and temperature conditions. However, an emblio of the clusterd dislocations in the slip plains and subgrain formation may occurred in some shocked grains as seen in Figures 1b and 1d. This observation seems to be consistent with low temperature and high stress (LT/HS) type dislocations observed in L6 chondrites [*Karato and Matsui*, 1981]. It is, however, likely that the relation between the dislocation density and subgrain size for shock compression differs from that of low strain rate experiments [*Karato et al.*, 1980]. Strain rate dependence on this relation would not be so simple due partly to the transient deformation processes concerned and partly to the heterogeneous generation rate of dislocations.

As shown in Figure 2, dislocation densities of the present experiments are much less than those in L6 chondrites ($\geq 10^{13}$ m^{-2}), probably due to low temperatures and low shock pressures. Although comparisons of dislocation textures between terrestrial olivines and ordinary chondrites are not enough at present, shock compression experiments with varied temperature could give some clues to the quantitative estimates of shock pressures in ordinary chondrites.

Further investigations are obviously needed to clarify the effects of transient deformation and recovery as well as the deformation textures on the shock processes recorded in chondrites.

REFERENCES

[1] Dodd, R.T.(1981)*Meteorites; A Petrological-Chemical Synthesis*, Cambridge Univ., 432p.
[2] Dodd, R.T. and Jarosewich, E. (1979) *Earth Planet. Sci. Lett.* **44**, 335-40.
[3] Jeanloz, R. (1980) *J. Geophys. Res.*, **85**, 3163-3176.
[4] Karato, S. (1987) *Phys. Chem. Minerals*, **14**, 245-248.
[5] Karato, S. Toriumi, M., and Fujii, T. (1980) *Geophys. Res. Lett.*, **7**, 649-652.
[6] Karato, S. and Matsui, T. (1981) *Progr. & Abst., Seism. Soc. Japan*, **No.1**, D36, 216.
[7] Köhlstedt, *et al.*, (1976) *Science*, **191**, 1045-1046.
[8] Fujii, N. and Kanamaru, T. (1989) *Proc. 22nd ISAS Lunar Planet. Symp.*, ISAS, 141-144.
[9] Reimond, W.U. and Stöffler, D.(1978) *Proc. Lunar Planet. Sci. Conf.*, **9th**, 2805-2824.
[10] Toriumi, M. and Karato, S. (1978) *Tectonophys.*, **49**, 79-95.
[11] Toriumi, M. and Karato, S. (1984) In I. Sunagawa (ed.), *Materials Science of the Earth's Interior*, 281-300, Terra Pub., Tokyo.

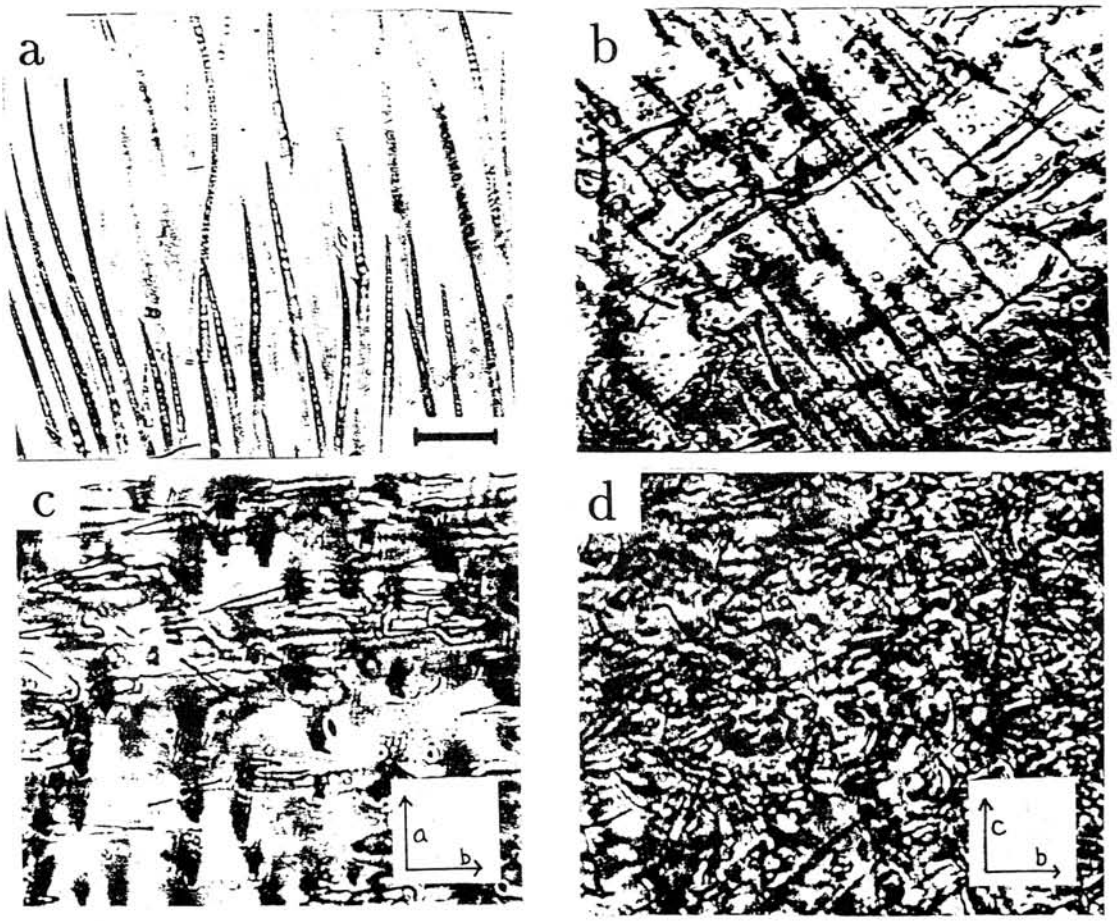

Figure 1. Examples of dislocations under optical microscope, for (a) unshocked and (b) 620 *MPa* from San Carlos olivines, and oriented grains from Kilborn Hole olivines for (c) unshocked and (d) 750 *MPa*, respectively. A scale bar in (a) shows 10 microns and scales are all the same for others.

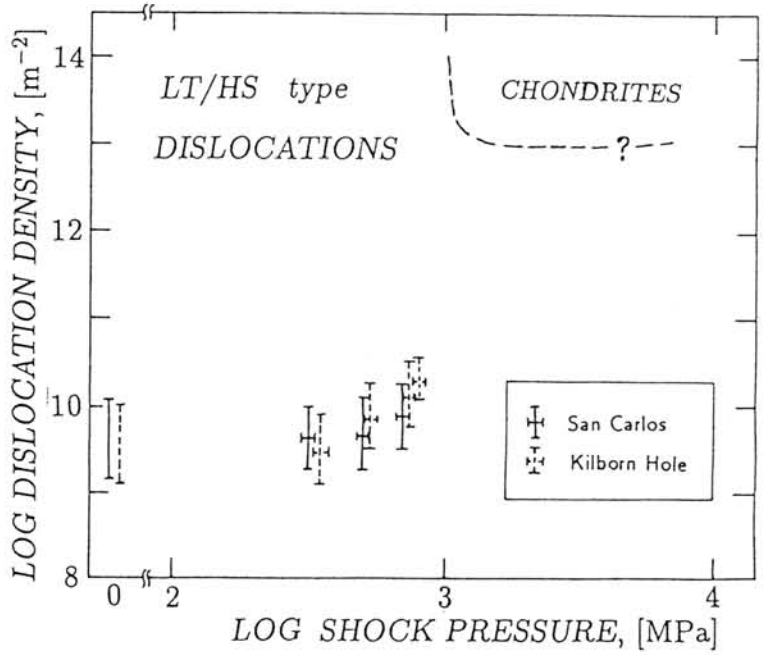

Figure 2.

Dislocation density *vs* shock pressures for olivines.

Formation of Chondrules by Collisions between Planetesimals

Mizutani[1], H., Yamamoto, T.[1], Kozasa, T.[2], and Honda, R.[1,3]

1)Institute of Space and Astronauticakl Science,
Yoshinodai 3-1-1, Sagamihara, Kanagawa 229
2) Max-Planck-Institut für Kernphysik,
Heidelberg 1, F.R.G.
3) Department of Earth Science, Nagoya University,
Furo-chou, Chikusa-ku, Nagoya 464

It is considered that chondrules are a primitive material that conserves memories of the events occurred in the early solar system. Important constraints upon the formation conditions have been obtained from laboratory experiments (*e.g.* [1, 2]). We take account of the following constraints on the chondrule formation: (1) Chondrules passed through a liquid phase as suggested by their spherical appearance. (2) The cooling rate at crystallization of many of the chondrules are in the range of $-dT/dt \sim 1 - 10^{-3}$ K s^{-1}. It is noted that this cooling rate is much faster than that of the solar nebula itself, but much slower than that expected in the cooling of a mm-sized body in a vacuum. (3) The radius of most of the chondrules is $0.1 < a < 10$ mm. (4) The oxygen partial pressure in an environment where chondrules were formed is much higher than that expected for a solar nebula gas. (5) Relict grains are observed in a substantial part of the chondrules.

We propose a model of chondrule formation through condesation of grains in cooling of a hot vapor produced at collisions of planetesimals, and examine whether this model satisfies the experimental constraints as stated above.

The Model

Let us consider a collision of planetesimals with a relative velocity of $1 \sim 10$ km/s. At a collision, a part of the kinetic energy is converted to thermal energy in the vicinity of the collision point. As a result, a portion of the target and projectile materials are heated and vaporize. At the same time some portion of the planetesimals that does not reach the vaporization temperature will be fractured by shock wave due to impact, and ejected into the surrounding space as dusts. This process results in a cloud consisting of hot vapor and dust particles. Subsequently the cloud begins to cool down with expansion. When the cloud cools down to a condensation temperature of the vapor, grains are formed by recondensation of the vapor. We regard the grains to be chondrules.

The chondrule formation by this mechanism is studied on the basis of the thermodynamics of the vapor cloud and of a kinetic theory of condensation including nucleation and grain growth [3, 4]. It is assumed for simplicity that the cloud is spherical and expands uniformly with a constant velocity equal to the initial sound velocity. Futhermore it is assumed that the vapor and the grains condensed are in thermal equilibrium in the optically thick cloud. The energetics of the cloud is determined by cooling due to thermal emission from the cloud surface and heating due to absorption of incident solar radiation. During the condensation period, the latent heat released by grain growth is included as a heating source.

The elemental composition of the vapor is expected to be similar to that of the planetesimals. We take an olivine composition as the elemental composition of the vapor, which is given by Mg : Si : Fe : O = 1 : 1 : 1 : 4. The condensation reaction that we consider is:

$$2\mathrm{Mg} + \mathrm{SiO} + \frac{3}{2}\mathrm{O_2} \longrightarrow \mathrm{Mg_2SiO_4(s)}.$$

The initial temperature T_0 and pressure P_0 is determined from the condition of thermal equilibrium: $P_0 = \rho_0 k T_0/\mu m_{\mathrm{H}} = P_{\mathrm{e}}(T_0)$, where P_{e} is the saturated vapor pressure, ρ_0 is the initial density, μ is the mean molecular weight, and k the Boltzmann constant. We put $\rho_0 = 1$ g cm^{-3} $\sim$ planetesimal density. These conditions imply the initial vapor temperature of about 7000 K. A parameter involved in the model is a total mass of the vapor M_{vap}.

Formation Process of Chondrules

When the vapor cools down to the liquidus temperature, the vapor reaches an equilibrium temperature, at which a vapor and a bulk liquid can be in chemical equilibrium. Further cooling leads to a supersaturation state, in which grains are nucleated and begin to grow. The growth of a grain is accompanied by deposition of the latent heat, and as a result the grain temperature increases and returns to the liquidus temperature. After that, the growth of a grain proceeds along the liquidus line. During the growth, the energy balance is almost realized between the heating by the latent heat deposition and the radiative cooling. Thus the cooling is a very slow at this stage, and the grains are in the liquid phase. This situation is realized irrespective of detailed behavior of the cooling of the vapor at the early stage down to the liquidus temperature, since latent heat deposition due to grain growth always controls the cooling curve to pass along the liquidus line. When the vapor is consumed up by the growth of grain size, the cooling curve begins to deviate from the liquidus line, and the grains of liquid droplets begin to solidify when the cooling curve crosses the solidus. The grains thus formed cool by thermal emission, and finally their temperature approaches a temperature determined by the balance between heating due to absorption of solar radiation and cooling due to thermal emission.

Conclusions

The results derived from the model are summarized as follows:

(1) It is confirmed that chondrules pass through a liquid phase during condensation. Latent heat deposition accompanying condensation plays a key role in realizing a liquid phase.

(2) The observed cooling rate of $-dT/dt < 1$ K s $^{-1}$ is realized for the collisions that produce the vapor mass larger than 10^{21} g. The chondrules condensed under this condition will not escape from a sphere of influence of planetesimal gravity, if the mass of a target planetesimals is larger than 10^{24} g.

(3) It must be pointed out that the size of chondrules bears importnat information on the origin of chondrules. In our model the size indicates the mass of the vapor produced at a planetsimal collision. It is shown that the observed size are produced for the vapor mass less than 10^{22}.

(4) The high oxygen partial pressure is self-evident in our model, since condensation of chondrules occurs in the vapor of planetesimal composition and its pressure is much higher than the oxygen partial pressure expected for the ambient solar nebula.

(5) Within a framework of our model, it is expected that the orgin of relict grains have some relevance to the ejected dust particles. Study of chondrule formation in a dusty cloud is in progress, and tentative results of this study will also be presented.

REFERENCES

1 Nagahara, H., 1983: *Mem. Natl. Inst. Polar Res. Special Issue* **30**, 61.

2 *Meteorites and the Early Solar System*, 1988: eds. J.F. Kerridge and M.S. Matthews, Univ. Arizona Press.

3 Yamamoto, T. and Hasegawa, H., 1977: *Prog. Theor. Phys.* **58**, 816.

4 Kozasa, T. and Hasegawa, H., 1987: *Prog. Theor. Phys.* **77**, 1402.

METAMORPHISM OF CO AND CO-LIKE CHONDRITES AND COMPARISONS WITH TYPE 3 ORDINARY CHONDRITES. Derek W.G. Sears, J. David Batchelor, Lu Jie and Bradly D. Keck. Cosmochemistry Group, Department of Chemistry and Biochemistry, University of Arkansas, Fayetteville, AR 72701, USA.

Introduction CO chondrites differ from type 3 ordinary chondrites in their bulk compositional and isotopic properties [1,2], abundance of refractory-rich inclusions (ameboid olivine inclusions and other CAI similar to those in Allende [3]), and their relatively small chondrule sizes [4]. However, like the ordinary chondrites, CO chondrites are essentially olivine and pyroxene, with minor amounts of plagioclase, metal and sulfide [3]. They may also be sorted into a metamorphic sequence similar to that for the type 3 ordinary chondrites. With increasing levels of metamorphism, CO chondrites show similar variations to those of type 3 ordinary chondrites in silicate heterogeneity, metal composition, TL sensitivity and cathodoluminescence (CL) petrography [3,5,6,7]. On the basis of metamorphism experienced, McSween divided the CO chondrites into petrographic types I, II and III [3], while Scott and Jones divided the group into types 3.0-3.9 [7]. Underlying this is the important issue of the similarity of the thermal histories of the CO and ordinary chondrite classes. In this paper we present new TL data for ten CO and CO-related chondrites (Table 1), and we discuss the thermal histories of the CO and ordinary chondrite classes.

Results Table 1 lists TL data for the new carbonaceous chondrites, and Figs. 1 and 2 compare these data with data for other CO chondrites. Most CO chondrites produce two TL peaks, one at 110-130C whose intensity shows a 100-fold variation which is metamorphism-dependent, and one at 220C which is relatively constant in intensity. Colony and ALHA77307, like the type 3.0-3.1 ordinary chondrites, have broad glow curves, mainly due to an additional peak at 350C. This peak is erratic in its behavior and the curves are reminiscent of those produced by Allende CAI [8]. LEW85332, the three paired MAC samples and Y-82020 produce such glow curves. Allan Hills 85003 and A82101 and Yamato 791717, 81050 and 82094 have curves with dominant peaks at 110-130C with little contribution from a peak at 350C.

Discussion Using the present TL sensitivity data for the 'metamorphic' peak and the petrographic type definitions suggested for type 3 ordinary chondrites [9], Yamato 791717, 81020 and 82050 are petrographic type 3.4 and Yamato 82094 is petrographic type 3.5. These assignments are consistent with the brief descriptions of these samples by Yanai and Kojima [10] and of Y-81020 by Graham and Yanai [11]. ALH85003, ALHA82101, LEW85332 and the MAC87300 group have TL sensitivity based petrographic types of 3.5, 3.6, 3.1 and 3.2, respectively. ALHA82101 was described as type 3.3 by Scott and Jones [7] and LEW85332 was described by Rubin and Kallemeyn [12] as one of the least equilibrated chondrites known; they also regard the meteorite as a unique carbonaceous chondrite.

Table 2 lists TL-based petrographic types for CO chondrites from the Keck and Sears [6] study, along with petrographic type assignments based on petrographic data [3,13,14,7]. We may also use CL petrography to

Table 1. New induced thermoluminescence data for CO and CO-like chondrites.

		TL Sensitivity (Dhajala = 1)			Peak Temperature (C)			Recommended
Meteorite	Source	Peak 1	Peak 2	Peak 3	Peak 1	Peak 2	Peak 3	Pet. Type
ALH82101,12	MWG	0.33±0.095	0.07±0.01	---	138±21	268±26	---	3.6
ALH82101,13	MWG	0.2±0.1	0.041±0.009	---	134±18	270±26	---	3.6
ALH85003,2	MWG	0.28±0.08	0.05±0.02	---	118±11	266±25	---	3.5
ALH85003,18	MWG	0.15±0.07	0.031±0.008	---	117±11	267±25	---	3.5
Y82094,95	NIPR	0.188±0.041	---	---	137±1	---	---	3.5
Y791717,93	NIPR	0.072±0.006	0.019±0.004	---	120±3	232±2	---	3.4
Y81020,25	NIPR	0.07±0.02	0.082±0.018	0.055±0.012	125±5	216±1	321±6	3.4
Y82050,73	NIPR	0.054±0.008	0.019±0.004	---	116±8	231±7	---	3.4
LEW85332,13	MWG	0.0098±0.0005	0.017±0.002	0.016±0.001	120±11	258±25	412±40	3.0
LEW85332,2	MWG	0.0010±0.0008	0.019±0.004	0.018±0.005	119±11	240±25	395±36	3.0
MAC88107,3	MWG	0.02±0.01	0.07±0.04	0.07±0.04	125±5	202±3	292±10	3.1
MAC87301,3	MWG	0.03±0.02	0.07±0.03	0.07±0.03	125±5	210±11	300±10	3.1
MAC87300,3	MWG	0.012±0.003	0.031±0.002	0.032±0.005	125±5	212±7	311±7	3.1

Table 2. Petrographic type for CO chondrites.

Meteorite	McSween	TL sens	CL	Scott/ Jones
Colony	I	3.2	3.0-3.1	3.0
ALHA77307	I	3.3	3.0-3.1	3.0
Ornans	II	3.4	3.2-3.4	3.3
Kainsaz	I	3.5	3.1-3.2	3.1
ALHA77003	II	3.5	3.2-3.4	3.4
Felix	II	3.5	3.2-3.4	3.2
Lance	II	3.6	3.2-3.4	3.4
Warrenton	III	3.6	3.5-3.9	3.6
Isna	III	3.8	3.5-3.9	3.7

assign petrographic types, particularly for the lower types (Table 2). The CL of type 3.0 ordinary chondrites consists of yellow CL from the mesostasis of magnesian chondrules, red CL from low-Fe olivines and pyroxenes in chondrules and matrix, and blue CL from chondrule mesostases with plagioclase-normative compositions. Additionally, a significant number of chondrules contain quartz-normative mesostases which are non-luminescent. With increasing metamorphism, this diversity in color disappears, to be replaced by the ubiquitous blue CL of sodic plagioclase as calcic chondrule mesostases 'equilibrate' toward oligoclase, and magnesian silicates become relatively Fe-rich and therefore non-luminescent [15,16,17]. The CO chondrites of McSween's type III are comparable in their CL properties to ordinary chondrites of type 3.5-3.9. Isna and Warrenton have matrix with little or no CL and a uniform distribution of grains and chondrules with blue CL. Chondrules in Isna have mesostasis which is usually bright blue or bluish/white and only occasionally yellow or orange. The CO chondrites of type II resemble ordinary chondrites of type 3.2-3.4 in their CL properties. Lance, Felix, ALHA77003 and Ornans have matrices which are largely non-luminescent but with scattered isolated grains with red CL (presumably forsterite), somewhat larger matrix 'grains' (probably grain aggregates) with blue CL and which grade into CAI, and chondrules whose mesostases have blue or bluish/white CL and whose grains have either red CL or are non-luminescent. The CO chondrites of McSween's type I have CL properties comparable to type 3.0-3.1 ordinary chondrites. Colony and ALHA77307 have abundant red CL matrices and grains, with inclusions and chondrules which are either non-luminescent or whose mesostasis luminesces white (probably over-exposed blue) or yellow. Kainsaz is also McSween type I, but has CL properties intermediate to those of the other type I and the type II CO chondrites, tending towards the latter.

With the exception of Kainsaz, for which CL and petrologic data suggest a much lower value than TL sensitivity, the types assigned by TL, CL and mineral chemistry are in reasonable agreement. However, there are two points to stress. (1) CO chondrites differed significantly in thermal history from the ordinary chondrites. Unlike CO chondrites, ordinary chondrites contain a single metamorphism-dependent TL peak which shifts from 100 to 200C with increasing metamorphism, the change in peak temperature occurs at metamorphic intensities equivalent to type 3.5. Since the change is thought to be associated with disordering of feldspar [18], type 3.5 ordinary chondrites probably experienced temperatures of 500-600C. Apparently while some CO chondrites suffered devitrification of their chondrule glasses to the extents observed for ordinary chondrites of type 3.5-3.8, they did not experience the same relatively high temperatures. Presumably either the CO chondrites suffered metamorphism for much longer periods than the ordinary chondrites [6] or their higher water content facilitated devitrification and other metamorphic reactions. The recent calculations of Jones and Rubie [20] also indicate that the metamorphism of the CO chondrites was the result of various times at a modest range of temperatures below 600C. (2) While CL data (and the mineral and matrix compositions) suggest that metamorphic intensities for Colony and ALHA77307 were comparable to those of type 3.0-3.1 ordinary chondrites, their TL sensitivities are higher. This most probably reflects interference of the metamorphic peak by the higher temperature TL peaks, and we prefer the 3.0 assignment for Colony and ALHA77307. We also suspect the TL assignments for LEW85332 and the MAC87300 group are high by about 0.1, and this is reflected in our recommended petrographic type assignments in Table 1.

Conclusions TL sensitivity, CL petrography and mineral and matrix composition data suggest that the CO chondrites form a metamorphic sequence analogous to that of type 3 ordinary chondrites and subdivision in an analogous manner is appropriate. However, while these observations suggest that the degree of metamorphic alteration for some CO chondrites may approach that observed for type 3.6-3.8 ordinary chondrites, induced TL data make it clear that they did not experience temperatures as high. CO chondrites did not experience temperatures greater than those experienced by type 3.5 ordinary chondrites (presumed to be 500-600C). LEW-85332, MAC87300/87301/88107 and Y-81020 have glow curves similar to those of Colony and ALHA77307; these may be either particularly primitive CO chondrites, members of a new primitive carbonaceous chondrite class, or intermediate between existing carbonaceous chondrite classes. Our recommended petrographic types for the present samples are listed in Table 1.

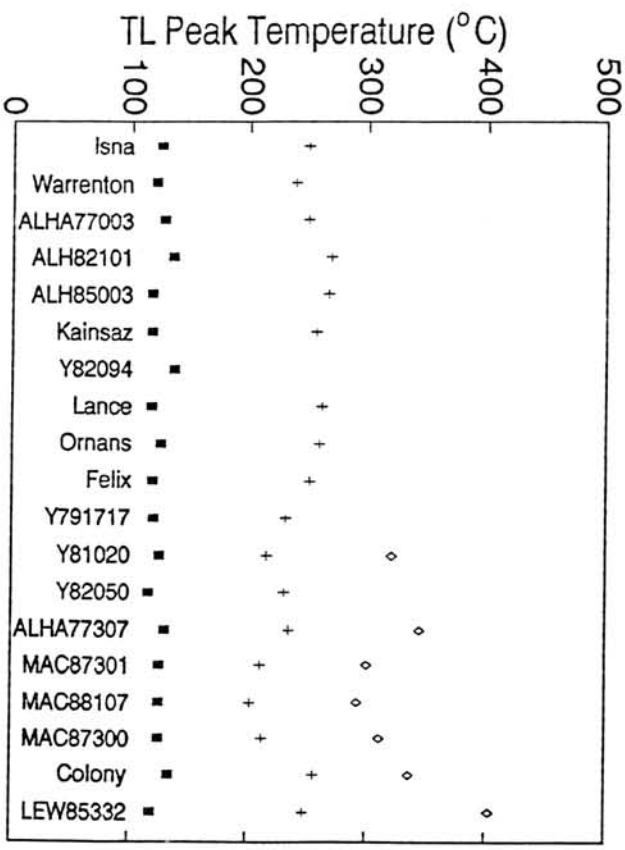

Fig. 1. TL peak temperatures for CO and CO-like chondrites. The 100-120C peak is metamorphism-related, the others are not.

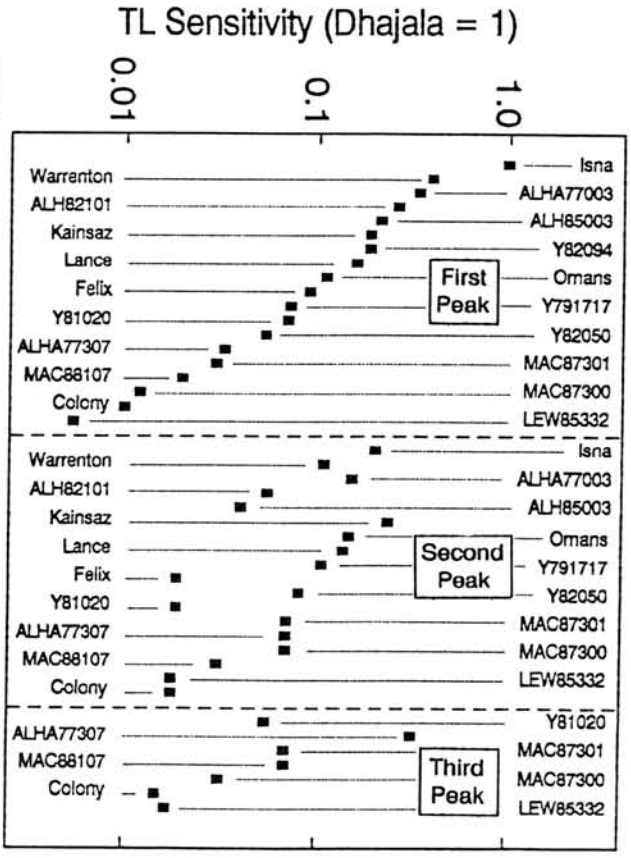

Fig. 2. TL sensitivity data for the present samples compared with those of the CO chondrites of Keck and Sears [6].

Supported by NASA grant NAG9-81.

References 1. Kallemeyn G.W. and Wasson J.T. (1981) GCA 45, 1217-1230. 2. Clayton R.N. and Mayeda T.K. (1984) EPSL 67, 151-161. 3. McSween H.Y .(1977) GCA 41, 477-491. 4. Rubin A.E. (1989) Meteoritics 24, 179-189. 5. Keck B.D. and Sears D.W.G. (1986) Meteoritics 21, 411-412. 6. Keck B.D. and Sears D.W.G. (1987) GCA 51, 3013-3021. 7. Scott E.R.D. and Jones R.H. (1990) GCA (submitted). 8. Guimon R.K. and Sears D.W.G. (1986) Meteoritics 21, 381-383. 9. Sears D.W., Grossman J.N., Melcher C.L., Ross L.M. and Mills A.A. (1980) Nature 287, 791-795. 10. Yanai K. and Kojima H. (1987) Photographic Catalog of the Antarctic Meteorites NIPR, Tokyo. 11. Graham A.L. and Yanai K. (1986) Proc. 10th Symp. Antarct. Meteor., 1985, 167-180. 12. Rubin A.E. and Kallemeyn G.W. (1990) LPS XXI, 1045-1046. 13. Scott E.R.D., Taylor G.J., McSween H.Y., Okada A., Maggiore P., Keil K. and McKinley S.G. (1981) Meteoritics 16, 385. 14. Rubin A.E., James J.A., Keck B.D., Weeks K.S., Sears D.W.G. and Jarosewich E. (1985) Meteoritics 20, 175-195. 15. Sears D.W.G., DeHart J.M., Hasan F.A. and Lofgren G.E. (1989) In Spectroscopic Characterization of Minerals and Their Surfaces (L.M. Coyne, S.W.S. McKeever and D.F. Blake, eds.), 190-222. 16. DeHart J.M. and Sears D.W.G. (1986) LPS XVII, 160-161. 17. DeHart J.M., Lofgren G.E. and Sears D.W.G. (1990) GCA (submitted). 18. Sears D.W.G. (1988) Nucl. Tracks Radiat. Meas. 14, 5-17. 19. Guimon R.K., Keck B.D. and Sears D.W.G. (1985) GCA 49, 1515-1524. 20. Jones R.H. and Rubie D.C. (1990) LPS XXI, 583-584.

Thursday, May 31, 1990

0900-1815 *Symposium, Auditorium*

1010-1125 *Special Session (I); CI Chondrites*

1125-1345 *Special Session (II); Unique Meteorites*

1345-1730 *Special Session (III); Lunar Meteorites*

REE ABUNDANCES AND COSMOCHRONOLOGY OF SEVERAL UREILITES

Kazuya Takahashi[1] and Akimasa Masuda[2]
1) The Institute of Physical and Chemical Research
2) Department of Chemistry, The University of Tokyo

Ureilites are characterized by chemically ultramafic composition and the existence of carbonaceous material between silicate grains. According to the mineralogical study by Takeda (1987), ureilites have been roughly classified into 3 groups, calcic, ordinary and magnesian groups and planetesimal collision model has been proposed for the genesis of ureilites. We have performed the Rb-Sr and Sm-Nd dating and measurements of REE abundances on MET-78008, one of the most Ca-rich ureilites. This meteorite consists of mainly olivine and augite. Each mineral was separated by fractional dissolution and heavy liquid separation methods.

REE patterns of MET-78008 are shown in Fig. 1 with the patterns of separated samples and the pattern of ALH-77257(Shimizu and Masuda, 1981). ALH-77257 belongs to the ordinary group and olivine is dominant in mineral composition. As shown in Fig. 1, the REE patterns of ALH-77257 are quite different from each other and this difference is considered to reflects the difference of mineral and chemical compositions between these two meteorites.

The result of Rb-Sr dating on MET-78008 is shown in Fig. 2. In this isochron, following three characteristics can be seen. (1) The age is 4.01 $\pm$0.06 b.y. (2) The point of whole rock falls on the 4.5 b.y. isochron formed by other meteorites such as Juvinas eucrite. (3) Although the analytical error limits are small for each sample , the deviation of each data point from the calculated isochron of 4.01 b.y. and each data are rather large. This age, 4.0 b.y., can be regarded as the age of last igneous event or shock metamorphism. The second characteristic mentioned above suggests that the Ca-rich feature of this meteorite had been established 4.5 b.y. ago. On the other hand, the Sm-Nd isotopic data of the whole rock sample have been obtained to be $^{143}Nd/^{144}Nd=0.515153$ and $^{147}Sm/^{144}Nd=0.2801$. The model age of whole rock, calculated from these values and the initial value of solar system, is around 4.5-4.6 b.y. This result is consistent with the Rb-Sr data mentioned above. This Sm-Nd isotopic data also suggest that the difference of REE patterns between MET-78008 and ALH-77257 shown in Fig 1. had been caused at the stage of differentiation 4.5-4.6 b.y. ago. The third characteristic of Rb-Sr system indicates that the scale of the differentiation 4.0 b.y. ago was not so large or that many small scale metamorphism had occurred. From these observations, it is considered that MET-78008 would have been formed from Ca-rich source material, whose REE patters had been already fractionated, 4.0 b.y. ago and this source material might have undergone large differentiation 4.5 b.y. ago. And these observations do not indicate the single collision by planetesimal for the genesis of ureilites but indicate plural and complicated process. We are going to analyze the different type of ureilite, Y-791538 (Mg-rich), to compare with the MET-78008.

References:
Takeda (1987) Earth Planet. Sci. Lett., 81, 358-370.
Shimizu and Masuda (1981) Mem. Natl. Inst. Polar Res., Spec. Issue, 20, 211-220.

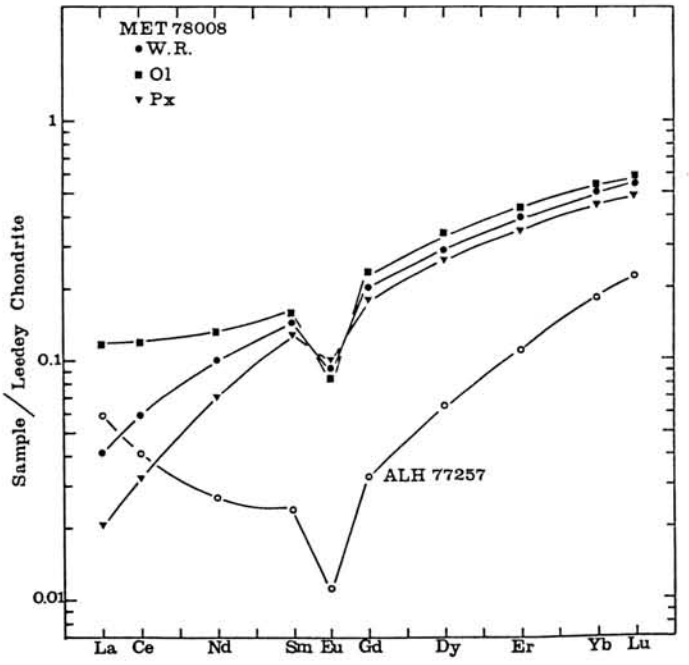

Fig. 1 REE abundance pattern of some ureilite samples

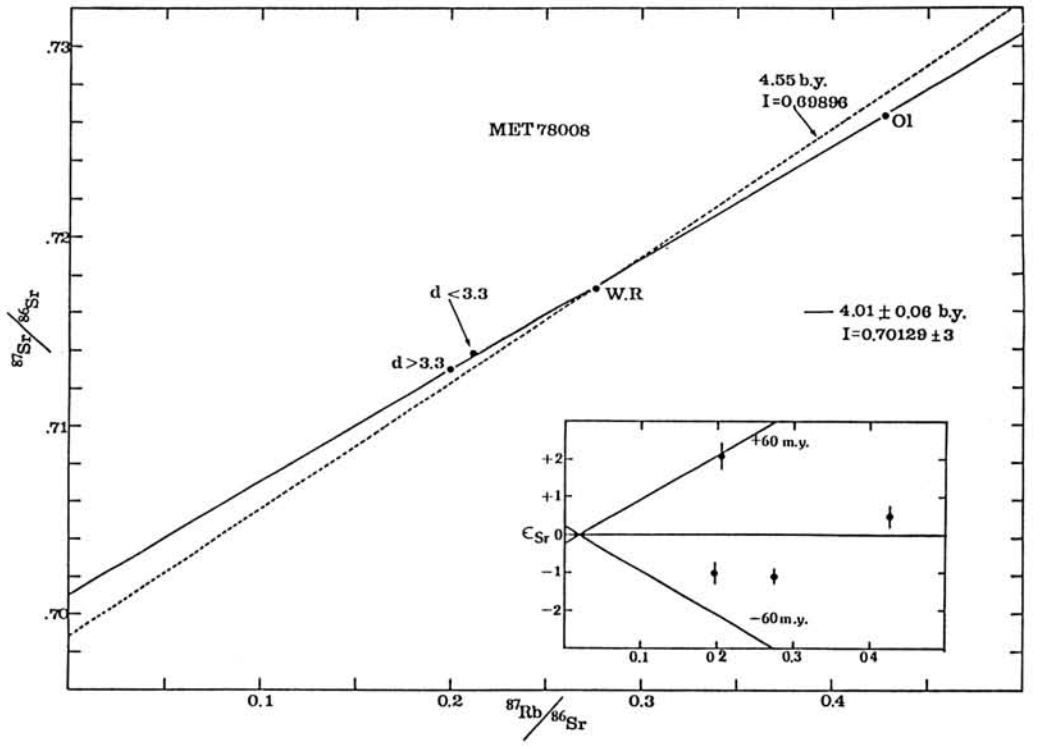

Fig. 2 The Rb-Sr isochron plot of MET-78008

REE and Y Abundances in Allende Group II Inclusions

Shigekazu Yoneda, Kazunori Shinotsuka, Hisanori Mihara,
Hisao Nagai and Masatake Honda
College of Humanities and Sciences, Nihon University
Sakurajousui, Setagaya, Tokyo 156, Japan

Extensively fractionated mixtures of rare earth elements in Group II inclusions in Allende and other meteorites are considered to be condensed materials from the residual gases which lost highly refractory elements in the early solar nebula (1). Although Ho and Y have almost the same ionic radii and partition coefficients in igneous processes, a different behavior between Ho and Y could be expected because of their different volatilities.

In this study, the abundances of rare earth elements and Y in the Allende and other meteorites, especially Allende Group II inclusions are investigated by radiochemical neutron activation analyses (neutron dose:10^{17}-10^{18}n/cm^2). The activities of REE are determined by γ-ray countings and those of Y are β-ray countings for ^{90}Y. The details of the analytical procedure are described in ref.(2).

An inclusion named 3-C (3-C3 and 3-C5) in the Allende meteorite is a typical Group II fine-grained inclusion containing spinel, and showing a fractionation between light and heavy REE, and a large positive Tm anomaly (Fig.1). Allende 4-A and 5-A are also Group II inclusions. Allende 2-C has high REE abundances with a negative Ce anomaly but no L-H REE fractionation. Ness County fusion crust also has a negative Ce anomaly and small negative slope pattern to H REE. Murchison 1-M is enriched in H REE except for Tm and Yb; it seems to be a mixture of a counter part of Group II inclusions and bulk chondritic materials. Ordinary chondrites (Ness County: NCA1, NCB1; Jilin), terrestrial rocks (JB-1a, JB-2, JB-3) and all of the inclusions other than Group II have no evidence of different behavior between Ho and Y, and only Allende Group II inclusions are found in a depletion of Y relative to Ho (Fig.2). C1-normalized Y/Ho ratios of Group II inclusions are changed from 0.1 to 0.6. Since Allende 3-C5 sample (Y/Ho:0.6) is supposed to be diluted by chondritic sources, Y/Ho of Group II is estimated to be less than 0.2.

References

(1)Boynton (1975) *Geochim. Cosmochim. Acta*, **39**,569-584
Davis and Grossman (1979) *Geochim. Cosmochim. Acta*, **43**,1611-1632
(2)Yoneda *et al.*(1989) Abstract on *14th Symp. Ant. Met.*,94-95

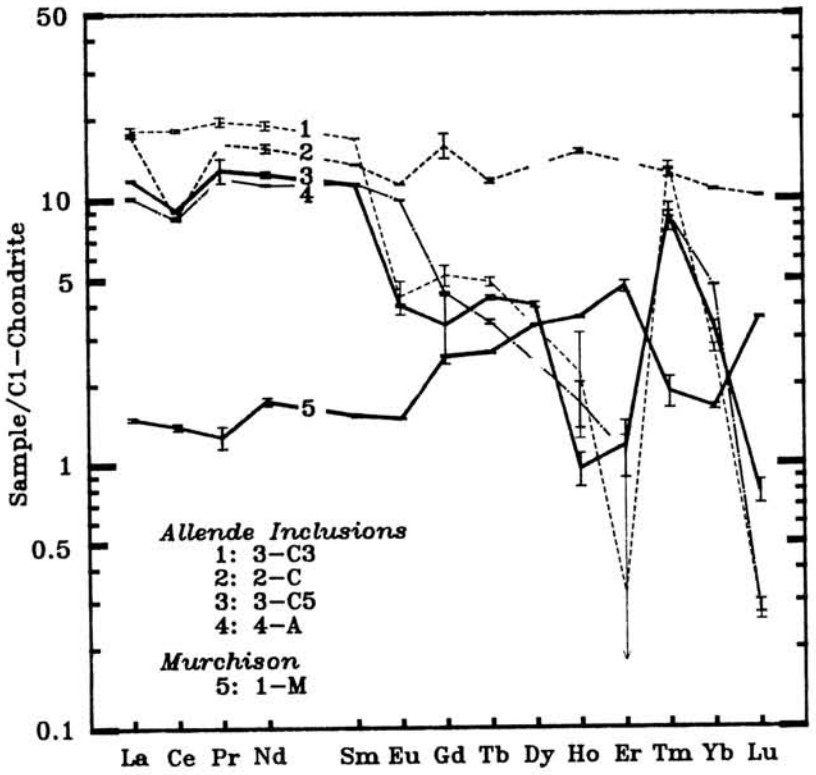

Fig. 1 REE patterns of Allende and Murchison inclusions.

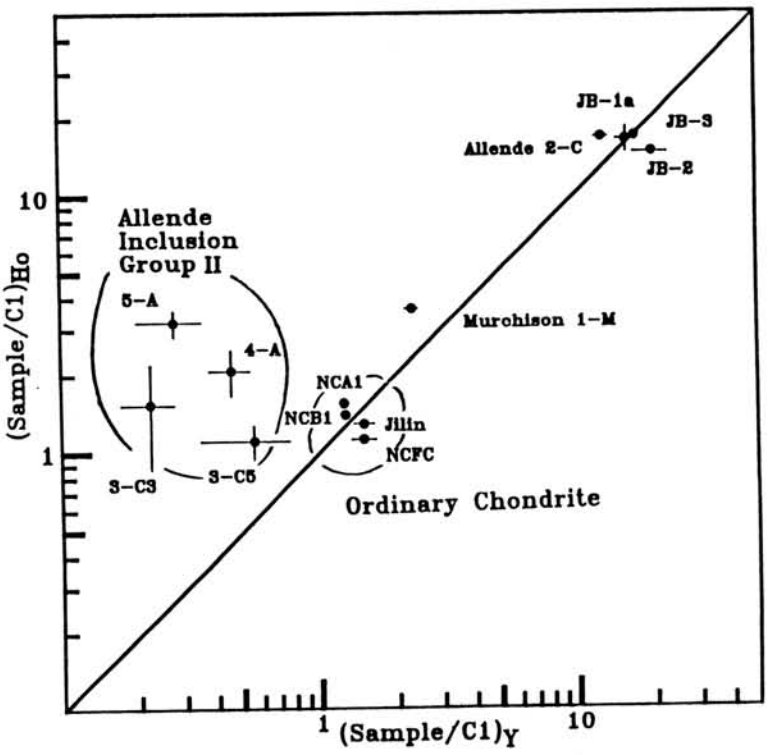

Fig. 2 Correlation between C1-normalized Y and Ho. Allende Group II inclusions are depleted in Y.

ANTARCTIC WEATHERING AND REE REMOBILIZATION IN ANTARCTIC EUCRITES. Christine Floss and Ghislaine Crozaz. Earth and Planetary Sciences Department and McDonnell Center for the Space Sciences, Washington University, St. Louis, MO 63130 USA.

In recent years, the Antarctic meteorite collections have become increasingly important additional sources of extraterrestrial material. Although a weathering classification exists for these meteorites, it was originally assumed that storage in the Antarctic "icebox" had left most of these rocks largely unaltered. However, recent evidence suggests that remobilization of some elements, including the rare-earth-elements (REE), may be widespread.

During most geochemical processes, the REE in the trivalent state are fractionated as a smooth function of ionic radius. Anomalies in the REE pattern are commonly exhibited by Eu, which can exist in the divalent state under reducing conditions. Less frequently, Ce is oxidised to Ce (IV). Terrestrially this occurs primarily in the marine environment. The lower solubility of tetravalent Ce than the trivalent REE [1] results in a strong negative Ce anomaly for seawater and many associated authigenic and biogenic phases. Exceptional are ferromanganese nodules which apparently scavenge Ce and thus have large positive anomalies. Studies on altered submarine basalts [2,3] show that Ce behaves inconsistently, being either enriched or depleted relative to basalt interiors; different water-to-rock ratios may be responsible. In meteorites, numerous examples of Ce anomalies have been reported [4-6]. Although there are exceptions [7], the bulk of Ce-anomalous meteorites appear to come from Antarctica, and have positive anomalies, with reported Ce/Ce* (where Ce is the measured value and Ce* the value obtained from interpolation between La and Pr) ratios up to 2.56. These studies also suggest that the eucrites dominate the population of Ce-anomalous Antarctic meteorites.

Shimizu *et al.* [8] analysed inner and outer portions of the polymict eucrite ALHA 78132, in an attempt to determine if the anomalies could be attributed to terrestrial or pre-terrestrial processes. An inner sample of the meteorite has a small negative Ce anomaly, while four outer portions have positive ones as well as lower REE abundances. The latter also have slightly lower contents of FeO, MgO and CaO. The authors concluded that weathering in the Antarctic ice was responsible for these observations.

A recent comparison of Antarctic and non-Antarctic eucrites [9] has revealed interesting differences between the two groups. A significant fraction of Antarctic eucrites have high Ce/La ratios at low La concentrations, while non-Antarctic eucrites lack this component. The implication is that Ce is oxidised and preferentially retained over the trivalent REE during alteration in the Antarctic ice.

In this study we have focussed on one Antarctic polymict eucrite, LEW 85300. Our specific goal was to determine in which phase or phases the Ce anomalies were found and whether or not they were spatially associated with cracks or a given lithology. The meteorite has been classified as weathering grade A/B, with few rust stains and minor fractures. We used secondary ion mass spectrometry (SIMS) to analyse individual minerals in two polished thin-sections. The sections contain a number of distinct basaltic clasts, consisting of calcic plagioclase and inverted pigeonite, embedded in a glassy matrix. Isolated fragmented and shocked plagioclase and pyroxene grains also occur in the matrix. One of the thin-sections also contains patches of silica, which optically appear to have undergone some alteration. We primarily selected fresh-looking, seemingly unweathered pyroxene and plagioclase grains, although a few analyses were also made of the silica and the glassy matrix. The bulk of the REE in the eucrites must reside in tiny Ca phosphate grains, as they do in many other achondrites. If weathering took place in this meteorite, the phosphates would probably be affected first. However, we were unable to find any to analyse in our thin-sections.

Of 17 plagioclase grains analysed, only two have Ce anomalies, both of them negative (Ce/Ce* = 0.34 and 0.53). Figure 1 shows the C1-chondrite normalized REE patterns for two adjacent plagioclase grains; the plagioclase with the negative anomaly has the same Ce abundance as its normal counterpart, but higher abundances of the other REE. Three analyses

of glassy matrix have relatively flat, non-anomalous REE patterns with concentrations of ~10 x C1, similar to typical bulk eucrite analyses. Pyroxene analyses are more interesting: of 52 apparently unweathered pyroxene grains, 32 have positive Ce anomalies ($1.64 \leq Ce/Ce^* \leq 30.0$), 6 have negative anomalies ($0.31 \leq Ce/Ce^* \leq 0.54$), and the remainder are normal. Shown in Figure 2 are the REE patterns for the pyroxene grains with the largest positive and negative Ce anomalies. A traverse of eight analyses across a single pyroxene grain revealed anomalies of both types, but no obvious trend. Positive and negative Ce anomalies are found adjacent to each other, and next to non-anomalous analyses. A magmatic source for the Ce anomalies is thus ruled out. A plot of Ce/Ce* ratio vs. Nd concentration shows that the highest ratios are found at low Nd concentrations, consistent with leaching of the REE in the Antarctic ice and preferential retention of Ce. Deposition of Ce-depleted REE might then account for the negative Ce anomalies found in some plagioclase and pyroxene.

Three analyses in a large patch of altered silica reveal variably fractionated REE patterns (Figure 3) with large negative Ce anomalies. Major and minor element variations in the analyses corresponding to the two upper patterns show the presence of pyroxene, consistent with the observation by [10] that such silica patches contain granules of orthopyroxene. The third analysis appears to consist only of silica. Because silica is an inhospitable host for the REE, we believe that the pattern shown in Figure 3 may be caused by weathering. It appears that the silica inherited some of the mobilized REE, and we furthermore suggest that these REE were originally hosted in Ca phosphate. The LREE-enriched pattern with a negative Eu anomaly is what one might expect if the REE were leached from phosphates, with Ce being preferentially left behind.

The anomalies appear to be randomly distributed in all clasts, as well as in the matrix. They are not preferentially associated with a given lithology, nor are they necessarily located near fractures in the sections. The exact mechanism for REE mobilization is unclear, but it is most probably due to weathering in the Antarctic ice. Even samples which appear relatively fresh and unweathered have apparently undergone some alteration, the extent of which varies on the microscale. The pyroxene contains extensive microcracks along cleavage planes; this may have facilitated remobilization in this mineral. This study has important implications for the use of REE and other trace element data in petrogenetic modelling of the Antarctic eucrites. Terrestrial processing must be ruled out before such data can be used to interpret the petrogenesis of these meteorites.

[1] A.J. Fleet (1984) In *Rare Earth Element Geochemistry*., P. Henderson (ed.) 510 pp.
[2] F.A. Frey, W.B. Bryan and G. Thompson (1974) J. Geophys. Res. **79**, 5507-5527.
[3] J.N. Ludden and G. Thompson (1979) Earth Planet. Sci. Let. **43**, 85-92.
[4] N. Nakamura and A. Masuda (1980) Proc. 5th Symp. Ant. Met., 159-167.
[5] H. Shimizu and A. Masuda (1981) Proc. 6th Symp. Ant. Met., 211-220.
[6] H. Shimizu and A. Masuda (1982) Proc. 7th Symp. Ant. Met., 145-152.
[7] A. Masuda and T. Tanaka (1980) Earth Planet. Sci. Let. **49**, 109-116.
[8] H. Shimizu, A. Masuda and T. Tanaka (1983) Proc. 8th Symp. Ant. Met., 341-348.
[9] D.W. Mittlefehldt and M.M. Lindstrom (1990) Geochim. Cosmochim. Acta (submitted).
[10] R.H. Hewins (1990) LPSC XXI, 509-510.

Figure 1

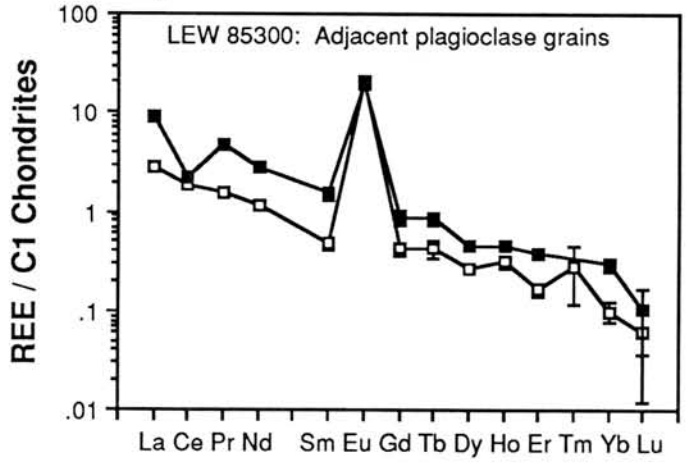

Figure 2

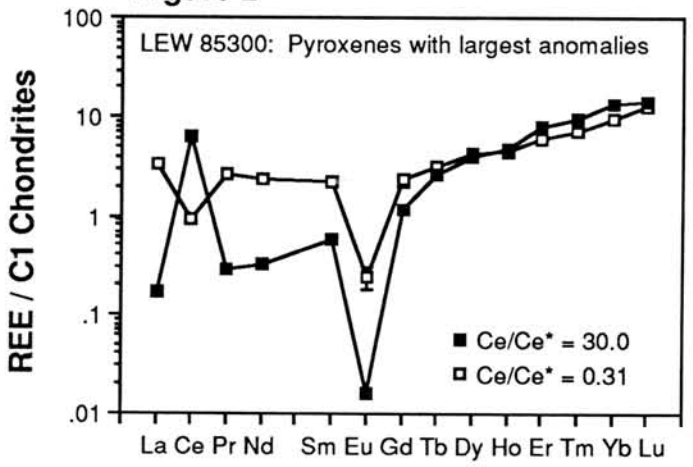

Figure 3

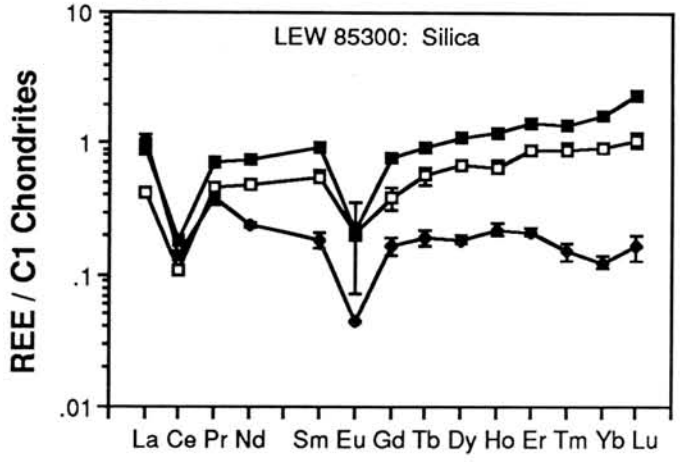

THE METAMORPHOSED CARBONACEOUS CHONDRITES - A NEW METEORITE GROUP?

Geiger T.[1,2] and Bischoff A.[1]
[1] Institute of Planetology, University of Muenster, Wilhelm-Klemm-Str. 10, 4400 Muenster, FRG. [2] Institute of Meteoritics, University of New Mexico, Dept. of Geology, Albuquerque, NM 87131, USA.

In comparison to other meteorite groups, less work has been done studying the metamorphosed carbonaceous chondrites (C4-6). One of the reasons might be the small number of samples available. However in the last few years more meteorites of this group were collected on Antarctic ice-fields by Japanese and U.S. expeditions. To date 25 different meteorites have been classified as C4-6 carbonaceous chondrites - 17 samples are considered in this study. These are Karoonda, Coolidge, Mulga (West) and the Antarctic samples from Allan Hills (82135, 84038, 84096, 85002), from Elephant Moraine (83311, 87507, 87514, 87519, 87626, 87529,87860), from Lewis Cliff (86258, 87009), from Pecora Escarpment (82500), and from the Yamato Mountains (6903). Detailed petrographic studies are only given for Karoonda, Coolidge, and PCA82500 by *Scott & Taylor* (1985) and *McSween* (1977a,b). *Binns et al.* (1977) studied Mulga (West) and *Okada* (1975) Y-6903. The Allan Hills samples were investigated recently by *Geiger & Bischoff* (1989b, 1990).
Bulk chemical analysis as well as oxygen isotopic data are reported by *Kallemeyn & Wasson* (1982), *Kallemeyn* (1985, 1987, 1989), and by *Clayton & Mayeda* (1984, 1989). A comparison of the results from petrographic, bulk chemistry, and oxygen isotopic analyses of these meteorites reveal discrepancies in the properties used for classification. Based on oxygen isotopic data almost all analyzed samples plot in the range found for the CO3 chondrites *(Clayton & Mayeda* 1989). However bulk chemical analysis by neutron activation analysis classifies most of these meteorites intermediate between CO-CM and CV (*Kallemeyn* 1987, 1989). From a petrographic point of view Karoonda and Coolidge have been classified as CO4, and CV4 (*McSween* 1977a,b), respectively.
Here we report the first results from petrographic studies of the Elephant Morraine and Lewis Cliff samples.

All samples of the metamorphosed carbonaceous chondrites can be subdivided into two main groups, reduced and oxidized (*Geiger & Bischoff* 1989b, 1990). The reduced group is comprised of only two meteorites, Coolidge and ALH84096. All other samples are in the oxidized group. This differentiation is based on the presence of metal or magnetite and is not connected to McSween's (1977b) subdivision made for the CV group.
Huss et al. (1981) have shown that matrix olivines in ordinary chondrites become more

homogeneous and coarse grained with increasing petrologic type. A similar sequence is observed in C3-6 carbonaceous chondrites. Coolidge with a very fine-grained, dark matrix and 67 Vol% chondrules (*McSween* 1977b) and LEW87009 with a transparent, coarse grained matrix and no chondrules visible, seem to be the end members of this sequence. Coolidge has been classified as CV4, but from textural features it appears intermediate between CV3 and CV4, whereas LEW87009 seems to be the first meteorite classified as C6. Between these two end members of the sequence one can find intermediate stages of metamorphism. These stages are characterized by increasingly blurred chondrules and coarsening of matrix material. However, it is not possible to establish a metamorphic sequence only by considering textural features, because most of the samples have undergone brecciation, which complicates exact classification.

In all the investigated samples the matrix olivines are well equilibrated. Most mean Fa-contents plot between 27 and 33 mol% Fa. with very similar standard deviations of 0.6 to 1.0 Mol%. One exception is Coolidge with mean Fa content of matrix olivines of 14.6±0.7 mol% Fa (*Geiger & Bischoff* 1989b). These well equilibrated matrix olivine in Coolidge do not fit with textural features, which are more C3 like as mentioned above. *Scott & Taylor* (1985) report very low CaO contents of matrix olivines as evidence for a metamorphic origin of these homogeneous olivines. The low-Ca-pyroxenes in the matrix of all analyzed samples are not as well equilibrated as the olivines. This is because the cation diffusion rates in olivines are much higher than in pyroxenes. In all investigated meteorites the feldspars in the matrix show a wide variation of composition, e.g. in PCA82500 from 13 to 95 mol% An (*Geiger & Bischoff* 1989b).

The opaque mineralogy of all Antarctic meteorites in the oxidized group is surprisingly similar. Only the abundance of opaque minerals varies from sample to sample. But magnetite is always the most abundant opaque phase. It occurs mostly in two different populations. First as small grains finely dispersed in the matrix on grain boundaries of olivine grains or as inclusions in olivines. And second as larger (up to 1mm) grains. All these larger grains contain exsolution features of ilmenites and spinels (*Geiger & Bischoff* 1990).

The oxidized group has also similar sulfide occurrences. The most abundant sulfides are pyrrhotite intergrown with pentlandite. Small amounts of pyrite and chalcopyrite occur as well.

Another peculiarity of the metamorphosed carbonaceous chondrites seem to be the occurrence of platinum group minerals. *Geiger & Bischoff* (1989a,b) report the minerals laurite-ehrlichmanite, cooperite, chengbolite, and alloys containing high amounts of refractory siderophile elements. These phases have been described previously only in

terrestrial assemblages but not in meteorites.
The metals in Coolidge and ALH84096 are different. The kamacites in Coolidge have high Ni contents of 7% Ni and Co contents of about 0.5% Co, whereas the taenite composition is about 18% Ni and 0.3% Co. *Scott & Taylor* (1985) report fast cooling rates of >> 10^3 °/m.y.. Kamacites in ALH84096 have 5% Ni and very high Co contents of about 2.7% Co. Taenites are varying between 34 and 48% Ni and 1.06 to 0.62% Co. The sulfide in these two meteorites of the reduced group is troilite.

There are difficulties in classifying the samples of the metamorphosed carbonaceous chondrites. The more strongly the samples are metamorphosed the more difficult it is to associate them with the CO or CV group based on petrographic features. These difficulties hold also for a classification based on bulk chemical or oxygen isotopic data. The question that then arises is: Are the metamorphosed carbonaceous chondrites related to the CO or CV groups at all? That means, are they a product of heated CO or CV precursors? Or are they derived from parent bodies which are independent bodies but still similar to CO or CV bodies. Based on the present results the possibility remains that the analyzed metamorphosed C-chondrites form a new and independent group of carbonaceous chondrites. However, this conclusion has to be confirmed by further investigations.

References:

Binns R.A. et al. (1977), Meteoritics 12, 179; *Clayton R.N. & Mayeda T.K.* (1984), EPSL 67, 151-161; *Clayton R.N. & Mayeda T.K.* (1989), LPSC XX, 169-170; *Huss et al.* (1981), GCA 45, 33-51; *Geiger T. & Bischoff A.* (1989a), LPSC XX, 335-336; *Geiger T. & Bischoff A.* (1989b), Meteoritics 24, 4, 269; *Geiger T. & Bischoff A.* (1990), LPSC XXI, 409-410; *Kallemeyn G.W.* (1985), Abstr. 10th Symp. of Antarctic Meteorites, 45; *Kallemeyn G.W.* (1987), Mem. Natl Inst. Polar Res., Spec. Issue 46, 151-161; *Kallemeyn G.W.* (1989), Meteoritics 24, 4, 283; *Kallemeyn G.W. & Wasson J.T.* (1982), GCA 46, 2217-2228; *McSween H.Y.Jr.* (1977a), GCA 41, 477-491; *McSween H.Y.Jr.* (1977b), GCA 41, 1777-1790; *Okada A.* (1975), Mem. Natl Inst. Polar Res., Spec. Issue 5, 14-44.

Special Session (I)

CI Chondrites

Special Session (II)

Unique Meteorites

MINERALOGY OF CLASTS IN THE Y-82162 CHONDRITE (C1)

Ikeda, Y.
Ibaraki University, Mito, 310

The Y-82162 chondrite shows a breccia-in-breccia structure and consists of many kinds of clasts, mineral fragments, ordinary-chondrite fragments, and matrix. They are shown in Table 1, and the mineral assemblages are in Table 2.

Clasts in Y-82162 are smaller than about 300 microns across and show various textures and mineral assemblages. The phyllosilicate clasts consist mainly of sodian talc and chlorite, and sodian talc-rich clasts are predominant. Carbonate clasts often show a concentric texture of ankerite core and dolomite rim.

Unusual clasts are very-fine-grained aggregates, and CaO-rich unusual clasts often have a carbonate mantle which surrounds completely a fine-grained oxide aggregate including periclase, "Beta-phase", and "Alpha-polyphase". The periclase is smaller than 10 microns and surrounded by Beta-phase which has a chemical composition similar to $8FeS \cdot 9(Ca_{0.8}Fe_{0.2})O \cdot 0.3P_2O_5$. Alpha-polyphase is fine-grained aggregates having a chemical composition between periclase (or an aggregate of FeO-poor periclase and magnetite) and dolomite. The periclase and Alpha-polyphase are intimately associated with carbonates, suggesting that they were produced from Mg-Fe-carbonate by the decomposition.

Magnetite-rich clasts include MnO-poor magnetites showing various morphology; framboidal aggregates, spheroidal grains, plaquettes, and irregular grains. Chlorite and dolomite occur in magnetite-rich clasts. Matrix is defined to be fine-grained aggregates of tiny grains smaller than 1 micron, and consists mainly of chlorite.

Chondrite fragments are probably projectiles colliding on the carbonaceous parent body during the gardening process. They seem not to have suffered any alteration, suggesting that Y-82162 had not suffered any reaction during and after the gardening process.

Table 1. The constituents of Y-82162.

Phyllosilicate Clasts	Sodian Talc-rich Clasts
	Chlorite-rich Clasts
Carbonate Clasts	
Unusual Clasts	CaO-rich Unusual Clasts
	MnO-rich Unusual Clasts
	CaO-MnO-poor Unusual Clasts
Apatite-Magnetite-rich Clasts	
Magnetite-rich Clasts	
Apatite-rich Clasts	
Mineral Fragments	Sulfide Mineral Fragments
	Oxide Mineral Fragments
	Phosphate Mineral Fragments
Matrix	Others
Chondrite Fragments	

Table 2. Mineral assemblages of clasts and fragments in the Y-82162 carbonaceous chondrite.

	Sodian Talc Clasts	Chl-rich Clasts	Carbo-nate Clasts	Ca-rich Unusual Clasts	Mn-rich Unusual Clasts	Mt-rich Clasts	Ap-rich Clasts	Sulfide Mineral Frag.	Oxide Mineral Frag.	Matrix	Chondrite Fragments
Sodian Talc	+++	+					+				
Chlorite	+	+++				+	+			+++	
Ankerite	+	+	+++	+			+				
Dolomite			+	+		+					
Rhodochrosite					+						
Magnetite		+	+	+	+	+++			+		
Periclase				+							
Alpha-polyphase			+	+++							
Beta-phase				+							
Gamma-polyphase				+	+++						
Delta-polyphase					+++						
Ilmenite									+		
Apatite	+		+	+		+	+++				
Pyrrhotite	+	+	+	+	+		+	+			
Pentlandite								+			
Chalcopyrite								+			
Awaruite								+			
Ferrihydrite								+			
Olivine											+
Protoenstatite											+
Low-Ca Cpx											+
Augite											+
Fassaite											+
Plagioclase											+
Chromite											+
Whitlockite											+
Troilite											+

Alpha-polyphase is a fine-grained aggregate probably of Gamma-polyphase and dolomite.
Beta-phase has a chemical composition similar to $8FeS \cdot 9(Ca,Fe)O$ with a small amount of P.
Gamma-polyphase is a fine-grained aggregate probably of FeO-poor periclase and magnetite.
Delta-polyphase is a fine-grained aggregate probably of Gamma-polyphase and rhodochrosite.

THE ORIGIN OF PHYLLOSILICATES IN THE YAMATO-82162 CI CARBONACEOUS CHONDRITE

Kazushige Tomeoka

Mineralogical Institute, Faculty of Science, University of Tokyo, Hongo, Tokyo 113, Japan

CI and CM carbonaceous chondrites consist mainly of fine-grained phyllosilicates, which are responsible for most of the water (5 to 20 H_2O wt%). The origin of the phyllosilicates has been interpreted in terms of condensation from the solar nebula or aqueous alteration on the meteorite parent body, although most previous studies have suggested the latter origin. The most convincing evidence for the aqueous alteration is probably the presence of veins of sulfates and carbonates in CI chondrites [1-4]. However, such veins of phyllosilicates have not been known. I present here the first observation of fracture-filling veins of phyllosilicates in the Yamato-82162 CI chondrite. I studied the phyllosilicates by using scanning and transmission electron microscopes (SEM and TEM) and found that they are coherent intergrowths of Fe-bearing, Na-rich saponite and minor chlorite-like phyllosilicate, thus they are similar to the phyllosilicates in the Orgueil CI chondrite [5].

Y82162 is one of the new CI chondrites from Antarctica that has been a subject of the consortium study for the last couple of years. It can be classified into CI group but shows many unusual mineralogical and chemical features [e.g., 6,7]; thus, it may have experienced a considerably different history from other CI chondrites. Like many other carbonaceous chondrites, it is a breccia composed of submillimeter to millimeter clasts. In addition to the fine-grained phyllosilicates in the matrix, this meteorite contains abundant coarsely crystallized phyllosilicates. Our previous study showed that they occur as isolated clusters ranging from 50 to 300 μm in diameter [5]. The present study reveals that they also occur as fracture-filling veins, which vary in width from 1 to 200 μm and extend up to 500 μm. Some veins branch out to narrower veins (2 to 5 μm in width), forming a network. They terminate at clast boundaries (Fig. 1), which indicates that the phyllosilicate veins were formed prior to some of the brecciation events that occurred on the meteorite parent body.

The phyllosilicates in the veins contain major amounts of Mg and minor Fe, Al and Na. The phyllosilicates in the clusters and the veins show no compositional differences [cf. Table 3 in Ref. 6]; thus they are probably the same phyllosilicates. High-resolution TEM observations show that the phyllosilicates occur in coherent, disordered intergrowths of two types of layers; one has an interlayer spacing of ∿10 A, and the other has variable spacings from 13 to 15 A. The latter commonly occur as single layers. The 10-A layers probably correspond to Na-rich saponite. Based on the spacing, the layers of wider spacings may be chlorite. The coherent intergrowth of the two different types of phyllosilicates resembles that in Orgueil, although the phyllosilicates in Orgueil consist of saponite and serpentine.

It has been suggested that CI chondrites have undergone a multi-stage aqueous alteration and that the sulfate veins formed in a relatively late alteration stage [1-3, 5]. In Orgueil, the coarse phyllosilicates appear to have been degraded to finer phyllosilicates and altered to matrix during the aqueous alteration that produced the sulfate veins [5]. From these observa-

tions and evidence, Tomeoka et al. [6] suggested that Y82162 has not experienced the late aqueous alteration stage, thus it does not contain sulfates and retains abundant coarse phyllosilicates. The present study shows that the coarse phyllosilicates in the CI chondrites were probably produced initially as vein-fillings during the aqueous alteration. Therefore it is conceivable that the phyllosilicates in the CI chondrite matrices formed through the repetition of vein formation and degadation by the activity of aqueous solutions.

The presence of phyllosilicate veins suggests that the aqueous alteration responsible for the phyllosilicate formation occurred in regolith regions, simultaneously with the period of regolith gardening. A recent theoretical study suggests that the water probably accreted onto the parent body originally as ice [8]; thus, a heat is required to melt ice. If the alteration really overlapped with the regolith gardening, the heat may have been supplied in situ by shock impact on the regolith rather than by decay of radionuclides from internal regions of the parent body.

REFERENCES

[1] DuFresne, E.R. and Anders, E. (1962) Geochim. Cosmochim. Acta, 26, 1085-1114.
[2] Bostrom, K. and Fredriksson, K. (1966) Smithson. Misc. Collect., 151, 1-39.
[3] Richardson, S. M. (1978) Meteoritics, 13, 141-159.
[4] Fredriksson, K. and Kerridge, J.F. (1988) Meteoritics, 13, 141-159.
[5] Tomeoka, K. and Buseck, P.R. (1988) Geochim. Cosmochim. Acta, 52, 1627-1640.
[6] Tomeoka, K., Kojima, H. and Yanai, K. (1989) Proc. NIPR Symp. Antarct. Meteorites, 2, 36-54.
[7] Paul, P. L. and Lipschutz, M. E. (1989) Z. Naturf., A44, 979-987.
[8] Prinn, R.G. and Fegley, B. (1988) in Origin and Evolution of Planetary and Satellite Atmosphere, 78-136. (University of Arizona Press).

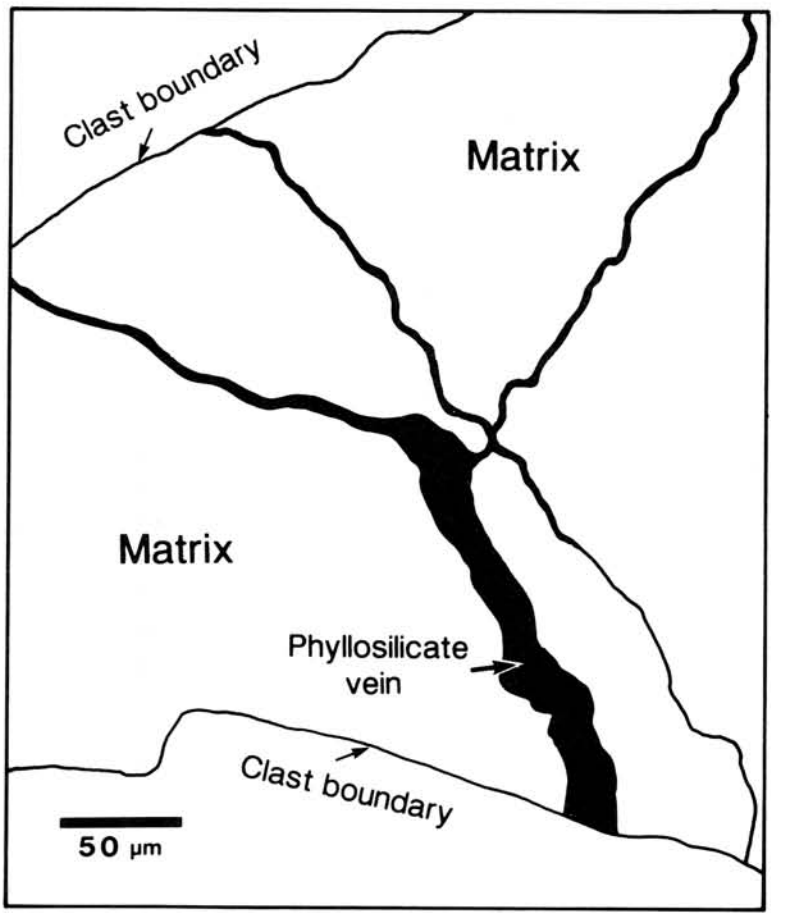

Fig.1 Illustration showing a portion of a clast containing phyllosilicate veins and clast boundaries.

Thermal metamorphism in four Antarctic carbonaceous chondrites and its temperature scale estimated by T-T-T diagram

Junji Akai
Deptm. of Geology and Mineralogy, Fac. Science, Niigata Univ.,Niigata 950-21

Among Antarctic C1 or C2 type carbonaceous chondrites found, four unique specimens which were thermally metamorphosed have been reported(1,2,3),Y-793321 B-7904, Y-86720 and Y-82162 are the four specimens. The degree and maximum temperaures of the metamorphism have been variously estimated (1,4). Duration and cause of the heating are also unknown. In this study , heating experiments of serpentine and saponite in vacuo were carried out to establish temperature scale of such metamorphism . Based on the data , T-T-T diagrams were obtained.

Among the four carbonaceous chondrites, detailed description of B-7904 by EM has not been given yet. Examination on B-7904 by EM and AEM was carried out prior to heating experiments.

Matrix of B—7904

Mineral grains in Fig.1 can be estimated as originally saponite. their compositions are fundamentally similar to those found in Y-86720 and Y-82162. Layer structures of saponite are not confirmed in these specimens because of metamorphism.

Precise identification of mineral grains transformed from serpentine is difficult probably because of utterly transformed features.

Heating Experiment of phyllosilicates

Specimens used were serpentine in Murchison chondrite and terresrial saponite which occurred at Green tuff region. Powdered specimens were heated in vacuo for diffrent durations at different temperatures and cooled.

Heated specimens were examined mainly by EM and AEM , and the degrees of the transformation were estimated. ED pattern of serpentine change in the following order;

I : Appearance of halo diffraction maintaining layer structures , II: Disappearance of layer structure and appearance of diffuse olivine spots , III:Disappearance of diffraction halos and appearance of sharp olivine spots + (enstatite?)

In the Dark Field EM image of mineral grains corresponding to stage II in Y-793321 , newly formed small olivine domains are found and transformation mechanism is suggested.

On the other hand, saponite changes to enstatite more rapidly without definite transitional stage .

T—T—T diagram and temperature estimation

Summarizing all the results on these thermally changed products, T-T-T diagrams for rising temperature were obtained. Fig.2 shows T-T-T diagram of ser

pentine . Fig.3 shows T-T-T diagram of saponite.

Combining , previously described data on phyllosilicates and their thermally changed products in Y-793321, Y-86720, Y-82162 and B-7904(this study), and Figs.2 and 3 , degree of thermal metamorphism in each specimens could be estimated as follows.(Temperatures estimated are also shown.)

B-7904 ≃or > Y-86720 > Y-82162 > Y-793321

T ⩾ ~750°C ~ ,T ⩾ 750 ~700℃,T ~700~600°C ~ , T ⩾ ~400°C ~

Ref.

(1) Akai,J. (1988),GCA, 52, 1593-1599. : (2) Akai,J. (1990) , Proc.NIPR Symp. Ant. Met.(accepted) : (3) Tomeoka et al. (1989a,b) Proc NIPR Symp. Ant.Met.55-74,75-108 : (4) Paul,R.L. and Lipschutz M.E. (1989) 14th Symp.Ant.Meteor.(abs) 32-33.

Fig. 1 Thermally affected saponite grains in B-7904 matrix.

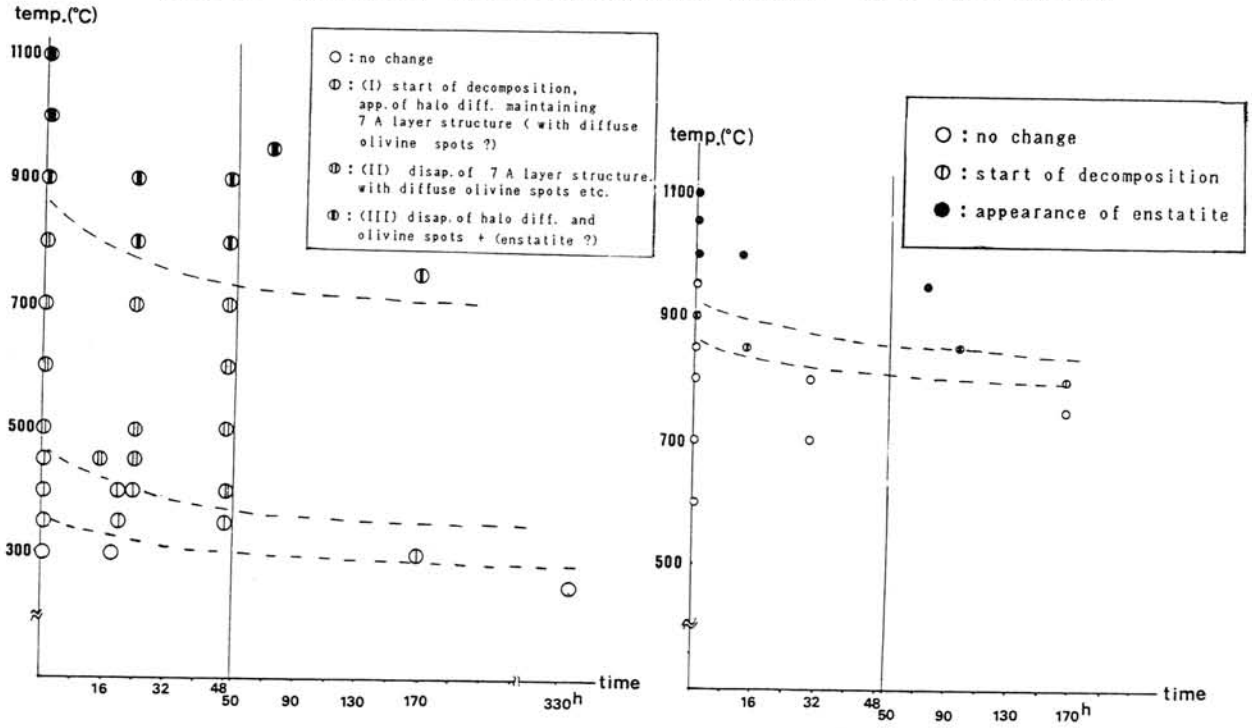

Fig.2 (left) and Fig.3 (right) : T-T-T diagram of serpentine and saponite, respecively, indicated by change of ED patteren for elevated temperature.

COMPOSITIONAL HETEROGENEITY OF ALTERATION PRODUCTS IN YAMATO-86720 CHONDRITE

S. MATSUNAMI, H. NISHIMURA AND H. TAKESHI: NARUTO UNIVERSITY OF EDUCATION, NARUTO, TOKUSHIMA 772, JAPAN.

Phyllosilicates are the most abundant and ubiquitous minerals in the alteration products of chondrules, inclusions and matrix materials in CM chondrites. Especially, formation of PCP and groundmass phyllosilicates in several CM chondrites seems to be records of aqueous alteration processes in the early solar system (McSween, 1979; Ikeda, 1983; Kojima et al., 1984; Tomeoka and Buseck, 1985). They may give clues to understanding of exact formation processes of alteration products.

As already suggested by many investigators, Ca appears to be easily transported from primary Ca-rich materials to Ca-rich alteration product at earlier stage of aqueous alteration (Kojima et al., 1984). The formation of Ca-carbonate observed in several carbonaceous chondrites may be the results of deposition of Ca from aqueous solution. However, detailed behaviour of Ca during aqueous alteration of CM chondrites is poorly known. Detailed study of mode of occurrence of Ca-bearing alteration products may offer clues to clarifying redistribution of Ca during extensive alteration. In this study, especially, Ca distribution of alteration products in 22 altered chondrules and inclusions of Yamato-86720 was petrographically investigated in detail using EPMA.

Among characteristics of composition of alteration products, the CaO content appears to be remarkably variable. It is revealed that alteration products from chondrules and inclusions in Yamato-86720 may contain a significant amount of CaO as much as 41.2 wt%. Using the CaO content of alteration products from chondrules and inclusions, three distinct modes of occurrence of alteration products are observed: type I, type II and type III. Type I is characterized by both the relatively high CaO content and the relatively uniform distribution of Ca in altered objects. The CaO contents are ranging from 4.2 to 41.2 wt%. Some of alteration products are enriched in both CaO and P_2O_5 contents (as much as CaO=26.5 wt% and P_2O_5=13.1 wt%), although P_2O_5 contents of the alteration products are generally low (< 0.9 wt%). The high CaO and P_2O_5 contents are due to the presence of Ca-phosphates. An inclusion (A12) contains porous aggregates composed of tube-shaped phyllosilicates. The composition of the aggregates indicates that they are composed mainly of smectite. The pore spaces around the deformed tubes are possibly filled with Ca-carbonates. Type II is characterized by heterogeneous distribution of Ca in altered chondrules and inclusions. The CaO contents of alteration products show remarkable variablities, ranging from 0.05 to 35.3 wt%. A small amount of alteration products contain high P_2O_5 contents as much as 13.8 wt%. Type III is characterized by the CaO contents of the alteration products lower than 2.4 wt%.

From three types of occurrences, we can infer the origin of compositional heterogeneity of alteration products in Y-86720 chondrite. It is suggested that the remarkable variablities of Ca distribution in alteration products can be explained mainly by the variable mixing ratios of phyllosilicates (smectite), Ca-carbonates and Ca-phosphates. The presence of types I, II and III suggests that most of altered chondrules and inclusions of Y-86720 may reflect the original contents of Ca and P prior to aqueous alteration. Type I may correspond to products derived from aqueous alteration of Ca,Al-rich inclusions (CAIs). Types II and III may be formed through aqueous alteration of chondrules with variable contents of CaO.

MIDINFRARED DIFFUSE REFLECTANCE SPECTRA OF SOME ANTARCTIC CARBONACEOUS CHONDRITES.

Miyamoto, M.

Dept. of Pure and Applied Sciences, University of Tokyo, Komaba, Tokyo 153.

Infrared diffuse reflectance spectra (2.53-25 μm) of some Antarctic carbonaceous chondrites were measured to study effects of thermal metamorphism on the spectra, because mineralogical and petrologic investigations have shown thermal metamorphic features of carbonaceous chondrites with CI-CM affinities among Antarctic carbonaceous chondrites(1-9). Spectra of powder samples (<37 μm) of Murchison(CM2) heated in H_2 environment(1 atm) at 300-700 ^{o}C were also measured to examine spectral changes by thermal metamorphism and were compared with those of thermally metamorphosed carbonaceous chondrites. Details of diffuse reflectance measurements are described in Miyamoto(10).

Absorption bands near 3 μm due to hydrous minerals

The spectrum of Yamato(Y-)791198 shows strong absorption bands near 3 μm similar to those of Murchison caused by primary hydrous minerals (Fig. 1). Belgica(B-)7904, Y-793321, Y-82162, and Y-86720 carbonaceous chondrites show weaker absorption bands near 3 μm compared with Y-791198 (Fig. 1)(11). The carbonaceous chondrites which show weak 3 μm bands contain less amount of hydrous minerals compared with Y-791198 and Murchison, because the integrated intensity of absorption bands near 3 μm is related to the amount of hydrous minerals.

According to mineralogical studies(1-9), B-7904, Y-793321, Y-82162, and Y-86720 are more or less thermally metamorphosed and Y-791198 resembles ordinary CM chondrites. Absorption features near 3 μm are consistent with mineralogical and petrologic studies. Thermally metamorphosed carbonaceous chondrites show weak absorption bands near 3 μm (Fig. 1), suggesting that hydrous minerals in the carbonaceous chondrites were dehydrated by thermal metamorphism.

Major absorption intensities near 3 μm of the thermally metamorphosed carbonaceous chondrites may be due to secondary hydrous minerals produced by terrestrial weathering (Fig. 1), because the shape of spectral curves near 3 μm is similar to that of Antarctic ordinary chondrites(10) which contain weathering-produced hydrous minerals and the wavelength position of reflectance minima is slightly different from that of Y-791198 (Fig. 1).

Fig. 1 also shows spectral features around 3 μm of an unheated sample and heated samples of Murchison. As heating temperature increases, the intensity of the 3 μm band decreases and the 3 μm band disappears in the spectra of the samples of Murchison heated above 500 ^{o}C, that is, most hydrous minerals in Murchison are dehydrated at ca. 500 ^{o}C (12). Although reflectance minimum near 3 μm of the unheated sample of Murchison is about 2.81 μm (3560 cm^{-1}), those of the 300 and 400^{o}C samples is about 2.73 μm (3660 cm^{-1})(Fig. 1)(12), which is similar to the reflectance minimum of serpentine (e.g., 13). This result suggests that some hydrous minerals which have longer wavelength position of reflectance minima were dehydrated at 300 ^{o}C. This may be due to the decomposition of tochilinite before coexisting serpentine(3,14).

Absorption bands near 7 μm due to carbonates

The spectrum of Y-791198 shows absorption bands near 6.9 μm(1450 cm^{-1}) similar to Murchison, probably due to primary calcite(15)(Fig. 2). The spectra of B-7904, Y-793321, and Y-86720 which are thermally metamorphosed show no absorption bands near 6.9 μm (Fig. 2)(11), suggesting that most carbonates were decomposed during heating events. Although Y-82162 shows weak absorption bands near 3 μm as a result of dehydration (Fig. 1), absorption bands near 6.9 μm are seen in the spectrum (Fig. 2), that is, Y-82162 contains relatively large amount of carbonates compared with the other thermally metamorphosed carbonaceous chondrites(3).

The spectra of Antarctic carbonaceous chondrites show faint absorption bands near 7.4 μm (1350 cm^{-1}) probably due to hydrous carbonates formed by terrestrial weathering (Fig. 2), because Antarctic ordinary chondrites usually show the 7.4 μm band due to hydrous carbonates produced by terrestrial weathering (16). The presence of weathering-produced hydrous carbonates is in line with weak absorption bands near 3 μm caused by weathering-produced hydrous minerals in the spectra of thermally metamorphosed Antarctic carbonaceous chondrites (Fig. 1). We cannot, however, exclude the possibility that the hydrous carbonates are primary.

Although the 400 and 450 °C samples show weak absorption bands near 6.9 μm (1450 cm^{-1}), the 500 °C sample shows no absorption bands. This result suggests that most carbonates in Murchison are decomposed by heating above 500 °C (12).

The results of heating experiments show that both the 3 and 6.9 μm bands disappear in the spectra of the samples heated above 500 °C, suggesting that metamorphic temperature is > ca. 500°C for thermally metamorphosed Antarctic carbonaceous chondrites (B-7904, Y-793321, and Y-86720), because they show weaker absorption bands near 3 and 6.9 μm compared with Murchison (Figs. 1 and 2).

Akai(5,7) proposed metamorphic temperatures of some Antarctic carbonaceous chondrites on the basis of mineralogical observations of the Murchison samples heated at various temperatures: 500-600 °C for Y-793321, about 800 °C for Y-82162 and Y-86720, >800 °C for B-7904. Tomeoka et al. (3) discussed metamorphic temperatures and proposed that the thermal metamorphism probably occurred at >500 °C in a reduced condition. Our results are consistent with previous studies.

The author thanks Drs. M. Zolensky, T. Fujii, M. Toriumi, and K. Ito for discussion.

References: (1) Kojima H., Ikeda Y., Yanai K. (1984) Mem. Natl. Inst. Polar Res., Spec. Issue, 35, 184-199. (2) Kojima H. and Yanai K. (1987) 12th Symp. Antarctic Meteorites, 15. (3) Tomeoka K., Kojima H., and Yanai K. (1989a, b) Proc. NIPR Symp. Antarct. Meteorites, 2, 36-54 and 55-74. (4) Watanabe S., Tsuchiyama A., and Kitamura M. (1988) 13th Symp. Antarctic Meteorites, 128-129. (5) Akai J. (1988) Geochim. Cosmochim. Acta 52, 1593-1599. (6) Tomeoka K. (1989) 14th Symp. Antarctic Meteorites, 18-20. (7) Akai J. (1989) 14th Symp. Antarctic Meteorites, 22-23. (8) Zolensky M., Barrett R., and Prinz M. (1989) 14th Symp. Antarctic Meteorites, 24-26. (9) Zolensky M. E., Barrett R. A., and Gooding J. L. (1989) Lunar Planet. Sci. XX, 1249-1250. (10) Miyamoto M. (1988) Earth Planet. Sci. Lett. 89, 398-402. (11) Miyamoto M. (1990) Lunar Planet. Sci. XXI, 799-800. (12) Miyamoto M. (1990) Lunar Planet. Sci. XXI, 797-798. (13) Miyamoto M. (1989) Proc. 22nd ISAS Lunar Planet. Symp., 99-105, Inst. Space Astronaut. Sci.,

Tokyo. (14) Mackinnon I. D. R. and Zolensky M. (1984) Nature 309, 240-242. (15) Miyamoto M. (1987) Icarus 70, 146-152. (16) Miyamoto M. (1989) Earth Planet. Sci. Lett. 96, 229-234.

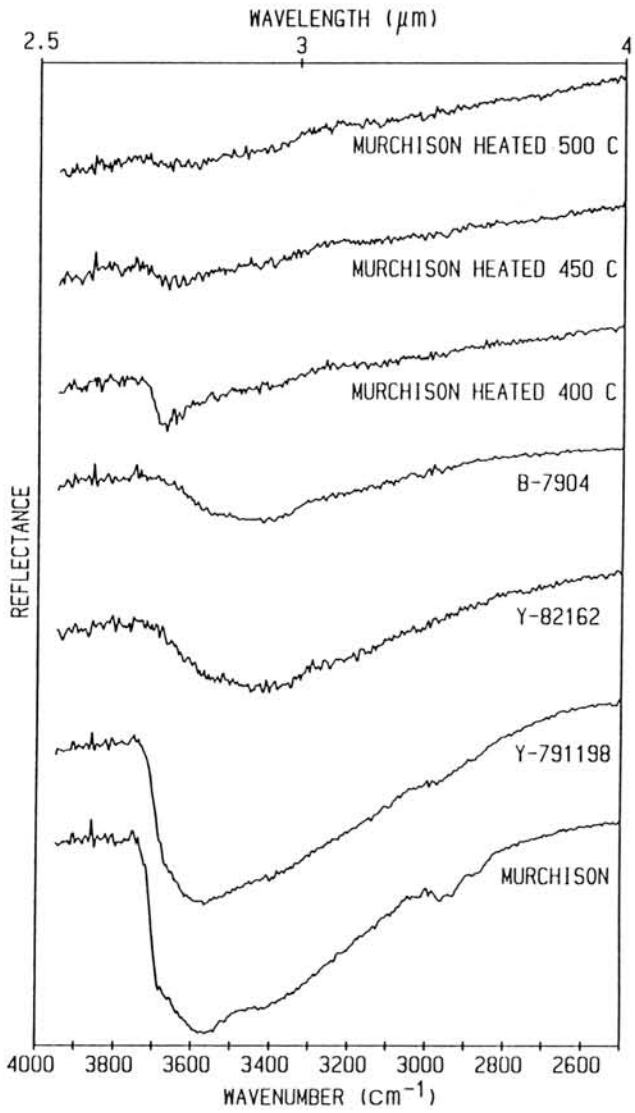

Fig.1. Infrared diffuse reflectance spectra near 3 μm of some carbonaceous chondrites and heated samples (400, 450, and 500 °C for 6 hours) of Murchison (CM2).

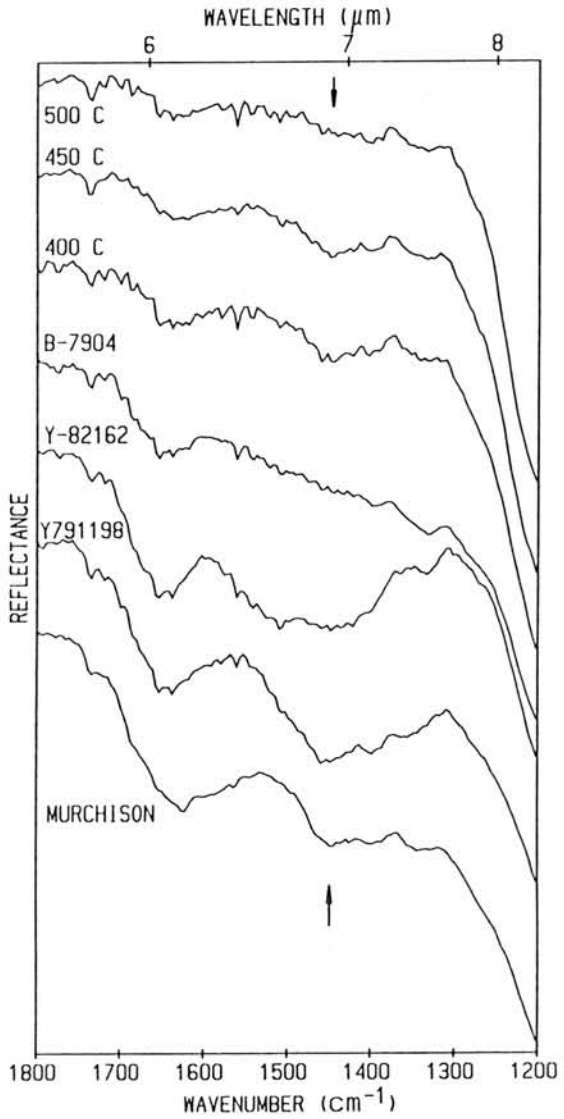

Fig.2. Infrared diffuse reflectance spectra near 7μm of some carbonaceous chondrites and heated samples (400, 450, and 500 °C for 6 hours) of Murchison. Arrows indicate the 6.9 μm (1450 cm^{-1}) band.

PETROLOGY OF UNIQUE METEORITES, Y-74063, Y-74357, Y-75261, Y-75274, Y-75300, Y-75305, A-77081, A-78230, AND Y-8002

H. Nagahara[1], T. Fukuoka[2], I. Kaneoka[3]M. Kimura[4], H. Kojima[5], I. Kushiro[1], H. Takeda[6], and A. Tsuchiyama[7], K. Yanai[5]
1) Geol. Inst., Univ. Tokyo, Tokyo 113, 2) Dept. Chemistry, Gakushuin Univ., Tokyo 171, 3) Geophys. Inst., Univ. Tokyo, Tokyo 113, 4) Dept. Earth Sci., Ibaraki Univ., Mito 310, 5) Natl. Inst. Polar Res., Tokyo 173, 6) Mineral. Inst., Univ. Tokyo, Tokyo 113, 7) College Gener. Edu., Osaka Univ., Osaka 560

As a part of a consortium study on the Antarctic unique meteorites, seven unique meteorites, Yamato-74063, Y-74357, Y-75261, Y-75274, Y-75300, Y-75305, ALH-77081, A-78230, and Y-8002 were petrologically and chemically studied in comparison with related meteorites Y-74025 [1,2] and Y-741493 [3]. A-77081 was previously studied [4] and three (Y74357, Y75274, and Y8002) briefly [5-7]. The meteorites are characterized by roughly chondritic compositions and non-chondritic textures. Oxygen isotopic compositions have been already reported [8-10]. They are divided into three groups on the basis of petrological features: one is related to Acapulco and Lodran, the second is related to Winona and Pontlyfni, and the last is related to enstatite chondrites.

1. Y-74063, Y-74357, Y-75274, A-77081, A78230, and Y-8002

Y-74063, Y-74357, Y-75274, A-77081, A-78230, and Y-8002, are texturally, mineralogically, and chemically related to each other and also to Lodran, Acapulco, and Y-791493. They are coarse-grained and exhibit an equigranular texture. They consist of olivine, orthopyroxene, clinopyroxene, plagioclase, chromite, Fe-Ni metals, and troilite with accessory apatite, merrillite, schreibersite, daubreelite, and graphite. Olivine and orthopyroxene are usually coarser grained than other minerals, of which modal abundances are highly variable according to meteorites. Plagioclase is interstitial and the modal abundance vary from a few to more than 10 vol%.

The meteorites are igneous in origin; olivine and pyroxenes are cumulus phases, and plagioclase, trace apatite and/or merrillite are intercumulus. Because cumulus and intercumulus phases did not crystallized simultaneously, the modal abundance of intercumulus phases does not represent the degree of melting. Difference in the REE patterns for Y-74063 [11], A-77081 [12], Acapulco [13], and Lodran [14] is due to the different degree of melt extraction and/or addition.

The degree of melting is shown by the mineral compositions. The Cr/(Cr+Al) ratio of spinel increases with increasing An mol% of plagioclase. The Cr/(Cr+Al) ratio of spinel in residual peridotites generally becomes higher with higher degree of melting [i.e., 15], and accordingly, the increasing number of the Cr/(Cr+Al) ratio and An mol% represents the increasing in degree of melting from a common precursor. The degree of melting is highest in Y-75274 and Y-8002, and becomes smaller through Y-791493, Y-74063, Y-74257, A-77081, and Acapulco, to A-78230. Trace elements such as Mn and Ti in pyroxenes covary with those in spinel, representing enrichment of those elements in bulk rocks. The precursor material of the meteorites are richer in Cr, Mn, V, and P and poorer in Ti than ordinary chondrites.

The iron-magnesium relationships among olivine, orthopyroxene, and clinopyroxene of the meteorites are almost in equilibrium, and they are divided

into two groups, one is highly magnesian (Y-75274 and Y-8002) and the other is less magnesian (Y-74357, A-77081, A-78230, Y-791493, Acapulco, and Lodran). Although olivines in some of the meteorites appear to have been reduced after crystallization, it is not significant in most cases. Olivine in Y-74357 is, however, exceptionally magnesian when compared to pyroxenes, which is supposed to be due to reduction. This suggests that those meteorites should not be classified based simply on olivine composition.

Above observations show that the meteorites were derived from a common precursor through different degree of melting. Petrofabric for olivines in Y-74063 and Y-741493 show concentrations of Y(c) axes which could be formed in magmatic laminar flows. The fact that the meteorites are essentially chondritic in major elemental composition shows that they were formed in melt pockets in a chondritic body but that the loss of partial melt was not significant. The heat source for melting is still unclear. The cooling rate estimated for Y-74063 and Y-791493 by using the method of grain size and composition of spinel and olivine [16] is about 10^3 deg/Ma from 800 to 600°C, which suggests that the melting occurred in fairly large areas.

2. Y-74025, Y-75300, and Y-75305

Y-74025, Y-75300, and Y-75305 are genetically related to Winona, Pontlyfni, and Mount Morris. These meteorites are texturally and mineralogically similar except that Y-74300 have coarse- and fine-grained portions. They consists mainly of olivine (Fo_{98-99}), orthopyroxene (En_{96-97}, $Wo_{0.4-1.6}$), Fe-Ni metals and troilite with smaller amounts of clinopyroxene (En_{51-56}, Wo_{44-48}), plagioclase (An_{15-22}), spinel, apatite, merrillite, daubreelite, and schreibersite. Rare pentlandite, pyrrhotite, rutile, zircon, and Mn-Cu sulfide are observed in Y-75305. Modal abundance of opaque minerals varies largely from meteorite to meteorite (about 10 tp 40 vol%) which is also the case in the "winonaites" (20-55 % [17]), and the metal/kamacite ratio is highly variable. Olivine, pyroxenes, plagioclase are homogeneous, but spinel is highly heterogeneous especially in Y-75305 (Cr_2O_3 56-74wt%, Al_2O_3 5-18%, MgO 2-20%), most of which coexist with metals and /or troilite.

Although these meteorites are texturally similar to the Lodran-Acapulco type meteorites, mineralogy of pyroxenes, plagioclase, and spinels show that they are different from the Lodran-Acapulco type meteorites. The formers are poorer in Cr and Mn than the latter, and spinels in the formers are much more magnesian, as well as olivine and pyroxenes, than those in the formers.

The textural similarity and REE patterns [2, 11] show that the meteorites of this group were formed also through partial melting in melt pockets in a parent body. Loss of the partial melt was not significant in most cases resulted in fairly chondritic major elemental compositions. The assemblage and compositions of minerals show that they were formed in a condition more reducing than the Lodran-Acapulco type meteorites but more oxidizing than enstatite chondrites. It is not clear whether the parent body of this group is the same as that of the Lodran-Acapulco type meteorites. The oxygen isotopic composition for the two groups are slightly different, but the diversities in the two groups are wider than the difference between the two groups.

3. Y-75261

Y-75261 is very fine-grained (less than several tens um) and consists of the porphyritic and non-porphyritic portions. The porphyritic portion have forsterite and enstatite phenocrysts embedded in glassy groundmass rich in Al, Si. Ca, and Na. Sodium and Al are exclusively distributed in the porphyritic portion. The non-porphyritic portion is an aggregate of enstatite and kamacite with lesser amount of forsterite. Pyroxenes in the two portions are compositionally indistinguishable, which are highly pure enstatite with trace element contents less than 0.5 wt%. Enstatite grains contains tiny blebs of kamacite, which is similar to the occurrence of kamacite blebs in enstatite chondrites.

Petrological and mineralogical observations along with oxygen isotopic compositions suggest that Y-75261 is an enstatite chondrites with a unique texture. It possibly be a shocked enstatite chondrite.

References: [1] Kimura, M. (1987) *Abst. 12th NIPR sympo.* 47, [2] Fukuoka, T. and Kimura, M. (1988) *Abst. 13th NIPR sympo.* 44-45, [3] Nagahara, H. and Ozawa, K. (1986) *Mem. Natl. Inst. Polar Res. Spec. Issue* No. **41**, 181-205, [4] Takeda, H. et al. (1980) *Mem. Natl. Inst. Polar Res. Sepc. Issue* No. **17**, 119-144, [5] Matsumoto, Y. et al. (1983) *Abst. 8th NIPR sympo.* 7, [6] Mori, H. et al. (1984) *Lunar Planet. Sci.*, **XV**, 567-568, [7] Yanai, K. et al. (1984) *Abst. 9th NIPR sympo.* 24-28, [8] Clayton, R. N. et al. (1984) *Mem. Natl. Inst. Polar Res. Spec. Issue* No. **35**, 267-271, [9] Mayeda, T. K. et al. (1986) *Mem. Natl. Inst. Polar Res. Spec. Issue*, No. **46**, 144-150, [10] Mayeda, T. K. and Clayton, R. N. (1989) *Abst. 14th NIPR sympo.*, 71, [11] Nakamura, N. (1990) *this volume*, [12] Kallemeyn, G. W. and Wasson, J. T. (1985) *Geochim. Cosmochim. Acta*, **49**, 261-270, [13] Palme, H. et al. (1981) *Geochim. Cosmochim. Acta*, **45**, 727-752, [14] Fukuoka, T. et al. (1978) *Lunar Planet. Sci.*, **IX**, 356-358, [15] Jaques, A. L. and Green, D. H. (1980) *Contrib. Miner. Petrol.*, **73**, 287-310, [16] Ozawa, K. (1984) *Geochim. Cosmochim. Acta*, **48**, 2597-2611, [17] Prinz, M. et al.(1980) *Lunar Planet Sci.*, **XI**, 902-904.

Y-74063: UNIQUE METEORITE CLASSIFIED BETWEEN E AND H CHONDRITE

Keizo Yanai and Hideyasu Kojima
Department of Meteorites, National Institute of Polar Research
9-10, Kaga 1-chome, Itabashi-ku, Tokyo 173 Japan

Introduction: In classification of chondrites, any meteorites have not been classified in a field between E and H chondrite until Antarctic meteorites collected. Recently several specimens in Antarctic meteorites were preliminary identified in this space (field) as "chondrite" which have chondritic composition with poor chondritic texture.

General features: The Antarctic meteorite **Yamato-74063** is a chondritic meteorite, 35.41grams nearly complete rounded stone with dull black fusion crust showing general features most of chondritic meteorites. It does not appear belong to any unique specimen. Y-74063 was originally identified as only an unique specimen[1], but new petrographic and chemical evidence from the Y-74063 indicate that it is a new type of chondrite between E and H chondrite.

General petrography: Y-74063 consists of relatively coarse-grained olivine and pyroxene with nickel-iron in recrystallized matrix. Sometime chondrule-like appearances were poorly traced in the thin section. One of them looks like originally radial pyroxene chondrule, but it is not clear in any cases. Most of olivine and pyroxene contain much more and very fine-grained dusty-like opaques. Matrix of Y-74063 is being integrated with the fine-grained granular ground mass which consists mainly of olivine and pyroxene with minor amount of nickel-iron, troilite and plagioclase. Olivine and pyroxene have homogeneous compositions, average Fa10.9 and average Fs10.9 respectively, however those compositions and quite different from those of any enstatite chondrite and ordinary chondrites (Fig.1). Some Ca-rich pyroxene, En50.7-52.1 Fs4.1-4.7 Wo43.4-45.0 are recognized. Plagioclase is Na-rich, Ab83.7 An13.5 Or2.8.

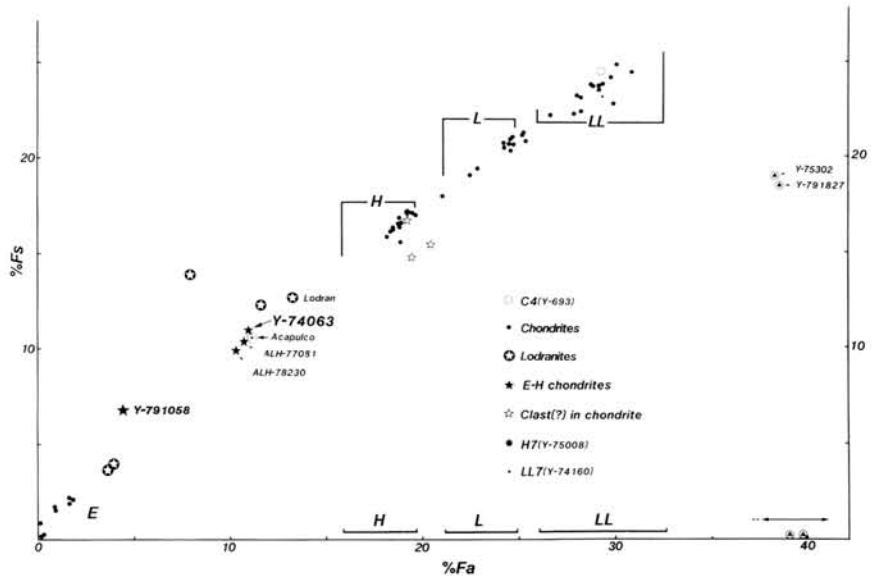

Fig.1: Y-74063 is plotted between E and H chondrite on the %Fa-%Fs diagram.

Bulk composition: The bulk chemical composition of Y-74063 analyzed shows in the Table 1 with those of known type chondrites for comparison each other. Showing the table, Y-74063 is characterized it's unique composition; this meteorite is the lowest total Fe in all chondrite types, Nickel-iron is nearly same value of L chondrite, but troilite is much higher than ordinary chondrites and lower than E chondrite. Fe in silicates is lower than ordinary chondrites and higher than E chondrite. MgO is much higher them other chondrites, and CaO is slightly higher. Other components are almost same. As showing Fig.2, Fe in metals vs Fe in silicates of Y-74063 distinct from all known chondrites.

Conclusion: Y-74063 is unique chondrite which is classified as a new type between E and H chondrites from those of petrological and chemical characteristics.

Reference: [1]Yanai K & H Kojima(1979) NIPR Catalog. 298p.

	Y-74063	Y-691 (E)	Y-74370 (E)	H	L	LL
SiO_2	38.98	36.31	34.14	35.64	39.32	39.58
TiO_2	0.08	0.08	0.12	0.10	0.10	0.14
Al_2O_3	2.96	2.93	2.51	2.00	2.39	2.52
Fe_2O_3	0.91	0	0	-	-	-
FeO	9.69	0.96	3.9	11.71	15.13	19.86
MnO	0.19	0.24	0.23	0.28	0.33	0.34
MgO	27.01	19.59	18.20	23.73	25.52	25.70
CaO	2.68	1.29	1.10	1.76	1.85	1.78
Na_2O	0.83	0.83	0.74	0.73	0.90	0.87
K_2O	0.07	0.07	0.09	0.08	0.09	0.11
$H_2O(-)$	0.04	0.50	1.05	0.07	0.10	0.10
$H_2O(+)$	0.3	0.5	5.9	0.22	0.17	0.39
P_2O_5	0.46	0.46	0.46	0.23	0.24	0.25
Cr_2O_3	0.34	0.45	0.43	0.46	0.52	0.58
FeS	9.31	16.31	12.77	5.45	6.04	5.27
Fe	4.89	17.8	16.6	15.80	6.10	1.33
Ni	0.98	1.71	1.51	1.70	1.10	0.95
Co	0.031	0.077	0.051	0.058	0.036	0.025
Total	99.75	100.10	99.80	100.01	99.93	99.79
Total Fe	18.65	28.90	27.75	28.36	21.70	20.11

H, L, LL: average

Table 1. The bulk composition with those of known type chondrites.

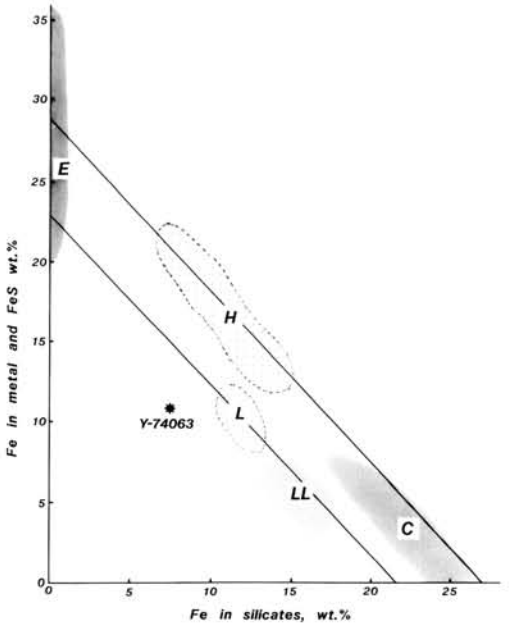

Fig.2: Y-74063 is on the UC diagram. Y-74063 distinct from all known chondrites.

LITHOPHILE TRACE ELEMENT ABUNDANCES IN ANTARCTIC UNIQUE METEORITES AND IN UNIQUE CLASTS FROM L6 CHONDRITES

Koshi Yamamoto[1], Noboru Nakamura[1], Keiji Misawa[2], Keizo Yanai[3] and Y. Matsumoto[4]
[1]Dept. Earth Sci., Faculty of Sci., Kobe University, Nada, Kobe 657, Japan, [2]Inst. Cosmic Ray Res., University of Tokyo, Tanashi, Tokyo 188, Japan, [3]Natl. Inst. Polar Res., Kaga, Itabashi, Tokyo 173, Japan, [4]Dept. of Mineral. Sci. Geol., Yamaguchi University, Yoshida, Yamaguchi 753, Japan

As one of consortium studies on unique Antarctic meteorites, we have carried out isotope dilution analyses of lithophile trace elements (including REE) together with some major elements (Mg, Fe, Ca) for three unique meteorites Yamato-75300, -74063 and -8002. The Sr isotopic analyses are also in progress for the meteorites. In addition, the analytical results for two unique clasts from L-chondrites (Yamato-75097 and -793241) are presented for comparison. The samples sizes used for isotope dilution analyses were ~10mg for Y-75300 and -8002. The Y-74063 specimen were taken from a powder aliquote weighing ~120mg.

Yamato-75300 The meteorite has the oxygen isotopic composition of winonaites (Mayeda and Clayton, 1989). As shown in Fig. 1, it indicates the remarkable REE fractionation (~0.1~1xCI) with V-shaped general pattern and a large positive Eu anomaly, and depletion of alkali metals. The REE pattern is quite similar to those of unique clasts from L6 chondrites Y-75097 and -703241 (Nakamura et al., 1984; Warren and Kallemeyn 1989), and seems to be a kind of fractionation patterns for ungrouped chondritic meteorites reported by Kallemeyn and Wasson (1985). The relative enrichment of Eu together with Sr (~1xCI), and of both lighter and heavier REE suggest that the trace element fractionations were established mainly by partitioning of elements into plagioclase and olivine during the thermal processes which might have formed the meteorite.

Yamato-8002 The meteorite is classified into lodranite and has the oxygen isotopic composition similar to Sombrerete. This meteorite have higher but quite similar REE fractionation pattern compared with that of Y-75300 meteorite, and is depleted in Fe and Rb (Fig. 1). The relative enrichment of both Eu and Sr together with the fractionated REE patterns suggest that the meteorite was formed by the similar fractionation processes to that of Y-75300 meteorite.

Yamato-74063 The meteorite shows a flat REE pattern with minor negative Eu anomaly, which is normal to ordinary chondrites. In spite of relatively unfractionated lithothphile abundances (~1.5xCI), Rb is too much depleted (~0.1xCI). It is also noted that all the unique meteorites examined here show extreme

depletion of Rb relative to other lithophiles (even compared to K), which is not well understood. We have undertaken the Rb-Sr isotopic analyses for the meteorites. The isotopic analyses of bulk and mineral seprates are now in progress.

References: Kallemeyn G.W. and Wasson J.T. (1985), Geochim. Cosmochim. Acta 49, 261-270; Nakamura N., Yanai K. and Matsumoto Y. (1984), Meteoritics 19, 278-279. Warren P.H. and Kallemeyn G.W. (1989), Proc. Lunar Sci. Conf. 19th, 475-486.

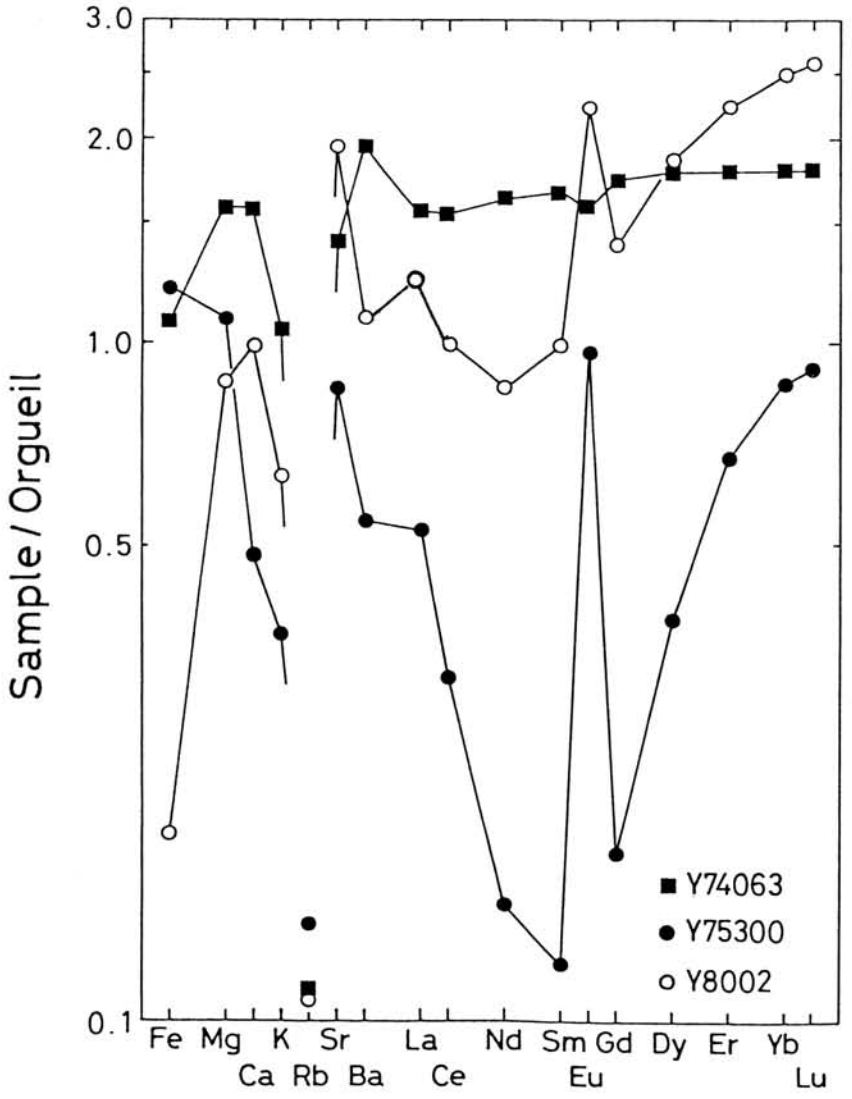

Fig. 1. Orgueil (CI)-normalized lithophile element patterns for unique Antarctic meteorites.

CHEMISTRY OF Y-74063, -74357 AND ALH-78230 UNIQUE METEORITES

Fukuoka, T.[1] and Kimura, M.[2]

1. Department of Chemistry, Gakushuin University, Mejiro, Tokyo 171.
2. Department of Earth Sciences, Ibaraki University, Mito 310.

Yamato 74063 (Y-74063) meteorite was classified as unique (1), chondrite (2) and (E-H) 7 (3), previously. Kimura (4) carried out the mineral and petrological investigations of Y-74063 and discussed the relationships between Y-74063 and the unique meteorite such as winonaites (5), lodranites etc. He suggested that Y-74063 belongs to group of Acapulco (6) and ALH-77081 (7). Yamato 74357 (Y-74357) meteorite was classified as lodranite (1,2,3), previously. Fukuoka *et al.* (8) presented chemical composition of Lodran. Allan Hills 78230 (ALH-78230) meteorite was classified as unique (2) and (E-H) 7 (3), previously.

In this study, to discuss the classification of these three meteorites based on the chemical features, we are analizing more than 20 major, minor and trace elements in two chips of Y-74063 and in chips of Y-74357 and ALH-78230 by instrumental neutron activation analysis (INAA) as a part of consortium study. The samples were provided from the National Institute of Polar Research of Japan.

The preliminary analytical results are shown in Table 1. The chemical abundances of two chips of Y-74063 show the chemical hetelogeneity (especially Sm). The C1 chondrites (non-volatile) normalized REE abundance pattern of Y-74063 (weighted mean) is similar to those of ALH-78230 and Y-74025 (9) and is not similar to Lodran (8). The chemical abundances of Y-74063 and ALH-78230 are basically chondritic, but Y-74357 is not chond ritic. Y-74357 show the fractionated C1 chondrites normalized REE pattern which is similar to that of Lodran (8). The chemical abundances of Y-74357 are depleted in most lithophile elements compared with those of C1 chondrites.

REFERENCES:

(1) Kojima, H. and Yanai, K, (1984) Abstract 9th Sym. Antarctic Meteorites, 11. (2) Yanai, K. and Kojima, H. (1987) Photographic Catalog of the Antarctic Meteorits, 298p. (3) Natl Inst Polar Res. (1987) Science in Antarctica, 6, Antarctic Meteorites, 440p. (in Japanese). (4) Kimura, M. (1987) Abstract 12th Sym. Antarctic Meteorites, 47. (5) Prinz, M. *et al.* (1980) Lunar Planet. Sci., 11, 902. (6) Palme, H. *et al.* (1981) Geochim. Cosmochim. Acta, **45**, 727. (7) Takeda, H. *et al.* (1980) Mem. Natl Inst. Polar Res., **17**, 119. (8) Fukuoka T. *et al.* (1978) Lunar Planet. Sci., 9, 356.
(9) Fukuoka, T. and Kimura, M. (1988) Abstract 13th Sym. Antarctic Meteorites, 44.

Table 1. Preliminary results of chemical abundances by INAA

		Y-74357	YAMATO 74063			ALH 78230	Error*
		-72	A	B	wtd.mean	-56	%
Wt	mg	102.9	95.5	82.2		97.2	
Ti	%		0.072	0.11	0.090		20-30
Al	%		1.22	1.34	1.28		1-2
Fe[1)]	%	24.2	20.1	19.0	19.6	23.3	0.5
Mg	%		15.6	16.0	15.8		2-5
Ca	%		1.03	1.79	1.38		4-10
Na	%	0.108	0.674	0.740	0.705	0.753	0.5-1
K	%	0.005	-	-	-	0.054	13-50
Mn	%		0.262	0.265	0.263		0.5-1
Cr	%	0.124	0.292	0.245	0.270	0.500	0.5
Sc	ppm	7.59	8.20	11.9	9.91	10.5	0.5
V	ppm		94	88	91		2-3
La	ppm	0.064	0.32	0.39	0.35	0.36	5-33
Ce	ppm		1.1	0.6	0.87		20-35
Sm	ppm	0.034	0.188	0.286	0.233	0.215	1-6
Eu	ppm	0.032	0.088	0.085	0.087	0.158	5-16
Dy	ppm		0.57	0.46	0.52		25
Yb	ppm	0.079	0.20	0.28	0.24	0.26	7-33
Lu	ppm	0.020	0.043	0.047	0.045	0.043	10-15
Hf	ppm	0.08	0.24	0.22	0.23	0.12	10-23
Zn	ppm		109	79	95		
As	ppm	2.16	1.77	1.68	1.73	1.77	6-17
Se	ppm		24	21	23		
Co	ppm	715	470	449	460	768	0.5
Ni	%	0.90	1.25	1.13	1.19	1.48	0.5
Os	ppb	465	220	150	190	500	6-14
Ir	ppb	568	306	236	274	522	1
Au	ppb	166	184	149	168	182	2

* Errors for INAA are due to counting statistics.
1) Total iron as FeO.

Noble gases in unique meteorite Y-74063

N. Takaoka and Y. Yoshida
Department of Earth Sciences, Faculty of Science
Yamagata University, Yamagata 990.

Y-74063 has been classified originally as unique chondrite by Yanai and Kojima (1987). It resembles a unique meteorite Acaplco (Palme et al,1981) in its recrystallized, achondritic texture and unique mineralogical composition. Noble gas compositions have been measured to obtain data which can give a useful guide to classification of the unique meteorite.

The sample used for analysis is a chip of 91.97 mg. Microscopic inspection of a 2 mm chip reveals that it consists of fine-grained olivine and pyroxene with minor amounts of Fe-Ni metal and troilite, and that the silicate minerals are characterized by many cleavages or cracks. In particular, majority of pyroxene minerals have many cleavages of about 10 um interval.

Concentrations and isotopic ratios of noble gases are given in Table 1. The meteorite contains huge amounts of primordial heavy noble gases, while it is depleted in primordial He and Ne. Fig. 1 displays comparison with carbonaceous chondrites, ureilites and some other unique meteorites. Primordial ^{36}Ar is comparable with C-chondrites and ureilites, but an order of magnitude higher than for Lodran (Zahringer, 1968) and Acapulco (Palme et al., 1981). In particular, primordial ^{132}Xe is abnormally abundant and even higher than for ureilites except Dyalpur(Mazor et al., 1970) and A-77257(Takaoka,1983). Y-74063 also contains the highest concentraion of radiogenic ^{129}Xe so far reported. Prmordial $(^{20}Ne/^{36}Ar)p$ is as low as compatible with ureilites. $(^{36}Ar/^{132}Xe)p$ is lower than for C-chondrites and ureilites (Fig. 1). In a correlation diagram (Fig. 2), the Y-74063 datum falls on an extended lower end of a reference line for ureilite bulk and carbon-rich samples (Gobel et al., 1978), reflecting enrichment in ^{132}Xe.

Helium is dominated by the spallogenic and radiogenic gases.

It is difficult to know the isotopic ratio of trapped Ne that is diagnostic for the trapped gas, beacuse spallogenic Ne is predominant. The concentration of spallogenic ^{21}Ne is between Acaplco and a Acaplco-type meteorite A-77081 (Schultz et al.,1982), whose cosmic-ray exposure ages are 8 m.y. (recalculated with the production rate normalized to Nishiizumi et al.,1980) and 6 m.y., respectively. Hence, the exposure age of about 7 m.y. is suggested for Y-74063, if there are no significant differences in target chemistry and shielding condition. Lodran has the longer exposure age, because spallogenic ^{21}Ne in the Lodran silicate is higher by a factor of 5.

The concentrations of ^{4}He and ^{40}Ar can be interpreted by radiogenic ^{4}He and ^{40}Ar produced by in-situ decays of 15 ppbU for 3.3 Ga and 450 ppmK for 4.5 Ga, respectively, although we can not give gas-retention ages because no data are available on K and U.

Y-74063 is characteristic of the anomalously high abundances of primordial Ar, Kr and Xe and the depletion of primordial He and Ne. This suggests a link with ureilites, but no carbonaceous material is found as in ureilites. The high abundance of primordial gas indicates that the meteorite contains unusually gas-retentive phase(s) which did not lost the gas at the recrystallization stage, or acquired the gas by highly adsorptive sites at or after recrystallization at ambient conditions such as abnormally high gas pressure. Further work is needed to identify the host phase(s) of the primordial gas.

References: Gobel et al.(1978), J.Geophys.Res.,83, 855-867; Mazor et al.(1970), Geochim.Cosmochim.Acta, 34, 781-824; Nishiizumi et al.(1980), Earth Planet.Sci.Lett.,50, 156-170; Palme et al.(1981) Geochim.Cosmochim.Acta, 45, 727-752; Schultz et al.(1982), Earth Planet.Sci.Lett., 61, 23-31; Takaoka(1983), Abstr.8th Symp.Antar. Meteor. 81-82; Yanai and Kojima(1987), Photogr. Catalog Antarct. Metor. NIPR; Zahringer(1968), Geochim.Cosmochim.Acta, 32,209-237.

Table 1. Noble gas compositions in Y-74063.

Sample	^{3}He	^{4}He	^{20}Ne	^{21}Ne	^{22}Ne	^{36}Ar	^{38}Ar	^{40}Ar	^{84}Kr	^{132}Xe
Y-74063	8.89	1530	2.36	1.09	1.49	102	19.7	3600	1.33	3.08

Concentration is given in unit of 10^{-8} cm^3/g.

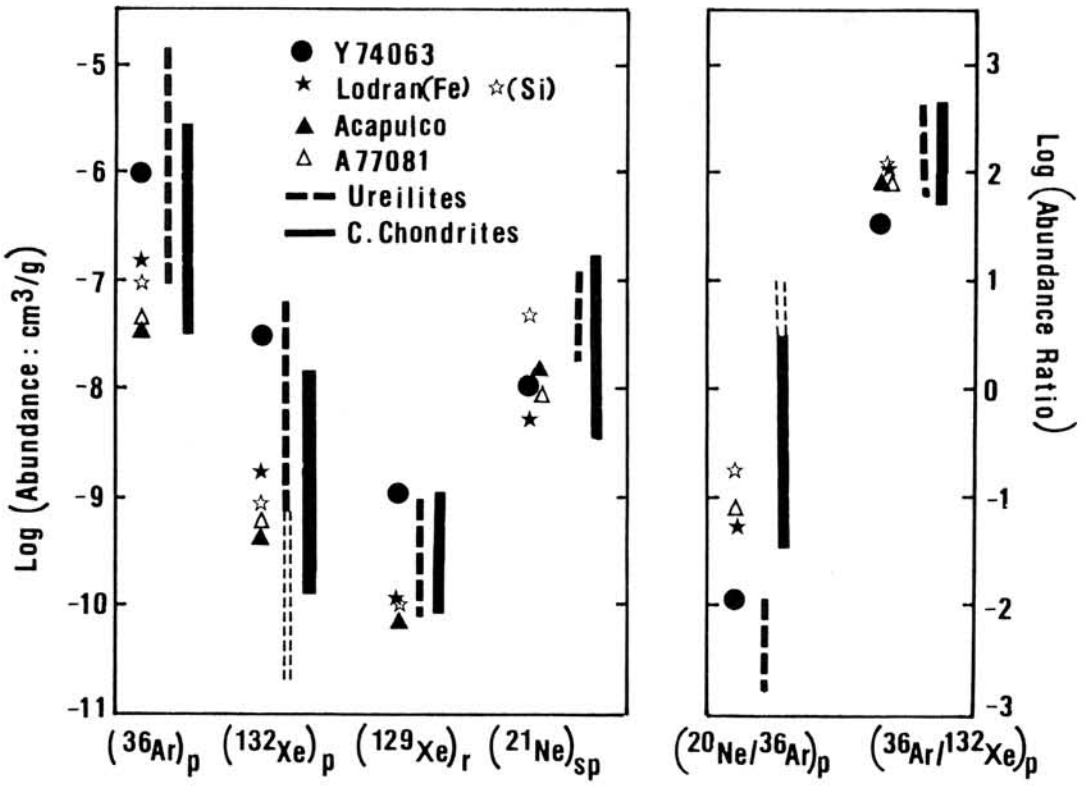

Fig.1

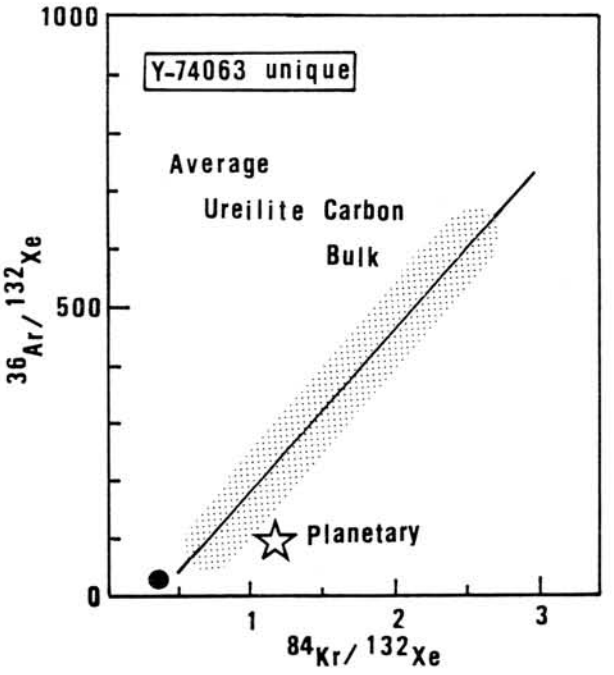

Fig.2

REFLECTANCE SPECTROSCOPY AND MINERALOGY OF PRIMITIVE ACHONDRITES — LODRANITES.

Takahiro HIROI and Hiroshi TAKEDA
Mineralogical Institute, Faculty of Science, University of Tokyo,
Hongo, Tokyo 113, Japan

As a part of consortium studies of unique achondrites, reflectance spectra of mineralogically characterized primitive achondrites (Acapulco-type meteorite and lodranites), have been measured for the first time. Their reflectance spectra were compared with that of an S-type asteroid 29 Amphitrite [1]. They are also compared with those of an H6 chondrite Y82111 (with recrystallized texture) and an iron meteorite Mundrabilla in Fig. 1. According to our model [2], one of the way to simulate the shallow absorption bands of Amphitrite is to reduce the silicate grains in chondrites.

As a good candidates for this reduced chondrite, we employed primitive achondrites [3]. We measured reflectance spectra of three primitive achondrites: an Acapulco type winonaite ALH77081, a lodranite Y791491, and a partly reduced lodranite Y74357, which are in order of ascending degree of reduction from chondrites. Those spectra are shown in Fig. 2. As those primitive achondrites become more reduced, their absorption bands become shallower.

We tried to simulate the Amphitrite spectrum by linear combinations of reflectance spectra of Mundrabilla and those primitive achondrites. The results are shown in Fig. 3. As the reduction of the primitive achondrite increases, the fitting is improved and the amount of Mundrabilla becomes smaller. The modal abundances and chemical compositions of those primitive achondrites are shown in Fig. 4 and 5, respectively. We can expect that a more reduced primitive achondrite than the Y74357 can reproduce the Amphitrite spectrum better by mixing less Fe-Ni metal than any others.

In conclusion, the S-type asteroids may have been derived from chondritic materials. The large chondritic asteroids may have experienced some modifications on its surface by collision etc., and the small ones may have remain unmodified.

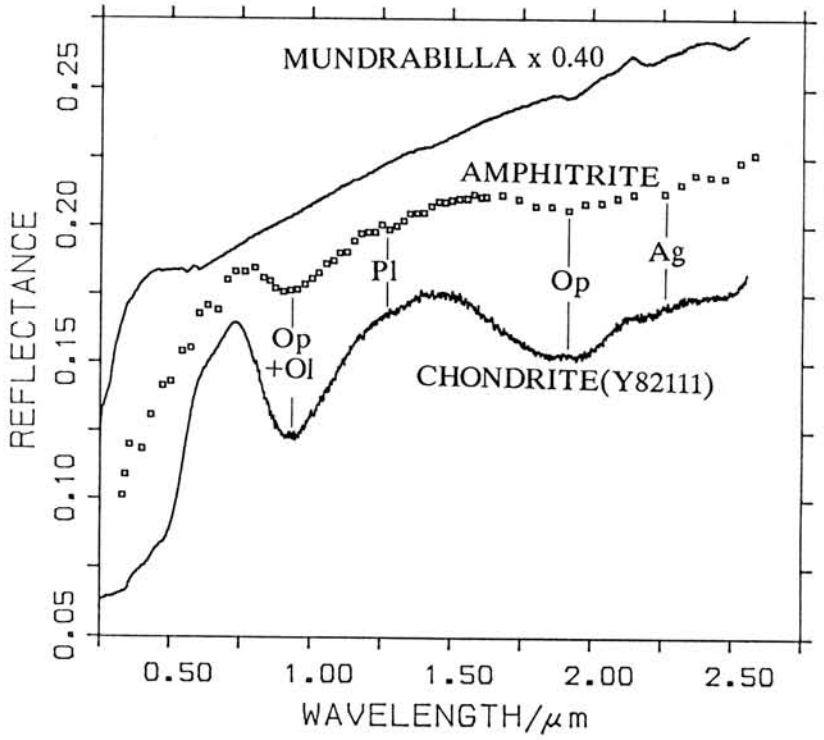

Fig. 1. Reflectance spectrum of an asteroid 29 Amphitrite (Bell et al., 1985) compared with those of an H6 chondrite Y82111 and an iron meteorite Mundrabilla.

We thank NIPR for the meteorite samples and Dr. M. Miyamoto for the spectrometer.

REFERENCES: [1] Bell J. F. et al. (1985) Lunar Planet. Sci. **XVI**, 47-48. [2] Hiroi et al. (1985b) Proc. **18th** ISAS Lunar Planet. Symp., 52-53. [3] Prinz M. et al. (1983) Lunar Planet. Sci. **XIV**, 616-617.

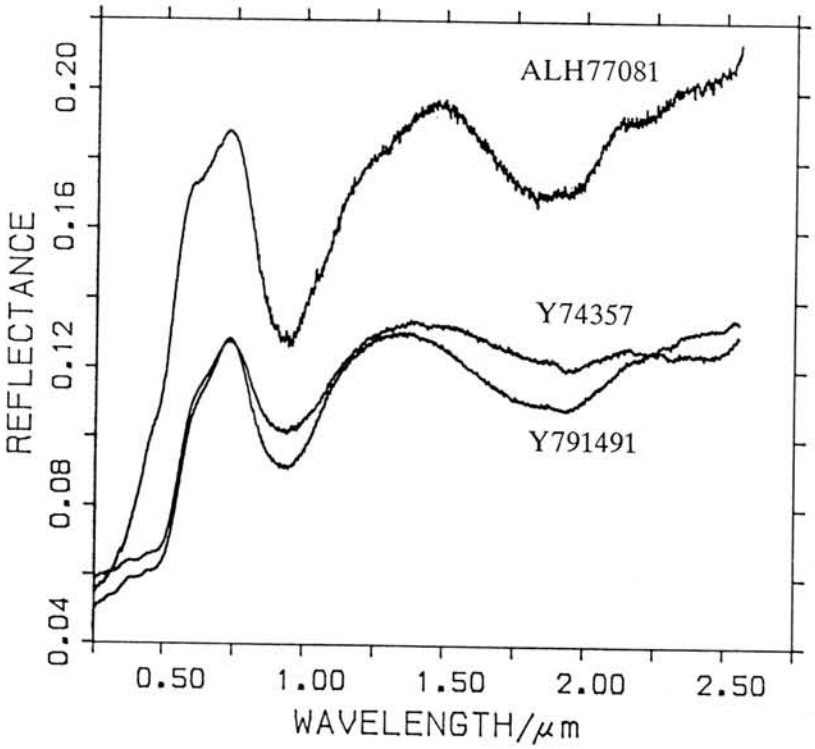

Fig. 2. Reflectance spectra of primitive achondrites: an Acapulco type winonaite Y77081, a lodranite Y791491, and a partly reduced lodranite Y74357.

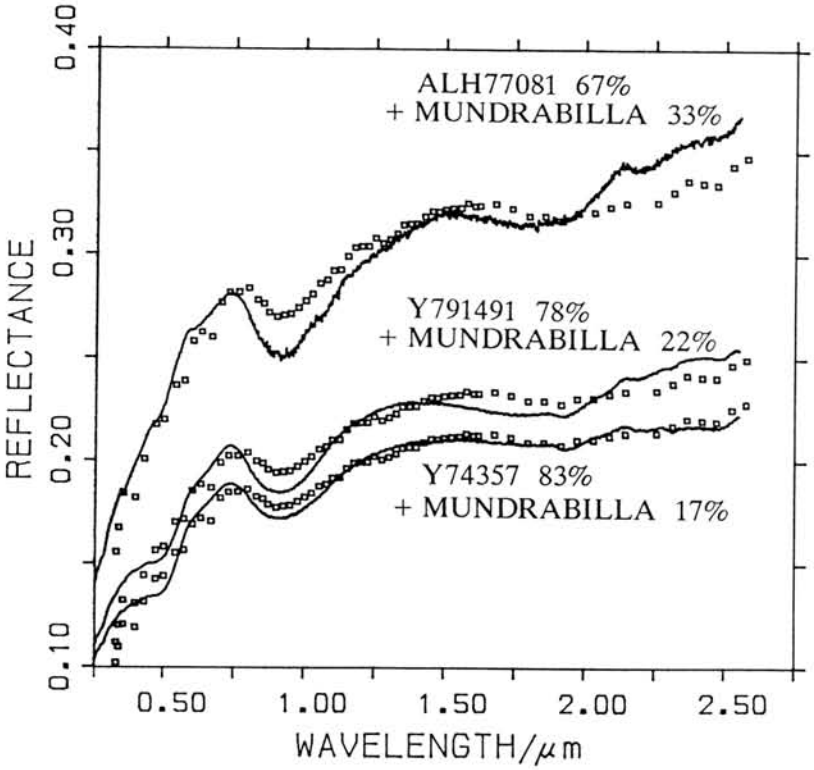

Fig. 3. Least square fittings of reflectance spectrum of Amphitrite by those of primitive achondrites and Mundrabilla.

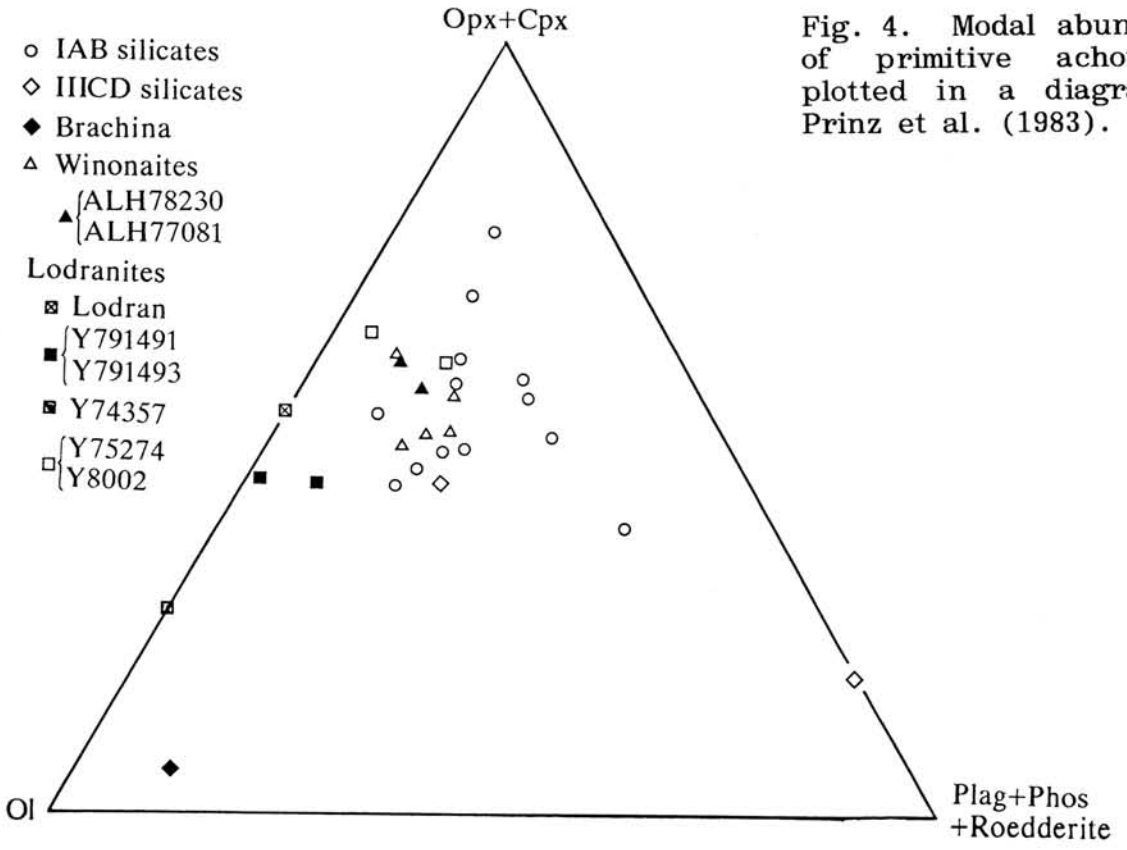

Fig. 4. Modal abundances of primitive achondrites plotted in a diagram by Prinz et al. (1983).

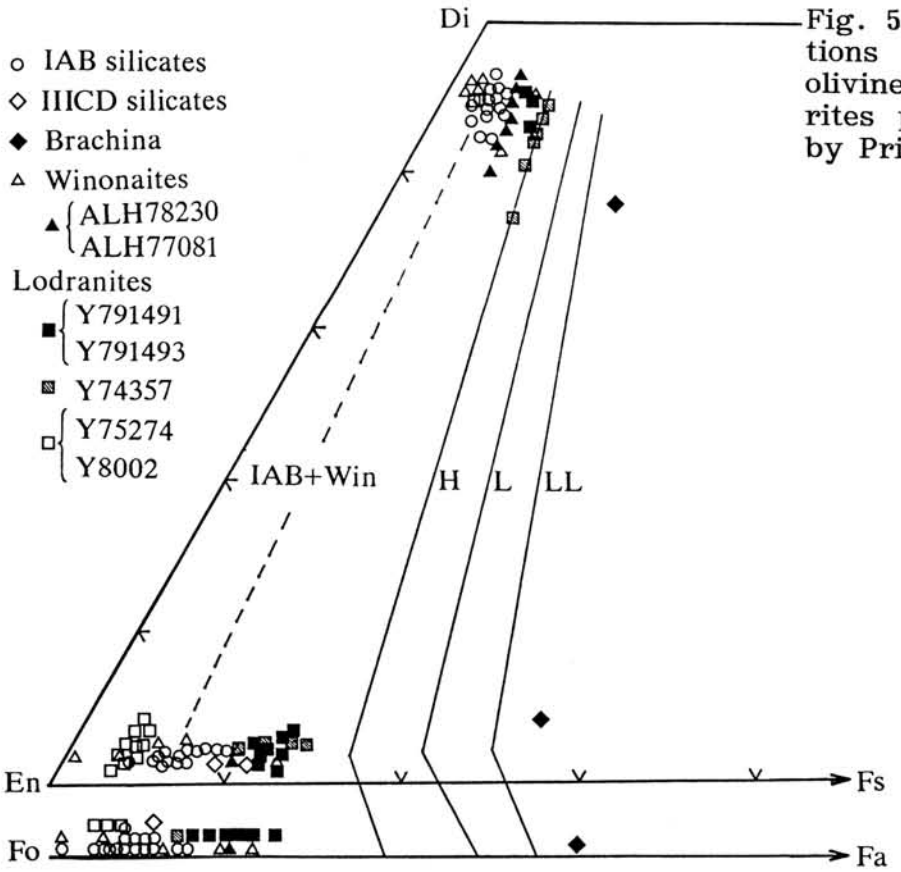

Fig. 5. Chemical compositions of pyroxenes and olivines in primitive achondrites plotted in a diagram by Prinz et al. (1983).

Special Session (III)

Lunar Meteorites

A STEP TOWARD THE PRIMARY LUNAR Pb COMPOSITION: U-Pb ISOTOPE SYSTEMATICS OF LUNAR NORITE 78235

Wayne R. Premo and M. Tatsumoto
U.S. Geol. Survey, Branch of Isotope Geology, Denver, Colorado 80225

One of the key problems with using the U-Th-Pb system for age determinations on lunar samples has been the absence of precise measurements of initial Pb compositions. Precise initial compositions are essential not only for precise lunar ages, but initial values for ancient highland rocks would provide vital information regarding the extent of volatile element depletion in the Moon. Therefore, we intent to investigate (as we have in the past [1,2]) ancient lunar highland rocks that may provide evidence of a primary lunar Pb isotopic composition and U/Pb ratio acquired during lunar formation. Lunar norite 78235, thought to be ancient, deep-seated, lunar crust, is described as a "coarse-grained, gabbroic rock with cumulate layering" that was shocked and melted [3,4]. The original cumulate layering is disrupted and crosscut by numerous veinlets of dark vesicular glass; the original mineralogy is reported to contain ~ 50% plagioclase and ~ 50% low-Ca pyroxene (bronzite) with minor high-Ca pyroxene, troilite, chromite, and whitlockite [3,4,5,6]. Other accessory phases reported include fluorapatite, rutile, Fe-Co-Ni metal, and baddellyite. Our subsample, however, contained ~ 70% deformed plagioclase (which ~ 30-40% is maskelynite), ~ 25% black to dark-brown vesicular glass, and < 5% pyroxene. Only the Fe-Co-Ni metal was observed as a minor constituent. After a whole-rock (WR) split was taken, four separates were hand-picked and include deformed plagioclase + pyroxene (D-Pl-Px), maskelynite (MA), dark vesicular glass (GL), and Fe-Co-Ni metal (ME). These separates were first treated with alcohol, then very dilute acids, in order to remove any terrestrial contamination and strip the grain surfaces of any adsorbed Pb component [7]. The remaining Pb in the residues should ideally represent initial Pb incorporated during noritic cumulate formation as well as radiogenic Pb that has since accumulated from the in situ decay of U and Th.

Pb isotopic data from residues of leached separates (solid circles), leaches (open triangles and diamonds), and washes (open squares) are shown in Figure 1, and are compared with the Pb composition of our laboratory contamination (blank Pb; large x). Washes and leaches define a trend (dashed line) between our blank Pb and a mixture of radiogenic Pb with an average age ~4300 Ma, and appear to have successfully removed any Pb contamination as well as adsorbed secondary Pb. Some leaches indicate that either a younger Pb component with a maximum age estimate of ~4100 Ma exists as a rind, coating grain surfaces in all separates except D-Pl-Px (the original norite), or Pb-loss experienced by this sample was restricted to the outer portions of grains. The Pb from all residues, except ME, is very

radiogenic (measured $^{206}Pb/^{204}Pb > 600$), plot very near the ordinate, and do not define a linear trend, indicating either sample heterogeneity or a disturbance to the U-Pb systematics.

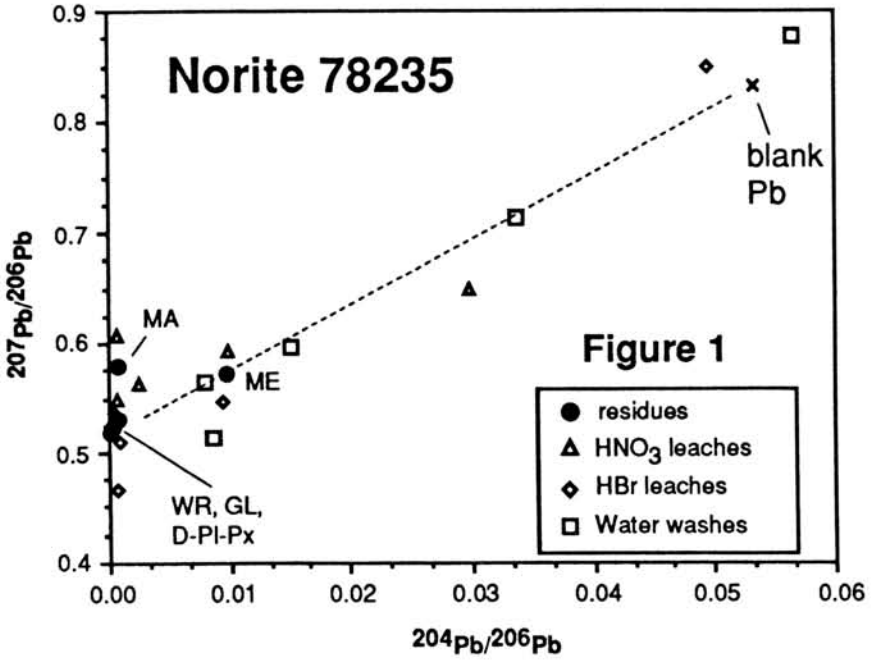

Assuming the Canyon Diablo troilite primordial Pb composition [8] for initial Pb values, the U and radiogenic Pb isotopes from 78235 define a formation age of 4425 ± 65 Ma for the original noritic material, and a metamorphic age of 3930 ± 210 Ma, apparently the age of the shock-melt event that caused an approximate 30 to 40% loss of Pb from the original norite. These two ages are indistinguishable from those defined by the cataclysm array of [9]. However, these ages are in conflict with previously reported Sm-Nd ages of 4.33 and 4.34 Ga for norite 78236, a sister sample [10,11]. Using the weighted mean of these two Sm-Nd ages, 4338 ± 43 Ma, as the crystallization age of norite 78235, we can calculate the initial Pb composition required to reproduce the same age and error in the U-Pb system (Fig. 2). That initial composition is $^{206}Pb/^{204}Pb = 44.19 \pm 0.1$, $^{207}Pb/^{204}Pb = 74.84 \pm 0.1$, $^{208}Pb/^{204}Pb = 55.21 \pm 0.2$; these values correspond to a $^{238}U/^{204}Pb$ (μ) of 508, assuming 4.56 Ga as the age of the Moon. The initial Pb compositions and μ value also agree with suggested initial compositions and μ values (~400 to 500) from several other samples of apparent ancient lunar crust, including 78155 [12], 67075 [2], and 60025 [13,14].

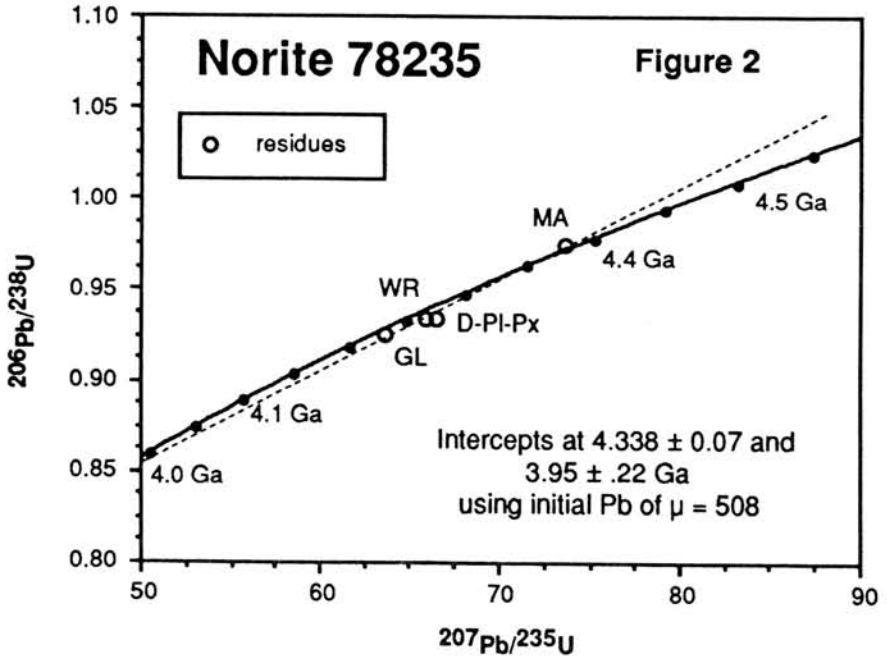

If we assume that these samples are products of the lunar magma ocean (primary differentiation event; 15), then the Moon must have started with a μ value of ~ 400 to 500. The μ values increase sharply if we assume younger ages for the Moon; for example, at 4.51 Ga, the initial μ is ~ 640; at 4.43 Ga, μ is ~ 1300. Such values are not inconsistent with the idea that the Moon was derived from part of Earth's early mantle ejected into orbit following an impact with a Mars-sized body between 4.43 and 4.56 Ga [16], as extreme temperatures could have caused an extreme U-Pb fractionation; the more volatile Pb being lost to space more readily than refractory U.

References:

[1] Tatsumoto, M., Premo, W.R., and Unruh, D.M. (1987) Proc. Lunar Planet. Sci. Conf. 17th, E361-E371.
[2] Premo, W.R., Tatsumoto, M., and Wang, J.-W. (1989) Proc. Lunar Planet. Sci. Conf. 19th, pp. 61-71.
[3] Jackson, E.D., Sutton, R.L., and Wilshire, H.G. (1975) GSA Bull 86, p. 433-442.
[4] Dymek, R.F., Albee, A.L., and Chodos, A.A. (1975) Proc Lunar Conf 6th, 301-341.
[5] Winzer, S.R., Nava, D.F., Lum, R.K.L., Schuhmann, S., Schuhmann, P., and Philpotts, J. A. (1975) Proc. Lunar Sci. Conf. 6th, p. 1219-1229.
[6] McCallum, I.S., and Mathez, E.A. (1975) Proc. Lunar Sci. Conf. 6th, p. 395-414.
[7] Tatsumoto, M. (1970) Proc Lunar Conf 1st, 1695-1612.
[8] Tatsumoto, M., Knight, R.J., and Allege, C.J. (1973) Science 180, p. 1279-1283.
[9] Tera, F., and Wasserburg, G.J. (1974) Proc. Lunar Sci. Conf. 5th, p. 1571-1599.
[10] Carlson, R.W., and Lugmair, G.W. (1981) EPSL 52, p. 227-238.
[11] Nyquist, L.E., Reimold, W.U., Bogard, D.D., Wooden, J.L., Bansal, B.M., Wiesman, H., and Shih, C.-Y. (1981) Proc. Lunar Planet. Sci. Conf. 12B, p. 67-97
[12] Nunes, P.D., Tatsumoto, M., and Unruh, D.M. (1975) Proc Lunar Conf 6th, p. 1431-1444.
[13] Hanan, B.B., and Tilton, G.R. (1987) EPSL 84, p. 15-21.
[14] Carlson, R.W., and Lugmair, G.W. (1988) EPSL 90, p. 119-130.
[15] Warren, P.H. (1985) Ann. Rev. Earth Planet. Sci. 13, p. 201-240.
[16] Cameron, A.G.W. (1986), in *Origin of the Moon*; (eds. Hartmann, Phillis, and Taylor), p. 609-616,

CONSORTIUM REPORTS OF LUNAR METEORITES Y-793274 AND Y-86032.

Takeda, Hiroshi, Saito, J. and Mori, H.
Mineralogical Institute, Faculty of Science,
University of Tokyo, Hongo, Tokyo 113.
Yanai, K. and Kojima, H.
National Institute of Polar Research, Kaga, Itabashi-ku, Tokyo 173.

Two allocations of two different sites of lunar meteorite Y-86032 have been made for our consortium study. Three preliminary reports (1-3) and several individual reports (4-6) have been published on these samples. The results indicated that Y-86032 is a feldspathic fragmental breccia with little regolith components and with low solar wind gases and KREEP components. The noble gas abundances, cosmic ray exposure ages and terrestrial ages (3) suggested that Y-86032 is paired with Y-82192 and Y-82193, in consistent with their mineralogical and petrographic data (1). At this symposium, the U-Pb isotopic characteristics of Y-86032 (7) and other results (8) will be reported.

Samples of another lunar meteorite Y-793274 has been separated on Feb. 22, 1990 and allocated to small numbers of consortium members for the maximum usage of the small sample. Y-793274 weighs only 8.66 g and has been classified as an anorthositic regolith breccia, which is the fourth lunar meteorite in the Yamato meteorite collection (9, 10). The pyroxene compositions in the pyroxene quadrilateral are distributed within more restricted region with a sharp cut at the magnesian side and extend more to the Fe-rich side (9, 10).

The sample weighed 8.411 g before processing and had a saw cut surface at the left side of the entire sample seeing on the B-view (Photo 321 of Yanai and Kojima, 1987) (10). About one third of the sample adjacent to and parallel to the cut surface was chipped. Two large fragments 1.4 X 1.2 cm in size (,10 2.125 g) and 0.5 X 0.8 cm (,61 0.172 g) have been produced, leaving 5.945 g of the original sample. At both sides of the two fragments, there is a large grayish clast (G1) 0.3 X 0.2 cm in size. This clast and a much smaller clast of this type (G2) and white feldspathic ones are set in a much smaller comminuted angular fragments of dark yellowish to pinkish and brownish pyroxenes and white plagioclase rimmed with glassy interstitial materials between them. The amounts of mafic fragments exceed that of plagioclase. A part of G1 (,93) was allocated to the INAA study.

The larger chip (,10) was further subdivided into more than ten fragments. One fragment containing clast G2 (,81 0.022 g) and matrix sample (,84 0.032 g) with numerous mafic and anothositic fragments were allocated to another INAA study. A sample of collection of small chips (,65 0.075 g) was allocated to an exposure age study, and another similar sample with matrix was allocated to a noble gas study (,85 0.028 g). The remainder of the large chip (,10 1.266 g) was further subdivided into several chips and allocated to the terrestrial and cosmic ray exposure age determination (,66 0.048 g), RNAA (,62 0.132 g) and the U-Pb systematics (,84 matrix-rich and ,86 0.042 g clast-rich). A chip with a part of G2 was use for the PTS preparation. Several chips were used for mineralogical studies and a PTS was prepared from the sawn sample (,91).

Microscopic observations of a PTS (,91-1) described previously and a new one (,91-2) show that this fragmental breccia is rich in angular mafic minerals than plagioclase. Clast-laden glassy breccia and small number of

glass spherule and glassy fragments are also present. One large clast, which should be a part of the G1-like clast includes fragments of pyroxene and olivine in a white (transparent) maskelinitized plagioclase matrix. A swirly glass is present at a corner of the clast. One gabbroic clast consists of rounded olivine in plagioclase. No lithic clast of apparent plutonic origin can be recognized in the PTS. Inverted pigeonite or pyroxenes with coarse exsolution lamellae have not been found.

The chemical compositions of pyroxene fragments analyzed by electron microprobe (Fig. 1) distribute the same mannar as previously reported (10). The chemical compositions analyzed within each pyroxene grain show variation (Fig. 1). By combining zoning trends of all fragments measured, we find that their variation covers the entire range, except for the Mg-rich fragments. The most Mg-rich trend is similar to an exsolution trend, but true lamellae were not detected. Some grains show fine lamellae-like texture suggestive of exsolution. The results suggest that the chemical variation is not due to the presence of many pyroxene-types of crustal rocks as other lunar meteorites exhibited (11), and that the trend may represent zoned pyroxenes such as those reported for rare mare rock clasts found in Apollo 16 breccias and Luna 16 (12), and lunar mare meteorites (13-18). The original rock may be coarse-grained.

The chemical compositions (An) of plagioclase fragments range from 98 to 88. Some fragments are chemically zoned within the above range. Rare fragments have extremely Ab-rich composition as a lunar plagioclase, with $An_{67}Ab_{30}Or_3$ and $An_{54}Ab_{44}Or_2$. The olivine compositions (Fa) vary from 8 to 85. The presence of large grain of silica mineral, fayalite and hedenbergite suggest fractionation within a possible intrusion. Minor ilmenite is present within the G1 clast.

In summary, Y-793274 is a fragmental breccia with minor regolith components and is rich in pyroxenes suggestive of mare origin (or non-crustal). The mare components are not basaltic, but may be a coase-grained rock similar to 60019, Ba-2 described by Takeda et al. (12), and meteoritic lunar mare materials (13-16). We thank NIPR for the samples.

References:

(1) Takeda, H., Kojima, H., Nishio, F., Yanai, K. and Lindstrom M. M. (1989) Preliminary report on the Yamato-86032 lunar meteorite: I. Recovery, sample descriptions, mineralogy and petrography. Proc. NIPR Symp. Antarct. Meteorites, 2, 3-14.

(2) Koeberl, C., Warren, P. H., Lindstrom, M. M., Spettel, B. and Fukuoka, T. (1989) Preliminary examination on the Yamato-86032 lunar meteorite; II, Major and trace element chemistry. Ibid., 2, 15-24.

(3) Eugster, O., Niedermann, S., Burger, M., Krähenbühl, U., Weber, H., Clayton, R.N., and Mayeda, T.K. (1989) Preliminary report on the Yamato-86032 lunar meteorite; III, Ages, noble gas, isotopes, oxygen isotopes and chemical abundances. Ibid., 2, 25-35.

(4) Koeberl, C., Kurat, G. and Brandstätter, F. (1990) Lunar Meteorite Y-86032, mineralogical, petrological and geochemical studies. Proc. NIPR Antarct. Meteorites Symp., 3, in press.

(5) Wang, M. S. and Lipschutz, M. E. (1990) Labile trace elements in lunar meteorite, Y-86032. Ibid., 3, in press.

(6) Warren, P. H., Jerde, E. A. and Kallemeyn, G. W. (1989) Lunar meteorites: Siderophile element contents and implications for the

composition and origin of the Moon. Earth Planet. Sci. Lett., 91, 245-260.
(7) Tatsumoto, M. (1990) U-Pb isotopic characteristics of the lunar meteorite, Yamato-86032. Abstr. 15th Symp. Antarct. Meteorites, this volume.
(8) Kurat, G., Brandstätter, F. and Koeberl, C. (1990) Lunar meteorite Yamato-793274: A lunar highland sample possibly rich in mare minerals. Abstr. 15th Symp. Antarct. Meteorites, this volume.
(9) Yanai, K. and Kojima, H. (1987) New lunar meteorite: Yamato-793274 abstract. Abstr. 12th Symp. Antarct. Meteorites, 17-18.
(10) Yanai, K., Kojima, H. (compiled) (1987) Photographic Catalog of the Antarctic Meteorites, p. 216, NIPR, Tokyo.
(11) Takeda, H., Miyamoto, M., Mori, H., Wentworth, S. J. and McKay, D. S. (1990) Mineralogical comparison of the Y86032-type lunar meteorites to feldspathic fragmental breccia 67016. Proc. Lunar and Planet. Sci. Conf. 20th, pp. 91-100.
(12) Takeda, H., Miyamoto, M., Galindo, C. and Ishii, T. (1987) Mineralogy of a basaltic clast in lunar highland regolith breccia 60019. Proc. Lunar Planet. Sci. Conf. 7th, J.G.R. 92, E462-E470.
(13) Warren, P. H. and Kallemeyn, G. W. (1989) Elephant Moraine 87521: A unique achondrite, possibly the first from a lunar mare. Geochim. Cosmochim. Acta, in press.
(14) Delaney, J. S., Sutton, S. R. (1990) Petrography of meteoritic VLT basalt breccia (87521) from Elephant Moraine, Antarctica. Lunar and Planet. Sci. XXI, 274-275.
(15) Warren, P. H., Kallemeyn, G. W. and Jerde, E. A. (1990) Compositional-petrographic investigation of two newly-aquired moon rocks. Lunar and Planet. Sci. XXI, 1297-1298.
(16) Yanai, K. (1990) Anorthositic gabbro: Cumulate meteorite from Antarctica. Lunar and Planet. Sci. XXI, 1365-1366.
(17) Lindstrom, M. M. and Martinaz, R. R. (1990) Lunar Meteorite Y793274: A second basaltic breccia. Abstr. 15th Symp. Antarct. Meteorites, this volume.
(18) Warren, P. H. (1990) Lunar Meteorites. A survey of the eight distinct moon rocks from Antarctica. Ibid.

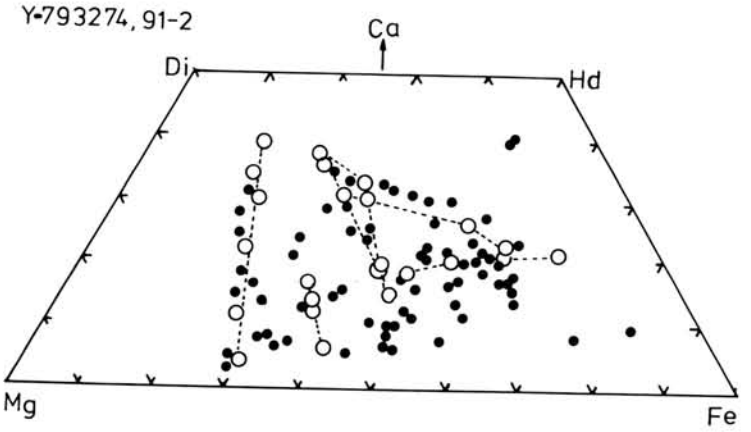

Fig. 1. Pyroxene quadrilateral of Y-793274,91-2. Solid circles are individual measurements; open circles with dotted lines represent zoning trends within one crystal fragment.

MINERALOGY OF LUNAR METEORITES, Y-86032, Y-793274 AND MAC88105.

Mori, H., Saito, J. and Takeda, H.
Mineralogical Institute, Faculty of Science,
University of Tokyo, Hongo, Tokyo 113.

A preliminary report on Y-86032 has been published as a part of the consortium study (1). The polished thin section of the representative portion of Y-86032 has petrographic characteristics very much like those of Y-82192/3. Very low abundance of regolith component, and solar wind gases (2) indicated that Y-86032 is similar to feldspathic fragmental breccia such as 67016. Y-86032 has been compared mineralogically with 67016 (3), MAC88105 and Y-793274. Granulitic clasts and clast-laden vitric (devitrified) breccia clasts are dominant in Y-86032. The mineral fragments consist of plagioclase, pyroxene, and olivine. The distribution of pyroxene compositions in the pyroxene quadrilateral is similar to those of Y-82192/3 and 67016,111 (3). Plagioclase compositions are also much like those in Y-82192/3 and 67016. Y-86032 is characterized by brown clast-laden glassy veins, which penetrate into breccia matrices.

To characterize crustal rock components, we searched for pyroxenes of plutonic origin. One large fragment of inverted pigeonite in Y-86032 contains blebby augites and another of orthopyroxene shows exsolution lamellae of augite on (100). They are from lunar crustal plutonic rocks, which are rare in MAC88105 and Y-793274.

TEM observation of Y86032,110 and ,111 showed that the fine-grained matrix material of both samples is composed of micron-sized angular fragments of plagioclase and very fine-grained (submicron-sized) interstitial material. The very fine-grained material is manly composed of plagioclase and minor mafic silicate minerals with a recrystallized texture. No glassy material was observed in the matrix. Microtextures of five lunar meteorite matrices have been compared to identify the pairing of these specimens. Mineralogy and size distribution of fine-grained matrices (micron to submicron sized) of these lunar meteorites are not much different. The degrees of recrystallization of matrices of Y-86032, Y-82192, Y-791197 and ALH81005 are similar and is lowest for MAC88105. Shock-produced glasses including both impact melt and maskelinite are not present in Y-86032, Y-82192, ALH81005 and have been observed only in Y-791197 and MAC88105.

In summary, the above information is consistent with the proposed pairing of the lunar meteorites (1) and Y-793274 and MAC88105 are unique.

We thank NIPR and Meteorite Working Group for the samples.

References:

(1) Takeda, H., Kojima, H., Nishio, F., Yanai, K. and Lindstrom M. M. (1989) Proc. NIPR Symp. Antarc. Meteorites, 2, 3-14.
(2) Euster, O., Niedermann, S., Burger, M., Krahenbuhl, U., Weber, H., Clayton, R. N. and Mayeda, T.K. (1989) Proc. NIPR Symp. Antarct. Meteorites, 2, 25-35.
(3) Takeda, H., Miyamoto, M., Mori, H., Wentworth, S. J. and McKay, D. S. (1990) Proc. Lunar and Planet. Sci. Conf. 20th, 91-100.

LUNAR METEORITE Y793274: A SECOND BASALTIC BRECCIA. Marilyn M. Lindstrom, NASA Johnson Space Center, Houston TX 77058, and Rene R. Martinez, Lockheed, Houston TX 77058.

Yamato 793274 was classified as an anorthositic lunar meteorite (1). Our current studies reveal that it is a basaltic breccia similar to EET87521 (2,3) and distinct from the seven anorthositic lunar meteorites (4).

Y793274,62 is a 130mg split of the 8.7g meteorite which we shared with Lipschutz. He is analyzing the smaller 30mg chip, while we separated the larger chip into four subsamples; bulk, glass-poor, black glass and green glass. We analyzed each by INAA and fused bead EMP. Preliminary results, based only on the first week's counting, are given in the table. The samples will be sent to Lipschutz for RNAA after INAA is complete.

The bulk composition of Y793274 is that of a mare basalt breccia. It has high concentrations of Feo (15%), Sc (38ppm), Cr (2200), Mn (1850), and Co (41), which are characteristic of mare basalts (5). Its TiO2 (0.57) is in the VLT basalt range, and its Fe/Mn (66) is typical of lunar samples. Most of these transition metal concentrations are lower than in EET87521 and other VLT basalts. Mass balance calculations suggest that 75-90% of the breccia is mare basalt, with the remainder mostly highlands material seen as white clasts (1). Concentrations of REE (figure 1) and other incompatible elements are lower than those of EET87521, but higher than those of VLT basalts. The pattern, like that of EET87521, has a REE slope similar to that of KREEP, and may indicate a small KREEP component in the breccia. Concentrations of siderophiles Au and Ir hint at meteorite contamination, as would be expected for lunar polymict breccias.

Basaltic breccias Y793274 and EET87521 are texturally distinct from mare gabbros Asuka 31 and Y793169, which were recently described by Yanai (6 and oral presentation), yet their modal proportions and mineral compositions suggest that they are generally similar to the others in bulk composition. Y793274 is a complex breccia consisting mostly of dark basalt clasts and mineral fragments in a glassy matrix, with scattered white lithic fragments. EET87521 is a polymict fragmental breccia consisting of coarse-grained mare basalt clasts in a matrix of mineral fragments and glass (2,3). One highland clast has been identified in thin section (3), and two others are visible on the hand specimen. In contrast Asuka 31 and Y793169 are unbrecciated coarse-grained igneous rocks with pyroxenes of variable composition (1).

The four basaltic lunar meteorites were found in three different regions of Antarctica. They appear to be petrographically distinct from each other. Y793274 and EET87521 are similar, yet distinct, in composition, while the mare gabbros have not yet been analyzed for major and trace elements. None of the basaltic lunar meteorites are paired specimens. This contrasts with the seven anorthositic lunar meteorites which, after considering pairing, represent only four falls. Although these anorthositic samples show some variations in petrography (regolith components and clast types), they are all very similar to each other in composition. The 4-4 distribution of highland-mare lunar meteorites contrasts with photogeologic surveys of the lunar surface which are 83-17 highland-mare. The dominant basalt among lunar meteorites appears to be VLT basalt, which is uncommon among Apollo samples.

Interpretations of the lunar meteorites and their differences from Apollo samples pertain to the nature and evolution of the lunar crust, and lead to more questions than answers. How many impacts do the eight lunar meteorites represent? and how many regions of the lunar surface were samples? Are lunar meteorites really random samples of the lunar crust? Why are the lunar meteorites found only in Antarctica? and are there

other lunar meteorites hidden among world eucrites? The answers to some of these questions await bulk geochemical studies of the remaining mare gabbros and cosmogenic nuclide studies of all four basaltic lunar meteorites. The answers to the last two questions are being addressed by curators of non-Antarctic meteorites.

REFERENCES: (1) K. Yanai and H. Kojima (1987) NIPR Catalog. (2) J.S. Delaney (1989) Nature 342, 889-890. (3) P.H. Warren and G.W. Kallemeyn (1989) GCA 53, 3323-3330. (4) M.M. Lindstrom et al (1990) LPS XXI, 704-705. (5) Basaltic Volcanism Study Project (1981) Pergamon. (6) K. Yanai (1990) LPS XXI, 1365-1366.

ACKNOWLEDGEMENTS: We thank Dr. K. Yanai and NIPR for the opportunity to study this very small and very interesting meteorite. This work was supported by NASA RTOP 152-13-40-21.

Compositions of Lunar Meteorites and VLT Basalts

	Y793274	EET87521	A17VLT	L24VLT	Y86032	Y791197
SiO2 (%)	48.3	48.4	46.7	46.2	44.1	
TiO2	0.57	1.12	0.92	0.85	0.20	0.34
Al2O3	13.7	12.6	10.0	13.1	29.3	26.1
FeO	15.1	19.0	18.6	18.6	4.22	6.39
MgO	9.03	6.34	12.2	6.71	6.11	5.24
CaO	12.0	11.6	10.0	13.0	16.2	15.4
Na2O	0.33	0.41	0.12	0.30	0.43	0.33
K2O	0.06	0.07	0.01	0.03	0.02	0.03
Sc (ppm)	37.7	44.	51.	48.	8.27	13.3
Cr	2190	1480	5070	1600	666	900
Mn	1850	1870	2020	2200	458	660
Co	41.1	46.	45.	43.	14.4	18.7
La	4.7	8.3	1.2	1.9	1.33	2.11
Sm	2.4	3.9	1.0	1.5	0.63	1.05
Yb	2.0	3.2	1.4	1.4	0.60	0.99
Hf	1.8	2.9	0.5	1.0	0.47	0.84

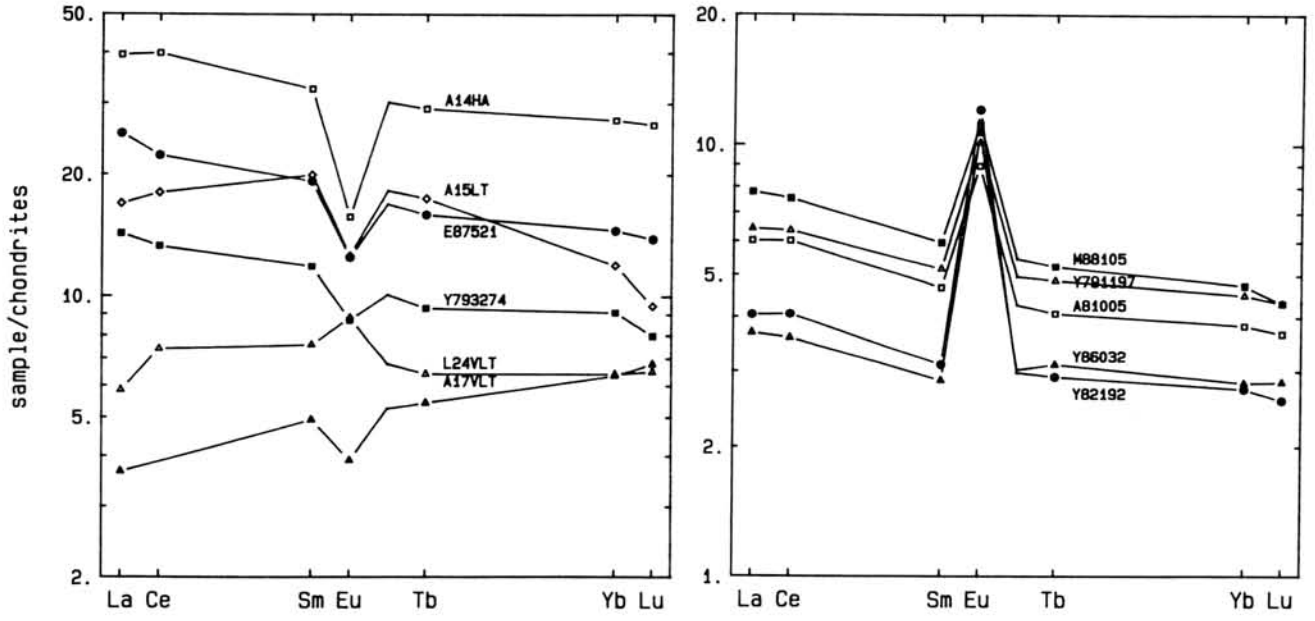

THE ELEPHANT MORAINE MARE BASALT BRECCIA AND THE IMPORTANCE OF THE LUNAR METEORITES AS SAMPLES OF THE LUNAR CRUST.

Jeremy S. DELANEY[1], S.R. Sutton[2] and R.L. Hervig[3]: (1) Dept Geological Sciences, Rutgers University, New Brunswick, NJ08903; (2) Dept Applied Sciences, Brookhaven National Lab., Upton NY11973; (3) Dept Chemistry, Arizona State University, Tempe, AZ85287.

The Elephant Moraine meteorite 87521 was originally identified as a eucrite (1) but petrological and geochemical studies have demonstrated it to be a breccia dominated by mare basalt material (2,3). The lunar affinities of the meteorite were further strengthened by the oxygen isotope signature of the sample (Clayton & Mayeda, 1989, personal communication). EET87521 was the first meteorite with abundant mare basalt material recognized but the subsequent reporting of two new mare basalts in the NIPR collections (4) has increased the number of mare basalts to three. At present, the three meteorites are each represented by a single specimen, unlike many of the highlands meteorites which are often represented by paired specimens.

Petrography of EET87521 The lithological components in EET87521 are very-low-titanium (VLT) basalt, shock glass (Figure 1)and uncommon leucocratic clasts probably of highlands origin. Much of the petrography of the specimens available has been given by (2), (3), (5) and (6). Significant features of the sample, however, are the wide range of mafic mineral compositions in the VLT fraction (Figure 2) and the widespread veining by the shock glass. The meteorite, on a broken surface roughly through the center of the stone, reveals light and dark areas that seem to define the abundance of shock glass. Some portions of the meteorite, therefore, may be relatively glass free but this awaits confirmation by study of the newly identified material. Almost all the VLT lithic clasts are ferroan and comparable with the eucrites while the magnesian portion of the VLT basalt is represented only by mineral clasts. The highlands clasts are relatively uncommon but were seen in section {,8} (3). Using trace element microprobe techniques (ion and synchrotron x-ray fluorescence {SXRF} microprobes) the shock glass and the feldspar in VLT basalt clasts have been documented for REE and Sr, Ti, Mn and other trace elements. The VLT feldspar (measured by SXRF) shows a range of Fe/Mn from 45 to 87, values that are typical of shocked lunar samples but higher than the values shown by lunar samples such as anorthosite 15415 (15-40) or by 14310 (35-46). However, mare basalt feldspars 15555, 15076 and 24109 show higher ratios of 42-87, 65 and 40-74 respectively. Similarly polymict highlands meteorite ALHA 81005 has Fe/Mn in feldspar between 32 and 82. The wide range of Fe/Mn in feldspar contrasts with fairly constant high values typical of olivine and of bulk rock samples. Although (7;8) have suggested that the observed range of Fe/Mn in feldspar in lunar samples reflected a shock signature, the new data including 87521 and 81005 suggest that the large range of feldspathic Fe/Mn is in fact caused by equilibrium processes during the crystallization of the feldspar and that the difference between ratios in highlands and mare regions reflects some fundamental difference in the crystallization conditions. Ion probe measurements of the light rare earths in plagioclase and glass from 87521 reveal important differences. Although the bulk sample has REE at ≈20xCI, a value that is surprisingly high for typical VLT basalt, the lithic clast feldspar has Ce and Sm abundances of ≈2-4xCI that are very similar to the Luna 24 VLT basalts. In contrast, the shock glass that pervades the meteorite has Ce and Sm contents of ≈120xCI even though the major element composition of the glass is close to the measured bulk composition of the rock (3) These observations confirm the suggestion by (3) that the 87521 contains a KREEP like component that is responsible for the elevated bulk rock REE pattern. Since this glass has invaded most of the lithic material, it must be carefully characterised so that its influence on the data from the VLT basalt fraction can be corrected. Although this meteorite is dominantly VLT basalt, there is a significant contribution from the high REE glass that may reflect the presence of a small, but ubiquitous highlands component.

The significance of the lunar meteorites: The lunar meteorite suite presently contains at least eleven specimens collected at seven different sites in Antarctica. These eleven specimens are not however individual meteorites. Several samples are paired and appear to represent five distinct highlands meteorites and three distinct mare meteorites. These meteorites were collected steadily between 1979 and 1988. Thus, the average rate of collection is greater than one per year. This consistent rate of discovery is in marked contrast to the rate of collection of other rare "planetary"

meteorites such as the SNC clan, of which only two have been found in Antarctica since 1979. Although lunar meteorites are uncommon when compared with the basaltic achondrites that appear to be ubiquitous at most sites in Antarctica, the lunar samples have become a regular feature of the sample collecting expeditions to Antarctica. The regularity with which the lunar meteorites are being recovered suggests that they are sufficiently abundant in Antarctica to ensure that future collecting by the meteorite search teams will recover more lunar samples from Antarctica during the next decade. The meteorites can be clearly demonstrated to be samples that were ejected from the moon over an extended period (0.5-~11Ma)and to have followed different trajectories (2500-<100000 years) between the Moon and the Earth using cosmogenic isotopic data and thermoluminescence studies (9,10,11.). The highlands meteorites although grossly similar to one another, are distinct and appear to sample different sites on the Moon. The three mare basalt rich meteorites are petrographically quite distinct and are unlikely to be paired. The present number of lunar samples is still small and any inference about the distribution of their sources on the Moon must still be tentative. The distinctive isotope signatures, exposure ages and terrestrial residence ages of the individual meteorites preclude any possibility that they sample a single crater on the Moon. The presence of both highland and mare meteorites suggests, however, that the present suite is a generally random sample of the entire surface of the Moon although the ratio of highlands to mare samples (5:3) no longer matches the relative surface areas of these provinces (83:17) as well as earlier data (2). If the mare meteorites are truly samples of the nearside maria, rather than clasts or specimens from small, highland basaltic regions, then the nearside may have been sampled slightly more frequently than the farside. Clearly the collection of more lunar meteorites from Antarctica will improve or constrain the randomness of sampling of the lunar crust by meteorites..

Since the manned missions to the Moon brought back samples from a limited area of the nearside, models of lunar evolution based on those samples can be applied with greatest confidence only for the area sampled. Although, many models have strong global implications, no independent samples have been previously available to test their generality. The existence of the meteorites, which appear to be from randomly distributed sites on the entire Moon provides the first opportunity for testing the generality of models of lunar origin based on the Apollo and Luna samples. The highlands meteorites are all breccias of highland regolith that contain a variety of lithic clasts. These have been matched with lithologies known from the highlands landing sites, but the relative abundances of the observed lithologies in the meteorite breccias and in the Apollo samples are still unclear. The comparison of the lunar meteorites with the Apollo and Luna samples has two aspects: (a) a search for lithologies in the meteorites that are unknown in the manned mission samples; (b) a systematic examination of the relative abundances of similar lithic components in polymict breccias from both the meteorite suite and the returned sample suite.

(a) The identification of previously unknown lithologies in the meteorites will extend the known diversity of lunar rocks. Future exploration of the Moon both by orbital mapping and by new sample return missions may pinpoint the lunar locality for any new lithologies so identified. More important, however, is the capability of *current* models of lunar petrogenesis to predict the existence and compositions of such lithologies. Such predictive capabilities provide the most direct test of the generality of the model. For example, the diversity of basalt types that are associated with early highland volcanism is not particularly well represented by the Apollo samples although magma ocean scenarios and other models such as serial magmatism are compatible with a range of basaltic material in the highlands. The presence of recognizable highland basalts as lithic clasts in meteorites is, therefore, potentially of great importance. Many highlands breccias contain clasts of basaltic material with affinities to the VLT suite of mare basalts, and VLT clasts have been identified in several of the lunar meteorites. Since EET87521 is a breccia rich in VLT it may be either from a very-low-titanium mare region, or possibly from a smalller highlands basalt with VLT affinities. The simplest approach would be to assume that EET87521 is indeed a mare basalt similar to the Luna 24 VLT basalts as suggested by (2)and (3)The meteorite contains, however, basaltic matrix glass with a significant KREEP component and plagioclase rich lithic clasts that appear to be of highlands origin (cf. 3). The presence of these components in the breccia suggest that EET87521 may, in fact, sample a highlands region containing both VLT basalt and KREEP basalts rather than a VLT mare region. Detailed comparisons of this meteorite with VLT samples from the sample return missions and with VLT rich

clasts from the highlands breccias and meteorites are in progress but, at present, this sample is believed to be from one of the nearside maria dominated by VLT basalts.

(b) In addition to the search for new lithologies in the lunar meteorites, the relative abundance and associations of previously known lithologies in the polymict breccias needs to be documented. Different sites in the lunar crust may have similar lithologies represented in polymict breccias but have them present in sufficiently different relative abundances to preclude their sharing a common petrogenesis. It is therefore of fundamental importance to compare not only *what* lithologies are present in the meteoritic breccias, but also *how abundant* is each lithology and whether particular suites of lithologies are characteristic at any given site.

References (1)Mason B & C Schwarz (1989) Antarctic Meteorite Newsletter,NN,aa-bb; (2)Delaney JS (1989) Nature, 342,889-890; (3)Warren PH & GW Kallemeyn (1989) Geochim Cosmochim Acta, 53,3323-3300; (4)Yanai K (1990) Lunar Planet Sci. XXI, aaa-bbb; (5)Delaney JS & SR Sutton (1990) Lunar & planet Sci. XXI, 274-275; (6)Warren PH et al. (1990) Lunar Planet Sci. XXI, 1297-1298; (7)DelaneyJS, et al. (1988) Lunar Planet Sci. XIX, 267-268; (8)Delaney et al. (1989) Lunar Planet Sci. XX, 238-239; (9)Sutton SR (1986) Mem. Natl Inst Polar Res., Spec Issue 41,133-139; (10)Eugster (1988) Proc NIPR Symp Antarct. Meteorites,1, 135-141; (11)Eugster (1989) Science 245, 1197-1208

Figure 1: General Texture of EET 87521 showing lithic clast of VLT basalt, shock glass veining and finer grained breccia.

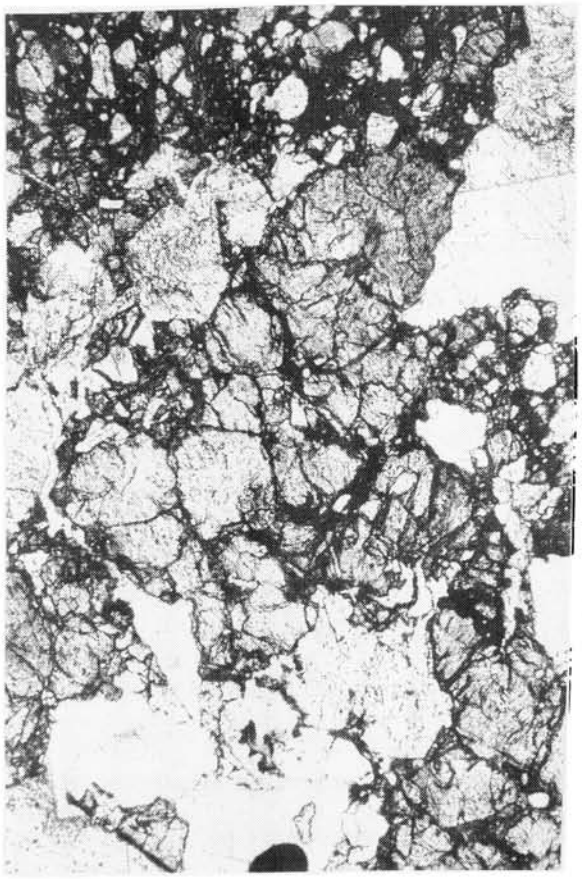

Figure 2: pyroxene quadrilateral and olivine and plagioclase composition histograms for EET87521.

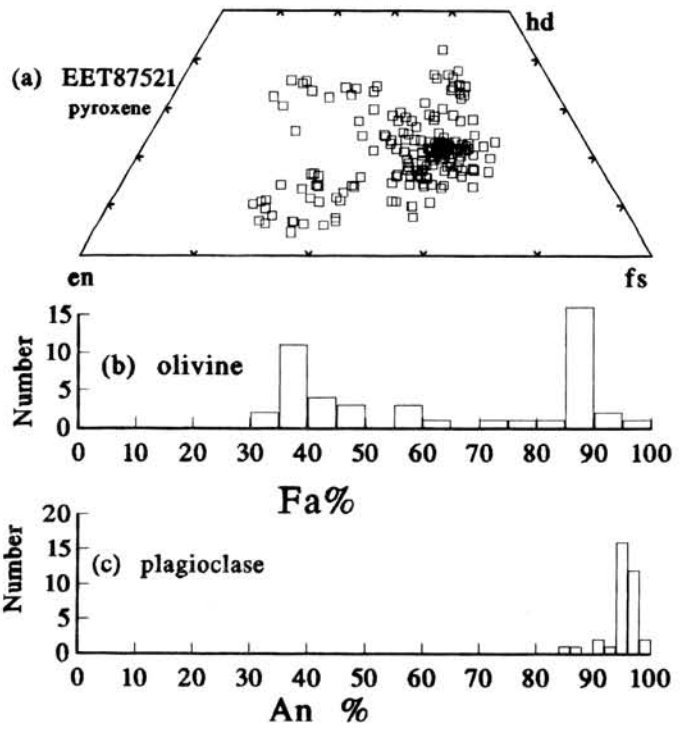

ASUKA-31: GABBROIC CUMULATE ORIGINATED FROM LUNAR MARE REGION

Keizo Yanai
Department of Meteorites, National Institute of Polar Research,
9-10, Kaga 1-chome, Itabashi-ku, Tokyo 173 Japan

Introduction: Antarctic meteorite **Asuka-31** (tentative name) is a lunar mare gabbro. This meteorite indicates that it is an unbrecciated, very coarse-grained cumulate closely related **very-low-titanium (VLT) lunar mare basalt**, and should be classified as a new type of lunar meteorites.

The ten Antarctic lunar meteorites collected previously at the Yamato Mountains, Allan Hills and MacAlpine Hills (**Y-791197, Y-793169, Y-793274, ALHA81005, Y-82192/193, Y-86032, EET87521 and MAC88104/105**)[1, 2, 3, 4, 5]. All of them except Y-793169 have sampled as breccia from the lunar crust. Asuka-31 indicates the lunar meteorites to include more varieties on the Moon rocks.

Asuka-31 meteorite: Asuka-31 was discovered as one of unusual specimen on the new site of Antarctic meteorites concentrated over 2,000 specimens, Dec. 20, 1988. There is on the ice field of Nansenisen (Nansen Ice Field), 130Km south of the Japanese Base "Asuka" (71°32'S, 24°08E). Asuka-31 is 442.12grams, near half stone with black-shiny fusion crust, and unbrecciated interior composed of reddish-brown pyroxene and translucent plagioclase with some black ilmenite. It appeared to coarse-grained and unbrecciated stone looks like very coarse-grained cumulate eucrites or ureilites. Preliminary examinations of thin section of the specimen shows that Asuka-31 is a coarse-grained and unbrecciated rock, consisting mainly of pyroxene and plagioclase (complete maskelynitized) with ilmenite and fine troilite, trace of olivine and nickel-iron. Asuka-31 is a typical subhedral granular and has a cumulate texture consisting of chains of pyroxene and isolated plagioclase crystals, ranging 2-4mm, 1-3mm respectively (Fig.1). The mode of Asuka-31 is roughly 59% pyroxene, 30% plagioclase, 6% ilmenite and 5% others including troilite and symplektite around ilmenite.

Pyroxene: Pyroxene is by far the most abundant component of the rock. It is almost colorless and occurs as subhedral cataclastic grains showing wavy extinction due to shock effect. The pyroxene range from En8.5-43.6, Fs30.7-68.2, Wo11.6-38.5, showing compositionally heterogeneous, although not zoned in any manner. Pyroxenes were plotted in wide range of Gabbro - Ferro-Gabbro region, however no pyroxenes were plotted over En50 (Fig.2). The FeO/MnO ratio of Asuka-31 pyroxenes remain within the range of lunar pyroxenes, which differs markedly from basaltic achondrites (Fig.3).

Plagioclase: Plagioclase appear as complete maskelynite and occur as isolated grains in chains of pyroxene crystals, however twining and zoning are not recognized. Most of the plagioclase are remarkably Ca-rich (An 85-96, Av 91.9). Only few grain of plagioclase among several dozen analyzed ran as low as An74 Ab23 Or3.4.

Opaque minerals and fusion crust: Ilmenite, troilite and trace of nickel-iron occur as opaque minerals. Ilmenite is subhedral-isolate grain within pyroxene and pyroxene-plagioclase, ranging 2-3mm. Troilite is fine grain of 10-30 microns. Most of troilite and some ilmenite grains were rimmed by symplektite like fine pyroxene aggregates. The fusion crust looks like very fresh shows green color with many fine bubbles.

Chemistry and Isotope: The bulk composition analyzed by H. Haramura is: 45.36%SiO_2, 1.66%TiO_2, 11.49%Al_2O_3, 0.17%Cr_2O_3, 21.18%FeO, 0.25%MnO,

6.41%MgO, 11.99%CaO, 0.50%Na_2O, 0.04%K_2O. Those data are consistent with those of Luna 24 VLT basalt and Apollo 17 VLT basalt from mare region. The bulk composition indicates that Asuka-31 is one of rocks from moon mare region, not highland as Fig.4 which shows FeO-MgO and TiO_2-Al_2O_3 values. It constrains especially related to VLT lunar mare basalt as Fig.5 which shows Mg/(Mg+Fe)-TiO_2 value. The oxygen isotope data is consistent with a luna origin; $\delta^{18}O$=5.69(pl), 5.33(px), $\delta^{17}O$=2.92(pl), 2.73(px)(R. N. Clayton, personal communication).

Conclusion: Asuka-31 is gabbroic cumulate; new type meteorite originated from lunar mare region, and it is closely related the very-low-titanium (VLT) lunar mare basalt. However it's lithology shows that it indicates plutonic, not volcanic flow.

References: [1]Yanai K & H Kojima(1979) NIPR Catalog. [2]Marvin VB(1983) LPSC XIV. 18-19. [3]Delaney JS(1989) Nature **342**, 889-890. [4]Warren PH & GW Kallemeyn(1989) GCA **53**, 3323-3330. [5]Delaney JS(1990) LPS XXI 273.

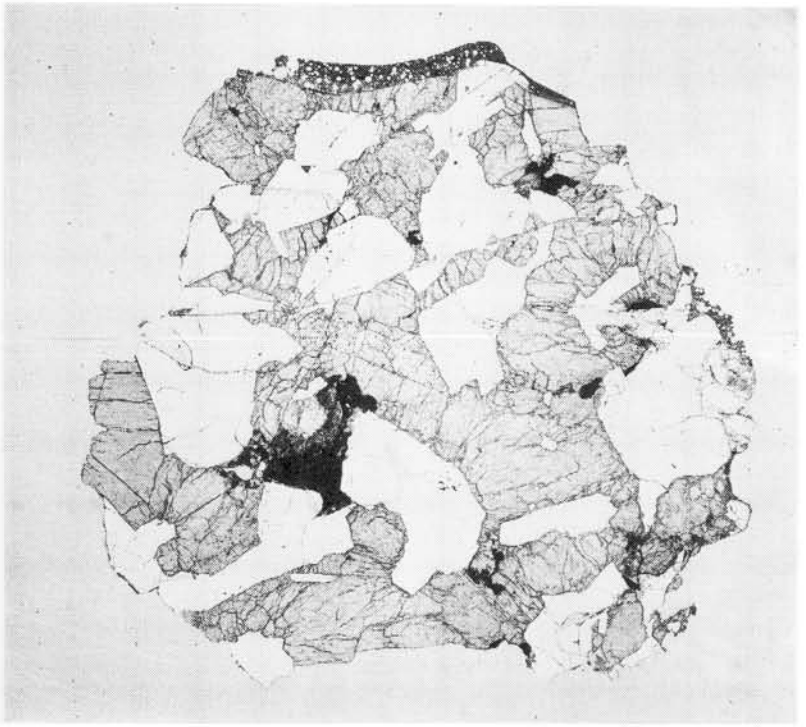

Fig.1: Photomicrograph of the thin section of Asuka-31, width 9mm.

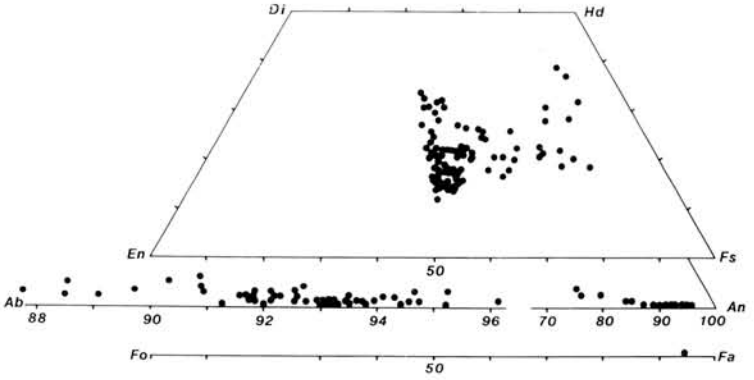

Fig.2: Compositional variation of pyroxenes, plagioclases and olivine in Asuka-31, determined by electron probe microanalysis.

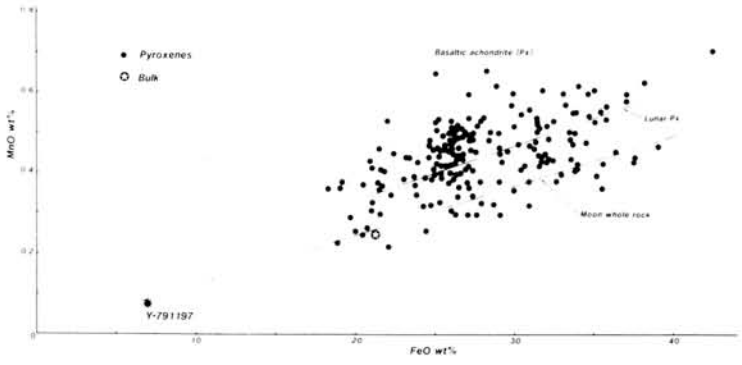

Fig.3: MnO-FeO values of pyroxenes in Asuka-31 as compared with those of lunar and achondritic pyroxenes and lunar whole rock analyses.

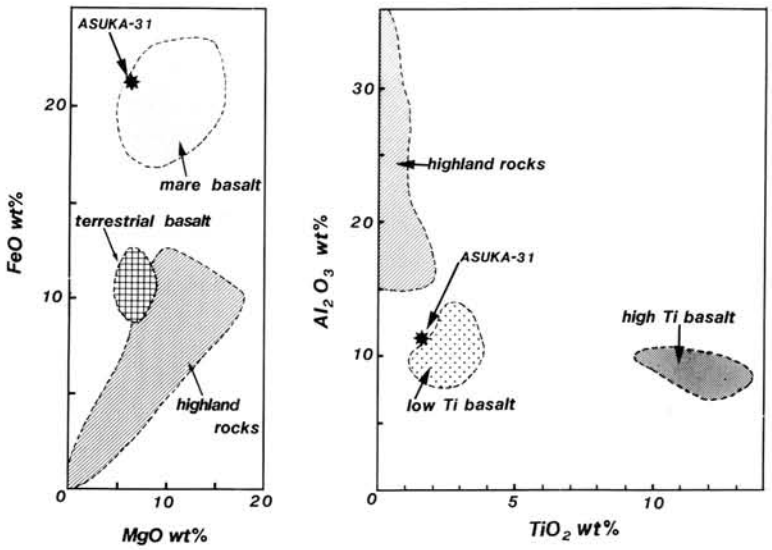

Fig.4: MgO-FeO and Ti_2O-Al_2O_3 values of Asuka-31 as compared with those of lunar rocks and terrestrial basalt.

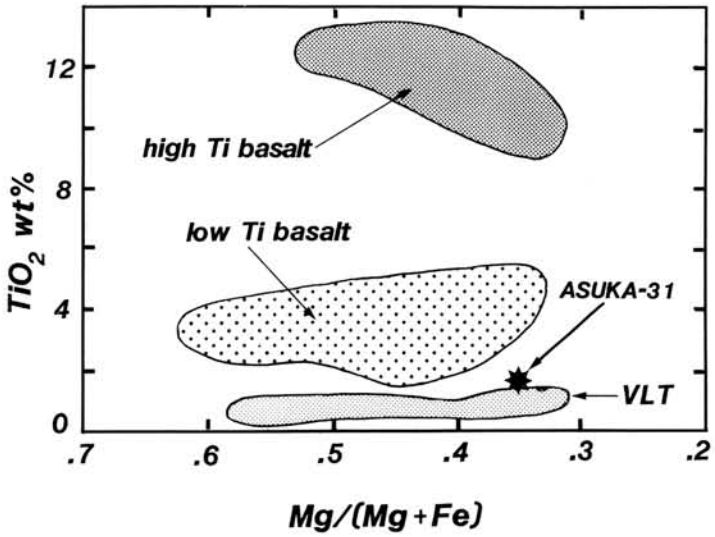

Fig.5: Mg/(Mg+Fe)-TiO_2 value. Asuka-31 is upper most in VLT basalt region and lower Mg'-value.

CHEMISTRY OF YAMATO-793274 LUNAR METEORITE

Fukuoka, T.

Department of Chemistry, Gakushuin University, Mejiro, Tokyo 171.

We are analizing more than 30 major, minor and trace elements in one white clast and two matrices from Yamato 793274 (Y-793274) meteorite by instrumental neutron activation analysis (INAA). One matrix sample (Sub. No.96) and one matrix sample with white clast (Sub. No.83) were provided from the National Institute of Polar Research of Japan. We separated the clast and the matrix from the matrix sample (Sub. No.83) and purified them prior to INAA. Preliminary analytical results are shown in Table 1 together with the chemical abundances of the matrices of Yamato-791197, -82192, -82193 and -86032 lunar meteorites.

Based on the well-established characteristic lunar and meteoritic ratios of FeO/MnO and K/La, and C1 chondrites normalized LIL patterns, Y-793274 meteorite is undoubtedly of lunar highland origin like other lunar meteorites (except EET 87521 (1,2)). Our conclusion is consistent with petrographic study (3).

The chemical composition of the clast, 83-1 is different from that of the matrices. This suggests that Y-793274 is a breccia. The chemical compositions of two matrices are slightly different. This indicates heterogeneous nature of the matrices which are attributed to their polymict character (3)and to the small sample size.

The chemical compositions of matrices of Y-793274 are highly different from those of other lunar meteorites such as Y-86032, -82192, -82193 and -791197 (see Table 1). Y-793274 lunar breccia includes the highest amount of KREEP component in lunar highland meteorites. These chemcal features suggest that Y-793274 meteorite is not pared origin with the other lunar meteorites and that the present 9 lunar meteorites originated possibly from more than 4 impact events on the lunar surface.

REFERENCES:

(1) Warren, P. and Kallemeyn, G. (1989) Geochim. Cosmochim. Acta,53, 3323. (2) Delany, J. (1989) Nature,342, 889. (3) Yanai, K. and Kojima, H. (1987) Abstract 12th Sym. Antarctic Meteorites, 17.

Table 1. Preliminary results of chemical abundances by INAA

		YAMATO 793274			Y86032[1]	Y82192[2]	Y82193[2]	Y791197[3]
		clast 83-1	matrix 83-2	matrix 96	matrix wtd.mean	matrix wtd.mean	matrix wtd.mean	matrix wtd.mean
Wt	mg	1.99	5.72	18.7				
TiO_2	%	0.61	0.60	0.66	0.24	0.22	0.27	0.30
Al_2O_3	%	30.3	18.8	15.0	27.9	27.0	25.8	27.1
FeO	%	5.29	13.82	14.30	4.46	4.60	5.70	6.7
MgO	%	8.0	8.9	10.1	5.2	4.5	5.1	6.4
CaO	%	19.1	13.3	11.5	15.8	15.1	16.7	15.3
Na_2O	%	0.57	0.45	0.37	0.45	0.49	0.41	0.34
K_2O	%	0.068	0.070	0.102	0.013	0.020	0.037	0.029
MnO	%	0.059	0.162	0.192	0.065	0.067	0.081	0.085
Cr_2O_3	%	0.074	0.240	0.319	0.094	0.110	0.154	0.120
Sr	ppm				180	190	180	137
Ba	ppm	79	97	85	23	26	28	39
Sc	ppm	9.26	29.4	34.4	8.55	8.68	12.2	12.9
V	ppm	24	85	140	23	27	31	28
La	ppm	4.72	6.99	5.13	1.22	1.11	1.27	2.17
Ce	ppm	11.0	19.4	16.1	3.1	2.7	3.6	5.4
Nd	ppm	6.9	11.6	7.4	2.1	1.5	2.0	34
Sm	ppm	2.05	3.12	2.08	0.62	0.54	0.65	1.04
Eu	ppm	1.37	1.10	0.77	0.90	1.10	1.00	0.78
Gd	ppm				0.83	0.80	0.80	1.3
Tb	ppm	0.39	0.64	0.46	0.14	0.12	0.15	0.24
Dy	ppm	2.8	3.6	2.7	0.9	0.9	1.0	1.5
Tm	ppm				0.12	0.08	0.11	0.16
Yb	ppm	2.15	3.02	2.29	0.58	0.55	0.73	1.03
Lu	ppm	0.31	0.42	0.33	0.088	0.082	0.117	0.15
Zr	ppm				20	20	20	32
Hf	ppm	1.94	2.76	1.93	0.39	0.36	0.45	0.81
Th	ppm	0.50	1.09	0.70	0.18	0.14	0.20	0.35
U	ppm	0.10	0.22	0.14	0.047	0.031	0.040	0.09
Ta	ppm				0.06	0.043	0.065	0.11
Co	ppm	17.5	44.1	46.9	15.4	14.4	19.2	19.8
Ni	ppm	150	120	100	162	121	150	180
Ir	ppb				5.0	2.9	6.0	6.5
Au	ppb				1.7	0.7	1.3	2.5

1) Fukuoka, T. et al.(1989) Abstract 14th Sym. Antarctic Meteorites 11.
2) Fukuoka, T. et al.(1986) Abstract 11th Sym. Antarctic Meteorites 40.
3) Fukuoka, T. et al.(1986) Mem. Natl Inst. Polar Res., Spec. Issue, 41 , 84.

U-Pb ISOTOPIC CHARACTERISTICS OF THE LUNAR METEORITE YAMATO-793274 AND 86032

M. Tatsumoto
U.S. Geological Survey, M.S. 963, Box 25046, Denver, CO 80225, USA

Lunar anorthositic samples have Pb isotopic signatures that are unique among all solar system material. The Moon was extremely depleted in volatile elements and, hence, the $^{238}U/^{204}Pb$ (μ) value was high (~300-400 ?) at its formation. Much Pb entered into sulfides and was removed to the deep lunar mantle and core from the lunar primary magma ocean. Pb partition coefficients for olivine and pyroxene are more than three times as high as the U and Th partition coefficients. Therefore, μ for the early cumulates (plus sulfides) from the lunar magma ocean to the lunar mantle was low (~50). The μ's of later cumulates gradually increased. The Pb partition coefficient for feldspar is large (probably ~0.5: Leemen, 1975), whereas those of U and Th are extremely small. Hence, anorthosite float from the lunar primary ocean has a very low μ and the Pb isotopic composition was changed only little since its formation. Thus, lunar highland Pb has a unique Pb isotopic composition (high $^{207}Pb/^{206}Pb$ and low $^{208}Pb/^{206}Pb$ values) compared to meteorites and terrestrial rocks.

Matrix material (150 mg) from Yamato-86032 was allocated from JSC, Houston, and subsequently 55 mg of white material (anorthosite-rich clast) was also allocated from NIPR, Tokyo. An attempt to separate a dark-colored portion from the white clast ended in fragmentation of 30 mg and 10 mg chunks, and numerous small pieces. Four fractions of the clast material and two separates of the matrix material were washed first with distilled ethanol and then with 0.1N HBr four times. Three clasts (Sub. No. 84, 86, 92) of 41, 32, and 16 mg each from Yamato-793274 were allocated. the clasts were washed with distilled ethanol and then leached with 0.1N HBr and 0.5 N HBr, four times each. Washes, HBr leaches, and residues of both meteorites were analyzed for U, Th, and Pb isotopes.

The $^{206}Pb/^{204}Pb$ and $^{207}Pb/^{204}Pb$ values for three clast residues of Yamato-793274 vary between 120 and 150, and 94 and 115 (~18 and ~15.6 for terrestrial basalts), respectively, as shown in Figure 1. The $^{208}Pb/^{206}Pb$ values are 1-1.1 (2.1 for terrestrial basalts). The Pb data of Yamato-793274 clearly show the high $^{207}Pb/^{206}Pb$ and $^{206}Pb/^{204}Pb$ values, as Y-791197 and ALHA 81005 did (Nakamura et al., 1985; Chen and Wasserburg, 1985) and thus provide strong, independent evidence of a lunar origin. Pb's of 0.1N HBr leaches and 0.5N HBr leaches are more radiogenic ($^{206}Pb/^{204}Pb$ values as high as 350) We interpret that this radiogenic Pb in leaches is probably lunar surface Pb which was incorporated into clasts at the brecciation and terrestrial Pb contamination is extremely small.

On the other hand, the 0.1N HBr leaches of Yamato-86032 yielded small amounts of Pb of near-terrestrial Pb isotopic composition. The Pb compositions

of the residues ($^{206}Pb/^{204}Pb$ up to ~60) were less than one-third as radiogenic as most lunar samples. However, they show a slight ^{207}Pb-rich signature and plot close to the Pb data for Yamato-791197 leaches, above the geochron. The data suggest either that the Moon has an unknown component of less-radiogenic Pb, or that the Pb is a mixture of lunar Pb with meteoritic and perhaps terrestrial Pb. Pb data of an acid-leach residue from Yamato-82192 (Nakamura et al., 1986) plot precisely on the geochron, suggesting contamination with a large amount of meteoritic or terrestrial Pb. Eugster (1989) suggested that Yamato 82192, 82193, and 86032 belong to the same fall, based on rare gas data. Pb of 86032 is similar to 82192 except for its ^{207}Pb-rich feature.

References:
Chen and Wasserburg (1985) Lunar Planet. Sci. XVI, 119-120.
Eugster (1989) Science 245, 244-245.
Leeman, W. P. (1975) Geochim. Cosmochim. Acta 43, 171-176.
Nakamura et al. (1985) 10th Symp. Antarctic meteorites, 45.
Nakamura et al. (1986) 11th Symp. Antarctic Meteorites, 18.

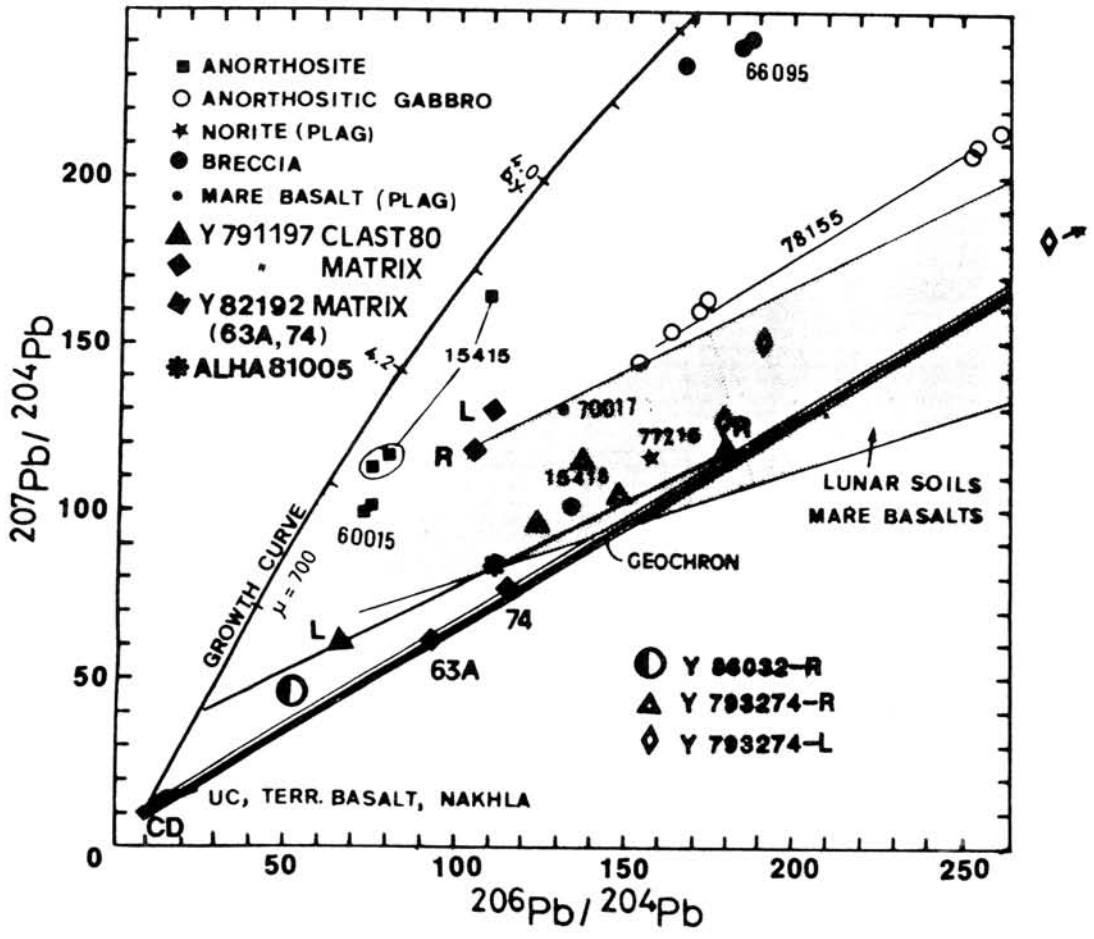

Fig. 1. $^{207}Pb/^{204}Pb$ vs. $^{206}Pb/^{204}Pb$ disgram for lunar meteorites and selected lunar samples.

Noble gases in lunar meteorites

N. Takaoka and Y. Yoshida
Department of Earth Sciences, Faculty of Science
Yamagata University, Yamagata 990.

Lunar meteorites are important because they can give information about new sites, which have never been sampled by Apollo and Lunar missions. Yamato-793274 and -86032 were originally classified as anorthositic regolith breccia (Yanai and Kojima, 1987). A recent mineralogical study reveals that Y-793274 is composed of mare basalt (Takada, private communication).

Specimens analysed in this work are Y-793274, 63, Y-86032, 63, ,66 and ,108. Y-793274, 63 (58 mg) was divided into three fractions: greenish glass, grain-size fractions of <25 um and >25 um. For Y-86032, 63 (224 mg) and ,66(206 mg), bulk samples and grain-size fractions (<25 and >25 um) were prepared. Y-86032,108(71 mg) is a white clast consisting mainly of felspar.

In this paper, we report results on noble gas isotopes in the Y-793274 glass and Y-86032 bulk samples. Noble gas analyses of the grain-size fractions of Y-793274 and Y-86032 specimens, and other studies are in progress.

The result on the noble gas isotopes is listed in Table 1. The Y-793274, 63 glass contains large amounts of noble gases trapped through solar wind implantation, indicating that the glass originated from solar-gas rich regoliths. Except for He, the abundance of trapped gases for the Y-793274 glass are two orders of magnitude higher than for Y-86032 (Table 2), and an order of magnitude lower than for Y-791197 (Takaoka, 1986), as found in Fig. 1. This trend is supported by preliminary data on noble gas compositions for the < 25 um fraction of Y-793274, which is not given in this paper. The abundance of trapped gases for Y-86032, 63 and ,66 is in good agreement with those for Y-82192 and -82193 (Takaoka,1987; Eugster and Niedermann, 1988). The trapped gases in Y-86032, 108 are low compared to the Y-86032 bulk (,63 and ,66). Y-86032, 108 lost most of trapped Ne and parts of trapped Ar, Kr and Xe. For He, the Y-793274 glass retains an appreciable amount of trapped

gas, while both Y-86032 bulk samples and feldspar-rich clast lost it to undetectable levels.

The concentrations of spallogenic ^{21}Ne and ^{38}Ar in the Y-86032 bulk samples agree with those in Y-82192 and -82193, indicating the same cosmic-ray exposure history. The concentrations of spallogenic ^{21}Ne and 38Ar in the Y-793274 glass are an order of magnitude higher than those in the Y-86032 bulk. With an assumption of the same production rate as for Y-82192, the upper limit of galactic cosmic-ray exposure age is about 100 m.y.

Fig. 2 is a three-isotope plot of Ne isotopes. The Y-793274 glass falls on a reference line, which ties between Ne-B (Black, 1972) and spallation Ne with $^{22}Ne/^{21}Ne$ = 1.27 at $^{20}Ne/^{22}Ne$ = 0.82. This suggests shallow shielding on the moon or a small meteoroid in space. The Y-86032 samples also correlate on this line to give the high $^{22}Ne/^{21}Ne$ ratio for spallation Ne.

Reference: Black,D.C.(1972) Geochim.Cosmochim.Acta, 36, 347-375. Eugster,O. and Niedermann,S.(1988) Earth Planet Sci. Lett.,89, 15-27. Takaoka,N.(1986) Mem. NIPR, Spec. Issue No.41, 124-132. Takaoka,N.(1987) Mem. NIPR, Spec. Issue No.46, 96-104. Yanai,K. and Kojima,H.(1987) Photographic Catalog of the Antarctic Meteorites, pp.298, NIPR.

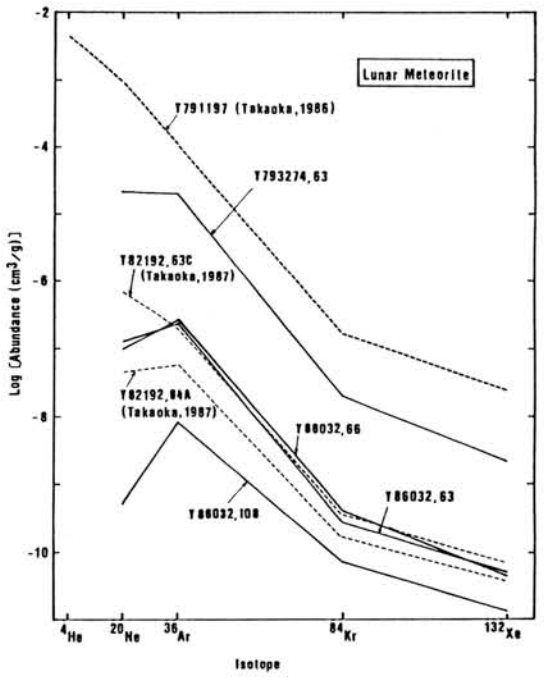

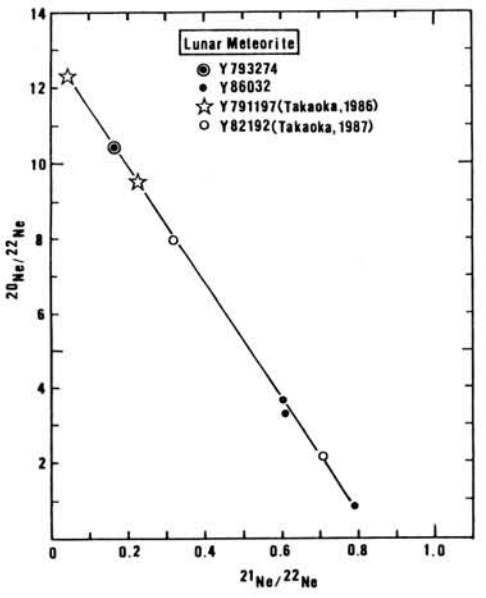

Table 1. Noble gases in Y-793274 and Y-86032 lunar meteorites.

Meteorite	Y-793274,63	Y-86032,63	Y-86032,66	Y-86032,108
Sample(mg)	Glass(8.76)	Bulk(62.7)	Bulk(55.4)	Clast(42.7)
^{4}He	1.9(E-4)	4.43(E-7)	3.80(E-7)	6.74(E-7)
$^{3}He/^{4}He$	9.6(E-4)	0.181	0.133	0.213
^{22}Ne	2.1(E-6)	4.28(E-8)	3.87(E-8)	2.44(E-8)
$^{20}Ne/^{22}Ne$	10.4	3.62	3.29	0.820
$^{21}Ne/^{22}Ne$	0.164	0.601	0.606	0.794
^{36}Ar	2.1(E-5)	2.58(E-7)	2.96(E-7)	2.85(E-7)
$^{38}Ar/^{36}Ar$	0.204	0.285	0.272	1.132
$^{40}Ar/^{36}Ar$	2.18	44.3	46.3	122
^{84}Kr	1.9(E-8)	2.8(E-10)	4.4(E-10)	7.3(E-11)
^{132}Xe	2.5(E-9)	5.0(E-11)	4.5(E-11)	1.4(E-11)

Concentrations are given in units of cm^3/g.

Table 2. Trapped and spallogenic gases in Y-793274 and Y-86032.

Meteorite	Y-793274,63	Y-86032,63	Y-86032,66	Y-86032,108
Sample	Glass	Bulk	Bulk	Clast
$(^{4}He)_t$	<1.9(E-4)	0	0	0
$(^{20}Ne)_t$	2.2(E-5)	1.29(E-7)	1.03(E-7)	5(E-10)
$(^{36}Ar)_t$	2.1(E-5)	2.40(E-7)	2.78(E-7)	8.6(E-9)
$(^{84}Kr)_t$	1.9(E-8)	2.8(E-10)	4.4(E-10)	7.2(E-11)
$(^{132}Xe)_t$	2.5(E-9)	5.0(E-11)	4.5(E-11)	1.4(E-11)
$(^{3}He)_s$	<1.8(E-7)	8.0(E-8)	5.1(E-8)	1.4(E-8)
$(^{21}Ne)_s$	2.9(E-7)	2.5(E-8)	2.3(E-8)	1.9(E-8)
$(^{38}Ar)_s$	3.1(E-7)	2.8(E-8)	2.8(E-8)	3.1(E-8)

Concentrations are given in units of cm^3/g.

VARIETIES OF THE LUNAR METEORITES COLLECTED FROM ANTARCTICA

Keizo Yanai and Hideyasu Kojima
Department of Meteorites, National Institutes of Polar Research
9-10, Kaga 1-chome, Itabashi-ku, Tokyo 173 Japan

Introduction: Over 10 specimens of lunar meteorite have been recovered from Antarctica by 1988-1989 field season. The specimens were at the **Yamato Mountains, Allan Hills** and **MacAlpine Hills(Y-791197, Y-82192/193, Y-86032**[1], **ALHA81005**[2], **MAC88104/105**[3]) have all sampled only plagioclase-rich highlands. **Y-793274** is pyroxene and plagioclase-rich breccia[4], and **EET87521**[5] is basaltic clasts-rich breccia: The both have much components from the basaltic provinces (the maria) of the lunar crust. **Asuka-31**[6] and **Y-793169**[6] are unbrecciated and coarse-grained cumulate rocks consisting mainly of pyroxene and plagioclase (maskelynitized) with ilmenite and troilite, trace of olivine and nickel-iron. The bulk composition of Asuka-31 and Y-793169 are very similar to those of **Luna 24 (VLT)** and **Apollo 17 (VLT) basalt** characterized **very-low-titanium (VLT) basalt.**

The oxygen isotope signature of all specimens is consistent a lunar origin, and the FeO/MnO ratios remain within the range of lunar pyroxenes, which differ markedly from that in basaltic achondrites as eucrites. However, in their pyroxene compositions there are large varieties as **Fig.1.** It seems that lunar meteorites were originated from several different places on the Moon surface which composed single rock facies or monomict-polymict breccia facies.

Conclusion: For their lithology, texture, petrography, chemistry and mineral compositions, the lunar meteorites divide to 4 or more different types as an **anorthosite regolith breccia** (included 2-3 different facies), **basaltic-anorthositic breccia, basaltic breccia, diabase and gabbroic cumulates** (Table 1). Those types indicate that each sample might originated from **at least 7 different sites** on the near and far-side sites of the Moon surface. Such varieties of the lunar meteorites strongly suggest that there are more varieties including **unknown type(s) of the lunar rock** in some where on the Earth and the Moon.

References: [1]Yanai K & H Kojima(1979) NIPR Catalog. [2]Marvin VB(1983) LPSC XIV 18-19. [3]Delaney JS(1990) LPS XXI 273. [4]Yanai K & H Kojima(1987) Abstracts, 12th Sym. A. M., 17-18. [5]Delaney JS(1989) Nature **342**, 889-890. Warren PH & GW Kallemeyn(1989) GCA **53**, 3323-3330. [6]Yanai K(1990) LPS XXI 1365-1366.

Table 1 Lunar Meteorites from Antarctica 1990.3

	Name	Wt.(g)	Lithology and type	Coll.
1	Y-791197	52.40	Anorthositic regolith breccia, A	Japan
2	Y-793169	6.07	Diabasic cumulate(VLT)	Japan
3	Y-793274	8.66	Basaltic-anorthositic breccia	Japan
4	ALHA81005	31.4	Anorthositic regolith breccia, A'	US
5	Y-82192	36.67	Anorthositic regolith breccia, B	Japan
6	Y-82193	27.04	Anorthositic regolith breccia, B	Japan
7	Y-86032	648.43	Anorthositic regolith breccia, B	Japan
8	EET87521	30.7	VLT basalt breccia	US
9	MAC88104	61.2	Anorthositic regolith breccia, B'	US
10	MAC88105	662.5	Anorthositic regolith breccia, B'	US
11	Asuka-31 (tentative)	442.12	Gabbroic cumulate(VLT) (VLT: very-low-titanium)	Japan

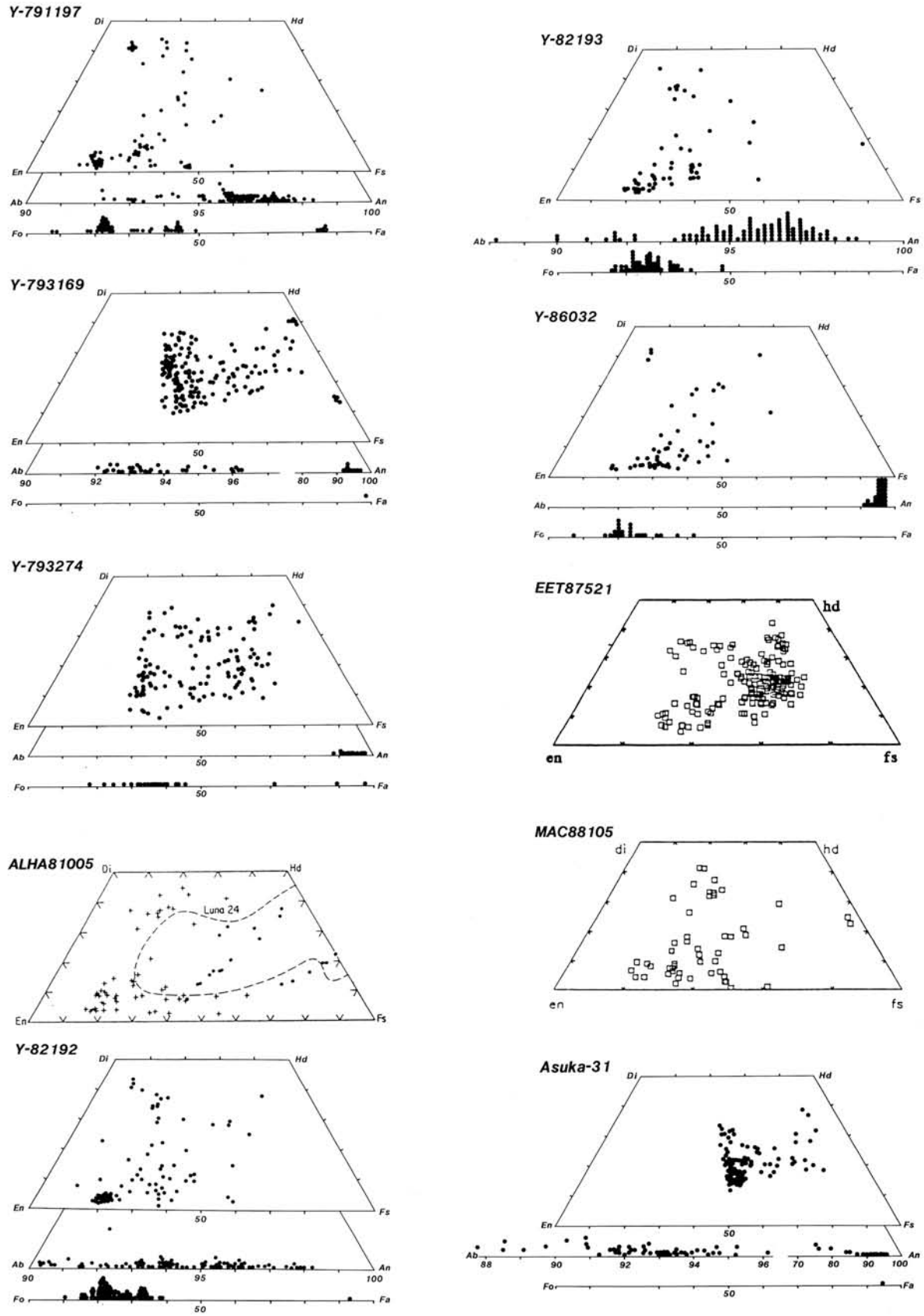

Fig.1: Pyroxene quadrilateral of all known lunar meteorites except MAC88104, with chemical compositions of olivines and plagioclases.

LUNAR METEORITES:
A SURVEY OF THE FIRST EIGHT DISTINCT MOON ROCKS FROM ANTARCTICA

Paul H. Warren

Institute of Geophysics and Planetary Physics, University of California, Los Angeles, CA 90024, USA

A total of 11 pieces of the Moon have now been found as meteorites collected by Japanese and American expeditions to Antarctica. This number includes one triplet plus one doublet of obviously "paired" samples. Thus, the total number of apparently distinct Antarctic Moon rocks currently stands at eight.

The value of this collection as an augmentation to previous sampling of the Moon can be appreciated by noting that the Moon has been directly sampled at only a total of nine sites (six US Apollo sites plus three USSR Luna sites). The Apollo sites were sampled most comprehensively, yielding 22-110 kg of material per site, mostly in the form of rocks (on average, about 135 rocks bigger than 5 g per site), from traverses that extended to points as far as 11 km apart. Sampling by the Luna probes was limited to 52-170 g of soil per site, obtained in the form of short cores. The representativeness of the Apollo and Luna samples is greatly enhanced by the "gardened" nature of the Moon's upper crust, thanks to its history of prolonged impact-bombardment. Thus, a significant fraction of the rocks at a typical point on the surface (especially if the point is in the ancient, heavily-cratered highlands) originally formed at points many tens, or even hundreds, of km away. However, six km-scale traverse zones, plus three 1-2 cm wide cores, hardly constitute an adequate sample of a heterogeneous, differentiated body with a circumference of 10,920 km. To make matters worse, for technological reasons the Apollo and Luna landings were clustered into a small region of the central nearside. A polyhedron drawn around all six Apollo sites covers only 2.8% of the Moon's surface, and adding the three Luna sites only stretches this coverage to 4.7%.

Lunar meteorites are delivered to the Earth by kinetic energy from random collisions (impacts) between other objects and the Moon. The 8 apparently distinct lunar meteorites do not necessarily represent 8 separate lunar impact sites. Hard evidence from cosmic-ray exposure (CRE) histories[1] (thus far measured isotopically for 4 of the 8 samples) guarantees a minimum of 2 separate lunar source craters, and the CRE data are only barely consistent with <3 sources [O. Eugster and K. Nishiizumi, presentations at 21st Lunar & Planetary Sci. Conf., 1990] (see also [1]). The 4 samples that have not yet been measured for CRE are petrographically distinct from one another, and totally unlike the 4 measured samples (i.e., dominantly mare, vs. dominantly nonmare). However, it is curious that 3 out of 8 samples are mare, and one of the others (Y793274) is a mixture of mare and nonmare material in roughly 2:1 proportions[2]. Only 1/6 of the Moon's surface appears (based mainly on albedos and crater-densities) to be of mare affinity. The remaining 5/6 of the surface appears to be highlands (nonmare) crust, and the maria are believed to be thin veneers (generally only a few hundred meters thick) covering nonmare materials. Simple probability theory indicates that the probability of finding 4 out of 8 instances of predominantly mare material, through random sampling of a population that is 1/6 mare, is only 0.031. Even ignoring the hybrid Y793274, the probability for 3 out of 7 random samples to be mare is only 0.095.

---

1 The relevant CRE age is the sum of the terrestrial age plus the "4π" exposure (Moon-Earth transit) age.

2 Based on our new data plus unpublished data from M. M. Lindstrom [pers. comm., 1990]. Our own data (preliminary, based on our microprobe fused bead technique only) indicate that the bulk composition of a 43-mg chip is (in wt%): SiO_2 47.1, MgO 9.0, Na_2O 0.33, Al_2O_3 17.4, FeO 12.2, MnO 0.178, Cr_2O_3 0.28, K_2O 0.07, CaO 12.1, and TiO_2 0.67. This meteorite probably originated as an immature soil near a highlands/mare boundary.

Short Petrological Descriptions of the Individual Meteorites: **Y791197** (mass: 52 g) is a relatively immature[3] regolith breccia composed of mainly highlands material [e.g., 2]. **Y793169** (6.1 g, not yet allocated for consortium investigation) is a medium-grained VLT (very-low Ti) mare basalt [K. Yanai, pers. comm., 1990]. **Y793274** (8.7 g) is a regolith breccia (probably relatively immature) composed of mare (probably VLT) and nonmare material in roughly 2:1 proportions [3] (see also footnote 1). **ALHA81005** (31.4 g) is a relatively mature regolith breccia composed of nearly pure highlands material. For a lunar regolith sample, it has an exceptionally high Mg/(Mg+Fe) ratio: 0.73. **Y86032** (712 g, including the far smaller paired specimens Y82192 and Y82193) is an extremely immature regolith breccia composed of mainly highlands material [e.g., 4]. **EET87521** (30.7 g) is a fragmental breccia (polymict, but with no indications of a surface regolith history). It is composed of nearly pure mare material. The mare component consists of relatively coarse-grained (cumulate?) diabases or gabbros, of VLT bulk composition [5,6]. **MAC88105** (724 g, including the far smaller paired specimen MAC88104) is an extremely immature regolith breccia [e.g., 7]. **Asuka-31** (tentative name, 442 g, not yet allocated for consortium investigation) is an uncommonly coarse-grained (cumulate) VLT mare diabase or gabbro [8].

Although the four dominantly-mare meteorites are petrographically distinct from one another, they might conceivably represent different samples of the debris from a single lunar source crater. Indeed, it is otherwise curious that they are so completely dominanted by VLT materials. The abundance of VLT types in the crust as a whole is difficult to gauge, however. Remote sensing techniques are far better at distinguishing between low-Ti and high-Ti mare basalts. Pieters [9] has recently used remote sensing to infer high proportions of augite within many large areas traditionally mapped as "pure" highlands. The minor mare components in ALHA81005, Y791197, Y86032 and MAC88105 seem to be dominantly VLT (see references in [6]). If CRE histories show that Y793169, Y793274, EET87521, and Asuka-31 represent 3-4 separate source craters, we will be able infer that VLT types are far more common than previously suspected.

The highlands meteorites are all regolith breccias (although in 2 of the 4 cases extremely immature). As such, they are compositionally equivalent to soils (or immature soils), formed by thorough blending of the upper-crustal materials of their respective locales of origin. In other words, their bulk compositions may be considered fairly representative of average compositions for large (scale of the order tens of km) zones of the lunar crust. Compared to the three highlands sites sampled previously (Ap-14, Ap-16, and Luna-20), these four meteorites show major-element compositions most like the relatively aluminous Ap-16. Al_2O_3 contents range from 25.6 wt% in ALHA81005 to ~28.3 wt% in MAC88105 [10]. These compositions thus confirm earlier assumptions that not only in the central nearside, but globally, the Moon's upper crust has a highly anorthositic bulk composition[4]. This highly anorthositic composition, so unlike the mafic sort expected for a simple amalgam of mantle-derived partial melts, is the single most important line of evidence in support of the "magma ocean" hypothesis of remarkably widespread primordial lunar melting.

For trace incompatible elements (which on the Moon tend to be concentrated into KREEP), the four highlands meteorites stand in stark contrast to all three of the highlands sites

---

3 Regolith breccias are rocks formed by shock-welding of pre-existing soil parcels. The maturity of a lunar soil is a measure of how long it has been exposured to lunar surface processes (most notably gardening and mixing). In general, a mature soil is a more thorough mixture of its regional crust than an immature soil.

4 Assuming that the 4 highlands meteorites come from 4 random points on the lunar surface, the statistical probability that all four are from the same (nearside) hemisphere as the Apollo and Luna sites is $0.5^4 = 0.063$.

sampled previously. Consider, for example, the typical rare earth element Sm. Regolith Sm contents are 26-38 μg/g at Ap-14, 1.3-9.8 μg/g at Ap-16, and ~3.2 μg/g at Luna-20 [10]. Yet among the four highlands meteorites Sm contents range from 0.63 in Y86032/8219X to 1.2 in MAC88105/4 [10]. Earlier estimations of the bulk composition of the lunar crust, and thus some estimations of the bulk composition of the Moon, should be revised downward for the extremely important refractory incompatible elements Th and U; and for K, REE, and many other incompatible elements.

When normalized to CI chondrites, the siderophile element patterns of the regoliths at the sampled highlands sites of the central nearside show large peaks at Au (Ap-16, Ap-14 and Luna-20) and Ni (Ap-16, Ap-14) [10]. The high CI-normalized Ni/Ir ratio at Ap-16 (~2.2) has been especially controversial. However, the lunar highlands meteorites, including our newest results for MAC88105, show flatter patterns and lower siderophile levels overall.

The handful of ages that have thus far been obtained from lunar meteorites [reviewed by 11] tend to cluster near 3.9 Ga. Many more data are needed, but if the lunar meteorites confirm that the clustering of highlands impact melt ages at 3.9 Ga is a global phenomenon (as opposed to being another idiosyncrasy of the central nearside), the main observational justification for the "cataclysm" hypothesis of lunar cratering history [12] would be greatly reinforced.

Another important means of testing the magma ocean (or magmasphere) hypothesis is through detailed investigations of petrochemical trends among "pristine" nonmare rocks, which are fragments (clasts or small rocks) that survived the extensive impact gardening of the upper lunar crust without having their original compositions altered by blending with other materials. Far more typical, among highlands rocks, are polymict breccias (e.g., impact-melt, fragmental, and regolith breccias) that are not directly relateable to endogenously lunar magmatic processes. The magmasphere hypothesis has generally been supported by investigators of pristine rocks, because these rocks manifest a sharp geochemical bimodality, with the most generally anorthositic type having distinctively "ferroan" Mg/(Mg+Fe) ratios, considering that they also possess relatively low Na/(Na+Ca) and Eu/Al ratios. Models of crystal fractionation and plagioclase flotation starting from a high-degree melt of lunar bulk matter predict compositions for the flotation crust similar to the average composition of the ferroan anorthositic suite of pristine rocks [e.g., 13]. The other, "Mg-rich" rocks of the ancient lunar crust are probably products of "serial" magmatism involving many separate layered intrusions. Several obviously pristine clasts have been found within the lunar meteorites. Most of these are ferroan or "hyperferroan" (more ferroan than any rock known from the Apollo/Luna collection). One clast from MAC88104 [7] is noteworthy for having geochemical parameters nearly intermediate between the ferroan type and the Mg-rich type. As additional lunar meteorites become available, we look forward to a greatly improved understanding of lunar gross evolution.

References: [1] Eugster, O. (1989) *Science* **245**, 1197-1202. [2] Ostertag R. et al. (1986) *Proc. 10th Sym. A. M.*, 17-44. [3] Yanai K. and Kojima H. (1987) *Abstracts, 12th Sym. A. M.*, 17-18. [4] Takeda H. et al. (1990) *PLPSC 20th*, 91-100. [5] Delaney J. S. (1989) *Nature* **342**, 889-890. [6] Warren P. H. and Kallemeyn G. W. (1989) *GCA* **53**, 3323-3330. [7] Warren P. H. et al. (1990) *LPS XXI*, 1297-1298. [8] Yanai K. (1990) *LPS XXI*, 1365-1366. [9] Pieters C. M. (1989) *LPS XX*, 848-849. [10] Averages of many literature analyses. [11] Kaneoka I. and Takaoka N. (1987) *Proc. 11th Sym. A. M.*, 105-112. [12] Ryder G. (1990) *Eos* **71**, 313-323. [13] Warren P. H. (1990) *Amer. Mineral.* **75**, 46-58.

55

Lin Wenzhu

Institute of Geochemistry, Academia Sinica, Guiyang, P. R. China

Alexey A. Marakushev

Department of Petrology, Moscow State University, USSR

57

Nikolai S. Gorbachev

Institute of Experimental Mineralogy, USSR Academy of Sciences, USSR

Friday, June 1, 1990

0900-1430 *Symposium, Auditorium*

1430-1545 *Special Lecture*

Professor Edward Anders

Invited Speaker,

Enrico Fermi Institute, University of Chicago

In-situ micro-Raman Observation on Some Differentiated Meteorites :Graphitic Materials in Antarctic Ureilites

Kagi, H.[1], Takahashi, K.[2], Shimizu, H.[1,2], Kitajima, F.[1] and Masuda, A.[1,2]

1) Department of Chemistry, The University of Tokyo
2) The Institute of Physical and Chemical Research

Ureilites, one of the most perplexing achondritic groups, contain a few wt.% of graphite and diamond filling spaces between the larger silicate minerals, i.e. olivine and calcium poor pyroxene. While the origin of the diamonds has been a controversial problem [1][2], few systematic studies of the graphitic material have been performed from the viewpoint of structure chemistry. The structure of graphitic material is interesting for its possibility as a new cosmo-thermometer[3].

We obtained Raman spectra of the graphite contained in four Antarctic ureilites; Allan Hills(ALH)-77257, ALH-78019, Meteorite Hills(MET)-78008 and Yamato(Y)-791538, using RAMANOR U-1000 laser Raman microprobe manufactured by Jobin Yvon. Polished thin sections, prepared only with alumina abrasive, were used for Raman microprobe measurements. The exciting frequency employed was the green line at 514.532 nm of argon ion laser, the slit width employed was 500 micrometer and laser power was 20 mW at the sample surface. The exciting light was focused into a spot of 1 micrometer on the graphite.

In Fig.1, Raman spectra of the graphite are displayed. Two band centered at 1350 cm^{-1} and 1580 cm^{-1} are observed in each spectrum. It is well known that the first-order Raman scattering from graphite produces two bands at 1580 cm^{-1} and 1350 cm^{-1}, and that the latter band is inversely proportional to the crystallite size along a-axis of the graphite crystal [4]. The calculated crystallite sizes, L_a, are shown in Table 1.

The order of the graphite crystal along a-axis is

ALH-78019 > ALH-77257 = Y-791538 > MET-78008.

The graphitization proceeds more rapidly corresponding to the increase of the temperature and pressure. Therefore, the results mean that ALH-78019, whose graphite is highly graphitized, suffered the most highest temperature among the four ureilites studied here.

We will also discuss the durability of the graphite to the acid treatment for mineral dissolution.

We thank National Institute of Polar Research for meteorite samples.

References:

[1]Fukunaga, K., Matsuda, J., Nagao, K., Miyamoto, M. and Ito, K. (1987) Nature, **328**, 141-143.
[2]Fukunaga, K., Matsuda, J. and Ito, K. 15th Symposium on Antarctic Meteorites (abstract) 130-131.
[3]Frans J. M. Rietmeijer and Ian D. R. Mackinnon (1985) Nature, **315**, 733-736.
[4]Tuinstra F. and Koenig J. L. (1970) Jour. Chem. Phys., **53**, 1126-1130.

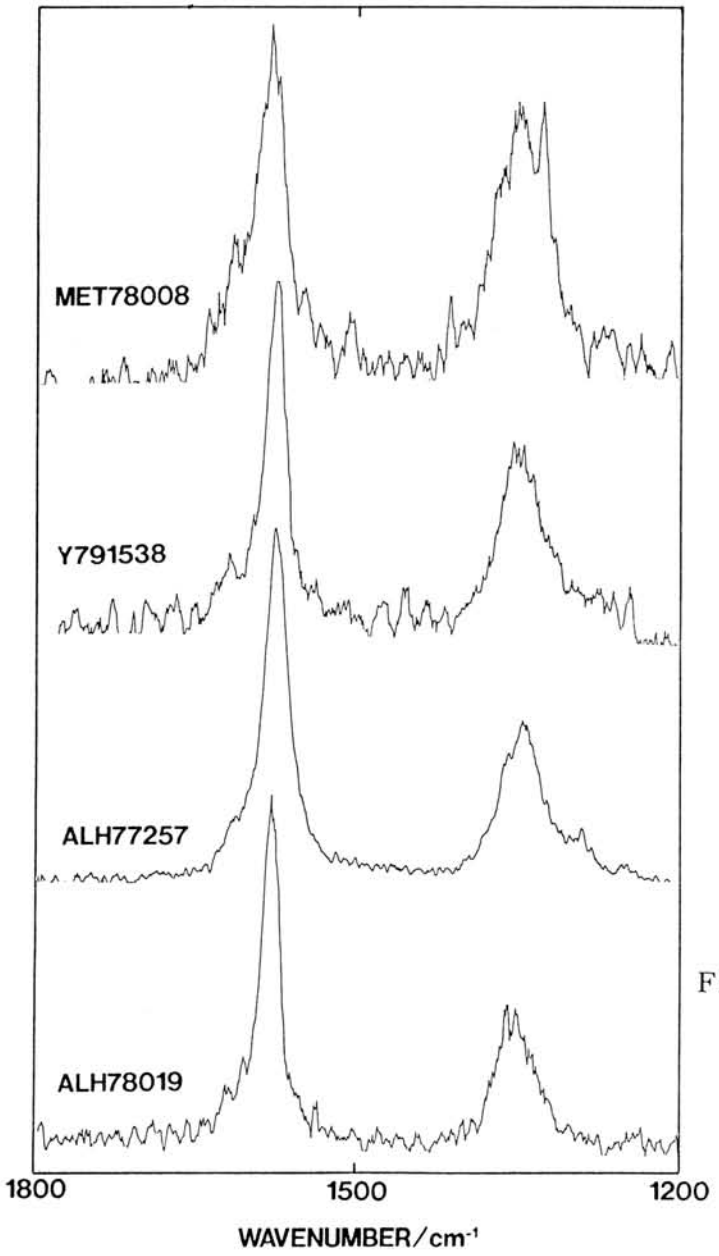

Fig. 1. Raman Spectra of graphitic materials in four Antarctic ureirites.

Table 1. Crystallite size along a-axis estimated from the ratio of the intensities of the two bands; 1350cm^{-1} and 1580 cm^{-1}

sample name	L_a / nm
MET-78008	7
ALH-77257	9
Y-791538	9
ALH-78019	12

CHEMICAL COMPOSITION OF ANTARCTIC METEORITES (1) - ORDINARY CHONDRITES

Ebihara, M. and Ozaki, H.

Department of Chemistry, Faculty of Science, Tokyo Metropolitan University, 2-1-1 Fukasawa, Setagaya, Tokyo 158.

One of the most characteristic features in the Antarctic meteorite collection is plentifulness of meteorites classified as petrologic type 3 in an ordinary chondrite group (unequilibrated ordinary chondrites, hereafter UOC's). By instrumental neutron activation analysis, we analyzed 32 ordinary chondrites from Antarctica, of which two thirds belong to petrologic type 3 (nine for H3, eight for L3 and four for LL3). The remaining samples are H-group chondrites of petrologic type 4-6 (equilibrated ordinary chondrites, hereafter EOC's). Based on the analytical data, we aimed to characterize Antarctic ordinary chondrites in terms of chemical composition. Weathering is highly concerned in Antarctic meteorites. This effect on chemical composition was also considered.

Of trace elements determined, only Zn shows a distinct difference in its Mg-normalized contents between UOC's and EOC's (Fig. 1). This is somewhat in contrast with the conclusion obtained by Kallemeyn et al. (1989) for non-Antarctic ordinary chondrites. No apparent difference in Zn contents was confirmed between H and L,LL groups of UOC's. Arsenic also shows a faint difference in its Ni-normalized values between UOC's and EOC's. These features observed in Zn and As abundances can be explained in terms of volatility of these elements.

Fig. 2 shows a histogram of Na contents. Degree of weathering is classified with symbols. There seems to be a correlation between Na content and degree of weathering: severely weathered meteorites (indexed with C) tend to have lower Na contents, suggesting that some Na has been lost due to weathering on Antarctica (possibly in the manner of chemical leaching). Another correlation could be confirmed between Au content and degree of weathering (Fig. 3), but its correlation seems to be in the opposite relation to the case of Na. Assuming aqueous alteration to be involved, Au can be mobile by making complex with halogens in meteorites (Ebihara et al., 1982). Transport of Au from outer part near surface to inner part, from which specimens for this work were taken, is a possible explanation. No other elements analyzed were found to be affected by terrestrial weathering.

REFERENCE: Ebihara M., Wolf R. and Anders E. (1982) Geochim. Cosmochim. Acta 46, 1849-1861. Kallemeyn G.W., Rubin A.E., Wang D. and Wasson J.T. (1989) Geochim. Cosmochim. Acta 53, 2747-2767.

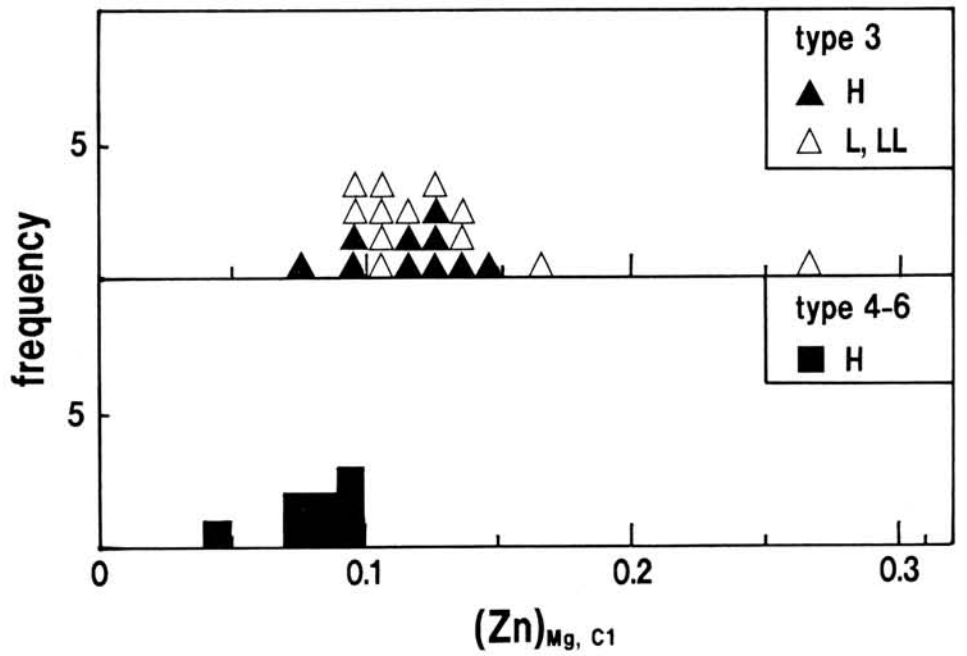

Figure 1
Distribution of Zn contents (normalized to Mg and C1 values) in type 3 and type 4-6 ordinary chondrites.

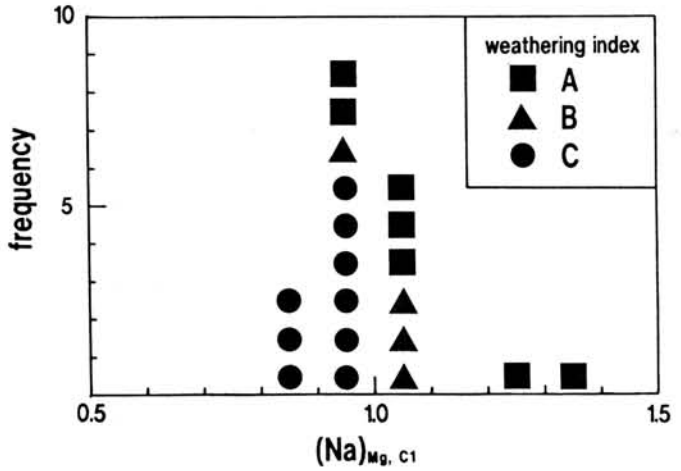

Figure 2
Histogram of Na contents (normalized to Mg and C1 values). Weathering degree is indicated with an A-B-C index (A: minor, B: moderate, C: severe).

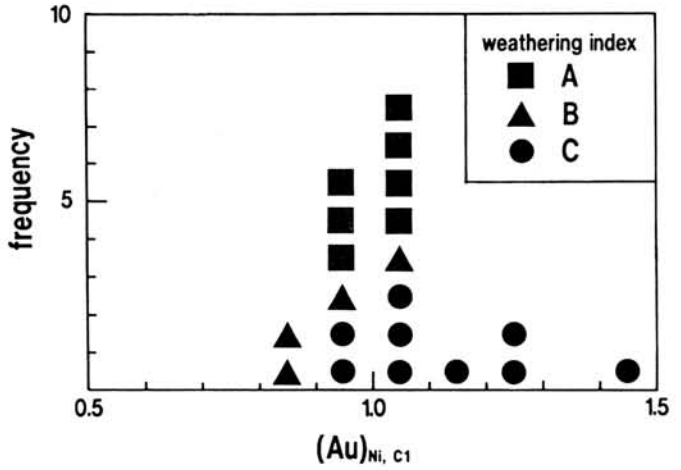

Figure 3
Histogram of Au contents (normalized to Ni and C1 values).

NOBLE GAS CONPOSITION IN THE VAPOUR GROWTH DIAMOND.

Fukunaga, K. and Matsuda, J.

Department of Earth Sciences, Faculty of Science, Kobe University, Nada, Kobe 657

Diamonds made by CVD (chemical vapour deposition) using microwave method from the gaseous mixture including noble gases contain large amounts of noble gases which are highly fractionated to be enriched in heavy noble gases (1,2). This noble gas pattern is coincident with the patterns in ureilite for heavy noble gases. On the other hand, diamonds made by CVD using thermal electron method contain small amounts of noble gases. These results suggest that the ionization method at the diamond syntheses is responsible to the trapping noble gases in CVD diamonds. In this study, we made diamonds by the thermal electron CVD by applying a electric voltage between the filament and the substrate.

Schematic drawing of our synthetic apparatus is shown in Figure 1. Gases were evacuated by a rotary pump and fed into a quartz tube in a furnace. The major component of the gas is H_2. The concentration of CH_4 and noble gas mixtures (1% He, 1% Ne, 96% Ar, 1% Kr and 1% Xe) were 1%, respectively. The total pressures were 23 torr. The substrates was heated to be at 800 C by furnace. Methane is resolved by thermal electrons released from hot W-filament. Diamonds are deposited on scratched silicon wafer substrate. The substrate holder made of stainless steel was set at positive or negative voltage relative to the W-filament.

Table 1 is synthesis conditions. By X-ray diffraction analysis all samples were identified as diamonds. Figure 2 is the secondary electron image by Scanning Electron Microscope of the synthesized diamond. Octahedron which make a diamond film can be seen.

Noble gases were examined by mass spectrometry employing stepwise heating technique. The precise experimental details are in our previous works (3,4). Temperature steps are 800 , 1400 and 2000 C, respectively. Results are listed in Table 2. For He and Ne, the concentrations of all samples of all temperature steps are blank level. For Ar, only the concentration of #109 at 2000 C step can be detected. For Kr and Xe, the small amount of noble gases released at 2000 C step. The amounts of noble gases of this experiment are much less than those of diamond made by the microwave method. This result may be on account on that the energy of thermal electron is not enough to ionization of noble gases.

References:

(1) Fukunaga, K., Matsuda, J., Nagao, K., Miyamoto, M. and Ito, K. (1987) Nature, 328, 141-143

(2) Matsuda, J., Fukunaga, K. and Ito, K. (1989) Lunar Planet. Sci., 20 630-631

(3) Matsuda, J., Matsubara, K., Yajima, H. and Yamamoto, K. (1989) Geochim. Cosmochim. Acta, 53, 3025-3033
(4) Yajima, H. and Matsuda, J. (1989) Mass Spectrosc. Japan, 37, 331-342

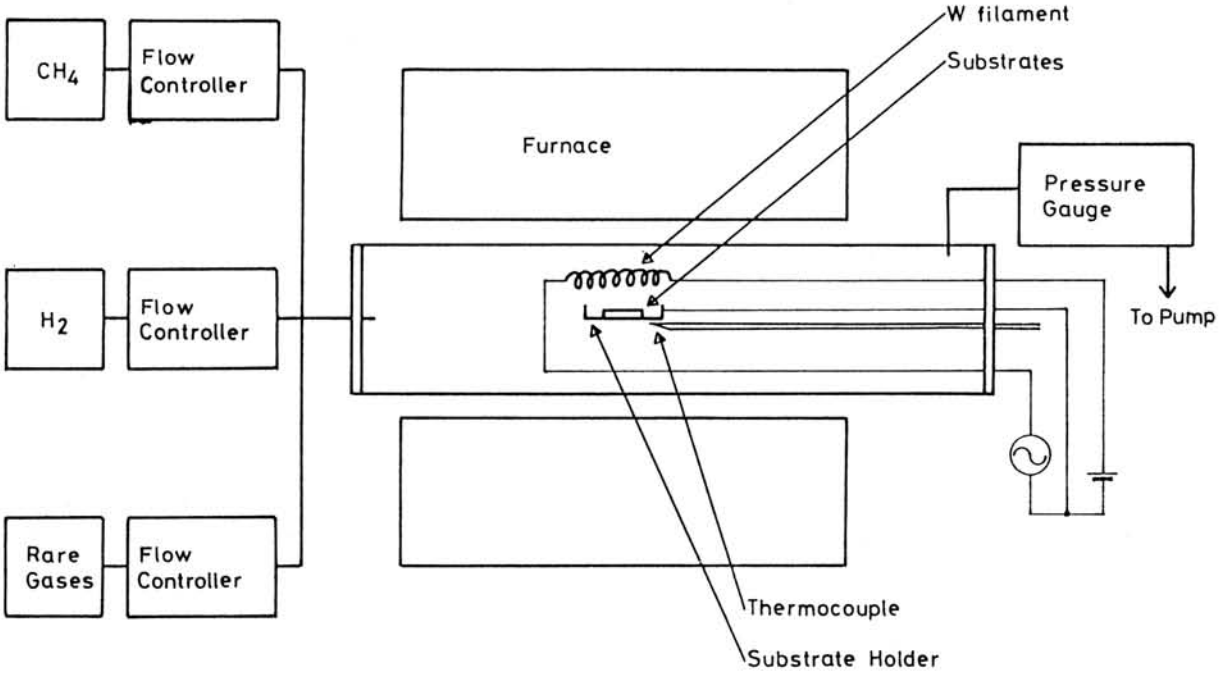

Figure 1
Schematic drawing of the experimental apparatus

Table 1: The electric potential of substrate holder relative to the W-filament.

Sample Number	Voltage (V)
#104	+25
#108	0
#109	-25

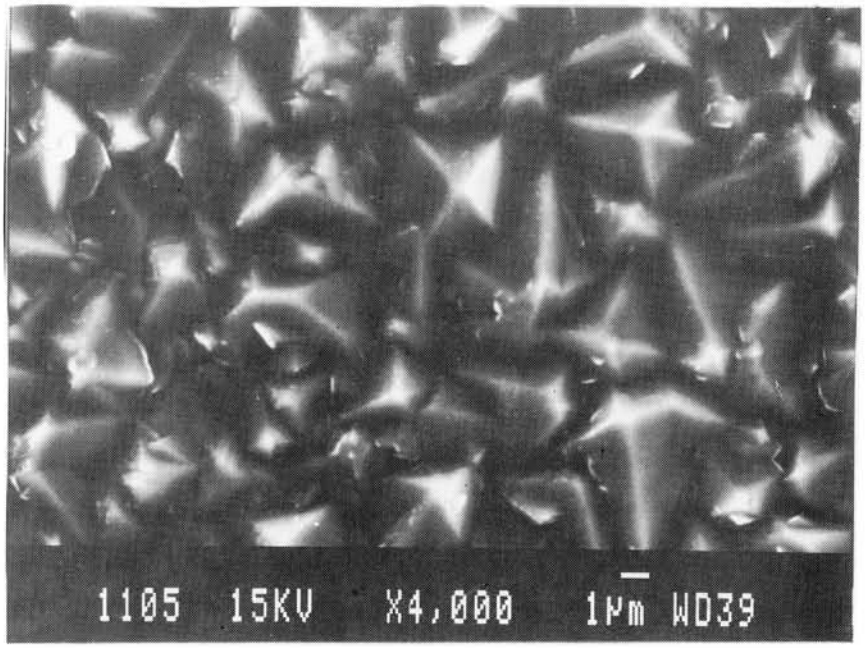

Figure 2
Secondary electron image by Scanning Electron Microscope of the diamond

Table 2 The concentrations of noble gases in diamonds

Sample Name	Weight (mg)	Temp. (C)	Concentration ($\times 10^{-10}$ cm^3STP/g)* ^{4}He	^{20}Ne	^{36}Ar	^{84}Kr	^{132}Xe
		800	N.D.	N.D.	N.D.	1.6 (48)	1.6 (27)
#104	2.841	1400	N.D.	N.D.	N.D.	N.D.	0.28(68)
		2000	N.D.	N.D.	N.D.	7.3 (17)	2.1 (22)
		800	N.D.	N.D.	N.D.	N.D.	N.D.
#108	3.791	1400	N.D.	N.D.	N.D.	N.D.	0.42(51)
		2000	N.D.	N.D.	N.D.	3.2 (27)	3.1 (12)
		800	N.D.	N.D.	N.D.	1.6 (48)	0.34(63)
#109	2.872	1400	N.D.	N.D.	N.D.	N.D.	0.40(59)
		2000	N.D.	N.D.	37 (42)	7.6 (17)	7.21(8)

N.D. : Not detected (blank correction exceeded 70%).
*The blank correction to the measured value is given in parentheses.

NOBLE GAS STUDIES IN SHOCK-PRODUCED DIAMONDS

Matsuda, J.*, Yajima, H.*, Kusaba, K.** and Syono, Y.**

* Department of Earth Sciences, Faculty of Science, Kobe University, Nada, Kobe 657.
**The Research Institute for Iron, Steel and Other Metals, Tohoku University, Katahira, Sendai 980.

Noble gases in diamonds are very important in studying the early history of our solar system. Diamonds are the host phases of Xe-X which is assumed to be of pre-solar origin (1). Noble gases in ureilites are contained in diamonds but not in graphite (2). Therefore, it interests us to examine the elemental fractionation and the isotopic effect of noble gases trapped at diamond syntheses in the laboratory. Fukunaga et al. (3) reported that the diamonds produced by chemical vapor deposition contained large amounts of noble gases, suggesting that ureilite diamonds also formed directly from the solar nebula. However, subsequent works showed that the noble gases were also enriched in the shock-produced diamonds compared to those in the raw material graphite (4, 5). As the shock-produced diamonds used in those studies were commercial ones, the synthetic conditions of diamonds were not well known. In this study, we actually synthesized the diamonds under shock-loading using a single-stage propellant gun to examine the effects of synthetic conditions on trapping noble gases in the shock-produced diamonds.

Graphite (purity 99.9%) were mixed with a copper powder (about 1:1 in volume and 1:9 in weight), and pressed into a small pellet by applying a load of 0.3GPa. The calculated porosity of the pellet sample is 12%. The copper was used to get high shock impedance and causes catalysis for the phase transition of graphite. The pellet specimen was encased in a copper container (a stainless steel container was also used for the higher pressure experiment). Shock-loading experiments were made by using a 25mm bore single-stage propellant gun installed at Tohoku University. The flyer velocity was measured from the time of flight of magnet embedded in the flyer by passing through between the two coils. The shock pressure (20-70GPa) was estimated from the flyer velocity on the basis of the shock-impedance match concept. We made two experiments for 50GPa to examine the reproducibility. The deformation of the container after shock-loading was shown in Fig. 1. The recovered matter was put in HNO_3 to dissolve the container (only for copper container) and the copper powder to isolate the carbon material. The graphite in the recovered carbon material was dissolved in hot H_2SO_4 + KNO_3 solution. The residual carbon material was identified by X-ray diffraction method, showing the lines of diamonds. The results in Table 1 show that the larger amount of diamond was

produced for the higher shock pressure.

Noble gas abundances in these shock-produced diamonds were examined by mass spectrometry using stepwise heating technique. The experimental procedures are given in our previous works (5, 6). The noble gases in graphite were mainly released at the lowest temperature of 800°C. The high release temperature of noble gases in the shock-produced diamonds indicates that the noble gases are tightly trapped inside the diamonds. The total gas amounts for the graphite, diamond under about 30GPa and under 50GPa are shown in Fig. 2. The reproducibility of our experiment at 50GPa seems very good. The noble gas abundances in shock-produced diamonds are much higher than those in the raw material graphite except for Xe. It is likely that the adsorbed component of Xe on graphite is responsible for the high Xe abundance. In Fig.2, there seems no clear relationship between the shock pressure and the noble gas abundances in diamonds. However, further studies should be necessary to confirm this.

References

(1) Lewis, R. S., Ming, T., Wacker, J. F., Anders, E. and Steel, E. (1987) *Nature, 326,* 160.
(2) Göbel, R., Ott, U. and Begemann, F. (1978) *J. Geophys. Res., 83,* 855.
(3) Fukunaga, K., Matsuda, J., Nagao, K., Miyamoto, M. and Ito, K. (1987) *Nature, 328,* 141.
(4) Matsuda, J. and Nagao, K. (1989) *Geochim. Cosmochim. Acta, 53,* 1117.
(5) Yajima, H. and Matsuda, J. (1989) *Mass Spectrosc. Japan, 37,* 333.
(6) Matsuda, J. Matsubara, K., Yajima, H. and Yamamoto, K. (1989) *Geochim. Cosmochim. Acta, 53,* 3025.

Table 1. Recovery and identification of diamond after shock loading.

Sample Name	Shock Pressure (GPa)	Carbon[a)] (mg)	Residue[b)] (mg)	X-ray Diffraction[c)]
SP2	19.5	126.7	0.5	-
SP7	29.1	134.7	1.8	+
SP3	42.2	126.6	6.1	+
SP5	50.7	121.4	10.4	+
SP4	52.0	117.4	13.4	+

a) The weight of carbon after dissloving in HNO_3.
b) The weight of residue after dissolving in KNO_3+H_2SO_4.
c) Diamond lines (+).

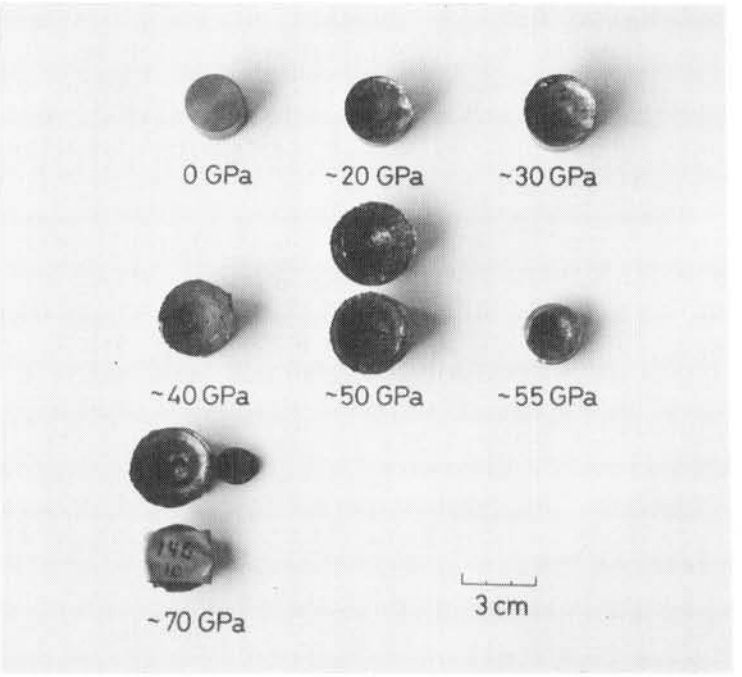

Fig. 1 Deformation of containers after shock-loading. Stainless steel container was used for 55 and 70GPa.

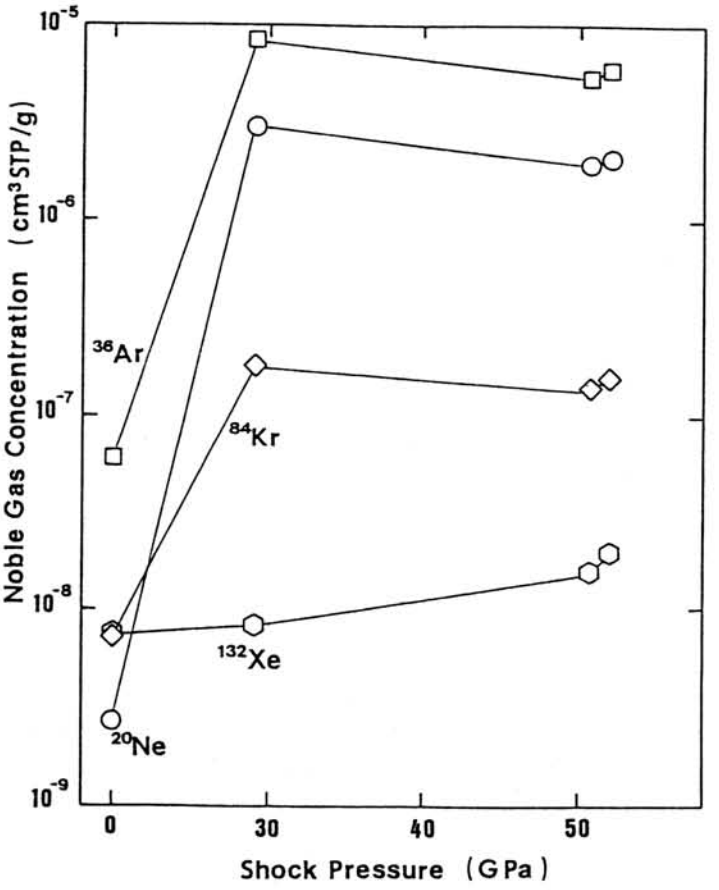

Fig. 2 Noble gas abundances in graphite and the shock-produced diamonds.

FRACTIONATED ALKALI METAL ABUNDANCES IN ALLENDE BO CHONDRULES: A CLUE TO MELTING PROCESSES

Noboru Nakamura, Hitoshi Matsuda, Saika Yokoyama, Hajime shimoda, Taro Shimaoka, and Koshi Yamamoto
Department of Earth Sciences, Faculty of Science, Kobe University, Nada, Kobe 657, Japan.

It has been shown that chondrules from unequilibrated chondrites (typically UOC's) retained considerable amounts (at the CI or higher levels) of alkalis, suggesting that they have not been subjected to ubiquitous vaporization loss of alkalis during the chondule-formation melting (Grossman and Wasson, 1983). Recently, we have reported olivine Fa-correlated and fractionated alkali (Rb/K) abundances for Allende BO chondrules (Matsuda et al., 1990), which has been taken as evidence of fractional vaporization of alkalis at the melting event. In order to confirm the reported correlations for K and Rb and to clarify more detailed distributions of alkalis in chondrules, additional 35 petrographically characterized Allende chondrules (15 BO, 20PO,POP) were analyzed for Na (by atomic absorption and EPMA), K and Rb (by isotope dilution) in this work.

Including previous works (Misawa & Nakamura, 1988; Matsuda et al., 1990), 40 Allende BO chondrules have been analyzed by us for K and Rb and partly for Na (in 30 BO), and additional 20 PO,POP for Na. From these analyses, the following features were found; (1) the majority of BO chondrules have higher abundances of alkalis with CI Rb/K ratio, while (2) BO chondrules with lower K/Ca show higher Rb/K, (3) the bulk abundance ratios of K/Ca and Na/Ca are positively correlated with olivine Fa contents for BO (Figs. 1 and 2) but not for PO and POP chondrules. These features are hold even inclusion of data by Rubin and Wasson (1987).

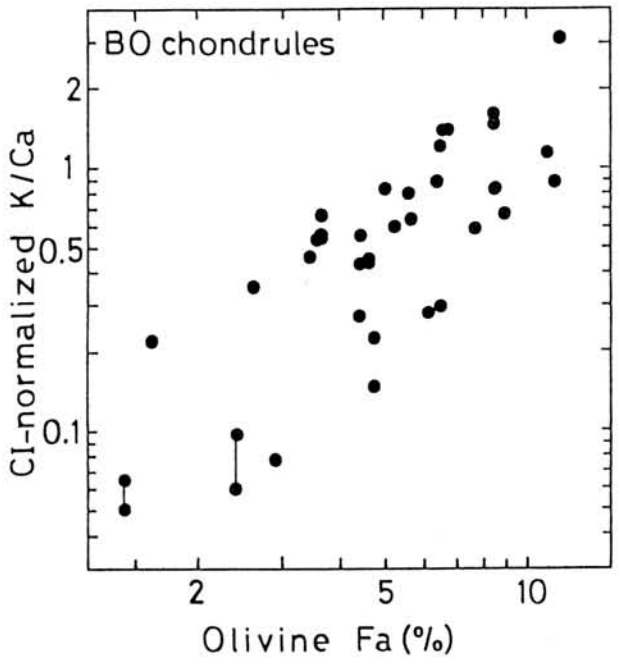

Fig. 1

Relationship between the bulk abundance (K/Ca) ratio and olivine Fa content for Allende BO chondrules.

The alkali (Rb/K) and alkali (Na, K, Rb)/refractory (Ca) fractionations observed for BO chondrules may be interpreted as having been produced by gas/solid(or melt) processes. Then, two possibilities may be considered: these features were produced prior to or during the formation of chondrules. The petrochemical observations as noted in (3) may favor the later case. If this is the case, the observed alkali abundance features may provide us a new constraint on the melting mechanism of BO chondrules. In view of lack of relationship between petrochemical feature as mentioned above with metallic abundance in BO chondrules, we suggest that the melting and vaporization loss of alkalis occurred without interaction with the nebular gas.

References:
Grossman J.N. and Wasson J.T. (1983), In Chondrules and Their Origins (ed. E.A. King) 88-121, Lunar Planet. Inst.; Matsuda H., Nakamura N. and Noda S. (1990), Meteoritics (in press); Misawa K. and Nakamura N. (1988), Geochim. Cosmochim Acta 52, 1699-1710; Rubin A.E. and Wasson J.T. (1987), Geochim. Cosmochim. Acta 51, 1925-1937.

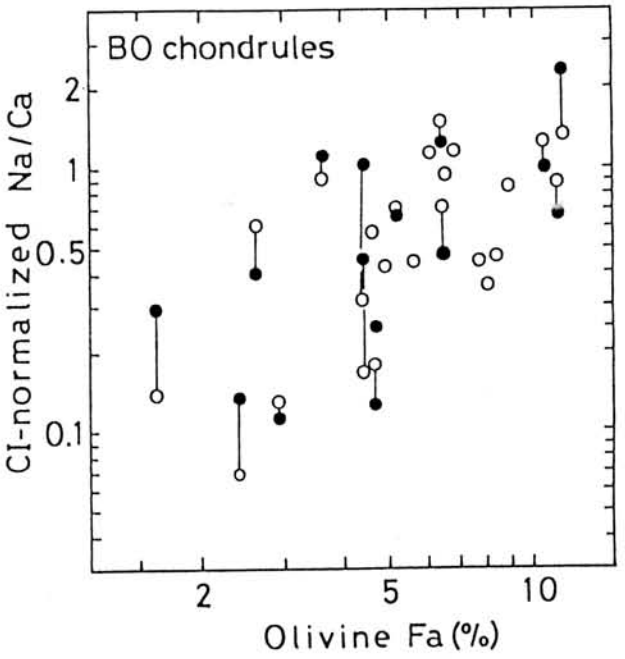

Fig. 2

Relationship between the bulk abundance (Na/Ca) ratio and olivine Fa content for Allende BO chondrules.

Volatilization Studies of Alkali Metals on a Chondritic Material (V) — an effect of total pressure —

TARO SHIMAOKA [1] and NOBORU NAKAMURA [1,2]

[1] *Department of Science of Material Differentiation, Graduate School of Science and Technology, Kobe University, Nada, Kobe 657, Japan,*
[2] *Department of Earth Sciences, Faculty of Science, Kobe University, Nada, Kobe 657, Japan.*

Since alkali metals are moderately volatile lithophiles,they can be used as indicators of physico-chemical conditions of high temperature gas/dust fractionation processes in the early solar nebula. Shimaoka and Nakamura (1989) performed a vaporization experiment of sodium on a chondritic material in the temperature range of 1150 $\sim$ 1450°C under pressure of 8×10^{-6} Torr and showed the similarity of mechanism for sodium vaporization between from the partial melt and from the total melt (Tsuchiyama *et al.*, 1981) despite the deferences of absolute values of vaporization rates. The reason of difference in vaporization rate between both experiments may be due to deferences in temperature, total pressure, oxygen fugacity and the chemical composition of charge. In order to investigate the most effective factor on change of vaporization rate, an additional heating experiment was carried out using a chondritic material under various pressure at constant temperature.

A fine grained starting material ($\phi < 10\mu m$) was prepared from the Etter chondrite (L5) . Sample was heated in a Ta-crucible at a constant heating rate up to a 1300°C and held at the temperature for 40 min. The experiments were carried out at various pressures ($10^{-6} \sim 10^{-3}$ Torr) controlled with bleeding He gas into the chamber except for 10^{-6} Torr. Quenched run products were analyzed for Na by the atomic absorption spectroscopy. Major chemical and petrographical examinations were made by EPMA and SEM-EDS system. The proportions of holes, glass materials and overgrowth rim materials to total samples were estimated from the SEM back-scattered electron images of run products using an on-line computer image reader.

Fig.1 and Fig.2 shows the positive relations between the proportions of holes or glass materials to the total charges and total pressure. There are no relations between relative concentration of Na in the heated samples and total pressure (Fig. 3). In Fig. 4, it is pointed out that the vaporization rates of Na for run products are substantially constant at the total pressure in the range of $10^{-6} \sim 10^{-3}$ Torr .

An Arrhenius plot of vaporization rate is shown in Fig. 5, together with those obtained by Tsuchiyama *et al.*(1981)(S1 and S2 in the figure). In this figure the higher values of

vaporization rate are observed in this work compared to those by Tsuchiyama *et al.*(1981). If the experimental results at the pressure of $10^{-6} \sim 10^{-3}$ Torr can extend to the the atmospheric pressure, the reason of the higher values of vaporization rate in this work may be considered to be due to differences in the oxygen fugacity and the chemical composition of charges. From olivine Fa content (= 20 %) in heated samples, we estimated the oxygen partial pressure prevailed during heating (Fig. 6), which correspond to that of experiments by Tsuchiyama *et al.* (hatched area in the figure).

In conclusion, it is suggested that the chemical composition of charges may be the most important factor which might have yielded the differences in the vaporization rates of Na in both experiments.

References

Shimaoka, T. and Nakamura, N. (1989): *Proc. NIPR Symp. Antarct. Meteorites*, 2, 252-267

Tsuchiyama, A. , Nagahara, H. and Kushiro, I. (1981): *Geochim. Cosmochim. Acta*, 45, 1357-1367

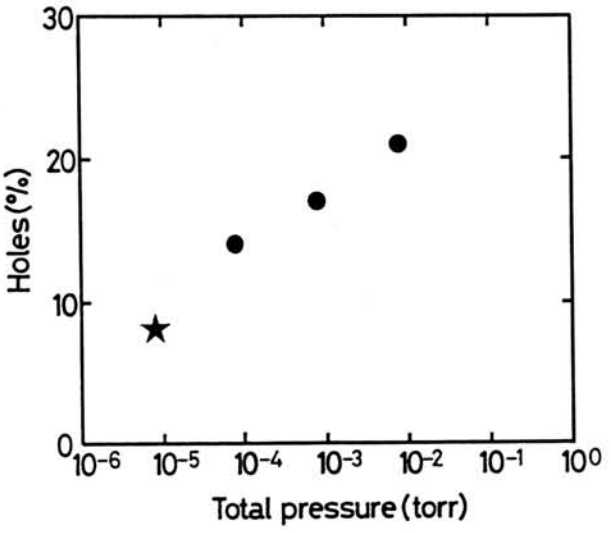

Fig. 1 Plot of areal proportion of holes to the total charge as a function of total pressure.

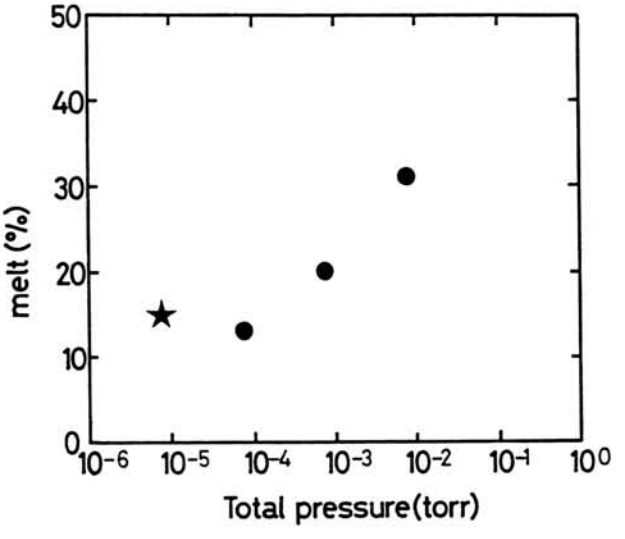

Fig. 2 Plot of areal proportion of melt to the total charge as a function of total pressure.

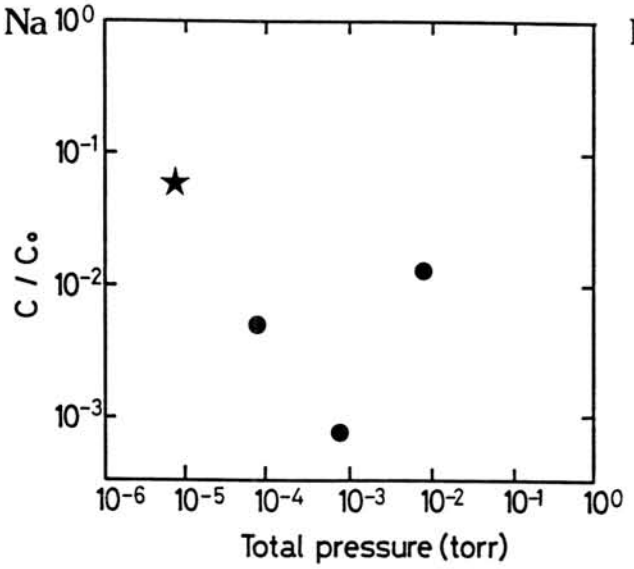

Fig. 3 Plot of relative concentration of Na as a function of total pressure.

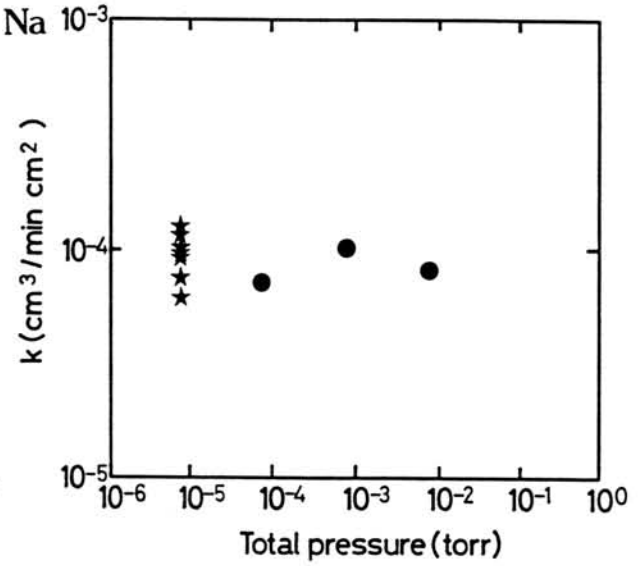

Fig. 4 Plot of the rates of Na vaporization as a function of total pressure.

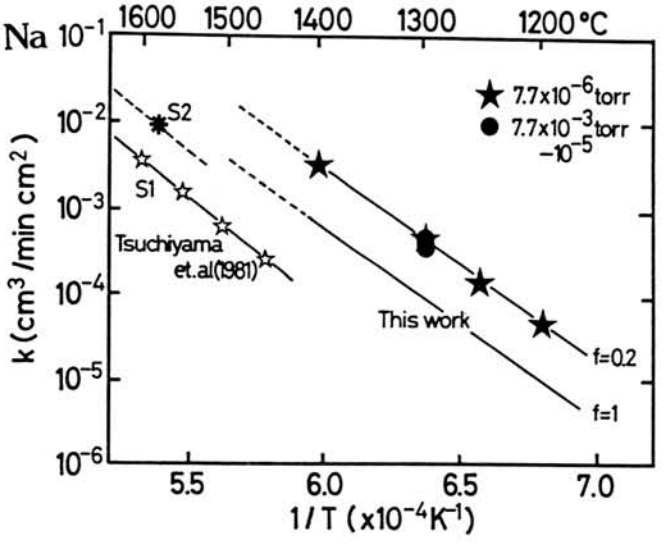

Fig. 5 Arrhenius plot of the rates of Na vaporization obtained in this work and Tsuchiyama et al.(1981).

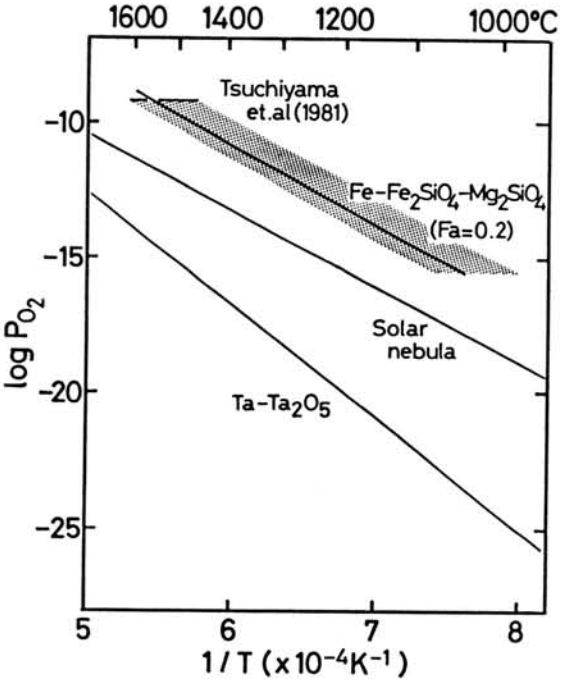

Fig. 6 Arrhenius plot of the oxygen partial pressure.

NE ENRICHMENT IN TEKTITES AND EXPERIMENT OF NE DIFFUSION INTO SILICA GLASS

Matsubara, K. and Matsuda, J.

The Graduate School of Science and Technology, Kobe University, Nada, Kobe 657.

Ne enrichment has been reported for natural silica-rich glasses, such as submarine glasses (1, 2), obsidians and Darwin glass (3) and tektite (4). The Ne/Ar ratio reported for Thailand tektite was the highest among those reported so far for these natural glasses. In order to investigate the Ne enrichment in more detail, [1] we measured all noble gas abundances and Ne isotopic compositions in five tektites collected from three different strewn fields on earth, and [2] we made an experiment of Ne diffusion into silica glass.

Noble gases in tektites were measured by a mass spectrometry using the stepwise heating technique. Figure 1 shows the noble gas abundance patterns of tektites, displayed as a fractionation factor F(m), defined by

$$F(m)=(^{m}X/^{36}Ar)_{sample}/(^{m}X/^{36}Ar)_{air}$$

where ^{m}X represents a noble gas isotope mass "m". The fractionations of tektites seem to show monotonic changes from Ar to Xe. The light noble gases, especially Ne, are enriched in tektites compared to the relative pattern of noble gases in air. F(20) values were various, which ranged 200-7130. It is surprising that F(20) value of TE5 is 7130, about four times higher than 1800 of Thailand tektite (4). For all tektite samples, Ne isotopic ratios agreed very well with those of air within errors. This suggests that Ne in tektite is that in air and has been diffused in from the atmosphere.

We made an experiment as shown in Fig.2 in order to confirm whether atmospheric Ne actually diffused into glass materials. We used 60-100 mesh fraction of obsidian (ME1) of which diffusion coefficient of Ne has been obtained by Matsuda et al. (3). About 10g of these samples was put into stainless steal crucible and was heated at 800 °C by a conventional Kantal heater. After degassing, we measured noble gases in the sample, and confirmed that all Ne in the sample was degassed. This sample was named "T0". About 1g of sample "T0" was put in the stainless steel cage and was heated in air. 40030 was heated at 400°C for 30 minutes in air. 50015, 50030, 50015H and 50064H were heated at 500°C in air for 15 min., 30 min., 15 hours and 64 hours, respectively. T012 and T034 were kept at room temperature for 12 days and 34 days, respectively.

Noble gases in these samples were extracted at 800 and 1600°C. We measured noble gases in ME1 for comparison. If blank corrections exceeded 20%, the measured amounts were shown as an upper limits without blank corrections. For He and Xe, the concentrations were shown as upper limits in all samples.

Almost all Ne was released by 800°C in all samples. Except for T012 and T034, Ne concentrations were almost the same in these samples, suggesting that these samples were saturated by Ne. The data of T012 and T034 indicate that Ne was easily diffused into glasses from the atmosphere even at room temperature.

The Ne concentration of about 3×10^{-8} cm^3STP/g is higher than that estimated from equilibrium solubility between air and silicate glass (5). Therefore, we suppose that Ne is in the vesicles rather than in the solid glass. If we assume that the partial pressure of ^{20}Ne in the vesicles is the same as that in the atmosphere at room temperature, the vesicle density in the sample would be about 0.5% in volume. The back-scattered electron image by the Scanning Electron Microscope observation shows many vesicles in the glass for our obsidian samples. We estimated vesicularity in them by image processing. It was 3% on the plane, much higher than the value we estimated. These results suggest that high ^{20}Ne concentration is in the void in the glass samples rather than that obtained by the solubility in the solid.

REFERENCES

(1) Dymond, J. and Hogan, L. (1973), Earth Planet. Sci. Lett., 20, 131-139.
(2) Ozima, M. and Zashu, S. (1983), Earth Planet. Sci. Lett., 62, 24-40.
(3) Matsuda, J., Matsubara, K., Yajima, H. and Yamamoto, K. (1989), Geochim. Cosmochim. Acta, 53, 3025-3033.
(4) Hennecke, E.W., Manuel, O.K. and Sabu, D.D. (1975), J. Geophys. Res., 80, 2931-2934.
(5) Lux, G. (1987), Geochim. Cosmochim. Acta, 51, 1549-1560.

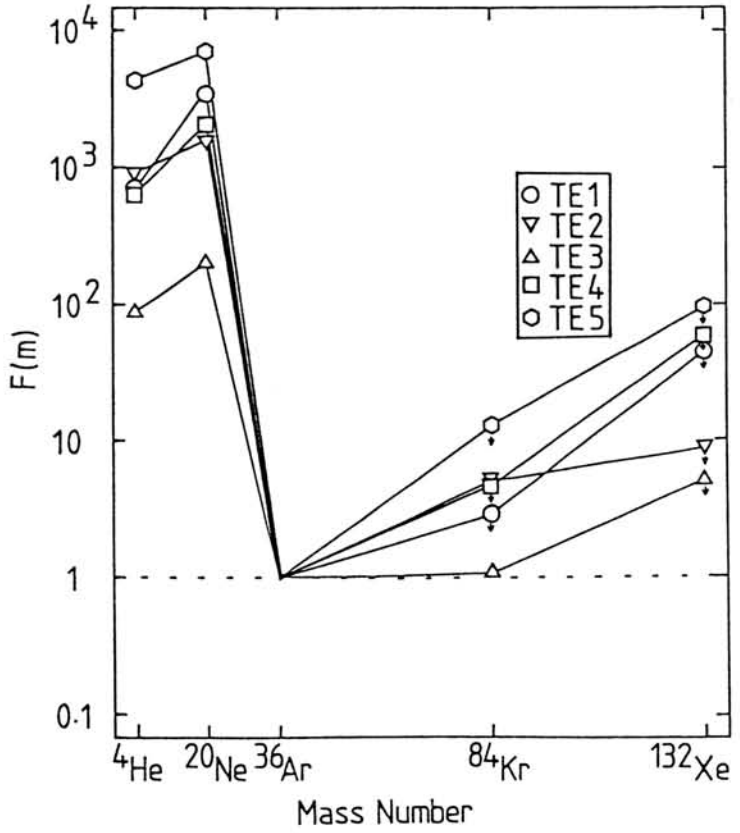

Fig.1 Elemental abundance pattern of noble gases in tektites.

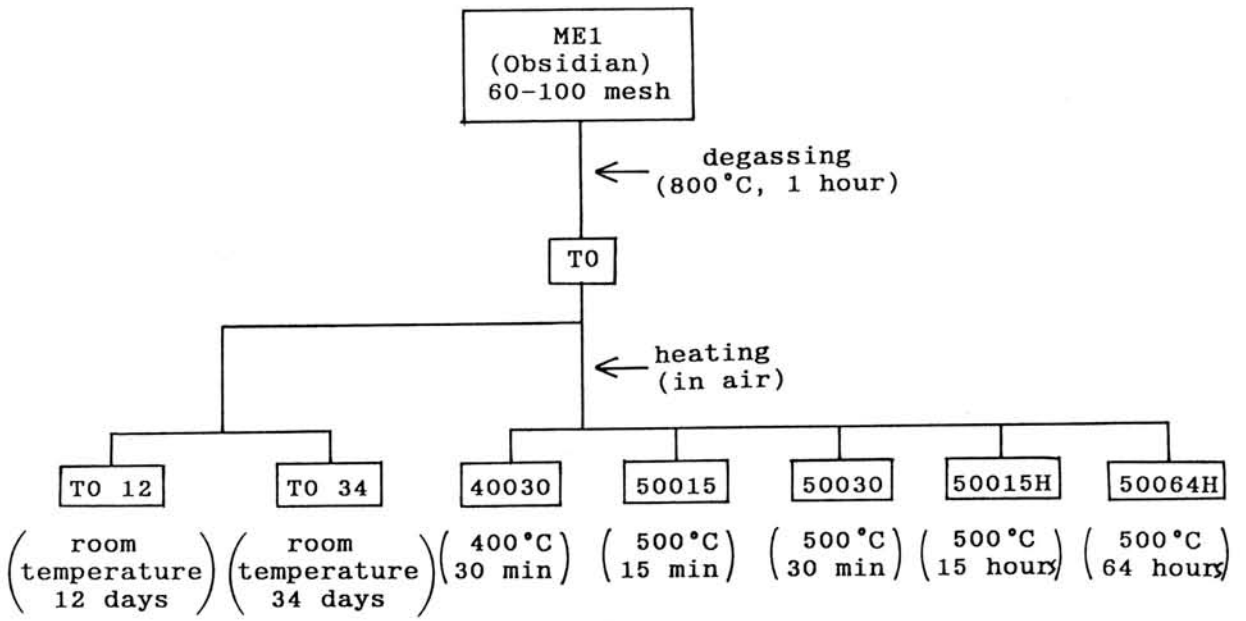

Fig.2 A schematic diagram of sample preparation.

PAIRING OF FIVE YAMATO'79 ACHONDRITES BY THE CHEMICAL COMPOSITIONS

Fukuoka, T.

Department of Chemistry, Gakushuin University, Mejiro, Tokyo 171

A large number of meteorite specimens were collected on the Antarctic ice field. These collections include a large number of howardites and polymict eucrites which are typical achondrites in the Antarctic meteorite cllection. Most of the specimens of these achondrites are probably pieces of some falls. In order to know the number of meteorite falls for the Yamato achondrites (especially polymict eucrites), the comparison of the chemical compositions of matrices of such polymict meteorites is one of the useful tools, because it is considered that the chemical compositions of matrix represent the average chemical compositions of polymict meteorites. Fukuoka (1) grouped 11 polymict eucrites into three based on the chemical compositions.

In this study, the abundances of 30 major, minor and trace elements in 5 matrix samples of 4 Yamato eucrites (monomict: Y-791186 and -792510, polymict: Y-791960 and -792769) and one howardite (Y-791962) have been determined by instrumental neutron activation analysis (INAA). The samples were provided from the National Institute of Polar Research of Japan. The small chips of clasts and fussion crust were excluded from the matrix sample specimens under stereo microscope to eliminate chemical effect from the clasts and the fusion crust prior to INAA. Preliminary analytical results are shown in Table 1.

The chemical compositions of any 5 Yamato achondrites are different from the others. Therefore every meteorite belongs to different chemical group. This conclusion does not agree with the groups of the mineralogical investigation (2) and the groups of the noble gas data (3). These discrepancies may be due to the chemical heterogeneity of the samples and the chemical weathering effects of the Antarctic meteorites. For our final purpose of this study, we have to carry out precise investigation of weathering mechanism of Antarctic achondrites.

REFERENCES:
(1) Fukuoka, T. (1984) Meteoritics 19, 227. (2) Takeda, H.*et al.* (1984) Abstract 9th Sym. Antarctic Meteorites, 20. (3) Nagao and Ogata (1989) Abstract 14th Sym. Antarctic Meteorites, 119.

Table 1. Preliminary results of chemical abundances by INAA

		Y-791186 -51	Y-791960 -52	Y-791962 -50	Y-792510 -41	Y-792769 -77	JB-1	Error* %
Wt	mg	109.7	131.2	93.7	108.6	128.2		
TiO_2	%	0.62	0.72	0.27	0.75	0.82	1.31	7-11
Al_2O_3	%	9.3	11.5	7.9	13.1	11.9	14.3	1-2
FeO[1)]	%	22.6	18.7	18.9	18.3	20.1	=8.11	0.5
MgO	%	8.3	9.1	15.4	6.5	5.5	7.7	3-7
CaO	%	7.6	8.8	5.7	10.3	9.8	9.5	3-5
Na_2O	%	0.37	0.42	0.27	0.49	0.59	=2.79	1
K_2O	%	0.06	0.04	0.03	0.12	0.05	1.4	17-35
MnO	%	0.62	0.53	0.54	0.52	0.56	0.15	1
Cr	ppm	2600	2800	4860	1730	1780	=414	0.5
Sr	ppm	38	52	-	114	76	=435	14-26
Ba	ppm	29	26	21	25	25	=490	28-50
Sc	ppm	29.9	29.4	24.4	33.1	34.5	=28.9	0.5
V	ppm	63	82	114	69	65	214	2-9
La	ppm	4.33	2.79	1.35	2.21	5.28	=38.8	2-5
Ce	ppm	10.5	7.3	3.8	4.3	9.5	=63	2-8
Nd	ppm	5.1	5.4	2.8	2.7	9.6	=27	4-14
Sm	ppm	1.66	1.71	0.88	0.89	2.93	=5.02	0.5-1
Eu	ppm	0.58	0.64	0.38	0.63	0.81	=1.59	3-4
Tb	ppm	0.33	0.38	0.17	0.25	0.68	=0.70	6-17
Dy	ppm	2.7	2.9	0.9	1.8	4.6	3.8	7-21
Yb	ppm	1.96	1.87	1.09	1.51	2.85	=2.4	2-3
Lu	ppm	0.32	0.30	0.17	0.27	0.45	=0.37	4-7
Hf	ppm	1.47	1.44	0.64	1.41	1.65	3.54	3-6
Th	ppm	0.49	0.28	0.14	0.32	0.40	9.23	6-24
U	ppm	0.51	0.06	0.06	0.07	0.11	1.65	5-20
Ta	ppm	0.23	0.30	0.09	0.26	0.23	=3.6	10-32
Co	ppm	28.4	9.41	35.7	5.43	7.32	=39.1	0.5-1
Ni	ppm	7	13	334	4	21	148	2-50
Ir	ppb	-	2.3	5.6	-	2.4	-	20-50
Au	ppb	-	-	2.8	-	-	-	20

* Errors for INAA are due to counting statistics.
1) Total iron as FeO.

Alterations in Ordinary Chondrite Fusion Crusts and their Relations to Chemical and Mineral Compositions of Spherules

Tazawa, Y.[1] and Sasaki, T.[2]
1) Dept. Physics, Kyoto Univ., Sakyo, Kyoto 606,
2) Sakuranomiya Osaka City High School, Miyakojima, Osaka 534.

So far, fusion crusts and artificially ablated debris of meteorites, especially of irons and carbonaceous chondrites, have been studied by several authors [1,2,3] with relation to origin of "Cosmic Spherules". We have been also studying several types of ordinary chondrites on chemical and mineralogical alterations in the fusion crusts and the next interiors. Samples studied are several hundred mg each of fragments including the fusion crusts taken from Antarctic collections provided by NIPR; Y-7304(L6), Y-74155(H3), Y-790448 (LL3) and ALH-77272(L6), and a fragment taken from a non-Antarctic fall;Aomori (L6). Thin-sections and fine-grained samples filed off from the crusts and the next interiors were used for EPMA, SEM/EDX and INAA.

As reported previously [4,5], INAA results on the abundances of trace elements cannot be clearly discriminated between the crusts' and the interiors' because of the inhomogeneous local constituents and the incomplete sample separation. While, EPMA/SEM/EDX results for the thin-sections show that abundances of major and minor elements in some main minerals are systematically altered in order of depth from the surface. In this paper, we mainly present the SEM/EDX results, especially focussed on main minerals (Ol, Px, Pl) of the L6 type and discuss some probable features of ablation products from ordinary chondrites.

General Features of the Fusion Crusts and the Next Interiors

1) Fusion crusts (FC) consist of two vitreous sub-layers; the outermost layer in which micron-sized magnetite grains are prevalent (FO) and the inner layer in which the grains are rare (FI), whose thickness are about 50 - 100 um and about 100 - 200 um, respectively.

2) Chemical compositions of FC are mostly homogenized in small (10 um) scale except um-sized magnetite grains but vary in large (10 um) scale, which seems to reflect those of original constituents.

3) Next to FC, a partially melted zone exists, whose thickness is about 200 - 500 um and the chemical compositions vary transitionally from unmelted inter -

iors toward FC (transition zone: TZ). Grain boundaries of olivines and pyroxenes are more or less deformed and chemically influenced by surrounding constituents. Plagioclases are mostly vitrified. Most of chinks developed in olivines and pyroxenes are filled with Fe-rich materials. The fillings occur both in Antarctic samples and Aomori, which seem to be formed not by terrestrial weathering but by heating during atmospheric entry.

4) Depletion of volatile elements in FC is less in ordinary chondrites than in carbonaceous chondrites.

References:

[1] Blanchard, M.B. (1972), J. Geophys. Res., 77,2442.

[2] Fruland, R.M. (1974), Meteoritics, 9,339.

[3] Brownlee, D.E. et al., (1975), J. Geophys. Res., 80, 4917.

[4] Tazawa, Y. & Sasaki, T,,(1987), abst. 12th Symp. Antarctic Meteor., NIPR.

[5] Tazawa, Y. & Sasaki, T.,(1988), abst. 13th Symp. Antarctic Meteor., NIPR.

CARBON-14 TERRESTRIAL, EXPOSED AND GLACIAL AGES OF ANTARCTIC METEORITES

Yasunori MIURA[1], Roelf BEUKENS[2] and John RUCKLIDGE[2]

[1] Faculty of Science, Yamaguchi University, Yamaguchi, 753.
[2] IsoTrace Laboratory, University of Toronto, Toronto, Ontario M5S 1A7.

1. Definition of C-14 ages

Meteoritic history of the Antarctica on the glacier can be discussed by ^{14}C terrestrial and exposed ages on Antarctic meteorites as follows:

^{14}C terrestrial age (T_{14}):
C-14 age of meteorite fallen to the Earth which is obtained at melt fraction of 1,600 °C.

^{14}C exposed age (E_{14}):
C-14 age of meteorite exposed on the glaciar surface which is obtained at fraction of 1,000 °C.

^{14}C glacial age (G_{14}):
C-14 age of meteorite stored (or buried) in the glacier.
$G_{14} = T_{14} - E_{14}$.

The previous ^{14}C ages obtained both fractions at melt and 1,000 °C used in this study are Yamato Mountains (Y-74191[L3], Y-74014[H6], Y-790448[LL3], Y-791500[H3]), Allan Hills (ALH-77231 [L6], ALHA-77004[H4], ALHA-77282[L6], ALHA-78084[H3]), Meteorite Hills (META-78028[L6]), Reckling Peak (RKPA-79001[L6]), Mount Baldr (MBRA-76001[H6]) and Elephant Moraine (EETA-79003[L6]) [1,2,3,4,5].

2. Interpretation of C-14 ages

Although there are only a few data of C-14 ages of the Antarctic meteorites, preliminary brief results of the C-14 ages and glacial weathering can be summaried as follows (cf. Fig. 1 and Table 1):

1) There are fairly good relations between the G_{14} or E_{14} age and the collection sites of the Antarctic meteorites as follows:

G_{14} age : MET>RKP>ALH>EET>MBR>Y.
E_{14} age : Y>MBR>EET>ALH>RKP>MET.

2) Yamato meteorites have remarkably younger values of T_{14} and G_{14} ages than the other Antarctic meteorites.
3) The fact that these ages are largely variated in the Yamato meteorites suggest that the great Yamato glacier shows "complex" movement; that is, fast movement and/or easy formation of liquid water on the glacial surface.

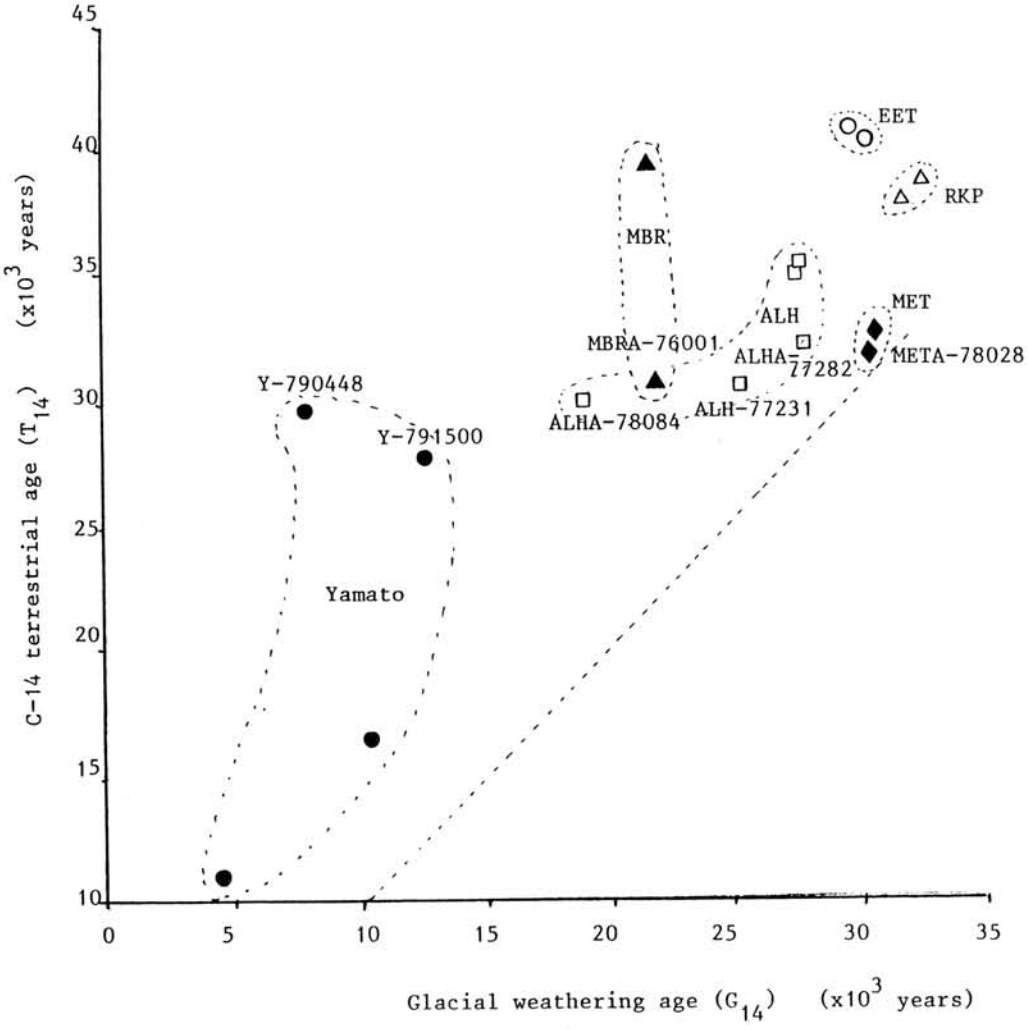

Fig. 1. Relation between C-14 terrestrial (T_{14}) and glacial (G_{14}) ages of the Antarctic meteorites discussed in this study.

4) Various changes of G_{14} age (i.e. glacial weathering) have been observed in many meteorites at ca. 30,000 years. The Yamato meteorites of Y-790448 and Y-791500 are easily exposed by fast glacial movement and weathered by liquid water, though the ALHA-78085 and ALHA-77231, and MBRA-76001 meteorites are fairly frozen (and buried) within the glacier.
5) The META, RKPA and META meteorites show older T_{14} and G_{14} ages which suggest that these meteorites are frozen within the glacier for a long time without any contamination and exposure.
6) The percentages of G_{14} and E_{14} ages from T_{14} ages are nearly constant in the same collection site of meteorites. Although there are various variations between E_{14} and G_{14} ages, it is found that two major groups of these ages are obtained, as listed in Table 1; that is,

Yamato type :
younger T_{14} and G_{14} ages, and
Allan Hills type :
younger E_{14} ages
(including ALH, MET, RKP, MBR and EET)

Table 1. Relation among E14, G14 and T14 ages of Antarctic meteorites.

Sample	[No.]	E_{14}(%)	G_{14}(%)	T_{14}(average, x10^3years)
ALHA (ALH)	[5]	23.1	76.9	33
EETA	[2]	24.6	74.5	41
MBRA	[2]	37.1	62.9	35
META	[2]	4.4	95.6	32
RKPA	[2]	15.4	84.6	38
Yamato	[4]	56.2	43.8	21

References:

[1] Beukens R. P. et al. (1988): Proc. NIPR Symp. Antarctic Meteorites, 224-230.
[2] Brown et al. (1984): Earth and Planetary Science Letters, 67, 1-8.
[3] Fireman E. L. (1983): Mem. Natl Inst. Polar Res., Spec. Issue, 30, 246-250.
[4] Jull A. J. T. et al. (1984): Proc. Lunar Planet. Sci. Conf., 15th, C329-C335.
[5] Miura et al. (1989): 14th Symposium of Antarctic Meteorites, 117-118.

THERMOLUMINESCENCE STUDY OF ORDINARY CHONDRITES BY TL SPATIAL DISTRIBUTION READOUT SYSTEM -II

NINAGAWA, K., KUBO, H., FUJIMURA, S., YAMAMOTO, I., WADA T.[1], MATSUNAMI S.[2] and NISHIMURA H.[2]

Okayama University of Science, 1-1, Ridai-cho, Okayama 700
[1]Okayama University, 1-1, Tsushimanaka 3-chome, Okayama 700
[2]Naruto University of Education, Takashima, Naruto, Tokushima 772

The artificial thermoluminescence(TL) images of unequilibrated ordinary chondridtes, ALH-77214(L3.4-3.5), Y-74191(L3.6), ALH-77216(L3.8) and equilibrated chondridtes, ALH-78043(L6), ALH-77294(H5), ALH-78128(H5), ALH-77182(H5) were measured by the TL spatial distribution readout system, combined with a microscope, and glow curves of many parts were investigated. The measurements were immediately done after γ -rays irradiation, at the rate of temperature rise 0.25 ℃/sec with a Corning band pass filter 4-96.

Figures 1 show a TL image change at various temperatures and BEI of ALH-77214. We found different types of glow in Fig.1. The glow curve of a square part A in Fig. 1 has a low peak temperature (about 90 ℃), and that of B has a high peak temperature (about 280℃). Their glow curves are shown in Figures 3a and 3b, respectively.

The TL glow curves of the other meteorites were also analyzed. But in these meteorites, we didn't find the glow curves with high peak temperature.

Table

Meteorite	the characteristics of TL glow curves
ALH-77214(L3.4-3.5)	two types of glow curves with about 90 and 280 ℃ peak temperature, respectively.
Y -74191(L3.6)	glow curves from 94 ℃ peak temperature and 68 ℃ FWHM to 138 ℃ peak temperature and 117 ℃ FWHM.
ALH-77216(L3.8)	glow curves with about 126 ℃ peak temperature.
ALH-78043(L6)	glow curves with about 125 ℃ peak temperature.
ALH-77294(H5)	glow curves with about 138 ℃ peak temperature.
ALH-78128(H5)	glow curves with about 136 ℃ peak temperature.
ALH-77182(H5)	glow curves with about 137 ℃ peak temperature.

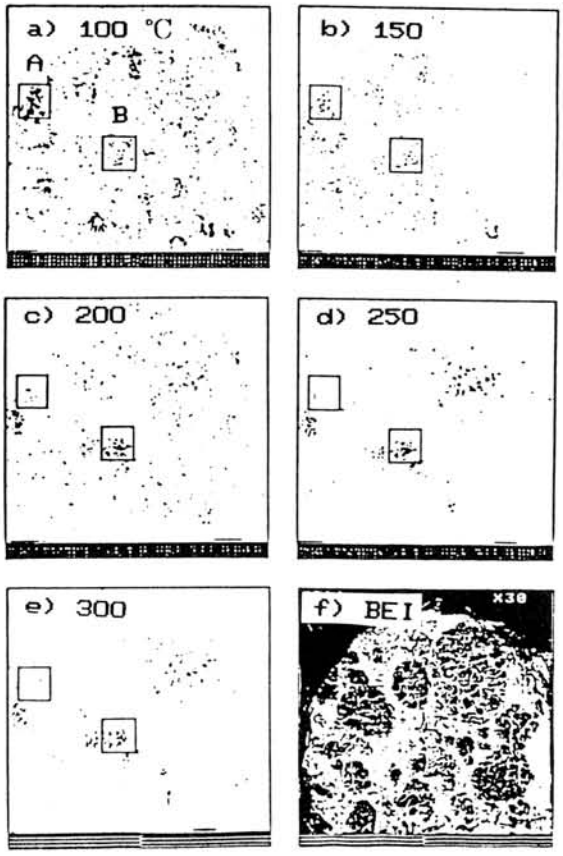

Fig.1 TL image change at various temperatures and BEI of ALH-77214.

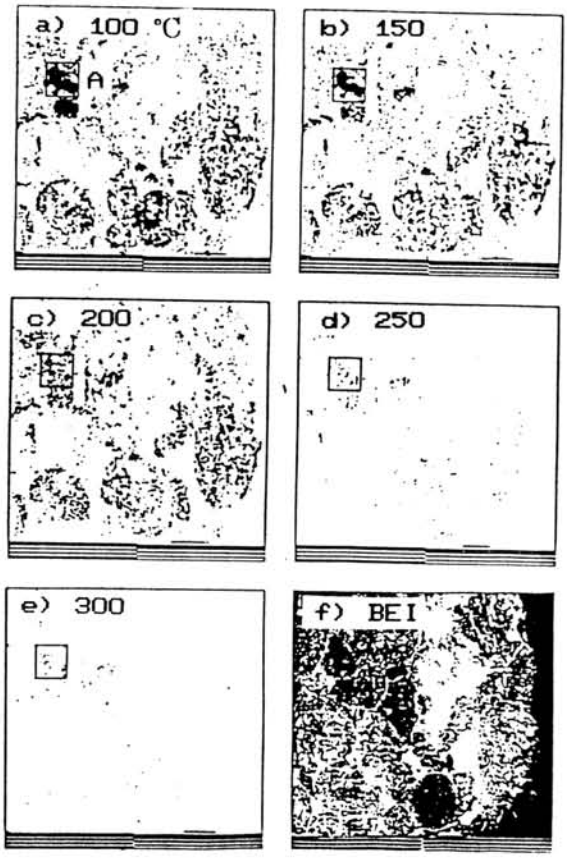

Fig.2 TL image change at various temperatures and BEI of Y-74191.

Figures 2 show the TL image change and BEI of Y-74191. The typical glow curves in Y-74191 and ALH-77216 are shown in Figures 3c and 3d. The TL characteristics of the meteorites are described in Table.

The manners of the artificial TL glow (TL sensitivity, TL peak width and peak temperature and emission spectra) are reflected to the minerals responsible for the TL. The minerals responsible for the TL in meteorites were to be mesostasis(feldspar) [TL sensitivity = 13.0], olivine[1.4], olivine +pyroxene[0.4], pyroxene[0.4], phosphates[2.05] and metal & sulphide[0.05][1]. But the EPMA measurements reveals that a silica mineral is also responsible to the TL in meteorites and shows the glow curves with high peak temperature, as well as the mineral responsible to the glow curves with low peak temperature is the mesostasis.

References

1)Lalou,C., Nordemann,D. and Labyrie J. (1970) C.R. Hebd. Seanc. Acad. Sci. (Paris), Serie B, **270**, 1706-1708

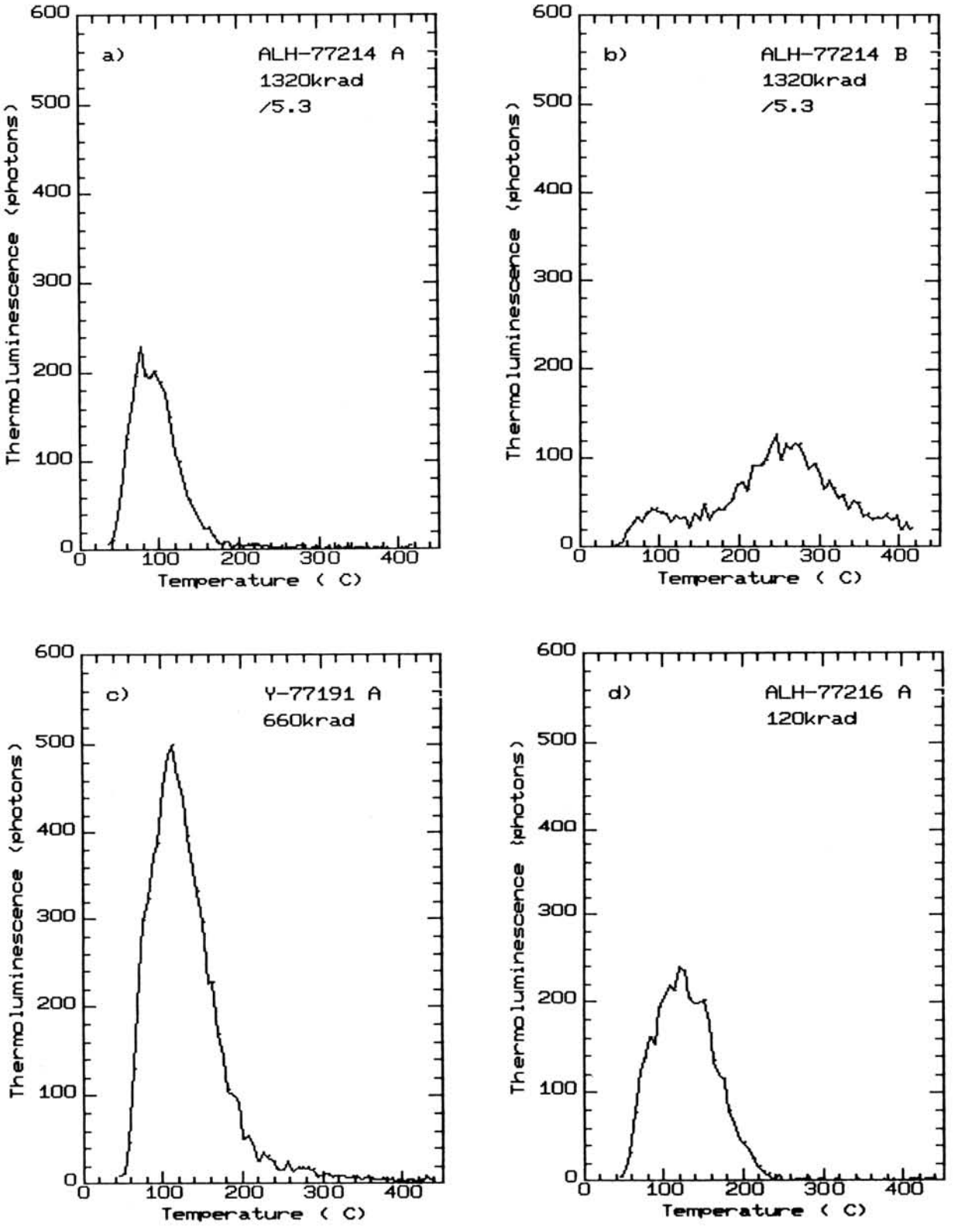

Fig.3 Glow curves a & b)the square parts A & B of ALH-77214 in Fig.1a. c)the square part A of Y-74191 in Fig.2a. d)a glow curve of ALH-77216.

NITROGEN ISOTOPE ANOMALY IN ORDINARY CHONDRITES

Ko HASHIZUME and Naoji SUGIURA
Geophysical institute, University of Tokyo, Tokyo, 113, JAPAN.

Ordinary chondrites are known to have suffered various degrees of metamorphism from the petrologic studies. It is observed for many volatile trace elements in ordinary chondrites that their concentrations decrease with the increase in the metamorphic grade of chondrites. There are two possible explanations for these observations. 1) Volatile trace elements have been lost from the parent body during the metamorphism of a intially homogeneous parent body. 2) Central part of a parent body must have accreted earlier at higher temperatures than the outer part of the parent body.

To provide a definite solution to this problem, we measured isotopic composition of nitrogen in ordinary chondrites. It is well known that in processes such as diffusion and distillation, light isotopes move more quickly than heavy isotopes, resulting in higher concentration of heavier isotopes (mass dependent isotope fractionation). The isotope fractionation may well occur if nitrogen has been degassed from the parent body, though nitrogen isotopic ratio is expected to be nearly constant if the trend of nitrogen concentration were established not after the accretion.

Isotopic ratio and abundance of nitrogen in ordinary chondrites were measured using a static mass-spectrometer. Isotopes of argon and neon were also measured. Chondrites are combusted stepwisely from 200°C to 1200°C. The major release of nitrogen occurs below 600°C. The isotopic ratio of this low temperature nitrogen is slightly positive ($\delta^{15}N \approx 15‰$). This nitrogen is probably due either to organic contamination or air nitrogen adsorbed on grain surface. At 800°C $\sim$ 1200°C, isotopic ratio for various chondrites varies quite widely ($-20‰ < \delta^{15}N < +80‰$). From studies of lunar samples, it has been established that ^{15}N produced by cosmic ray irradiation is released at high temperature fractions. Amounts of the cosmogenic nitrogen were estimated from our data of cosmogenic neon data. Nitrogen isotope anomaly observed above 800°C cannot be explained only by the cosmogenic nitrogen.

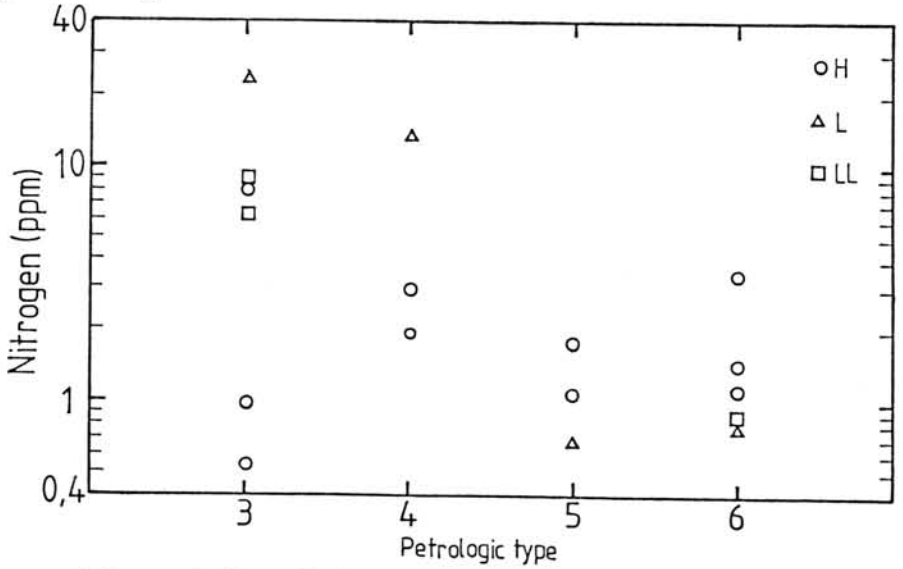

Figure 1. Petrologic type *versus* nitrogen concentration.

Nitrogen results for all the measured ordinary chondrites compiled from the 800°C ~ 1200°C fractions are described in the figures. The contribution of cosmogenic ^{15}N has been reduced for the $\delta^{15}N$ in the figures. Figure 1 is the petrologic type *versus* nitrogen concentration plots. Generally, nitrogen is abundant in type 3 chondrites and gradually becomes depleted as the petrologic type becomes high. The trend of the concentration agree with the well observed trend of volatile trace elements in ordinary chondrites. But, it must be noted that nitrogen is severely depleted in two H3s. Since they are both Antarctic meteorites (ALH78084 and Y791500), some unknown weathering effects are anticipated. Figure 2 is the petrologic type *versus* $\delta^{15}N$ plots. The increasing $\delta^{15}N$ from type 3 to type 5 can be interpreted as a result of nitrogen isotope fractionation caused by nitrogen escape from the parent body during metamorphism. The low $\delta^{15}N$ observed in type 6 chondrites can be a result of ineffective escape of nitrogen due to their low gas permeability. The observed nitrogen isotope anomaly is difficult to explain by the isotope fractionation caused by different accretion temperature. Figure 3 is the nitrogen concentration *versus* $\delta^{15}N$ plots for the H chondrites. The error bars are due to the uncertainty of the production rate of cosmogenic nitrogen used for the correction mentioned above. If nitrogen isotope fractionation occured starting from a parent body whose nitrogen concentration and nitrogen isotopic ratio were both completely homogenous before the metamorphism occured, nitrogen isotopic ratio is expected to be on a single fractionation line. The fractionation line in case nitrogen fractionated by atomic diffusion is shown in the figure. It is shown in the figure that no obvious correlation is observed between the nitrogen concentration and the nitrogen isotopic ratio. This may be the result of heterogenous nitrogen concentration in the parent body when accreted, or may be due to some effects occured after the metamorphism (*e.g.* shock impact, aqueous alteration or weathering after the meteorites falled on earth). One more possibility is that terrestrial contamination is still not completely separated even if we take the 800°C and above fractions.

As a conclusion, it can be said that the observed nitrogen isotope anomaly in ordinary chondrites seems to support the model of a parent body which was initially volatile-rich and open to volatile trace elements during the metamorphism.

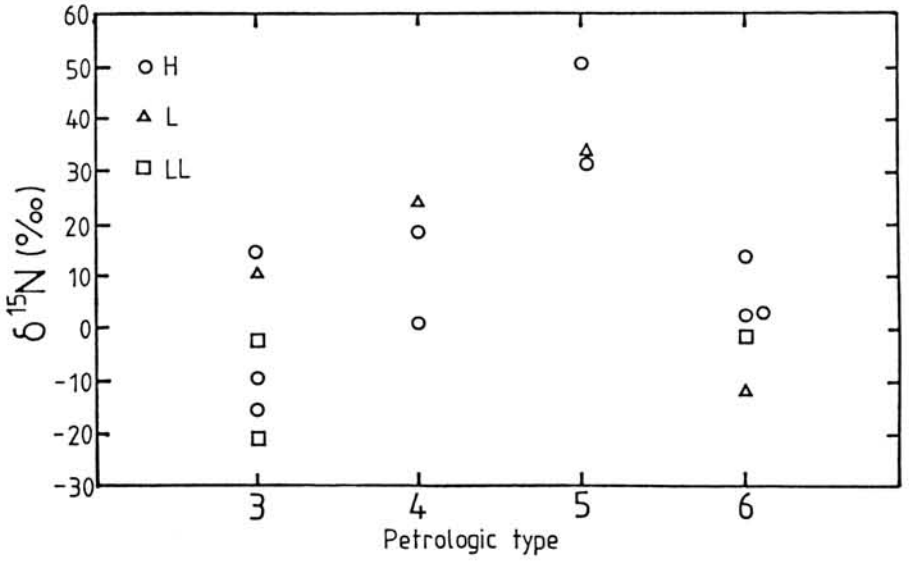

Figure 2. Petrologic type *versus* $\delta^{15}N$.

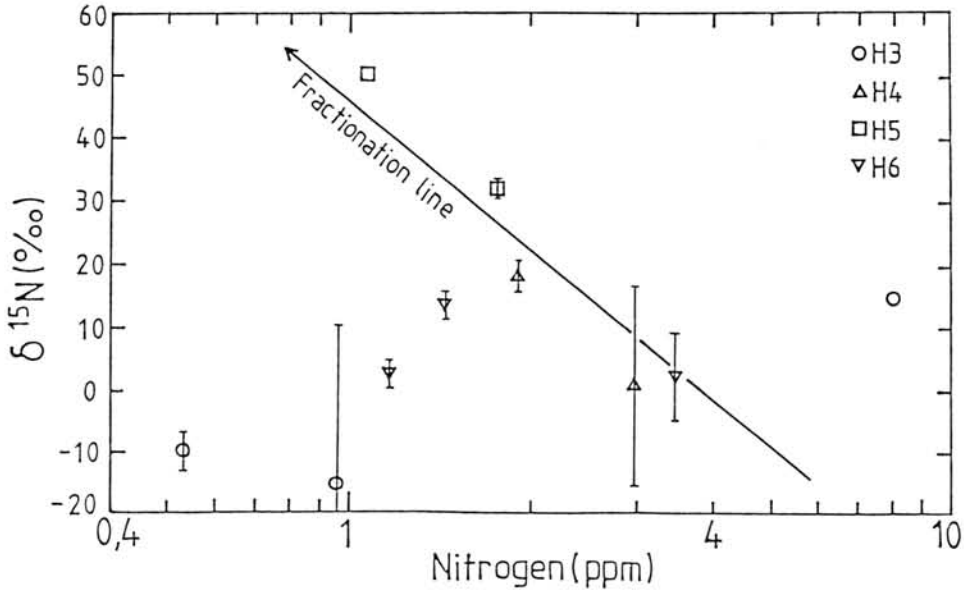

Figure 3. Nitrogen concentration *versus* $\delta^{15}N$ for H chondrites.

ANOMALOUS NITROGEN IN Y74191 (L3) CHONDRITE

Naoji SUGIURA and Ko HASHIZUME
Geophysical Institute, University of Tokyo, Tokyo, 113, JAPAN.

Presolar grains such as diamonds and SiC have been identified in primitive chondrites. Both diamonds and SiC are chemically stable, so they are enriched in HF/HCl residues and relatively easy to identify. Other presolar grains which are chemically less stable may exist in primitive meteorites. Isotope anomaly of nitrogen may be used as an indicator of the presence of presolar grains, because it tends to show huge isotope anomaly.

We have measured nitrogen isotope ratio of about 20 chondrites, and found a striking isotope anomaly ($\delta^{15}N = 750‰$.) in a L3 chondrite (Y74191). Neon and Argon are also measured to make sure that the anomaly is not due to spallogenic nitrogen. It is noted that the release pattern of the anomalous nitrogen is similar to that of primordial Ar. The anomalous nitrogen is not particularly enriched in the magnetic fraction, the non-magnetic fraction nor in the HF/HCl residue. The anomalous nitrogen seems to reside in Y74191 quite homogenously, at least in a *cm* scale, since the anomaly is reproduced for the different part of the *cm*-size sample. Compared with anomalous nitrogen in other meteorites (Bencubbin, Polymict Ureilites, ALH85085), the following similarity is noted. 1) Two or more components of anomalous nitrogen seem to exist in each meteorite. 2) The component released at higher temperature by combustion experiments has higher $\delta^{15}N$, and is dissolved by HF/HCl.

Table. Heavy nitrogen in meteorites

	Bencubbin	EET83309	ALH85085	Y74191
type	mesos.	ureilite	anomalous ch.	L3
component	N_α N_β	N_I N_{II}	N_A N_B N_C	N_a N_b
T comb. (C)*	900 600	300	250 550 >800	1100 700
	↓ ↓	↓	↓ ↓	↓ ↓
	1050 800	600	500 800	1200 1000
$\delta^{15}N$ (‰)	860 730	527	860 990 1497	750 200
Abundance (ppm)	50	49.6	190 50 <1	0.43 2.76
silicate	3 : 1			N_a rich
metal	15 : 1		- 60ppm	N_b rich
HF/HCl residue			(HCl residue)	
Abundance (ppm)**	0 3	0 17.9	96 0 0	0 1.45
$\delta^{15}N$ (‰)	- 1000	- 211	797 - -	- 180
T comb. (C)*	- 600	- 400	300 - -	- 500
			↓	↓
			600	700
reference	(1)	(2)	(3)	this study

*Combustion temperature.
**Abundance normalized by whole rock.

The presence of such common features for this anomalous nitrogen in different meteorites suggests that this component was ubiquitous in the primitive solar nebula. But, presolar grains cannot have existed as an independent fine grain in the solar nebula, since they are not common in the primitive meteorites. They are possible to form quite large size aggregates ($> m$ size?), since they are observed in multiple polymict ureilites.

References

(1) Franchi I,A., Wright I.P. and Pillinger C.T., 1986, *Nature*, **323**, 138.
(2) Grady M.M. and Pillinger C.T., 1988, *Nature*, **331**, 321.
(3) Grady M.M. and Pillinger C.T., 1990, *Earth Planet. Sci. Lett.*, **97**, 29.

Mg ISOTOPE COMPOSITION OF SILICATES PRODUCED FROM GAS-CONDENSATION FURNANCE

Keiji MISAWA[1] and Akira TSUCHIYAMA[2],

(1) Institute for Cosmic Ray Research, Univ. of Tokyo, Tanashi 188, JAPAN
(2) College of General Education, Osaka Univ., Toyonaka, Osaka 560, JAPAN

Vaporization and condensation are the most important processes in the early solar nebula. In order to investigate evaporation-condensation processes, one of the authors has undertaken condensation experiments in the system Mg-Si-O-H [1]. Here we report on Mg isotopes in the silicates produced by the experiment EC 18. Synthetic forsterite was subjected to distillation. Powdered forsterite (674.4 mg) was placed in Mo capsels and heated at 1610°C for 40.5 hrs. The total pressure of the chamber was kept at 1.4×10^{-5} bar by bleeding H_2 gas in the chamber. Mass loss is 60 wt%. The vaporized material was collected on the cold finger and identified using SEM-EDX, TEM-EDX and XRD [1].

The evaporation residue and the condensates were dissolved in a mixture of $HF+HClO_4$ acids and chemically separated Mg salts were loaded for isotopic analysis in the ICRR VG 354 mass spectrometer.

The data obtained in Table 1. show: 1) significant isotopic fractionation can be induced in the laboratory experiments; 2) both the evaporation residue and the evaporation condensate are enriched in the heavy Mg isotopes; 3) positive/negative mass fractionation is not necessarily correlated with residual negative/positive effects ($\delta^{26}Mg$). These features are partly inconsistent with the results of previous labolatory distillation experiments [2].

References. [1] A. Tsuchiyama LPS XX, 1136-1137 (1989). [2] T.M. Esat *et al.*, Nature 319, 576-578 (1986)

Table 1. Analytical Results.

Sample	Temperature (°C)	Phases	Fractionation $\Delta\ ^{25}Mg/^{24}Mg$ per mil AMU^{-1}	$\delta\ ^{26}Mg$ per mil
VR	1610	Fo	3.51	0.05
R2	1070 - 1170	Fo	9.37	0.01
R4	920 - 1100	Fo		
R5	820 - 920	Fo (+En ?)		
R6	690 - 820	En+Fo (En>Fo)	-0.59	-0.36
R8	500 - 640	En+Fo (partly amorphous)		
RT	room temp.	Amorphous (Mg/(Mg+Si)=0.8)		

$\Delta(^{25}Mg/^{24}Mg)=[(^{25}Mg/^{24}Mg)_{meas}/(^{25}Mg/^{24}Mg)_s-1]\times1000$, where s denotes the grand mean value; $^{25}Mg/^{24}Mg=0.12464$ for raw data determined from standards. $^{26}Mg/^{24}Mg$ are first corrected for mass fractionation by normalizing $^{25}Mg/^{24}Mg$ to 0.12663. Entries are in per mil relative to $(^{26}Mg/^{24}Mg)_o=0.139808$. Mg isotopic composition of unprocessed forsterite is normal.

[5] E.J. Catanzaro *et al.*, J. Res. NBS 70A 453-458 (1966)
[6] I.D. Hutcheon, Meteoritics 17, 230 (1982)
[7] D.A. Papanastassiou *et al.*, LPS XV, 629-630 (1984)

Table 1. Mg Isotopes in Allende Chondrules

Sample	Texture[a]	Fa (mol %)	Remarks	Fractionation[b] $\Delta^{25}Mg/^{24}Mg$ per mil AMU^{-1} $\pm 2\sigma$	$\delta^{26}Mg$[c] per mil $\pm 2\sigma_m$
S 2	PO	1.8-5.0	px; $En_{98}Fs_1Wo_1$ $En_{64}Fs_1Wo_{35}$	0.78 *±.64*	0.30 *±.56*
S 11	Unique	(4.1,17)	pl; An_{100}	0.93 *±1.11*	0.03 *±.18*
R 1	BO	9.8-11	Cr sp; $Mg_{.7}Fe_{.3}Al_{1.7}Cr_{.3}O_4$	1.87 *±1.68*	-0.12 *±.22*
R 13	BO	0.43-0.82		0.73 *±.82*	-0.42 *±.17*
G 3	BO	4.0-4.9		1.54 *±.67*	-0.42 *±.22*

(a) PO: porphyritic olivine, BO: barred olivine; (b) $\Delta(^{25}Mg/^{24}Mg) = [(^{25}Mg/^{24}Mg)_{meas}/(^{25}Mg/^{24}Mg)_s - 1] \times 1000$, where s denotes the grand mean value; $^{25}Mg/^{24}Mg = 0.12464$ for raw data determined from standards; (c) $^{26}Mg/^{24}Mg$ are first corrected for mass fractionation by normalizing $^{25}Mg/^{24}Mg$ to 0.12663. Entries are in per mil relative to $(^{26}Mg/^{24}Mg)_o = 0.139808$.

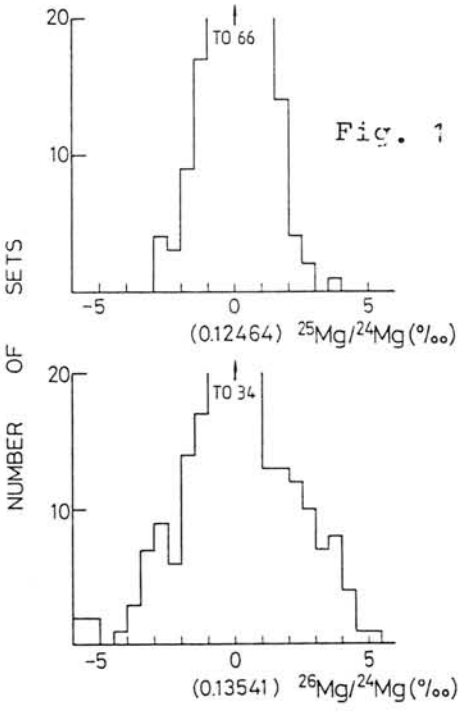

Fig. 1

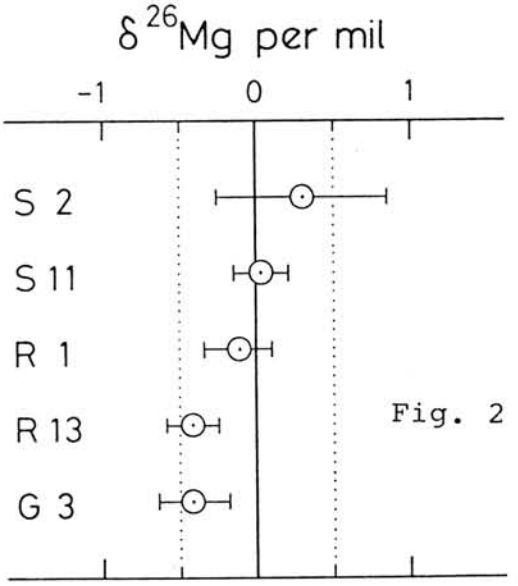

Fig. 2

Mg ISOTOPIC COMPOSITION OF CHONDRULES FROM THE ALLENDE METEORITE

Keiji MISAWA[1] and Noboru NAKAMURA[2]

(1) Institute for Cosmic Ray Research, Univ. of Tokyo, Tanashi 188, JAPAN
(2) Dep. of Earth Sci., Faculty of Science, Kobe Univ., Nada, Kobe 657, JAPAN

It is widely believed that chondrules were formed by melting of pre-existing solid precursor materials which may have been formed by multiple stages of condensation, vaporization and re-condensation. Extensive studies on Ca,Al-rich refractory inclusions (CAIs) revealed that CAIs show isotope fractionation primarily in O, Mg and Si [*e.g.* 1-3]. However, except for O isotope abundances [4], little is known about isotopic compositions of chondrules. We report on Mg isotopes in petrographically examined chondrules from the Allende meteorite, which would constrain the condition of the early solar nebula.

We analyzed one PO chondrule (S2), one plagioclase-rich chondrule (S11) and three BO (R1, R13, G3) chondrules. Chondrules S2, R13 and G3 are mainly consist of Fe-poor olivine (Table 1.).

For mass spectrometric analysis, typically 500 ng of Mg was loaded onto Re V-shaped filaments together with Si-gel and H_3PO_4 and analyzed using a serial peak jumping mode. Standards of normal Mg composition (reagent Mg, KLB1 olivine and Peace River) were analyzed regularly during these experiments. Figure 1. shows histograms of un-normalized Mg ratios. The reproducibility of raw measured isotopic ratios is $\pm$ 2 per mil for $^{25}Mg/^{24}Mg$ and $\pm$ 4 per mil for $^{26}Mg/^{24}Mg$, corresponding to a reproducibility of instrumental isotope fractionation of $\pm$ 2 per mil per amu.

We normalized the measured $^{25}Mg/^{24}Mg$ and then looked for variations in the corrected $^{26}Mg/^{24}Mg$. For normalization we use $^{25}Mg/^{24}Mg=0.12663$ [5] and mass fractionation was corrected by the power law. $\delta^{26}Mg$ is per mil deviation of $^{26}Mg/^{24}Mg$ relative to 0.139808 which is the grand mean value for standards normalized using the power law. In spite of difference of chondrule textures as well as bulk chemical compositions, 5 chondrules analyzed show normal Mg isotopic composition. That is, in all cases, the normalized $\delta^{26}Mg$ is, within errors, identical with normal Mg values (Fig. 2). The observations on the unique chondrule S11 are in agreement with previous results which showed the absence of $^{26}Mg^*$ from plagioclases in ol-pl inclusion and ol-pl chondrule [6,7].

We conclude that: 1) there are no large, easily identifiable, Mg isotope mass fractionation or nuclear effects in chondrules; 2) Vaporization loss of Mg during chondrule melting event is very minor; 3) Highly mass fractionated components produced by condensation and/or vaporization processes were subsequently mixed well with the precursor materials with normal Mg in the chondrule forming process.

References

[1] R.N. Clayton *et al.*, Science 182, 485-488 (1973)
[2] G.J. Wasserburg *et al.*, GRL 4, 299-302 (1977)
[3] C.A. Molini-Velsko *et al.*, GCA 50, 2719-2726 (1986)
[4] R.N. Clayton *et al.*, In *Chondrules and their origins* (ed. E.A. King), pp. 37-43. (1983)

MASS FRACTIONATIONS OF MINERALS PRODUCED FROM GAS-CONDENSATION PROCESS

Chiaki Uyeda and Akira Tsuchiyama
Institute of Geological Science, College of General Education,
Osaka University, Toyonaka, Osaka 560, Japan

Previously, we have reported the Mg mass fractionations of silicates produced through laboratory gas-condensation process[1]. The observed mass fractionations of condensates were strongly related with its condensation temperatures,Tc, and the result was explained qualitatively using the Rayleigh distillation model. In the present study the mass fractionations of silicon is newly measured in order to study the mechanism of the mass fractionation process in detail.

The condensates were produced in a vacuum furnace which was constructed by one of te present authors[2]. The samples measured in the present work (EC14) was produced under a relatively reduced condition compared to the samples measured previously(EC16-18)[1]. Powders of synthetic forsterite crystals(Mg_2SiO_4) was used as the starting material and was evaporated at about 1630℃. The evaporated gas firstly condensed as forsterite on the cold finger surface below 1100℃, and successively condensed at medium temperature(900℃-500℃) as mixtures of forsterite and Si, and below 600 ℃ as Mg-rich amorphous material. Isotope abundances of Mg and Si were measured by a ion microprobe analyser(Hitachi IMA-2A) for each condensate phase. Details of the measurements have been described before[1].

The relation of mass fractionation and condensation temperature is shown in Fig.1 for both Mg and Si. It is seen that the condensates with high T_c are fractionated toward the heavy isotopes with respect to the starting material, for both Mg and Si. As T_c decreases, the condensates became enriched with the light isotopes. Both $^{26}Mg/^{24}Mg$ and $^{30}Si/^{28}Si$ ratios showed reduction of about 40‰ as T_c decreased from 1100℃ to 400℃. The residue was enriched with the heavy isotopes. This range of variation is comparable to the samples measured previously(EC16-18), which where produced in a less reduced condition(compare EC16 in the figure). Esat et al.[4] has measured previously the Mg isotope abundance in laboratory distillated samples using terrestrial pyroxene as the starting material and the mass fractionations observed in condensates and residues fractionated towards the light and heavy isotopes, respectively. Our results indicate that under certain conditions, condensates can also be fractionated toward the heavy isotopes if their T_c are high.

In the present gas-condensation process, the silicate gas is considered to be oversaturated in the low temperature resion, because a large amount of condensates are observed below the equbrilium temperature down to room temperature. We therefore apply the Rayliegh fractionation model in analysing this large mass fractionation of the condensed silicate phases. For the present case we need to consider the time variation of the isotope component, since the starting material had a finite size(<10 μm) and therefore became enriched with the heavy isotopes as evaporation proceeded. We considered the amount of atoms which evaporated and condensed during a small time interval $\Delta\tau$, and then obtained the amount of mass fractionation as a function of time(τ) by taking the time integral of the condensed atoms during $\Delta\tau$,

$$\Delta 26_s(\tau) = \{\alpha f^{\alpha-1} p(\tau) - 1\} \times 1000\ (‰), \qquad (1)$$

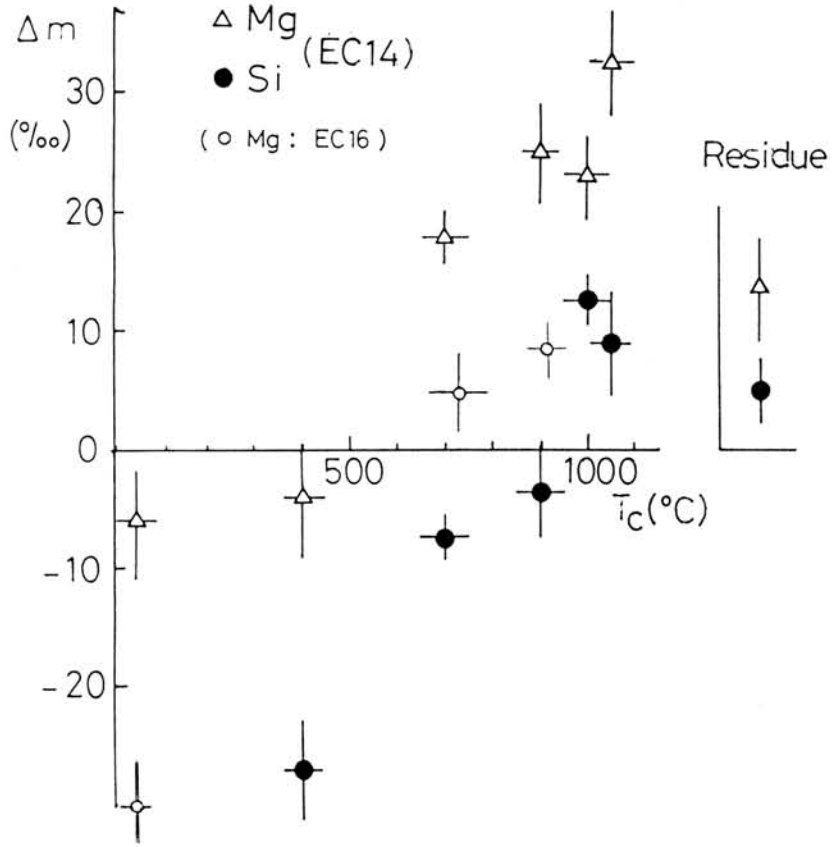

Fig.1 The relation between the amount of mass fractionation Δm, and condensation temperature T_c, for products of gas-condensation experiment. Δm is the mass fractionation with respect to the starting material, $\Delta m = \{({}^mM/{}^{m-2}M)_{sample}/({}^mM/{}^{m-2}M)_{starting} - 1\} \times 1000$ (‰); M=Si, m=30 for silicon and M=Mg, m=26 for magnesium.

where p(τ) represents the time average of the gas compnent, p(τ) ={1 - (1 - τ/τe)β}/(τ/τe). α is the coefficient of mass fractionation for the condensation process, and β is that of the evaporation process. τe is the amount of time needed to evaporate the starting material compelete-ly. f is the fraction of residual gas phase, which can be estimated from the actual amount of silicates which condensed on the cold finger. The theoretical temperature curves obtained from eq(1) will be compared with the experimental isotope values for both Mg and Si, and the mechanism of the condensation process will be discussed taking various experimental conditions into account.

References

1)Uyeda,C et al.(1989):Abst.14th symp.antarct.meteorites,87-89.
2)Tsuchiyama,A.(1988):Abst.13th symp.antarct.meteorites,123-125.
3)Uyeda,C. et al.(1989):Secondary Ion Mass Spectrmetry,SIMS VII in print.
4)Esat,M.T.et al.(1986):Nature 319,576-578.

AN ATTEMPT TO MEASURE COSMOGENIC 81KR IN ORDINARY CHONDRITES

Nakamura, Y., Ogata, A. and Nagao, K.
Institute for Study of the Earth's Interior, Okayama University, Misasa, Tottori 682-02, Japan.

1. Introduction

^{81}Kr is radioactive nuclide produced in meteorite by cosmic-ray irradiation in space. Its concentration in equiliblium state is as low as 10^{-14}cc/g in ordinary chondrites. Although it is difficult to make precise measurement of such low concentration of ^{81}Kr, the ^{81}Kr data combining with other cosmogenic noble gases provide us a useful information about cosmic-ray irradiation history of meteorites in space and about terrestrial ages of meteorites with long residence on the earth.

Since we want to measure ^{81}Kr-Kr terrestrial ages of antarctic meteorites systematically, we investigated detection limit and reliability of ^{81}Kr measurement with the mass spectrometer installed in our laboratory last year. We present the results on cosmogenic noble gases in four ordinary chondrites and the cosmic-ray exposure ages calculated with ^{81}Kr as well as other cosmogenic noble gases.

2. Samples and experimental method

The ordinary chondrites analyzed in this work are three nonantarctic meteorites, Long Island(L6), Densmore(H6) and Gladstone(H6) and an antarctic one, ALH-769(L6). Although they are finds, the terrestrial ages for nonantarctic chondrites are expected to be much shorter than the ^{81}Kr half life(2.1×10^{5}y) because of a rapid weathering on the earth. So, if ^{81}Kr-Kr exposure age for the meteorite is consistent with the cosmic-ray exposure ages based on cosmogenic ^{21}Ne and ^{38}Ar, the ^{81}Kr measurement is thought to be correct.

An analytical procedure of noble gases was standard one. Sensitivities and mass discrimination correction factors for noble gases were determined by measuring calibrated atomospheric noble gases. Noble gas amounts of blank run were 1.4, 0.6, 0.09, 0.003 and 0.0006 in unit of 10^{-10}ccSTP for ^{4}He, ^{20}Ne, ^{36}Ar, ^{84}Kr and ^{132}Xe, respectively. The blank levels are sufficiently lower than the noble gas amounts of samples measued in this work.

3. Results and discussion

Concentrations of cosmogenic ^{21}Ne and ^{38}Ar, production rates and cosmic-ray exposure ages obtaind in this work are summarized in Table 1. The results from duplicate analyses for Long Island are in good agreement with each other, which indicates good reproducibility in our noble gas analysis. Gladstone was a gas-rich meteorite and cosmogenic Ne was masked with large amount of solar-type Ne. For this meteorite the concentration of cosmogenic Ne could not be estimated. The production rates for ^{21}Ne and ^{38}Ar were calculated with the formulas presented by Eugster(1988). The formulas were evaluated from ^{81}Kr-Kr exposure ages for chondrites and include correction factors for chemical composition and shielding effect. Cosmogenic Kr

isotopic ratios are listed in Table 2. ^{81}Kr-Kr exposure age was calculated by $T_{81}=(1/\lambda)(P_{81}/P_{83})/(^{81}Kr/^{83}Kr)$, where λ is decay constant of ^{81}Kr. The production rate ratio P_{81}/P_{83} was estimated by following equations 1) $P_{81}/P_{83}=(0.95/2)(^{80}Kr/^{83}Kr + ^{82}Kr/^{83}Kr)$ and 2) $P_{81}/P_{83}=1.262(^{78}Kr/^{83}Kr)+0.381$. The ages T_{81} calculated with these equations are listed in Table 2.

There are systematic differences between two ^{81}Kr-Kr ages calculated by the two equations. The age obtained by the latter equation shows good agreement with T_{21} within experimental errors. The former age which is older than T_{21} and T_{38} seems to be caused by an overestimate of P_{81}/P_{83} ratio because of an interference of ^{40}Ar at ^{80}Kr peak caused by an incomplete separation between Kr and Ar. ^{80}Kr peak is affected by ^{40}Ar ion by charge transfer reaction in analyzer tube of mass spectrometer. This interfarence of ^{40}Ar at ^{80}Kr is expressed in Figure 1. According to Eugster(1988), P_{81}/P_{83} ratios for chondrites are plotted on a straight line in P_{81}/P_{83} vs. ^{22}Ne/^{21}Ne plot. Open symbols calculated by the equation 1) are plotted above the line in this Figure. However, the solid symbols by the equation 2) are on the line, which indicates that the estimation of P_{81}/P_{83} ratio by ^{78}Kr/^{83}Ke ratio is better than that by ^{80}Kr/^{83}Kr and ^{82}Kr/^{83}Kr ratios.

In conclusion, we think that the signal at ^{81}Kr obtained in this work is real one even though the noise level at this region is high and the mass separation between ^{81}Kr peak and isobaric hydrocarbon ones is inadequate. For more precise measuremernt of ^{81}Kr, following improvements should be applied to the analytical procedure and mass spectrometer. a) Complete separation of Ar from Kr in Kr analysis, b) resolving power should be increased, c) noise level caused by dark current in photomultiplier employed in collecter system of VG5400 should be lowered or should be replaced by other collecter system of low noise level.

Table 1. Cosmogenic ^{21}Ne and ^{38}Ar abundances, production rates and exposure ages.

Sample	$(^{21}Ne)_c$#	$^{22}Ne/^{21}Ne$	$P_{21}$$	T_{21}	$(^{38}Ar)_c$#	$P_{38}$$	T_{38}
Long Island	5.9	1.062±0.005	0.424	14	0.53	0.0496	11
(L6)	6.1	1.049±0.002	0.426	14	0.53	0.0505	10
Densmore(H6)	2.5	1.065±0.005	0.388	6.4	0.24	0.0534	4.5
Gladstone(H6)					1.2	0.0499&	24
ALH-769(L6)	6.0	1.086±0.005	0.372	16	0.71	0.0479	15

Concentrations of cosmogenic ^{21}Ne and ^{38}Ar are given in units of 10^{-8}cm^{3}STP/g.

$ Production rates of ^{21}Ne and ^{38}Ar in unit of 10^{-8}cm^{3}STP/g·Ma were calculated using the equations presented by Eugster(1988).

& For shielding corresponding to cosmogenic ^{22}Ne/^{21}Ne=1.11.

Table 2. Isotopic ratios of cosmogenic Kr and exposure ages based on cosmogenic Kr.

Meteorite	78 / 83 c	80 / 83 c	81 / 83 c	82 / 83 c	T_{81}(Ma) 1)	2)
	0.1559	0.979	0.0103	0.723	24	17
Long Island	±0.0062	±0.031	±0.0041	±0.047		±7
(L6)	0.1249	0.631	0.0107	0.743	18	15
	±0.0047	±0.026	±0.0016	±0.035		±2
Densmore	0.1397	0.980	0.0231	0.827	11	7.4
(H6)	±0.0121	±0.081	±0.0031	±0.145		±1.0
Gladstone	0.1335	1.821	0.0064	1.605	78	26
(H6)	±0.0181	±0.236	±0.0014	±0.248		±6
ALH-769	0.1764	1.278	n.d.	0.901		
(L6)	±0.0155	±0.093		±0.066		

1) Production rate ratios P_{81}/P_{83} were estimated from $^{80}Kr/^{83}Kr$ and $^{82}Kr/^{83}Kr$ ratios.
2) Production rate ratios P_{81}/P_{83} were estimated from $^{78}Kr/^{83}Kr$ ratios.

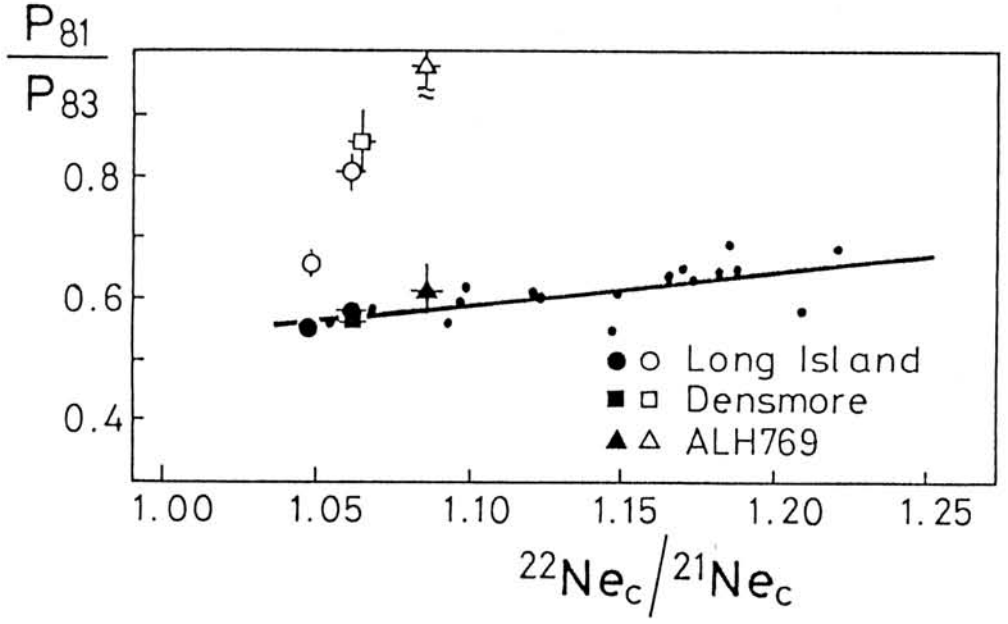

Figure 1. Correlation plot of production rate ratio P_{81}/P_{83} versus $(^{22}Ne/^{21}Ne)_c$. Open symbols were calculated with the formula $P_{81}/P_{83}=0.95\{(^{80}Kr/^{83}Kr)_c+(^{80}Kr/^{83}Kr)_c\}/2$, and solid symbols were calculated with $P_{81}/P_{83}=1.262(^{22}Ne/^{21}Ne)_c-0.029$ (Eugster, 1988). Data points (small solid circles) for chondrites are plotted on a straight line. Data points for three chondrites calculated by cosmogenic $^{78}Kr/^{83}Kr$ ratios are on the line, whereas those by $^{80}Kr/^{83}Kr$ and $^{82}Kr/^{83}Kr$ ratios are plotted above the line because of an interfering ^{40}Ar ion with ^{80}Kr peak. The P_{81}/P_{83} ratio corresponding to the point on the line produces ^{81}Kr-Kr exposure age which is in good agreement with the age by cosmogenic ^{21}Ne.

BE-10 AND AL-26 IN ANTARCTIC METEORITES.

H.Nagai, M.Honda, I.Kobayashi, Coll.of Humanities and Sci., Nihon Univ.,Tokyo
M.Imamura, Inst.Nuclear Study, Univ.Tokyo
K.Kobayashi,Res.Cent.,Nuclear Sci.Techn.,Univ.Tokyo

Cosmogenic ^{10}Be and ^{26}Al were determined in separated metal and stone fractions of meteorites by AMS, accelerator mass-spectrometry. The tandem van de Graaf accelerator, working terminal voltage: ca.3 MV, at the Univ. of Tokyo was employed for these measurements by applying the internal beam monitor method (1).

Chondrites, mainly antarctic chondrites, and stony irons were processed to separate their metal and stone phases. Because of higher ^{26}Al contents in their stone phases, extensive purifications for the metal grains had to be performed. The contamination levels must be lower than 0.1% stone in metals, and small stone corrections can be made. With chondrites, the levels were as low as 0.01%, the lowest at 0.004%, in our recent runs. Usually 5-10% of purified metal phases could be separated from bulk L-H chondrites respectively. Among antarctic meteorites, weathering effects were not seriously observed for the recoveries and the purities. From our two specimens of the Tsarev L-chondrite, however, only about 1% of metal could be isolated. For Y790981 the metal phases could not be recovered at useful size, 36mg of crude magnetic fraction were yielded out of 2.3 g bulk sample.

The sample sizes were 50-400 mg of metals and ca.100 mg of stones. Smaller amounts of the carriers were added for metal samples, down to 200 and 500 micro g.Be and Al respectively, and the observed atomic ratios of $^{10}Be/Be$ and $^{26}Al/Al$ of the samples were approximately 10^{-11}. Some examples of recent determinations are shown in Table 1 (2,3).

An extremely high production of ^{10}Be in carbon phases were observed in stone phases of the Y790981 and the Landes(3). Products in carbon in the Y790981 were extracted by bisulfate fusion after ignition at 900C. Based on the ignition loss, 2.5%

carbon were estimated in the bulk. In this extract about 16% C were found in decomposed silicates and 29 dpm ^{10}Be/kg was observed, in contrast to 18 dpm/kg in the remaining carbon free silicates. The difference suggests that 84 dpm/kgC and 18 dpm/kgstone. A similar situation was found more extensively in the Landes(15-30%C) and perhaps also in the El Taco, AI 8/9, stone(53%C). The production of ^{10}Be in C can be compared with that of ^{14}C in oxygen and ^{26}Al in Si. The nuclear reaction responsible to this production mainly attributed to ^{12}C(n,^{3}He) and ^{12}C(n,2pn), and this ^{10}Be in C may be classified as a typical low energy product corresponding to ΔA=. 3 (4).

Data obtained in the Y74094 may indicate undersaturations of these nuclides as already suggested by contents of other nuclides such as ^{53}Mn and ^{21}Ne, and productions at surface region of a large object like the Tsarev. On the other hand, those of the Y74165 can also be interpreted as the products in a fragment of a near surface of a relatively large object.

Ref. (1) H.Nagai et al(1987),Nucl.Instr.Method, B29,266-270; (1987) Meteoritics 22,467-469. (2) H.Nagai et al(1989) 14th Symp. Antarctic Meteorites,Jun.Tokyo; Workshop on "Production Rates of Cosmogenic Nuclides" Vienna. (3) H.Nagai et al(1990) 5th Intntl. Conf. on AMS, Paris, April. (4) M.Honda(1985) EPSL 75,77-80; (1988) Meteoritics 23,3-12.

TABLE 1 BE-10 AND AL-26 FOUND IN METAL AND STONE FRACTIONS

SAMPLE	CLASS	ID	METAL FRACTION sample mg.	dpm/kg Be-10	dpm/kg Al-26	stone %	STONE FRACTION sample mg	dpm/kg Be-10	dpm/kg Al-26
CHONDRITES:									
Y74094	H6	91	59	1.45±.43		.004			
Y74165	L4	61	166	3.47±.29	3.35±.29	.126	108	23.8±1.1	67.8±2.7
Y74191	L3	106	64	6.33±.36		.008			
Y74364	H4	74	119	5.39±.25	3.69±.20	.19			
Y74418	H6	71	112	6.06±.27	3.91±.25	.06			
Y75029	H3	51	73	2.71±1.6	3.9±.3	.32	112	18.2±.7	70.7±2.2
							300	18.7±.9	
Y790981	UREIL	72							
NESS Co.	L6		226	4.65±.26	3.34±.20	.095	104	24.4±1.1	62.6±2.2
TSAREV(2)	L5		57	1.33±.33		.006	178W	3.40±.19	13.9±.8
STONY IRONS and IRONS:									
ADMIRE	PAL		115	2.39±.12	2.29±.12	.01	81	16.9±.3	47.4±2.1
BUDULAN	MES	#	85.6	3.28±.18	2.55±.28	.40	101	20.3±.58	85.1±3.3
IMILAC	PAL	H202.20					176	20.9±1.0	48.7±1.8
MINCY	MES		162	5.31±.28	3.09±.16	.10	300	22.5±1.1	59.5±2.6
VACA MUERTA	MES	H300.16	201	2.38±.39	1.59±.10	.027	269	10.9±.2	45.2±2.2
CAMPO D.CIELO	IA	AI8/9&					269	0.48±.05	
(EL TACO)		1715& 1994		0.003±.003	0.014±.002				
		215& 2144		0.001±.001					
HENBURY	IIIA	H193.488	748	1.43±.10	0.95±.09				
LANDES	IA	H91.142	452	5.4±.12	3.8±.2	1.18	238	41 ±1.	85.5±2.7
UDEI STATION	IA	#	70	4.89±.22	3.97±.37	0.32	107	22.1±0.9	85.1±2.4

UREIL.: ureilite; PAL.: pallasite; MES: mesosiderite
Source: #: F.Begemann et al(1976); &: L.Schultz,Mainz
W: WHOLE ROCK

Special Lecture

Professor Edward Anders

INTERSTELLAR DIAMOND, GRAPHITE, AND SiC IN METEORITES

Edward Anders
Enrico Fermi Institute and Dept. of Chemistry, Univ. of Chicago, Chicago, IL 60637-1433, USA.

Murchison (C2) and other chondrites of types 1-3 contain small amounts of carbon-bearing interstellar grains: *diamond* (~400 ppm), *graphite* (<2 ppm) and *SiC* (~6 ppm). All are labelled with isotopically anomalous noble gases, which, by serving as "beacons" during separations, have made possible the isolation of these grains by a variety of chemical and physical techniques [*1,2,3,4*]. In contrast to oxide minerals, which generally show isotopic anomalies only in the permil range, these carbonaceous phases have very large anomalies, up to 10^1-$10^2\times$. The reason is their chemical inertness, which allowed them to survive intact, without isotopic exchange or dilution by solar-system minerals.

Diamond is present as submicroscopic grains [*1*] with median crystallite size ~26 Å [*5*]. It contains Xe-HL (enriched up to 2× in the *h*eavy and *l*ight isotopes, and presumably made by the *r*- and *p*-processes in a supernova) and associated components of the other noble gases [*4*]. Carbon and nitrogen are at most slightly anomalous ($\delta C^{13} = -38$ ‰, $\delta N^{15} = -340$ ‰). The diamond presumably was made by metastable condensation (CVD-process!) from a stellar atmosphere of C/O >1, and acquired its noble gases by ion implantation [*1,4*].

Graphite occurs as soot-like spherules of 1-6 μm [*6,7*]. It contains Ne-E(L), a nearly monoisotopic Ne^{22} component that may be derived from β^+ decay of Na^{22} ($t_{½}$ = 2.6 a). S-process Kr and Xe are also present [*6,8*]. The carbon itself is grossly anomalous, with C^{12}/C^{13} ranging from 0.08-50× the solar-system ratio [*6,7*]. Likely sources are novae [*9*] or red giants (AGB = *a*symptotic *g*iant *b*ranch stars).

SiC ranges from 0.01 to >10 μm in size [*3,10*], and most grains have cubic crystal structure [*11*]. Relative to solar isotopic ratios, Si, C, and N are anomalous by factors of 0.8-1.1×, 0.03-1.8×, and 0.22-22× [*3,11,12*]. SiC contains *s*-process Kr and Xe as well as a Ne component strongly enriched in Ne^{22} [= Ne-E(H)] [*2,3,14,15*]. Ion probe analysis of individual grains shows that they form ~6 tight clusters in δSi^{29}–δSi^{29}–δC^{13}-space, suggesting that most of the SiC in the early solar system came from only ~6 stars [*3,11,13*]. This is a surprising and important conclusion, which implies that the interstellar medium is less well-mixed than assumed in current models.

The presence of *s*-process Kr, Xe points to AGB stars as the source of the SiC. Some clues to *s*-process conditions are provided by Kr^{80} and Kr^{82}, which lie on branch points of the *s*-process path (through radioactive Se^{79} and Kr^{85}). The Kr^{80}/Kr^{82} ratio increases with grain size of SiC, whereas Kr^{80}/Kr^{82} decreases; the range of values corresponds to mean neutron densities of $(1.5\text{-}3) \times 10^9$ cm^{-3} and $T \simeq 150 \times 10^6$ K [*14,15*]. The latter temperature implies that C^{13}, not Ne^{22} is the principal neutron

source [*16*]. Surprisingly, the Kr isotopic ratios correlate with grain size of SiC [*14,17*], although one reflects conditions in the hot interior and the other, conditions in the cool atmosphere.

Neon in SiC contains some excess Ne^{21}, suggesting a presolar cosmic-ray exposure. The nominal cosmic ray ages average to 40 Ma [*3,18*], much less that the estimated 400 Ma lifetime of refractory interstellar grains [*19*]. But since a substantial part of the Ne^{21} may be nucleosynthetic rather than cosmogenic [*17*], the true ages must be even shorter, and the discrepancy correspondingly larger. Possible reasons are faster destruction of SiC in interstellar clouds due to its chemical instability at $C/O < 1$ or late degassing of SiC [*3,13*].

Because of their excellent state of preservation, these carbonaceous grains offer unique insights into nuclear processes in stars and chemical processes in the interstellar medium and the early solar system.

[*1*] Lewis, R. S., Tang, M., Wacker, J. F., Anders, E., and Steel E. (1987) *Nature* **326**, 160-162.
[*2*] Tang, M. and Anders, E. (1988) *Geochim. Cosmochim. Acta* **52**, 1221-1234.
[*3*] Zinner, E., Tang, M., and Anders, E. (1989) *Geochim. Cosmochim. Acta* **53**, 3273-3290.
[*4*] Anders, E. (1988) In *Meteorites and the Early Solar System* (eds. J. F. Kerridge and M. S. Matthews). Tucson: Univ. Arizona Press, 927-955.
[*5*] Lewis, R. S., Anders, E., and Draine, B. T. (1989) *Nature* **339**, 117-121.
[*6*] Amari, S., Anders, E., Virag, A., and Zinner, E. (1990) *Nature*, in press.
[*7*] Zinner, E., Wopenka, B., Amari, S., and Anders, E. (1990) *Lunar Planet. Sci.* **21**, 1379-1380.
[*8*] Amari, S., Lewis, R. S., and Anders, E. (1990) *Lunar Planet. Sci.* **21**, 19-20.
[*9*] Clayton, D. D. (1975) *Nature* **257**, 36-37.
[*10*] Amari, S. and Lewis, R. S. (1989) *Meteoritics* **24**, 247-248.
[*11*] Wopenka, B., Virag, A., Zinner, E., Amari, S., Lewis, R. S., and Anders, E. (1989) *Meteoritics* **24**, 342.
[*12*] Zinner, E., Tang, M., and Anders, E. (1987) *Nature* **330**, 728-730.
[*13*] Tang, M., Anders, E., Hoppe, P., and Zinner, E. (1989) *Nature* **339**, 351-354.
[*14*] Lewis, R. S. and Amari, S. (1989) *Meteoritics* **24**, 293.
[*15*] Lewis, R. S., Amari, S., and Anders, E. (1990) Paper presented at Meteoritical Soc. Mtg., Perth, Australia, 17-21 September.
[*16*] Gallino, R., Busso, M., Picchio, G., Raiteri, C. M., and Renzini, A. (1988) *Astrophys. J.* **334**, L45-L49.
[*17*] Amari, S., Lewis, R. S., and Anders, E. (1990) Paper presented at Meteoritical Soc. Mtg., Perth, Australia, 17-21 September.
[*18*] Tang, M. and Anders, E. (1988) *Astrophys. J.* **335**, L31-L34.
[*19*] McKee, C. F. (1989) In *Interstellar Dust [IAU Symposium 135]* (eds. L. J. Allamandola and A. G. G. M. Tielens). Dordrecht: Kluwer, 431-443.

Abstract Only

PETROGRAPHY AND CHEMISTRY OF THE THREE CARBONACEOUS CHONDRITES Y-86720, Y-82162, AND B-7904.

A. Bischoff and K. Metzler
Institut für Planetologie, Wilhelm-Klemm-Str. 10, 4400 Münster, Germany.

As a part of the consortium study on antarctic meteorites with affinities to CI-chondrites we studied the samples of Y-86720, Y-82162, and B-7904. These carbonaceous chondrites are unique samples and do not fit in the traditional classification schemes. Therefore, they have to be considered as very important samples to carry distinct information about processes in the early solar system. Based on the oxygen isotopic composition all three meteorites were classified as CI-chondrites (Mayeda et al., 1987; Clayton and Mayeda, 1989). B-7904, however, is chemically and petrologically a CM(C2)-chondrite (e.g. Skirius et al., 1986; Yanai and Kojima, 1987; Akai, 1988; Kallemeyn, 1988). Based on the petrology, mineralogy and chemistry Y-86720 has been classified as a CM- or an intermediate chondrite between CI and CM (e.g. Kallemeyn, 1988; Ebihara and Shinonaga, 1989). Y-82162 is classified by most authors as a CI-chondrite (e.g. Kallemeyn, 1988; Tomeoka et al., 1988). In this study we are presenting mineralogical and chemical data on B-7904, Y-82162, and Y-86720. Our main aim was to determine the abundances of individual components of these meteorites and to characterize these constituents chemically and mineralogically.

Yamato 82162.

Y-82162 is a very fine-grained carbonaceous chondrite; however, the sample is not homogeneous. Large, mm-sized fragment-like objects are visible (Fig.1). Many of such clasts are poorer in Fe than the surroundings. Y-82162 also contains abundant small (usually $<300\,\mu m$ in size) fragment-like components that include coarse-grained phyllosilicate-clusters with irregular shapes (Fig.2), aggregates of phosphates and magnetites, relicts of chondrule- and CAI-like objects, and various minerals (olivine, sulfides, whitlockite, orthopyroxene, Cr-spinel, SiC). Y-82162 appears to be a breccia. The dominating phases are phyllosilicates; abundant sulfide grains are scattered throughout the entire sample. However, the abundances of sulfides vary from clast to clast. All metals analysed in Y-82162 are Ni-rich (63-66 wt%) and smaller than 10μm in size. Abundant magnetites occur as isolated grains within the matrix or they form aggregates sometimes intergrown with phosphates.

Yamato 86720.

Based on an optical investigation with a polarizing microscope, Y-86720 contains abundant light-coloured objects embedded in a fine-grained, phyllosilicate-rich groundmass. In reflected light the great number of large (≤400μm in size) sulfide laths is obvious. We have determined the frequency distribution of various components larger than about 100μm in size. 528 mineral and lithic objects from an area of 133.85 mm^2 were analysed. The chondrite contains 14.35 vol% of components larger than≈100μm. Most abundant are rounded to irregularly-shaped (Fig.3), phyllosilicate-rich objects (9.42 vol%). Many similar objects also contain sulfide laths (3.55 vol%). Sulfide-rich, almost opaque aggregates and sulfide mineral grains constitute 0.57 and 0.81 vol%, respectively. The relict chondrules or aggregates (compare Fig.3) contain essentially no anhydrous silicates. These light objects exhibit, however, well-preserved accretionary dark dust mantles similar to those found in CM-chondrites (Metzler and Bischoff, 1987, 1989, 1990, this volume).

Belgica 7904.

B-7904 is an interesting carbonaceous chondrite, that is somehow similar to CM-chondrites. However, B-7904 contains abundant components, that never have been found in CM-chondrites before (see below). We have determined the frequency distribution of the components≥70 m in size. 435 mineral and lithic fragments were counted on a surface area of 61.2 mm^2. B-7904 contains≈18 vol% of objects larger than about 70μm. 42 vol% of these components are chondrules or chondrule fragments. The abundance of CAIs is far below 1 vol%. Most abundant components are olivine-bearing, fragment-like objects (45.9 vol%). Based on the optical observations the olivines are embedded in a fine-grained brownish-grey matrix (Fig.4). These objects are unknown from other CM-chondrites. About 9.4 vol% and 3.1 vol% of the components within B-7904 are olivine aggregates and olivine mineral fragments, respectively.
Most objects are surrounded by very dark, fine-grained, accretionary mantles (compare Metzler and Bischoff, this volume).

Distinct olivine compositions of various components have been obtained. About 50 vol% of olivines that occur within chondrules and chondrule fragments or as olivine mineral fragments are Fo-rich ($Fo_{>99.0}$); however, others can also be very Fa-rich ($\sim Fo_{40}$). More than 97% of the olivines analysed in olivine aggregates or within the olivine-bearing, fragment-like objects with the brownish-grey matrix are Fo-rich ($Fo_{>95}$). In other words the composition of olivine within different components is different. Another unusual observation in B-7904 is, that most chondrules, chondrule fragments and olivine-bearing, fragment-like objects contain spherical to egg-shaped fine-grained particles (Figs.5 and 6), which are rich in Cr_2O_3 (2-5 wt%) and Al_2O_3 (4-7 wt%). We do not have any idea about the formation of these spherules (up to ~200µm in size) and their incorporation in the host objects (e.g. chondrules, fragments).

References:
Akai J. (1988), GCA 52, 1593. Clayton R.N. and Mayeda T.K. (1989), Lunar Planet. Sci. Conf. XX, 169. Ebihara M. and Shinonaga T. (1989), Symp. Antarc. Meteor. 14th, 35. Kallemeyn G.W. (1988), Symp. Antarc. Meteor. 13th, 132. Mayeda K. et al. (1987), Mem. Natl. Inst. Polar Res., Spec. Issue 46, 144. Metzler K. and Bischoff A. (1987), Meteoritics 22, 458. Metzler K. and Bischoff A. (1989), Lunar Planet. Sci. XX, 689. Metzler K. and Bischoff A. (1990), this volume. Skirius C. et al. (1986), Mem. Natl. Inst. Polar Res., Spec. Issue 41, 243. Tomeoka K. et al. (1988), Symp. Antarc. Meteor. 13th, 126. Yanai K. and Kojima H. (1987), Catalog of the antarctic meteorites, published by NIPR.

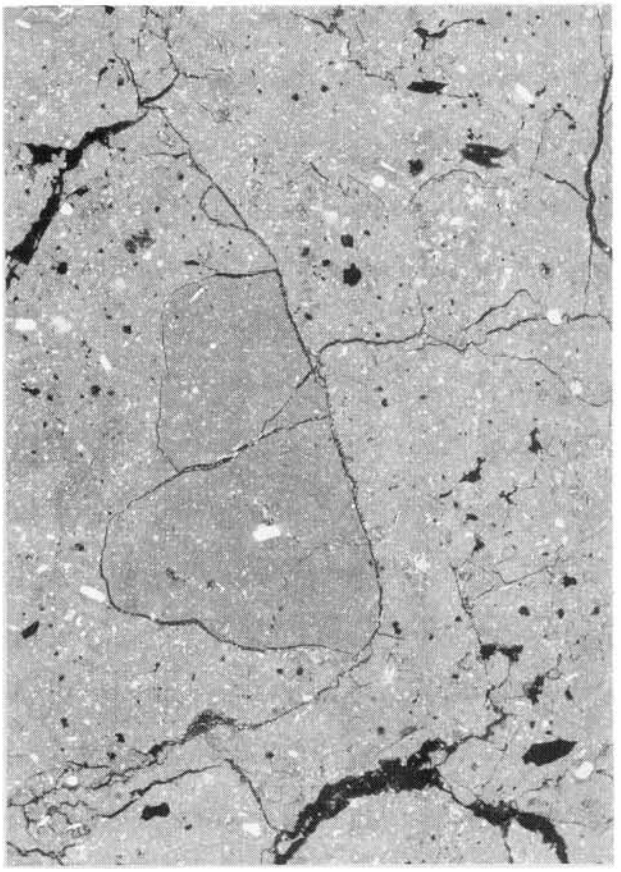

Fig.1: Large, mm-sized fragment-like object within Y-82162, that appears to be poorer in Fe than the surroundings (BSE-image)

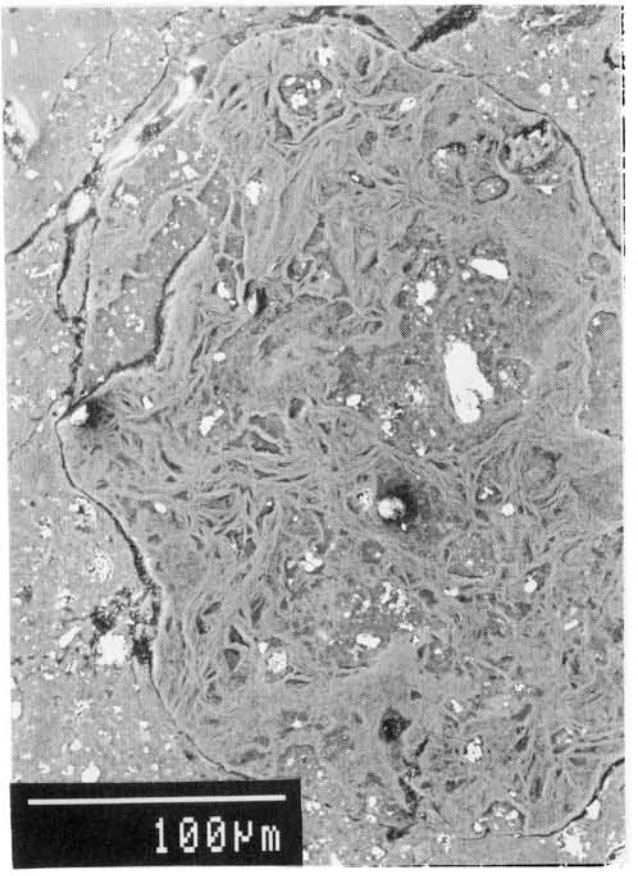

Fig.2: Coarse-grained, phyllosilicate-rich cluster within Y-82162 (BSE-image)

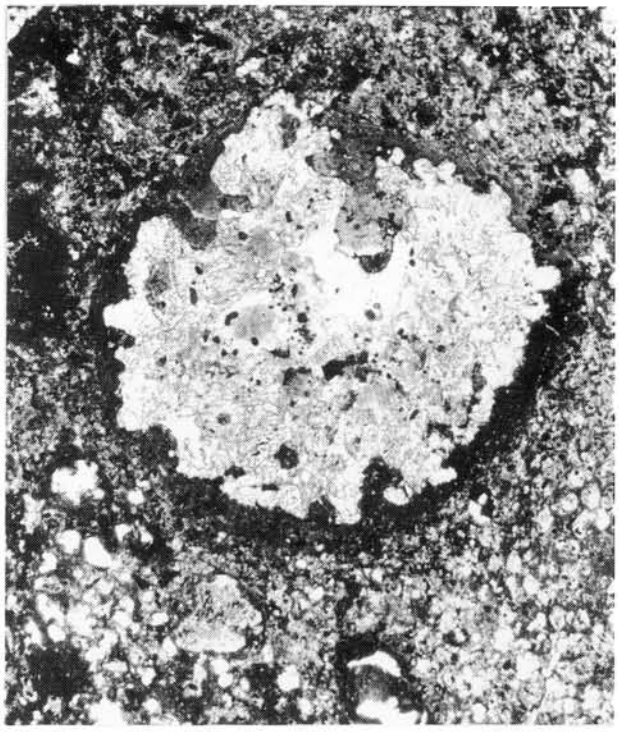

Fig.3: Rounded to irregularly-shaped, phyllosilicate-rich object (~1mm in size) within Y-86720; note the well-preserved, dark accretionary rim (transmitted light)

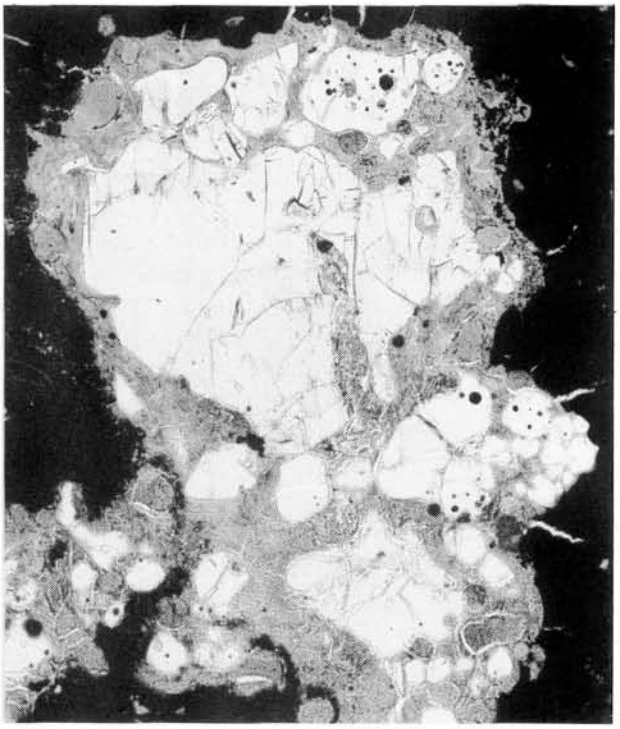

Fig.4: Unusual fragment-like object in B-7904 that consists of olivines (white) embedded in a brownish-grey, fine-grained matrix (transmitted light)

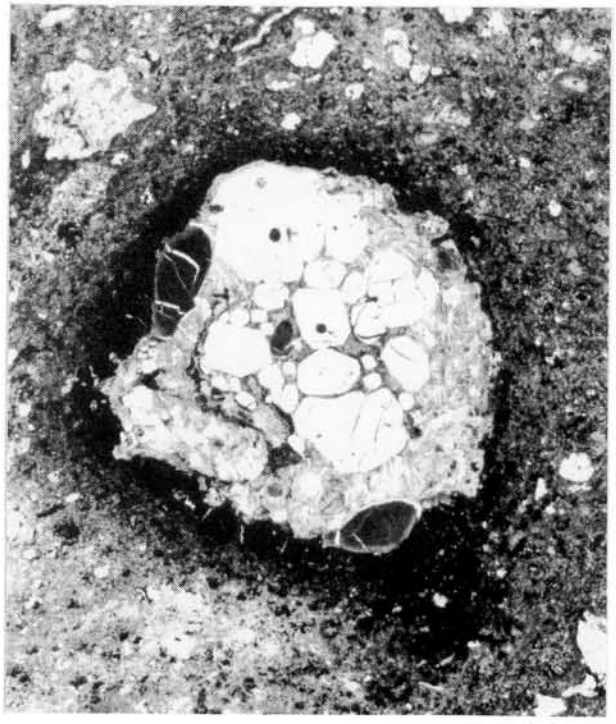

Fig.5: Chondrule-like object, rimmed by fine-grained accretionary dust, that contains abundant olivine (white) and some round or egg-shaped, Cr-rich inclusions (compare Fig.6; transmitted light)

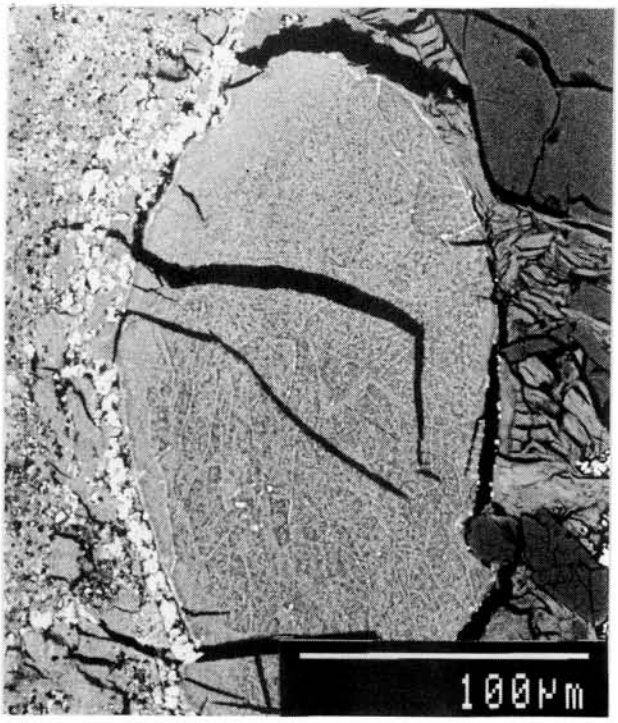

Fig.6: Typical texture of the fine-grained, Cr-rich inclusions (compare Fig.5; BSE-image)

LUNAR METEORITE YAMATO-793274: COSMIC-RAY PRODUCED AND SOLAR WIND NOBLE GASES. RELATION WITH ALLAN HILLS A81005?

Eugster, O.
Physikalisches Institut, University of Bern, Sidlerstrasse 5, 3012 Bern, Switzerland

In this paper I report the first results obtained for lunar meteorite Y-793274. Sample split Y-793274,66 (48 mg) was obtained for noble gas isotopic investigations. Two samples weighing 1.09 mg and 3.29 mg, resp., were chipped off with a stainless steel chisel and analysed applying our standard procedure using system B [1]. Results are given in Table 1.

Table 1 Results for samples from lunar meteorite Y-793274,66

	^{4}He	^{20}Ne	^{36}Ar	^{4}He	^{20}Ne	^{22}Ne	^{36}Ar	^{40}Ar
	10^{-8} cm^3 STP/g			^{3}He	^{22}Ne	^{21}Ne	^{38}Ar	^{36}Ar
1.09 mg	96370 ± 5000	28860 ± 1700	13560 ± 700	1929 ± 30	12.32 ± 0.20	21.18 ± 0.30	5.25 ±0.03	2.37 ±0.03
3.29 mg	97690 ± 5000	27430 ± 1400	11050 ± 600	1806 ± 20	12.40 ± 0.20	20.63 ± 0.30	5.20 ±0.03	2.54 ±0.03

Cosmic-ray exposure age

Table 2 gives the cosmogenic and trapped solar wind components. Because three He components are present (solar wind, radiogenic and cosmogenic) they could not be separated. The high concentration of trapped noble gases indicates that Y-793274 is a mature regolith breccia. For the calculation of the total duration of exposure to cosmic rays the same production rates as for ALHA81005 were adopted (10^{-8} cm^3 STP/g Ma): P_{21} = 0.12 and P_{38} = 0.13 [2]. An average cosmic-ray exposure duration of 340 Ma is obtained for Y-793274. The uncertainty is estimated to be about 30% due to the unknown chemical composition of Y-793274.

Table 2 Trapped (tr), cosmogenic (c) noble gases and cosmic-ray exposure ages of samples from Y-793274,66

	$^{20}Ne_{tr}$	$^{36}Ar_{tr}$	$^{21}Ne_{c}$	$^{38}Ar_{c}$	T_{21}	T_{38}	T_{av}
	10^{-8} cm^3 STP/g				Ma		
1.09 mg	28830 ± 1700	13530 ± 700	37.8 ± 4.0	39 ±20	320	300	340 ±100
3.29 mg	27400 ± 1400	11010 ± 600	38.0 ± 4.0	54.6 ±14.0	320	420	

Correlation of solar wind and cosmic-ray exposure

Figure 1 shows that the concentrations of cosmogenic and solar wind trapped noble gases in lunar meteorites are roughly correlated. The error bars shown for the $^{36}Ar_{tr}$ amounts take into account the inhomogeneity of the trapped gas concentrations observed for the different splits of a particular meteorite [1-9]. The linear display (Fig. 2) of $^{21}Ne_c$ vs. $^{36}Ar_{tr}$ shows that the ratio of cosmogenic to solar wind noble gases is strongly enhanced in the MAC88104/5, Y-82192/3, and Y-86032 meteorites compared to that in Y-793274, Y-791197, and ALHA81005. This indicates that for most of the exposure to cosmic rays the material of the former meteorites was shielded from solar wind irradiation either at depth within the lunar regolith or after breccia formation. On the other hand, the material of Y-793274, Y-791197, and ALHA81005 was exposed to cosmic rays and solar wind particles before breccia formation.

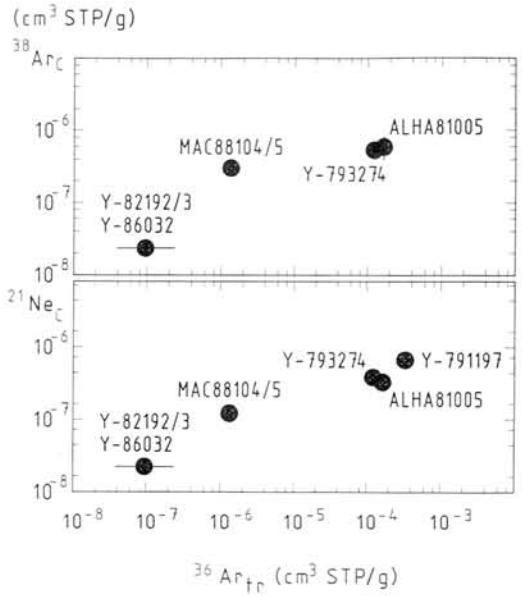

Fig. 1 Concentrations of cosmic-ray produced ^{38}Ar and ^{21}Ne, resp., versus solar wind trapped ^{36}Ar in lunar meteorites.

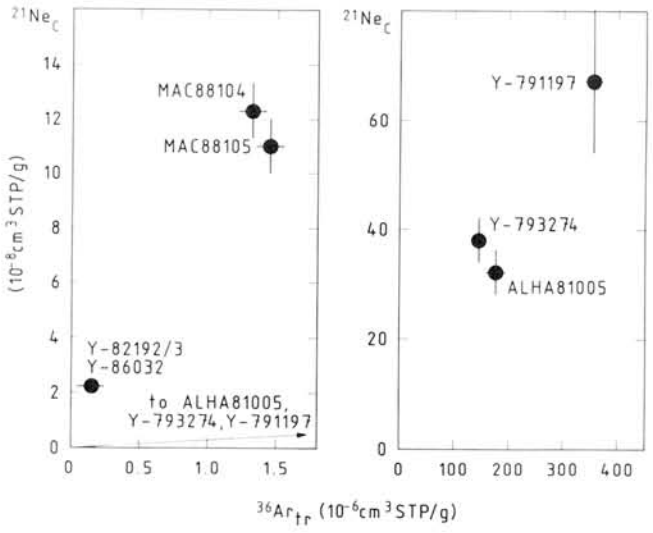

Fig. 2 Cosmic-ray produced ^{21}Ne versus solar wind trapped ^{36}Ar. Y-82192/3, Y-86032, and MAC88104/5 are enriched in cosmic-ray produced ^{21}Ne relative to the other lunar meteorites.

Relation of Y-793274 with ALHA81005?

As demonstrated in Figs. 1 and 2 the $^{21}Ne_c$, $^{38}Ar_c$, and $^{36}Ar_{tr}$ concentrations in Y-793274 and ALHA81005 are very similar. On the basis of these nuclides a relation between these two meteorites is possible. However, information on petrology, chemistry, and radionuclide activity is necessary to confirm or disprove such a relation. Considering the distance of about 3000 km between the collection sites of the Yamato and Allan Hills meteorites, pairing is very improbable, but the two meteorites might originate from the same ejection event on the moon, if they are really related.

Acknowledgements

I thank the National Institute of Polar Research for the valuable sample of Y-793274, H. Kojima and K. Yanai for sample preparation, and the members of the consortium group for their cooperation. The support by the Swiss National Science Foundation is acknowledged.

References

[1] Eugster O., Niedermann S., Burger M., Krähenbühl U., Weber H., Clayton R.N., and Mayeda K., Proc. NIPR Symposium on Antarctic Meteorites, No. 2, 25-35 (1989). [2] Eugster O., Geiss J., Krähenbühl U., and Niedermann S., Earth Planet. Sci. Lett. 78, 139-147 (1986). [3] Bogard D.D. and Johnson P., Geophys. Res. Lett. 10, 801-803 (1983). [4] Ostertag R., Stöffler D., Bischoff A., Palme H., Schultz L., Spettel B., Weber H., Weckwerth G., and Wänke H., Mem. Natl. Inst. Polar Res., Spec. Issue 41, 17-44 (1986). [5] Bischoff A., Palme H., Spettel B., Stöffler D., Wänke H., and Ostertag R., Abstract 11th Symp. Antarctic Meteorites, Tokyo, 13-1 (1986). [6] Takaoka N., Mem. Natl. Inst. Polar Res., Spec. Issue 41, 124-132 (1986). [7] Takaoka N., Mem. Natl. Inst. Polar Res., Spec. Issue 46, 96-104 (1987). [8] Eugster O. and Niedermann S., Earth Planet. Sci. Lett. 89, 15-27 (1988). [9] Eugster O., Lunar Planet. Sci. XXI, Lunar Planet. Inst., Houston, 337-338 (1990).

Antarctic two new winonaites, Y-74025 and Y-75305: Mineralogy and classification

Kimura M., Ibaraki University, Mito 310

Two new winonaites, Y-74025 and Y-75305, include various minor minerals such as K-rich feldspar, Nb-bearing rutile, magnesiochromite and others. Here, their mineralogy are briefly reported.

They consist mainly of minerals typical of O-chondrites, although they show allotriomorphic-granular texture. High amount of Fe-Ni metal (27.0 vol.%) characterizes Y-75305, whereas troilite (13.5%) is much more abundant than Fe-Ni metal (3.9) in Y-74025.

Kamacites contain 5.9-7.0% Ni and <0.05% Si, P and Cr. Taenites show wide compositional variation of Ni (19.6-42.9%). Schreibersites (Ni 48.3-53.8%) usually occur in Fe-Ni metals, and rarely with troilite. Troilites contain 0.2-0.6% Cr, and <0.05% Ni, Mn and Ti. Troilites often include daubreelites as lamellae. Daubreelites in Y-75305 are more depleted in Mn (0.15-0.21%) than those in Y-74025 (1.2-1.6%). One pyrrhotite grain occurs in Y-75305 which contains 1.1-1.9 Cr, 1.9-2.7 Ni. It contains tiny blebs of pentlandite, up to 2 microns. One rutile grain in Y-75305 occurs with troilite. This is the first discovery from winonaites. It contains 1.4% Cr_2O_3, 0.9 FeO, 0.09 ZrO_2, 3.8 NbO_2 and 0.2 TaO_2. Spinels occur abundantly in Fe-Ni metal, and rarely among silicates. They are not homogeneous, i.e., V_2O_3 0.14-0.55%, Cr_2O_3 56.0-74.1, MnO 0.6-3.1, TiO_2 0.1-2.2, ZnO 0.8-1.7, FeO 2.9-13.6, Al_2O_3 0.2-17.6, and MgO 11.2-20.5. They are magnesiochromites. The compositional zoning of spinel is very distinct with sharp boundary. In the peripheral parts, Fe, Cr, Mn, Zn and V are enriched. The composition of one spinel grain in Y-74025 is similar to those in Y-75305, although MnO (0.9%) is depleted in Y-74025 spinel. At any rate, the compositions of spinels in both meteorites resemble those in IAB iron meteorites and winonaite. One Fe-Ti phase (probalby ulvospinel) occurs in magnesiochromite as tiny bleb, 2 microns in size, in Y-75305. Apatites are always included in or attached to diopside, in both meteorites. Two zircon grains, up to 2 microns, occur in diopside and the boundary between magnesiochromite and plagioclase in Y-75305.

Olivines are very homogeneous. The average Fo contents are 98.2 in Y-75305 and 98.1 in Y-74025. Orthopyroxene is the most common silicate in these meteorites. Both Ca-poor and -rich pyroxenes are homogeneous, respectively. Their average compositions are $En_{96.9}Wo_{1.4}$ and $En_{50.6}Wo_{48.3}$ in Y-75305, and $En_{96.1}Wo_{1.6}$ and $En_{53.2}Wo_{45.9}$ in Y-74025. The average compositions of plagioclases are $Ab_{75.8}Or_{1.6}$ in Y-75305, and $Ab_{77.1}Or_{2.1}$ in Y-74025. Y-75305 contains one K-rich feldspar of $Ab_{79.0}Or_{18.8}$. It occurs in diopside as tiny spherules. K-rich feldspar ($Ab_{6.4}Or_{92.2}$) in Y-74025 is completely included in troilite.

Spinels are enriched in MnO in Y-75305, whereas Mn prefers daubreelite to spinel in Y-74025. Thus, these two meteorites are not paired, which is consistent with the differences of metal and troilite abundances between them. However, the mineral assemblage, texture and chemistry of olivine, pyroxene and spinel suggest that they surely belong to winonaite.

A POSSIBLE EFFECT OF ^{26}Al HEATING TO THE FORMATION OF CAI's

Masao KITAMURA
Department of Geology and Mineralogy, Faculty of Science, Kyoto University, Sakyo, Kyoto 606, Japan
and Masamichi MIYAMOTO
College of Arts and Sciences, University of Tokyo, Komaba 3-chome, Meguro, Tokyo 153, Japan

It has been discussed whether a Ca-Al-rich inclusion in chondrites is a residue of evaporation by reheating of a chondritic material or a cluster of condensates at high temperature. In both models, it has not been fully explained why CAI's are clusters separated from ferromagnesian silicates.

Minerals in CAI's have larger amount of Al than ferromagnesian minerals. If ^{26}Al exists, CAI's can be heated more than clusters of ferromagnesian silicates. From this point of view, a possible effect of ^{26}Al heating to the formation of CAI's during the condensation was proposed in the present study.

A present scenario on the formation process of CAI's with ^{26}Al is as follows. According to the condensation theory, minerals in CAI's precipitate at high temperature, followed by successive condensation of ferromagnesian minerals. When Al-rich minerals with ^{26}Al condense and form a cluster, the cluster must be heated by decay of ^{26}Al. Then, some parts of the heated cluster should evaporate again or melt. As temperature of the nebula surrounding the clusters decreases, ferromagnesian silicates can condense, but cannot accrete onto the cluster of CAI's, because ferromagnesian silicates should evaporate near the cluster. Then, the ferromagnesian silicates must be separated from the CAI's clusters.

Heating process of a CAI cluster by ^{26}Al was calculated to obtain a relation among maximum attainable temperature, radius and time, using a method by Miyamoto et al. (1981). An initial value of $^{26}Al/^{27}Al$ was taken as 5×10^{-5} (Lee et al., 1976). The calculation shows that the maximum attainable temperature increases rapidly as the radius increases. For an example, the clusters 30 and 60 m in radii have the maximum attainable temperature about $100^{o}C$ and $500^{o}C$ higher than temperatures of the surrounding nebula for about 5×10^{3} and 8×10^{3} years. respectively. This indicates that if the nebula is slowly cooled, the cluster should be small (less than 10^{2} m in radius). In a case of rapid cooling of the nebula with a cooling time scale of 10^{8} sec (Yamamoto and Hasegawa, 1977), the present simple calculation can not be applied directly. However, the heating of the ^{26}Al is considered to have the effect to the formation of CAI's.

Lee,T., Papanastassiou,D.A. and Wasserburg,G.J. (1976) Geophys. Res. Lett., 3, 41-44.
Miyamoto,M., Fujii,N. and Takeda,H. (1981) Proc. Lunar Planet. Sci. Conf., 12B, 1145-1152.
Yamamoto,T and Hasagawa,H. (1977) Prog. Theor. Phys. 58, 816-828

LUNAR METEORITE YAMATO-793274: A LUNAR HIGHLAND SAMPLE POSSIBLY RICH IN MARE MINERALS.

Gero Kurat[1], Franz Brandstätter[1], and Christian Koeberl[2]

[1]*Naturhistorisches Museum, P.O. Box 417, A-1014 Vienna, Austria*
[2]*Institute of Geochemistry, University of Vienna, Dr.-Karl-Lueger-Ring 1, A-1010 Vienna, Austria*

Yamato-793274 has been discovered by a Japanese Antarctic Research Expedition on January 3, 1980, in the Yamato Mountains in Antarctica and was first reported to be of lunar origin by Yanai and Kojima (1987). The sample is a single rock of 8.66 g and has a size of 2.6x1.8x1.2 cm with minor brownish to colorless vesicular fusion crust. Numerous relatively large mineral fragments and clasts are visible and are set in a dark matrix. Some analytical data were given by Yanai and Kojima (1987) and Yanai et al. (1987) and show a wide variation in plagioclase (An88.3-97.4), pyroxene (En4.2-67.5; Fs16.4-64.3), and olivine (Fa17.8-97.3) compositions. In view of the continuing interest in and importance of lunar meteorites, following the discovery of new large rocks at the Yamato Mountains and MacAlpine Hills, some samples of Y-793274 have recently been made available for a consortium study; despite the small size of the rock.

We have received sample Y-793274 in two fragments (,93: 31 mg, and ,94: 51 mg). Part of the larger fragment was used for a polished thin section, on which the following preliminary petrological and mineralogical results are based. The sample chips show a coarse grained texture, with some minor light brownish fusion crust on one side. The thin section shows a dense breccia consisting of relatively large and abundant mineral fragments (clinopyroxene, plagioclase, olivine, ilmenite), rare granulitic (poikilitic) breccias (very fine grained), and some devitrified glass, which is mostly brown to dark brown. The matrix is fairly dense, very abundant, consists of mineral fragments and interstitial partly recrystallized glass.

One large brownish, fine grained, recrystallized melt breccia was found. It contains pyroxene and plagioclase relics and is of anorthositic-noritic-troctolitic (ANT) composition (see analysis #1 in Table 1). Similar breccias of smaller size are present, but have not yet been analyzed (Fig. 1). Among large devitrified glass fragments, one dark brown glass was analyzed (#2 in Table 1). Its normative composition is highly mafic with 23 mol% olivine, 44 mol% pyroxene, and 32 mol% plagioclase of An95. This composition is unusual for lunar highland rocks and shows some similarity to Apollo 15 green glass.

Typical matrix glass compositions are given in #3 and 4 in Table 1. Analysis #3 is representative of anorthositic highland breccias, while #4 is considerably more mafic and indicates mixture with a low mg-component.

Throughout the thin section, pyroxenes are unusually abundant when compared to other lunar meteorites (e.g., Y-791197, Y-82192/3, Y-86032), and many are of pinkish color. They commonly show exsolution lamellae, and all phases are heavily shocked. The pyroxene compositions (Fig. 2) are highly variable and show a bimodal distribution. The higher mg- pyroxenes (analysis #5) are compatible with an origin from the lunar highlands, while the low-mg pyroxenes (#6,7) could be of mare origin (see also Fig. 3).

Their composition is similar to pyroxenes described from the mare meteorite EETA87521 (Warren and Kallemeyn, 1989) and Lunar 24 ferroan VLT basalts (Kurat and Kracher, 1981).

All plagioclase fragments encountered are highly anorthitic (An95-99). Olivine compositions analyzed range from Fo46-72 (Fig. 2), and the Fe-poor and Fe-rich endmembers are given in Tab. 1 (#8 and 9).

In conclusion, the lunar meteorite Y-793274 is a shock lithified fragmental highland breccia containing only a minor regolith component but an unusually high proportion of mafic mineral fragments, mostly ferroan pyroxenes. This meteorite is distinctly different from previously described lunar highland meteorites (e.g., the mineral and modal composition is quite different from Y-86032; Koeberl et al., 1990), because in addition to a typical highland component (without igneous rock clasts in our sample) it apparently also contains a mare component of possible VLT heritage. Major and trace element analyses are currently in progress. The data available so far indicate, however, that Y-793274 is not paired with any of the other known lunar meteorites.

References:

Koeberl, C., Kurat, G., and Brandstätter, F. (1990) Proc. NIPR Symp. Antarct. Meteorites 3, in press.

Kurat, G., and Kracher, A. (1981) Proc. Lunar Planet. Sci. Conf. 12B, 1-19.

Warren, P.H., and Kallemeyn, G.W. (1989) Geochim. Cosmochim. Acta 53, 3323-3300.

Yanai K., and Kojima, H. (1987) Papers presented to the 12th Symp. Antarct. Meteorites, NIPR, Tokyo, 17-18.

Yanai, K., Kojima, H., Koeberl, C., Graham, A.L., and Prinz, M. (1987) Photographic Catalog of the Antarctic Meteorites, NIPR, Tokyo, 298 pp.

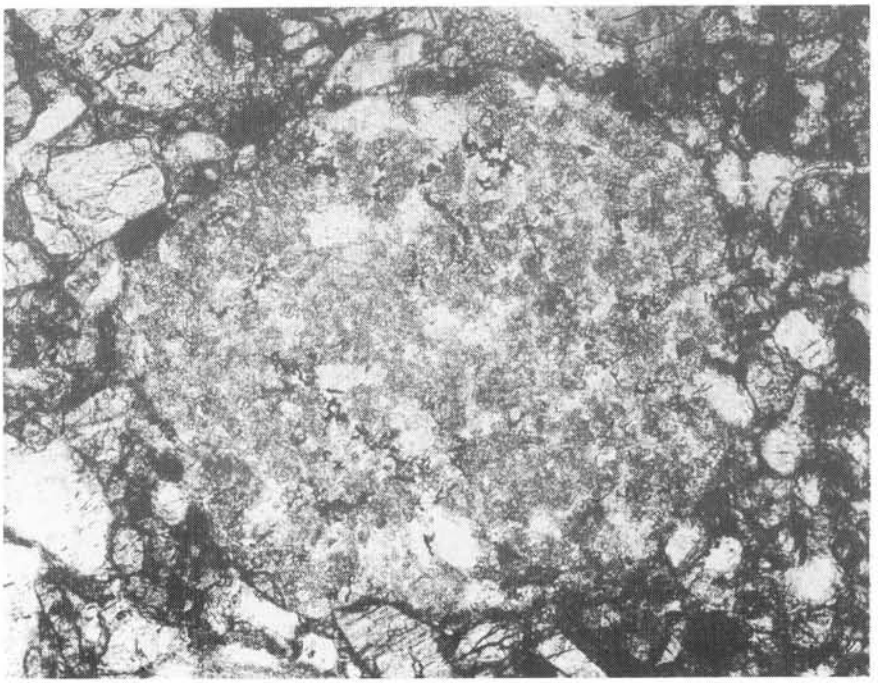

Fig. 1: Hornfelsic metabreccia of ANT composition, PPL, 8x

Table 1: Bulk and mineral compositions of Y-793274, obtained by EPMA

	(1)	(2)	(3)	(4)	(5)	(6)	(7)	(8)	(9)
SiO_2	44.7	46.2	42.4	47.1	51.4	48.2	48.0	35.5	33.9
TiO_2	0.29	0.38	0.30	0.57	0.28	0.88	1.02	0.11	0.05
Al_2O_3	29.4	11.4	28.0	18.1	2.69	0.85	1.22	0.12	-
Cr_2O_3	0.11	0.51	0.17	0.36	1.1	0.33	0.34	0.14	-
FeO	4.3	17.1	5.4	12.3	12.8	33.1	25.3	25.3	44.8
MnO	0.03	0.25	0.20	0.22	0.37	0.49	0.29	0.40	0.63
MgO	5.0	14.8	8.4	6.0	18.8	7.9	9.2	36.6	21.8
CaO	15.2	10.2	13.4	12.7	12.2	8.6	13.8	0.14	0.38
Na_2O	0.71	0.19	-	0.48	-	-	-	-	-
K_2O	0.03	-	-	-	-	-	-	-	-
Total	99.78	101.03	98.27	97.90	99.64	100.35	99.17	98.31	101.56

Identification of analyses: (1) ANT-breccia (2) dark brown glass, similarity to green glass (3) gabbroic anorthosite glass (4) matrix glass with mafic admixture (5) pyroxene, highland composition (6), (7) pyroxene, mare composition (8), (9) Fe-poor and Fe-rich olivines

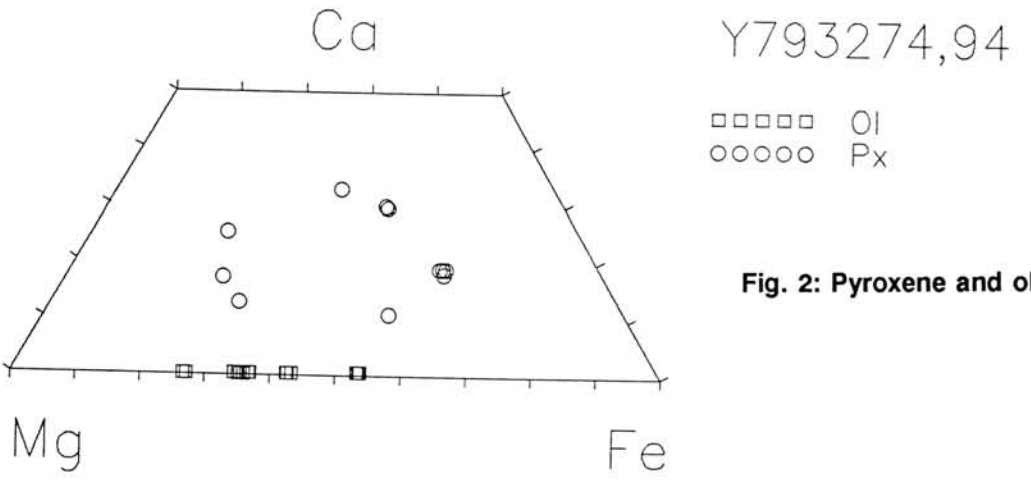

Fig. 2: Pyroxene and olivine compositions

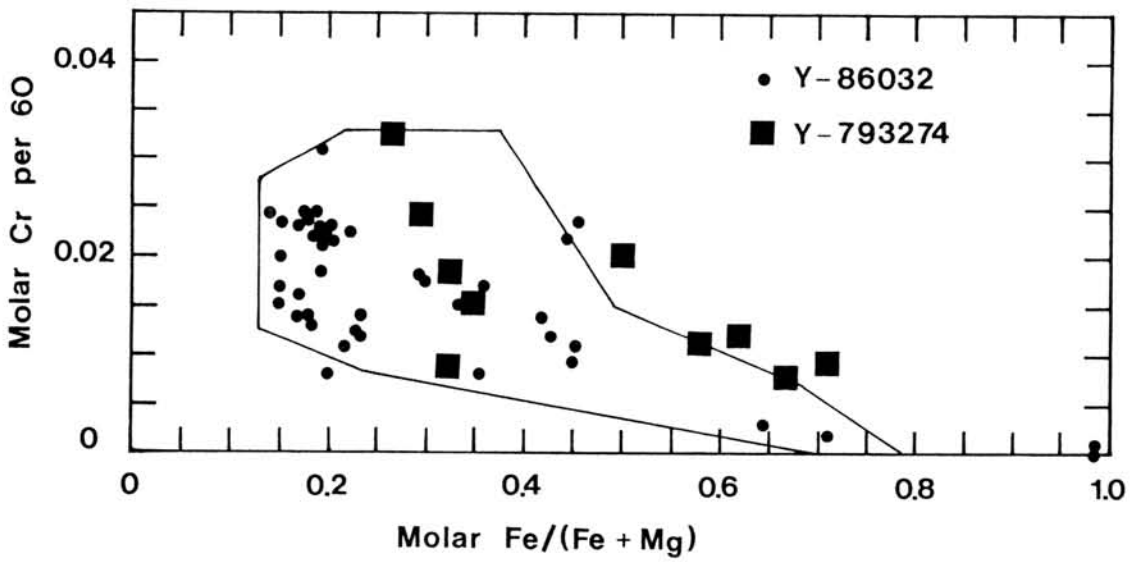

Fig. 3: Molar Cr in Y-793274 pyroxenes vs. molar Fe/(Fe+Mg) ratio, compared to Y-86032. The Fe-rich pyroxenes tend to plot outside the field defined by highland pyroxene compositions (see, e.g., Koeberl et al., 1990), indicating a possible mare component.

OXYGEN ISOTOPIC COMPOSITIONS OF B-7904, Y-82162, AND Y-86720

Toshiko K. Mayeda and Robert N. Clayton

Enrico Fermi Institute, University of Chicago, Chicago, IL 60637, USA

The oxygen isotopic compositions of whole-rock carbonaceous chondrites have recently been discussed by Clayton and Mayeda (1989). Five isotopic clusters are recognized as shown in Fig. 1: CI, CM, CR, CV, and CO. The metamorphosed C4 to C6 chondrites fall in the CO group. In the non-Antarctic samples the labels C1 and CI are synonymous, as are C2 and CM. However, in the more extensive collection of Antarctic meteorites, ambiguities arise in classifications based on different criteria: major element chemical composition, volatile element abundance, mineralogy, and oxygen isotopic composition. The oxygen isotope ratios of B-7904, Y-82162, and Y-86720 are clearly associated with the C1 or CI group, as is seen in Table 1 and Fig. 1. No analyses have been made of any separated mineral constituents.

Table 1

Oxygen Isotopic Compositions of Antarctic Carbonaceous Chondrites

Sample No.	$\delta^{18}O$ (‰)	$\delta^{17}O$ (‰)
B-7904	+21.28	+11.01
Y-82162	+21.56	+11.59
Y-86720	+22.29	+11.58

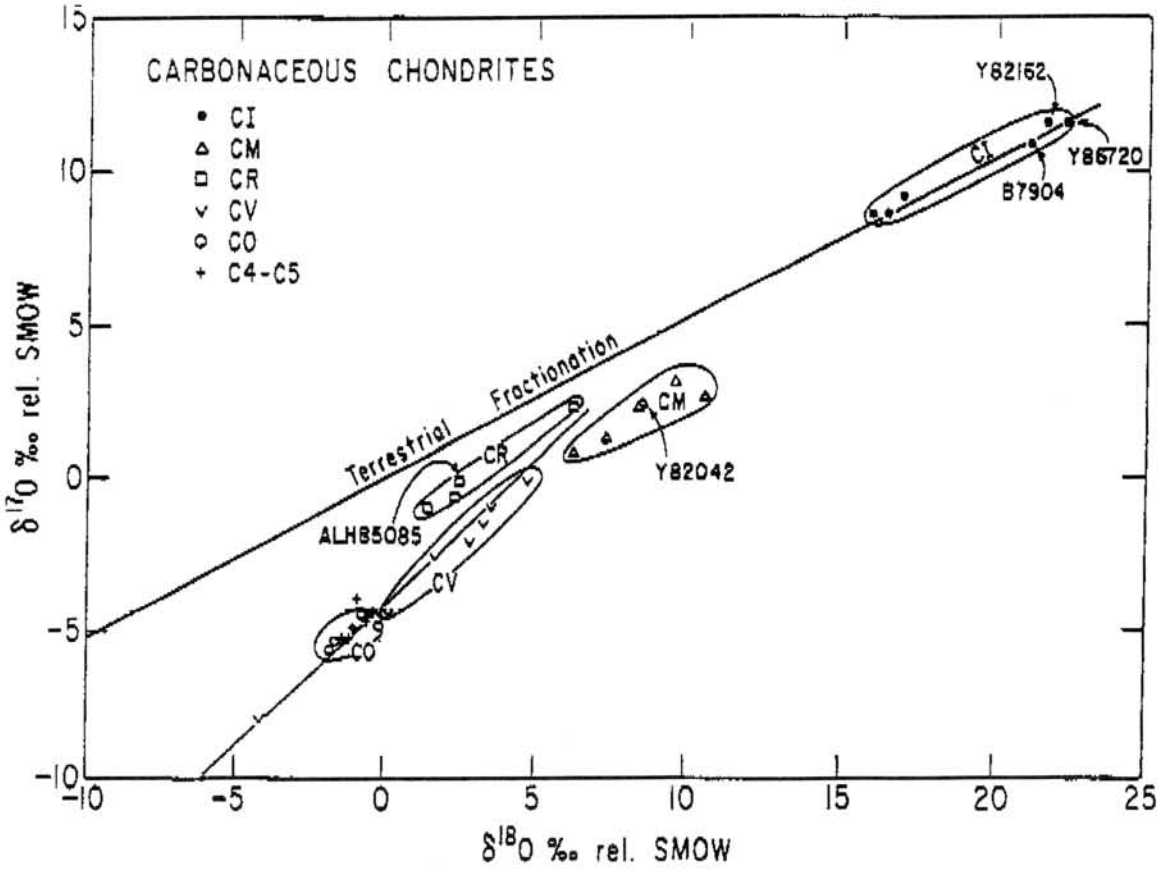

Fig. 1

The values of $\delta^{18}O$ and $\delta^{17}O$ in CI chondrites are much higher than those of all other meteorites, a fact which has been attributed to extensive aqueous alteration on the parent body at temperatures near 100°C (Clayton and Mayeda, 1984). It is likely that the three meteorites discussed here have also undergone such parent-body processes. Any subsequent heating and mineral reactions as discussed by Tomeoka et al. (1989a, b) apparently had only minor effects on the bulk oxygen isotopic abundances. Isotopic analyses of individual mineral phases should reveal more details of the thermal history.

References

Clayton R.N. and Mayeda T.K. (1984) Earth Planet. Sci. Lett. **67**, 151–161.

Clayton R.N. and Mayeda T.K. (1989) Lunar Planet. Sci. **XX**, 169–170.

Tomeoka K. et al. (1989a) Proc. N.I.P.R. Symp. Antarct. Meteorites **2**, 36–54.

Tomeoka K. et al. (1989b) Proc. N.I.P.R. Symp. Antarct. Meteorites **2**, 55–74.

PETROGRAPHY AND CHEMISTRY OF ACCRETIONARY DUST MANTLES IN THE CM-CHONDRITES Y-791198, Y-793321, Y-74662 and ALHA83100 - INDICATIONS FOR NEBULA PROCESSES

K. Metzler and A. Bischoff,
Institut für Planetologie, Wilhelm-Klemm-Str. 10, 4400 Münster, Germany

Carbonaceous chondrites are the most important source of information about processes in the early solar system. Many carbonaceous chondrites are, however, not regarded as pristine rocks unaffected by secondary alteration processes. The consensus of most petrographic studies is that the formation of phyllosilicates in CM-chondrites, for example, is basically the result of aqueous processes within meteorite parent bodies (i.e. after accretion). Based on a study of Y-791198, Y-793321, Y-74662, ALHA83100 and other non-antarctic CM-chondrites we believe that most phyllosilicates and calcites were already present in the solar nebula prior to parent body accretion.

Mineralogy of accretionary dust mantles.

Neglecting the influence of secondary impact processes at this point of the presentation the fundamental statement is that all coarse-grained components within Y-791198, Y-793321, Y-74662 and ALHA83100 are rimmed by fine-grained accretionary dust layers. One example is shown in Fig.1. Chondrules, chondrule fragments, CAIs, mineral fragments and PCP-rich components are separated from each other by accretionary dust mantles. We believe that these textures can only have been formed by a primary accretionary process in the solar nebula (compare Metzler and Bischoff, 1989a,b; Metzler et al., 1988). The entire thin section of Y-791198 shows such a texture. Within Y-793321, Y-74662 and ALHA83100 mm-sized lithic fragments with pristine accretionary fabrics (pristine fragments) exist embedded in a clastic matrix. The fine-grained clastic matrix, which is basically the result of repeated impact fragmentation on the meteorite parent body, has to be clearly distinguished from the fine-grained materials within the accretionary dust mantles mentioned before. Due to different degrees of brecciation the abundances of pristine rock fragments vary among the CM-chondrites (Y-791198: 100 vol%; Y-74662: 95 ± 3 vol%; Y-793321: 41 ± 7 vol%; ALHA83100: 29 ± 6 vol%).

As stated above, within such pristine rock fragments all coarse-grained components are surrounded by fine-grained accretionary dust mantles. In the following we will describe some typical examples. Fig.2 shows an irregulary-shaped, spinel-rich Ca,Al-rich inclusion from Y-791198 that is perfectly enclosed by the dust mantle. Similarly, a zoned olivine fragment in Y-74662 is embedded in fine-grained accretionary dust (Fig.3). Based on the appearence of zonation, it is obvious that the zonation certainly preceeded fragmentation of olivine and accretion of the dust mantle. In the same way PCP-rich components (Fig.4) and calcites are rimmed by accretionary dust mantles (compare Fig.1). Mineralogically and chemically the dust mantles from compositionally different enclosed components are similar; however, the maximum size of dust mantles surrounding the PCP-rich objects is less than that of those enclosing chondrules and CAIs (see Metzler and Bischoff, 1989b). Basically, the major minerals within the dust mantles are the same as those found within the PCP-rich objects; however, in general, Fe-rich phases are more abundant within the latter: serpentines like antigorite and cronstedtite and the S-bearing phase tochilinite are by far the most abundant minerals. These minerals, usually below 1μm in size, form a kind of groundmass embedding a great number of inclusions (mainly mineral fragments) with a size of up to 50μm. These components include PCP-rich objects, large serpentines, olivine fragments, enstatite, pentlandite, troilite, magnetite, Fe,Ni-metal and calcite. A typical example from Y-791198 is shown in Fig.5. The existence of fresh (unaltered) Fe,Ni-metals and olivines in the accretionary dust mantles embedded within H_2O-bearing phyllosilicates bears important information concerning the evolutionary history of the dust mantles and the CM-chondrites. We suggest that Fe,Ni-metals and olivines should have been affected by aqueous processes in the parent body.

Chemistry of accretionary dust mantles.

We have analysed 43 accretionary dust mantles from the four antarctic CM-chondrites by electron microprobe. The results are listed in Table 1. For comparison the bulk chemical analyses of Y-74662 and Y-791198 are given. In general, the accretionary dust mantles contain lower Mg/Fe- and Ca/Na-ratios compared to the bulk composition; the FeO-contents of the dust mantles are variable among the four chondrites. The very strong discrepancy in the Ca/Na-ratios between the composition of the dust mantles and the bulk composition is very surprising. The low Ca-concentration within the accretionary dust mantles can be explained by the lack of calcites and phases that usually occur within Ca,Al-rich inclusions.

Conclusions.

Based on a textural and chemical investigation of Y-791198, Y-793321, Y-74662, ALHA83100 and other non-antarctic CM-chondrites we suggest, that distinct features within these chondrites cannot be explained by parent body processes. It appears that the formation of fine-grained ("dusty") mantles surrounding various components within these chondrites can only be explained by accretionary processes in the solar nebula. Since fine-grained mantles also surround PCP-rich objects and calcites, we suggest that PCP-rich objects and calcites had to be present in the nebula prior to the aggregation of dusty materials and prior to the parent body formation. We also conclude that the undisturbed "pristine" fragments represent the freshly accreted parent body. The presence of unaltered Fe,Ni-metals and olivine within the accretionary dust mantles indicates that aqueous alteration on the parent body was only a minor process.

References:

Haramura et al. (1983), Proc. Symp. Antarctic Met. 8th., 109. Metzler and Bischoff (1989a), Meteoritics 24, 303. Metzler and Bischoff (1989b), Lunar Planet. Sci. XX, 689. Metzler et al. (1988), Lunar Planet. Sci. XIX, 772. Yanai and Haramura (1977), Proc. Symp. Antarctic Met. 2nd, 264.

Table 1: Chemical composition of accretionary dust mantles; the bulk compositions of Y-74662 and Y-791198 are taken from Yanai and Haramura (1977) and Haramura et al. (1983); a) composition of accretionary dust mantles; b) bulk composition of the CM-chondrite

No. of analyses	Y-74662 10 (a)	Y-74662 (b)	Y-791198 14 (a)	Y-791198 (b)	Y-793321 11 (a)	ALHA83100 8 (a)
SiO_2	27.3	29.18	28.3	28.41	26.2	27.4
TiO_2	0.09	0.22	0.06	0.12	0.09	0.09
Al_2O_3	2.41	2.38	2.05	2.62	2.46	2.09
Cr_2O_3	0.56	0.52	0.50	0.42	0.42	0.52
FeO	33.0	28.56	26.1	27.20	30.1	23.1
MnO	0.25	0.22	0.27	0.27	0.26	0.18
MgO	15.3	19.29	16.5	19.52	13.3	16.7
CaO	0.60	1.70	0.49	1.65	0.90	0.68
Na_2O	0.27	0.28	0.20	0.15	0.74	0.19
K_2O	0.04	0.04	0.08	0.03	0.06	0.03
P_2O_5	0.40	0.23	0.21	0.26	0.32	0.31
Ni	1.63	0.67	1.81	0.72	1.69	2.15
S	2.57	2.69	3.60	2.93	2.88	2.24
H_2O^+		13.26		12.81		
H_2O^-		1.56		2.85		
Total	84.42	100.80	80.17	99.96	79.42	75.68
Mg/Fe	0.36	0.52	0.49	0.56	0.34	0.56
Ca/Na	2.15	5.81	2.33	10.73	1.16	3.50

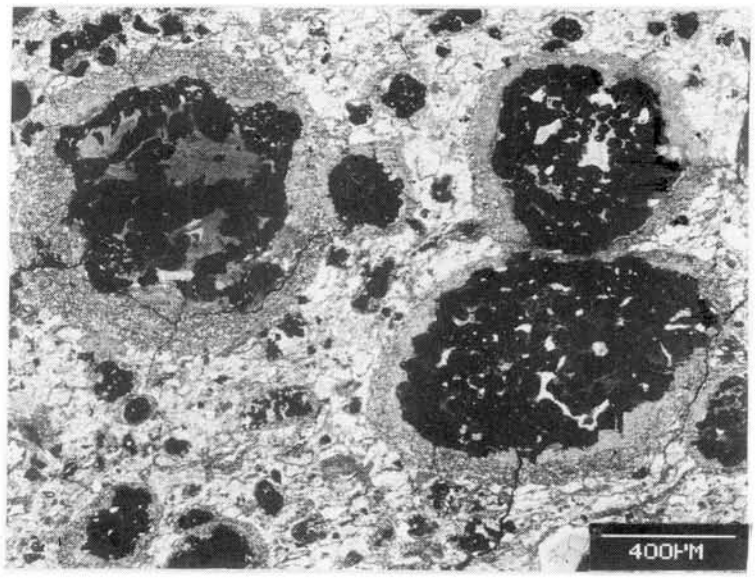

Fig. 1: Y-791198; chondrules, fragments and other components are surrounded by accretionary dust mantles; note that the light PCP-rich objects are also rimmed by a thin accretionary dust mantle.

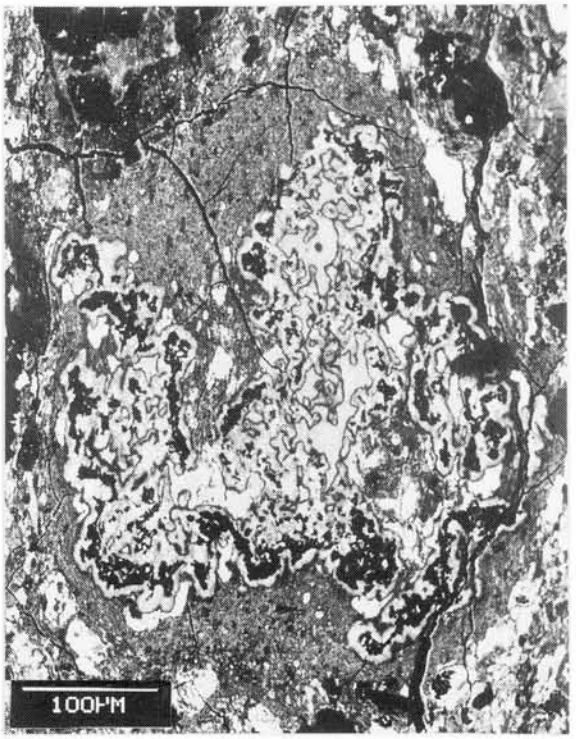

Fig. 2: Irregularly-shaped, spinel-rich Ca,Al-rich inclusion within Y-74662 rimmed by fine-grained accretionary dust.

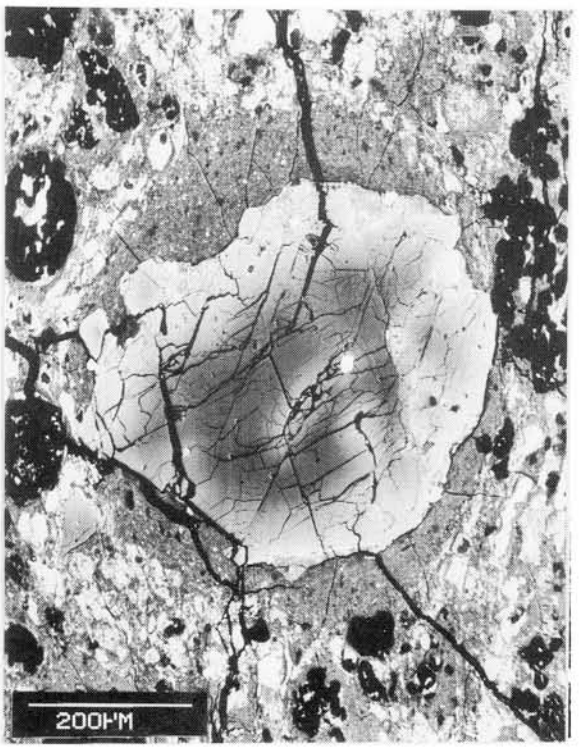

Fig. 3: Zoned olivine-fragment from Y-74662 enclosed by an accretionary dust mantle. The zoning process must have preceeded fragmentation and accretion of the dust mantle.

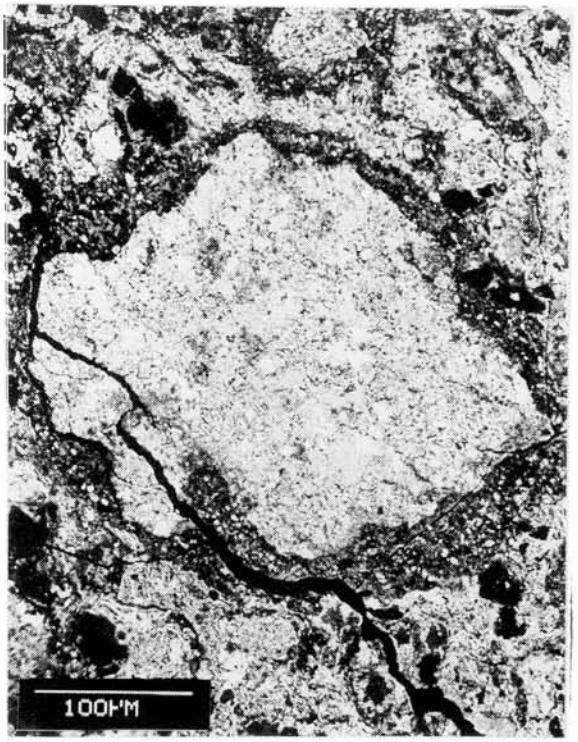

Fig. 4: PCP-rich object from Y-791198 rimmed by an accretionary dust mantle.

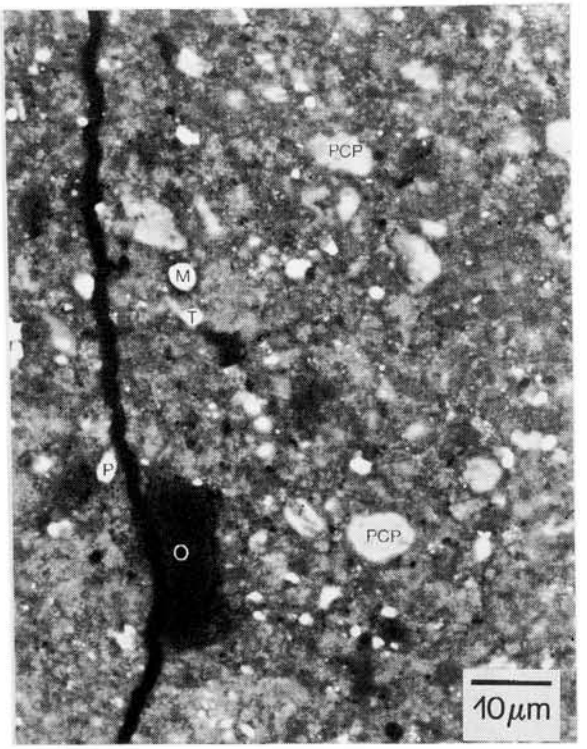

Fig. 5: Typical example of an accretionary dust mantle (Y-791198). The dust mantle contains small PCP-rich objects, troilites (T), pentlandites (P), Fe,Ni-metals (M) and olivines (O) with variable Fe-contents.

MAFIC CONTENTS AND DENSITIES OF METEORITIC PLAGIOCLASE - ESTIMATION OF IMPACT SITES

Yasunori Miúra
Dept. Min. Sci. & Geol., Fac. of Sci., Yamaguchi University,
Yamaguchi, 753, Japan.

Chemical composition (esp. mafic contents of FeO+MgO) and physical properties (esp. shocked lamellar texture and density change) are very important to estimate the degree of shocked metamorphism and source (i.e. host-rock) and distance from the center of the impact site in the meteoritic impact crater and impact fragments of meteorites and lunar rocks [1-8].

1. Problem of meteoritic plagioclase:

From the previous reports, there are major results on the meteoritic plagioclases as follows [3-8]:

1) High-temperature type plagioclases are obtained in type 6 chondrites from optical and powder X-ray properties [9].
2) Plagioclase (-like) compositions are obtained in all types of meteorites (esp. in calcic plagioclases of achondrites).
3) Among compositions and physical properties, anorthite (i.e. An) content is very useful data of meteoritic plagioclase(-like) phases.

But there are no detailed reports on compositions and structures of meteoritic plagioclase(-like) phases. This is mainly because (1) many standard data of terrestrial, lunar and shocked plagioclases are required to determine whether the meteoritic plagioclases is anomalous or not, (2) very tiny grains of chondritic plagioclases are difficult to obtain the detailed composition and structures, and (3) there are few data of compositions, structural data and source host-rocks of shocked plagioclase (-like) phases (esp. in diaplectic plagioclases and maskelynites).

The preliminary results are summarized on comparative data of mafic contents, structural data and impact site information as follows.

2. Mafic contents of meteoritic plagioclases (Fig. 1):

In order to discuss the meteoritic plagioclases, the comparative data of terrestrial and lunar data are briefly summarized as follows:

1) In terrestrial volcanic and plutonic plagioclases, mafic contents are less than 0.2 (wt.%), and crystals in volcanic rock have about 3 times the mafic contents (i.e. 0.6 wt.%).

2) In shocked plagioclases of the Manicouagan impact crater, the mafic contents are similar between crystals and diaplectic plagioclases, though the mafic contents among central peaks, intermediate and marginal rocks of the impact crater; that is about 20 times the mafic contents in the marginal melt rocks.

3) In lunar plagioclases, the mafic contents are almost similar to the terrestrial plagioclases, though the brecciated plagioclases of 77515, 67435 and 14066 have about 5 times the mafic contents.

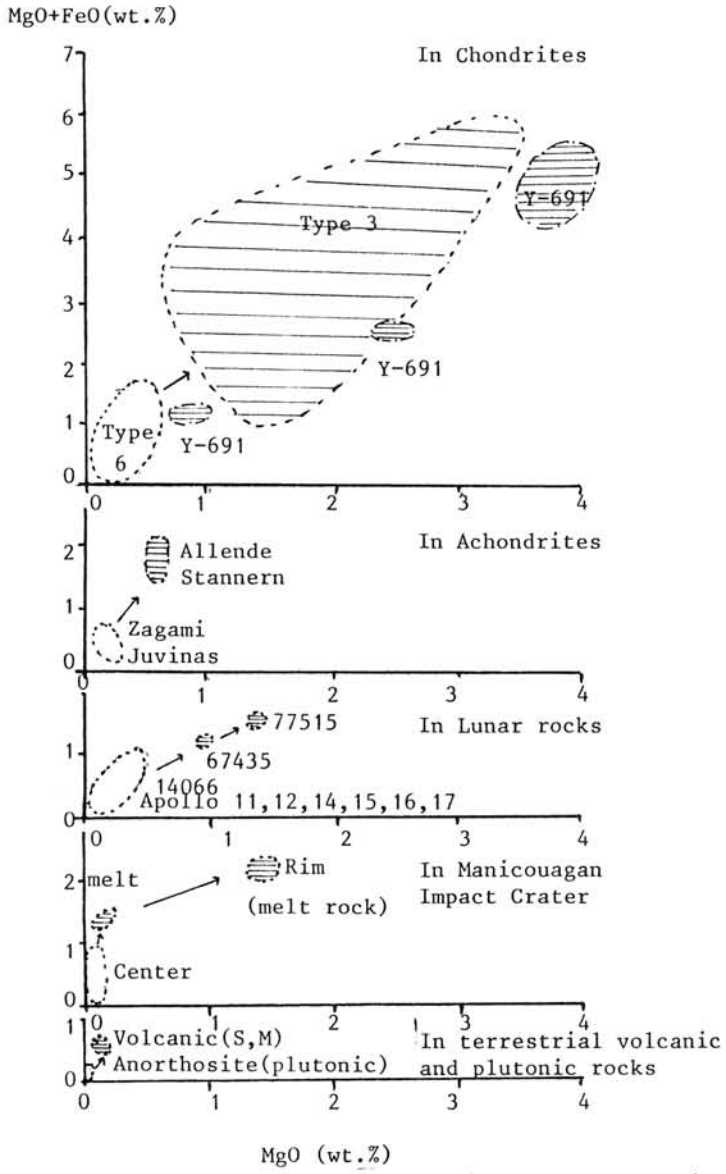

Fig. 1. Relation between mafic content (i.e. MgO+FeO) and MgO (wt.%) in chondritic, achondritic, lunar, Manicouagan impact, and terrestrial volcanic and plutonic plagioclases. Plagioclase(-like) phases of diaplectic and maskelynites are also plotted in chondritic plagioclases.

The mafic contents of meteoritic plagioclase(-like) compositions are shortly summarized as follows:

1) Crystalline plagioclases of Juvinas and Zagami achondrites show ca. 0.5(wt.%) of mafic contents which are similar to the mare basalts and lunar anorthosites but about 3 times than the terrestrial basalts and anorthosites.

2) Crystalline plagioclases of type 6 chondrites show various mafic contents of 0.3 (in L6), 1.0 (in LL6) and 1.6 wt.% (in H6).

3) Diaplectic plagioclase(-like) phases of type 3 chondrites show also much more MgO contents of 1.1 (in H3), 1.9 (in L3) and 3.4 wt.%(in LL3).

4) The compositions of the mafic contents are also different between crystalline and diaplectic (cf. maskelynite) plagioclases of meteorites.
5) plagioclase(-like) compositions of Y-691 (EH3) chondrite show three major groups of mafic contents; that is, 1.1 (optically and X-ray crystalline An_{74}), 4.7 (optically crystalline An_{58}) and 2.9 wt.% (glassy An_{30}).

Therefore, the mafic contents of plagioclase(-like) phases can be used as indicator of source host-rock, shocked metamorphism of impact sites.

3. Density change:

Density changes of various plagioclases have been obtained from the samples of terrestrial impact craters and achondritic plagioclases, based on the terrestrial igneous plagioclases, which are summarized as follows:

1) Densitie of plagioclases from the Manicouagan impact crater are changed from lower (2.57 in the center) to normal (2.70 in the rim).
2) Juvunas and Zagami SNC plagioclases show higher densities, though Stannern plagioclases have lower density. Meteoritic plagioclases has usually higher densities than the standard normal plagioclases.

4. Relation among composition, density and impact site:

1) Terrestrial shocked-plagioclases of Manicouagan impact crater show mainly lower density in the rim having minor foreign elements (Fe·Mg) and insufficient amounts of Na·Ca·K.
2) Lunar plagioclases of mare basalts and lunar anorthosites have mainly lower density with excess Ca·Mg·Fe amounts and insufficient Na content, compared with terrestrial igneous plagioclases. But lunar breccias show characteristics of excess mafic contents with lower density.
3) Eucritic plagioclases of Juvinas and Zagami reveal higher density with much more foreign elements (Fe·Mg) with complicated variation of ratio Al/Si.
4) Lower densities of terrestrial and lunar plagioclases are formed by shocked-metamorphism on the anorthositic crusts (with minor mafic contents). But, higher density of achondritic plagioclases suggests new formation process of insufficient crystallization process after impact events (i.e. relatively rapid-cooling after insufficient mixing with mafic minerals).

References:

[1] Grieve R.A.F. and Floran R.J. (1978): J.G.R., 83, 2761-2771.
[2] Arndt J., et al.(1982): P.C.M., 8, 230-239.
[3] Miura Y.(1984): Mem. Natl Inst. Polar Res., Sp. Issue,35, 226-242.
[4] Miura Y. and Tomisaka T.(1984): Ibid., 35, 210-225.
[5] Miura Y. (1988): LPSC XIX, 19, 794-795.
[6] Miura, Y. and Kato T.(1989): LPSC XX ,703-704.
[7] Miura Y., Yanai K. and Miura H. (1986): Meteoritics, 460-461.
[8] Miura Y. (1990): (in press).
[9] Van Schmus R. and Ribbe P.(1968): Geochim. Cosmchim. Acta, 32,1327.

THE CHIANG KHAN METEORITE SHOWER, LOEI PROVINCE, THAILAND

V. K. NAYAK
Department of Applied Geology, Indian School of Mines, Dhanbad, India

The meteorite known as the Chiang Khan meteorite fell as shower on 17th November, 1981, in an area located in the Loei Province, situated 524 kms. north-east of Bangkok, Thailand. According to an eye witness account (1981), it appeared like a fireball and plunged to the earth with an exploding sound. In all, 31 pieces were collected from a 24 square km. area. The total weight is 367 grams. The weight of the largest fragment is 51.3 grams while that of the smallest one is 0.2 grams. Professor R. Bhavilai, Department of Physics, Chulalongkorn University, Bangkok, Thailand, had kindly presented to me two fragments from the Chiang Khan meteorite shower. The morphological characteristics, dimensions, nature of the fusion crust and broken surfaces and texture of these meteorite pieces are presented.

Large Fragment:

This has 4.188 grams weight with a length varying from 8 mm to 10 mm, and a height of about 13.15 mm. The total form is rather difficult to construct but it appears to be a fragment of the original meteorite body. One of the surfaces shows a very low polyhedra appearance while the other surfaces are more or less flat. A minute chondrule and metallic minerals are present. 0.05 mm thick fusion crust is well developed. It has black-brown colour with dull lustre. It is coarse, somewhat corrugated without regmaglyptic relief. Another surface appears to be surface of the second kind. The two broken sides of the meteorite expose the inner surfaces which have whitish-grey colour, granular texture and mottled appearance. There are two fracture veinlets on the broken surface of the meteorite.

Small Fragment:

The small fragment has 2.7 grams weight and appears to be a single piece showing an irregular polyhedron shape. The fusion crust is excellently developed and shows black with a tinge of brown colour with dull lustre. Its thickness varies from 0.05 mm to 0.1 mm. The fusion crust is corrugated with inconspicuous regmaglypt features and

may represent the surface of the first kind. The fusion crust is peeled off from one surface and a corner and shows rusty appearance at some places.

The morphological characteristics, nature of the fusion crust and other features of the two meteorite fragments indicate the action of atmosphere. It is suggested that the investigation of all the fragments should be made to unravel the conditions of motion of the meteorite body in the atmosphere, its trajectory and mechanism of fragmentation etc.

The generous gift of two meteorite fragments from Professor R. Bhavilai, Chulalongkorn University, Bangkok, is gratefully acknowledged.

References:

Bhavilai, R. 1982. Personal Communication, 11th January 1981, Hindustan Times, New Delhi, 5th December

ELECTRON MICROSCOPE OBSERVATIONS OF Ca-Al-RICH INCLUSIONS IN THE YAMATO-791717 CO CARBONACEOUS CHONDRITE

Kouji Nomura, Kazushige Tomeoka and Hiroshi Takeda

Mineralogical Institute, Faculty of Science, University of Tokyo, Hongo, Bunkyou-ku, Tokyo 113

We present here the results of petrographic and scanning electron microscope observations of Ca-Al-rich inclusions (CAIs) in the Y791717 CO chondrite. All the CAIs in our specimen belong to the fine-grained type. Primary phases in the inclusions are spinel, fassaite, diopside, melilite, perovskite, and hibonite. Of particular interest and significance is that many of the inclusions contain variable amounts of nepheline and sodalite.

Most CAIs in Y791717 are composed of concentric objects having cores of spinel, mantles of nepheline and/or sodalite, and rims of aluminous diopside. Some occur as single concentric units, and others occur as aggregates of concentric units. These inclusions probably correspond to the fine-grained, "sinuous" rimmed complex (Kornacki and Wood, 1984). The aggregates of concentric units appear to be similar to the "fluffy" type A CAIs in Allende (MacPherson and Grossman, 1984), although melilite is rare in the CAIs in Y791717. It is evident from texture that nepheline and sodalite are secondary alteration products. So in order to compare the degrees of alteration, we classify these inclusions into three types based on the amounts of nepheline and sodalite, i.e., lightly altered, moderately altered, and heavily altered types.

Lightly altered inclusions have distinct concentric zones and rarely show textures indicative of alteration. However, in some inclusions, fassaite occurs inside of the diopside rim and is replaced by feldspathoids. Moderately altered inclusions contain spinel in the central part of inclusions, and 40 to 60 % of the internal areas are made up of nepheline and sodalite. There is much evidence that spinel is replaced by the feldspathoids. Most inclusions have aluminous diopside rims, but fassaite is rare. In heavily altered inclusions, more than 60 % in area are replaced by feldspathoids. Spinel occurs only as small relicts in the feldspathoid areas. Despite the extensive alteration, most inclusions retain aluminous diopside rims.

Our study reveals that CAIs in Y791717 contain major, variable amounts of nepheline and sodalite. The moderately and heavily altered inclusions provide much textural evidence that the feldspathoids were formed by alteration of primary minerals, mostly fassaite and spinel. The alteration probably proceeded with reaction of the primary phases with a low-temperature nebular gas prior to emplacement in the parent body. Based on our observations, the resistence of primary phases in the Y791717 inclusions increases in the order of fassaite, spinel, aluminous diopside.

REFERENCES

Kornacki, A.S. and Wood, J.A. (1984) Proc. 14th Lunar Planet. Sci. Conf., in J. Geophys. Res., 89, B573-B587.
MacPherson, G.J. and Grossman, L. (1984) Geochim. Cosmochim. Acta, 48, 29-46.

COSMIC RAY EXPOSURE HISTORY OF THE LUNAR METEORITES YAMATO 791197 and YAMATO 86032; S. Vogt, D. Aylmer and G.F. Herzog, Dept. Chemistry, Rutgers University, New Brunswick, NJ 08903; D. Fink, J. Klein and R. Middleton, Dept. Physics, University of Pennsylvania, Philadelphia, PA 19104.

Lunar meteorites are important for many reasons. First they offer a chance to study material from otherwise unsampled locations on the Moon; the Apollo and Luna missions returned samples representing only about 5% of the lunar surface. Second, they are the only meteorites whose parent body is known with certainty, and hence present the opportunity to test ideas concerning the frequency of large impact events and the evolution of ejecta orbits. Results for seven lunar meteorites show that either three or four impacts produced them. Two of them, Yamato 82192/3, lay buried a meter or more below the lunar surface for most of their history, were ejected less than 10 Ma ago and arrived on Earth within the last 0.1 Ma. Two other meteorites, ALHA 81005 and Yamato 791197, had a long exposure in the lunar regolith followed by a brief travel to Earth, either separately or jointly, that ended between 0.2 and 0.4 Ma ago [1, and refs. therein]. We report here results for cosmogenic radionuclides in the lunar meteorite Yamato 86032, recently made available for analyses and Yamato 791197. The purpose of the measurements is to reconstruct the exposure histories of the meteorites. Our ^{10}Be and ^{26}Al results are presented in Figure 1 and in Table 1 along with published cosmogenic radionuclide and ^{21}Ne data for lunar meteorites.

Yamato 86032 : The ^{10}Be and ^{26}Al concentrations obtained for Yamato 86032, which are not attainable in a 2π geometry [2,3,4], imply a long irradiation of several million years in a 4π geometry. An upper limit on the time of exposure to cosmic rays of no longer than 10 Ma is then set by the low ^{21}Ne contents [1]. As the material received most, if not all of its irradiation dose in a 4π geometry, we may compare the measured activities with the expected production rates. The latter were estimated by usingthe elemental production rates [5,6], and the elemental composition of Yamato 86032 given by Koeberl et al. [7]. The oxygen concentration was approximated as 45%, an average for lunar highland materials [8]. With these data we obtain a production rate P_{10} of about 23.5 dpm/kg and P_{26} of about 137 dpm/kg. Based on $P_{26} = 137$ dpm/kg we estimate a terrestrial age for Yamato 86032 of about 0.12 Ma, comparable to the ^{81}Kr/Kr terrestrial age of 0.072 ± 0.030 Ma given by Eugster [1]. As the measured ^{10}Be content equals its calculated production rate within limits of uncertainty, we conclude that the transit time must have lasted at least 5 Ma. The radionuclide concentrations obtained for Yamato 86032, along with the low ^{21}Ne contents indicate that this meteorite is paired with Yamato 82192/3 [see ref. 1].

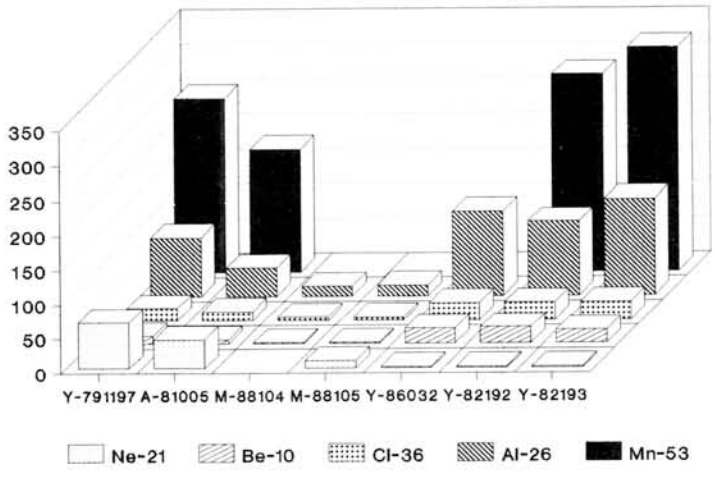

Figure 1: Cosmogenic nuclides in lunar meteorites
(for details see comments to Table 1)

Yamato 791197 : The high ^{21}Ne content of this meteorite indicates a long exposure to cosmic rays in the lunar regolith and/or transit time between Moon and Earth. Remarkably, the measured radionuclide concentrations agree well with measured saturation activities very close to the surface of the Moon. An irradiation for 150 Ma close to the surface, a very short transit time (< 0.1 Ma) and terrestrial

age (< 0.1 Ma) appears to be the simplest scenario for the exposure history of this meteorite [9]. In any case, the radionuclide pattern indicates that this material must have received most of its irradiation dose during the 2π irradiation on the Moon. An upper limit on the terrestrial age can be estimated, by assuming that the transit time was long enough for ^{26}Al to reach saturation. Estimating P_{26} as described above, we obtain $P_{26} = 130$ dpm/kg and calculate a terrestrial age T < 0.4 Ma. The corresponding production rates of the two longer lived radionuclides ^{10}Be and ^{53}Mn than limit the transit time to t < 1.5 Ma and the depth in the lunar regolith to < 50 g/cm^2. We conclude, that Yamato 791197 lay buried between 0 and 50 g/cm^2 on the Moon for most of its exposure to cosmic rays (150 Ma), was launched to Earth less than 1 Ma ago and its terrestrial age is less than 0.4 Ma. A pairing with any of the lunar meteorites identified so far appears unlikely. A joint launch with ALHA 81005 is not ruled out and would indicate that ALHA 81005 lay buried about 200 g/cm^2 deeper than Yamato 791197.

Table 1: Cosmogenic nuclides in lunar meteorites

Meteorite	Sample	$^{10}Be^a$	$^{26}Al^a$	$^{36}Cl^b$	$^{53}Mn^c$	$^{21}Ne^d$
ALHA 81005.		6.3±0.3[9]	41.3±4.1[9]	8.8±0.4[9]	173±12[9]	31[10]
	.75	4.1±0.5[11]	46 ±3[11]			
Y-791197	.75	11.6±0.5	85.1±8.5	12.3±0.9[9]	259±17[9]	67.1[12]
Y-82192	.73	24.0±1.2[9]	106.6±7.5[9]	18.0±1.1[9]	358±21[9]	2.2[12]
Y-82193	.101	20.1±1.0[9]	138.9±9.7[9]	18.9±0.7[9]	311±21[9]	2.3[12]
Y-86032	.					2.2[12]
	.114	22.8±1.2	122.0±7.9			
MAC 88104	.10	2.1±0.1[15]	14.4±1.2[15]			
MAC 88105	.24					10.8[13]
	.41	2.1±0.1[15]	15.7±1.3[15]			
	.		19.5±2.5[14]			

Notes: **a** activities in dpm/kg; **b** activities in dpm/kg (Fe+6Ca); **c** activities in dpm/kg$_{Fe}$; **d** content in 10^{-8} cc STP/g. **References:** 9 - 15 refs. [9] - [15].

Refs.: **[1]** Eugster (1988), Science 245, 1197-1202; **[2]** Nishiizumi et al. (1984), Earth Planet. Sci. Lett. 70, 157-163; **[3]** Nishiizumi et al. (1984), Earth Planet. Sci. Lett. 70, 164-168; **[4]** Klein et al. (1988), Lunar Planet. Sci. 19, 607; **[5]** Moniot et al. (1988), Geochim. Cosmochim. Acta 52, 499-504; **[6]** Hampel et al. (1980), Geochim. Cosmochim. Acta 44, 539-547; **[7]** Koeberl et al. (1989), Proc. 13th Symp. Antarctic Meteorites, Natl. Inst. Polar Res., in press; **[8]** Glass (1982), Cambridge Univ. Press, 469p.; **[9]** Nishiizumi et al. (1988), Meteoritics 23, 294; **[10]** Eugster et al. (1986), Earth Planet. Sci. Lett. 78, 139-147; **[11]** Tuniz et al. (1983), Geophys. Res. Lett 10, 804-806; **[12]** Eugster et al. (1989), Proc. NIPR Symp. Antarct. Meteorites 2, 25-35; **[13]** Eugster (1990), Proc. Lunar Planet. Sci. 21, 337-338; **[14]** Antarctic Meteorite Newsletter (1989), 12, No. 3, 21; **[15]** Vogt et al. (1990), Lunar Planet. Sci XXI, 1274-1275.

Acknowledgment: We thank K. Yanai for sending us the samples of Y-791197 and Y-86032.

LINKS BETWEEN STRUCTURAL FEATURES AND PHYSICAL PROPERTIES IN STONY METEORITES

Żbik Marek
SPACE RESEARCH CENTRE, ul Bartycka 18, 00-716 Warsaw POLAND

The structure of stony meteorites hage been studied. Several samples of ordinary chondrites various types were covered by micromorphometric analysis on scanning electron microscope/SEM/ equipped with an energy dispersive X-ray detector. Mutual grain and void distribution in the meteorite bodies interior have been observed.

Some physical properties as: porosity, elastic properties and density were compared. To elucidate the structural factors and to compare as well as contrast the mechanical properties of examined meteorites with regard to their microstructure /observed on SEM microphotographs/. The dynamic compressibility modulus has been used /1/. Tte formula which has been applied is:

$$E_d = \rho_{bulk} \cdot V_p^2$$

where E_d is the dynamic compressibility modulus, while V_p is the velocity of the compressional wave. The velocities V_p were determined with an Unipan 511 ultrasonic fault detector, applying the transmission method to 5-7 mm thick plane - parallel slabs. The density were determined by helium - air pycnometer. The results are sumarized in Table 1.

In Fig. 1 porosity is plotted against ultrasonic wave absorption. This figure shows that ultrasonic wave absorption in meteorites exponentially depends on porosity and increases sharply with porosity, ranging from 2% to 6%. It is observed that in meteorites where porosity are higher than 6% ultrasonic wave absorption depends from kind of contacts between mineral grains. If intergranular pores are prefered in meteorite sample ultrasonic wave can not pass through this sample. But if close type of voids dominates in meteorite pores system, ultrasonic wave can penetrate in spite of high porosity values.

Fig. 2 shows corelation between porosity /n/ and dynamic compressibility modulus/E_d/. The results obtained as we see on

the fig. 2 present three fields of the concentration of the measurement points. This is in good agreement with micromorphological obserwation. It should be emphasized that the same degree of metamorphism, characterized by the identity of the petrologic classification, was reached, for presented meteorites, apparently in different ways. Supported by the evidence as we have seen from fig. 2 meteorites are divided into three structural types:

I - type one collect the meteorites with porosity below 2% open porosity sistem and massive inner texture. On the SEM photographs visible vesicle, channels and vugs are representing closed type of porosity /2/.

II - type two collect the meteorites with porosity higher than 6%. On the SEM microphotographs of the meteorites representing this microstructural type we can see joints, fissures and intergranular pores illustrative for open porosity system /2/.

III - type three collect the meteorites with complicated inner structure and median porosity values. In this structural type, both open and closed porosity systems are present.

The analyses failed to show a link between physical properties and structural type of stony meteorites, and to be dependent on petrological type of meteorite, as it was stated in/3/. Obtained results lead to better understanding of the conditions of the origin and evolutionary history of meteorite parent bodies.

1-Żbik M. 1982 Bull.of the Polish Acad. of Sciences 33 No.1-2
2-Żbik M., Lang B. 1984 Earth and Plan. Sci. Lett. 70 No. 2
3-Yomogida K., Matsui T. 1983 Journal of Geophysical Research, 88 No. B11

Table 1

Name	density $g \cdot cm^{-3}$	bulk density $g \cdot cm^{-3}$	porosity %	velocity of ultrasonic wave $km \cdot s^{-1}$	Type
Dhajala	3.69	3.35	9.21	-	H3
Pultusk	3.76	3.50	6.91	3.85	H5
Faith	3.40	3.29	3.23	5.95	H5
Gnadenfrau	3.73	3.33	10.72	-	H5
Erksleben	3.75	3.57	4.80	5.10	H6
Djati-Pen.	3.73	3.73	0	6.10	H6
Melrose	3.45	3.45	0	6.29	L5
Tsarev 80	3.56	3.49	1.97	6.30	L5
Tsarev 84	3.54	3.54	0	6.50	L5
Tsarev 91	3.56	3.33	6.46	6.10	L5
Wilkanówko	3.57	3.51	1.68	3.45	L5
Alfianello	3.67	3.38	7.90	2.65	L6
Kniachinia	3.63	3.35	7.71	4.06	L5
Stannern	3.07	2.95	3.91	4.06	eucr.

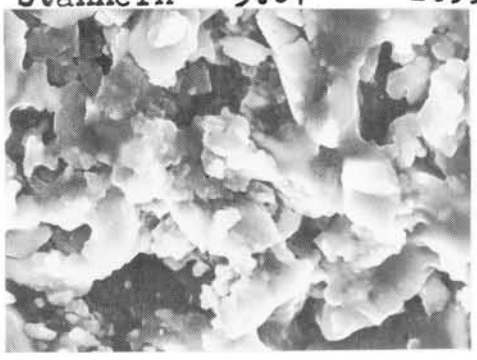

high and low porosity system in chondrite

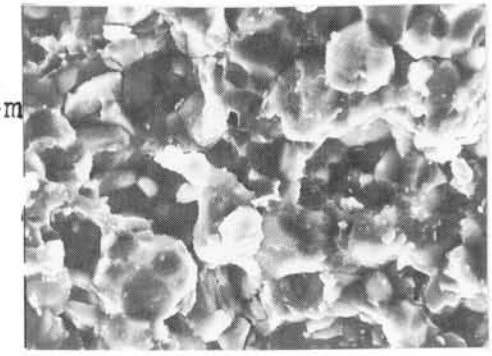

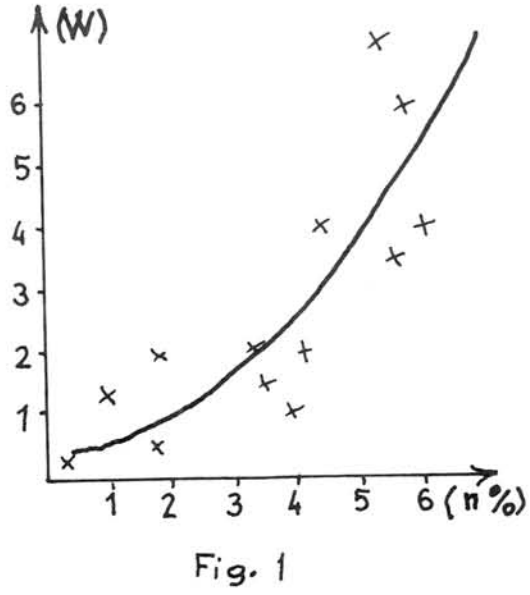

Fig. 1

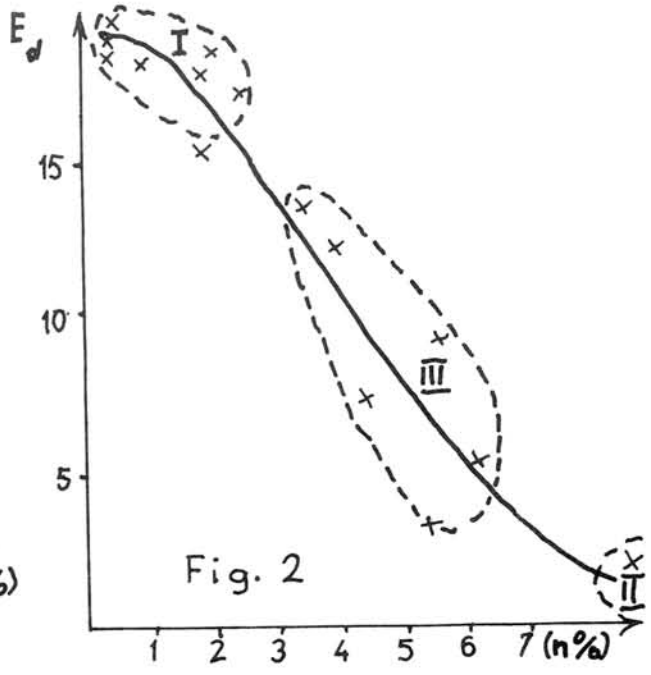

Fig. 2

Table 1. Noble gas compositions in Y-74063.

Sample	^{3}He	^{4}He	^{20}Ne	^{21}Ne	^{22}Ne	^{36}Ar	^{38}Ar	^{40}Ar	^{84}Kr	^{132}Xe
Y-74063	9.61	1610	2.37	1.08	1.53	156	30.0	5550	3.00	4.84

Concentration is given in unit of 10^{-8} cm^3/g.

Fig. 1.

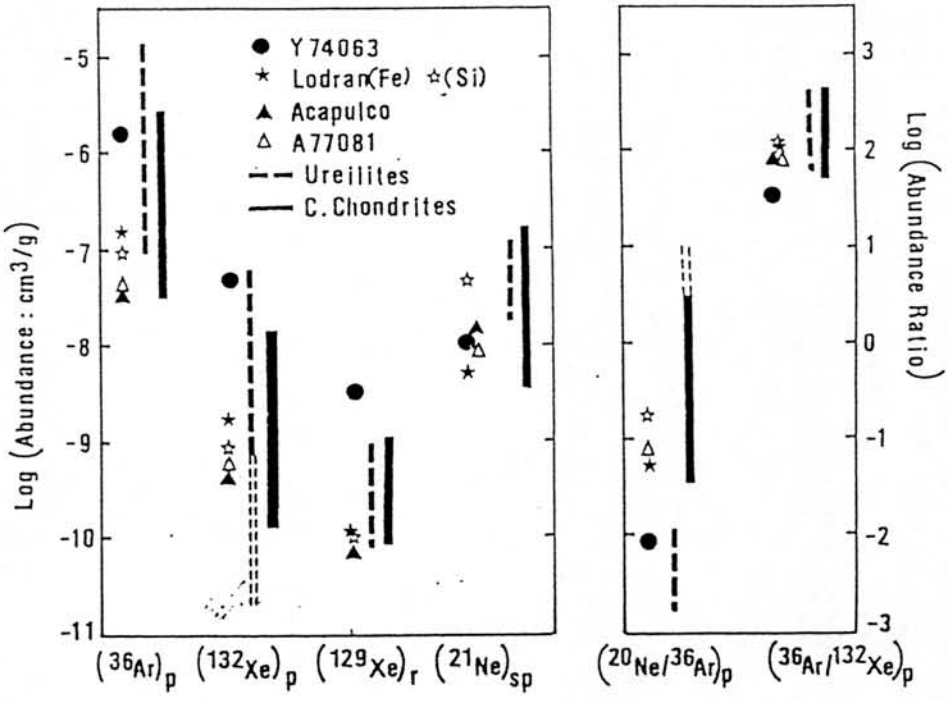

Fig. 2.

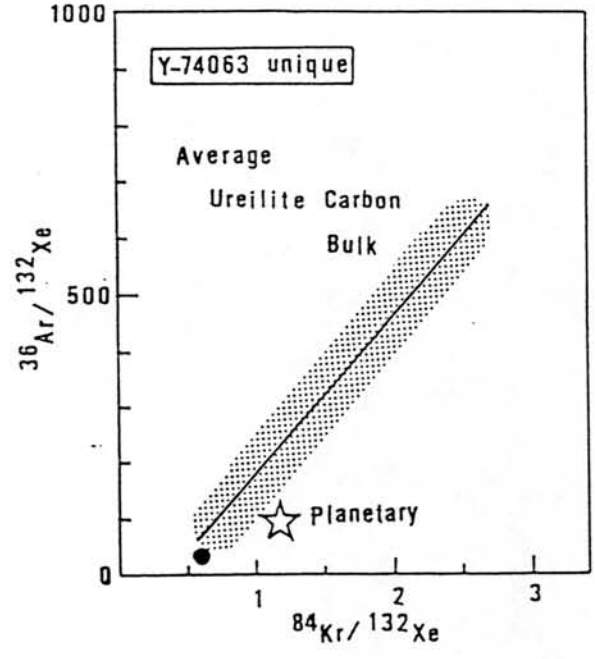

Spectral Reflectance of the Recently Fallen Chondrites in China

Lin Wenzhu

Institute of Geochemistry, Academia Sinica, Guiyang, Guizhou Province, China

Of late years, the scintific interest for asteroids greatly are growing. Specifically, near-Earth asteroids(Amors, Apllos and Atens)orbit cross-Earth, It probably are important impactor of terrestrial craters. Near-ultraviolet, visible and near-infrared spectral reflectance were most efficient technology to explore surface material of the asteroids. A good deal of spectral reflectance in the meteorites provided considerable insight to the asteroids. Through compare with out planetary, satellite and asteroids band between Mars and Jupiter not only explanation mystery of origin of some near-Earth asteroids, but in - ference " anomalous " asteroids could formed from solar nebula in lower temperature condensation.

In recent decades, a variety of spectral reflectance measurements of meteorites, mineral and terrestrial rocks have increased rapidly (1). The samples studies in the work were undertaken to provide for spectral reflectance of recently fallen chondrites in China (Jilin H5, Zaoyang H5, Laocheng H5, Xinyang H6, Qingzhen E3, Guangrao L5-6, and Suizhon L6) and Xinjiang iron meteorite. In addition, several igneous rocks were deteremined.

Impact was one of primarily process for planetary surface evolution and important mechanisum of formation asteroids. The planetary and great maiority of asteroids in solar system has been covered soil patches on surface that similar to the moon. The soil represent material composition of the asteroids and the geological elements of planetary (2). So, the samples were measured as powders. The crushing sampled were ground to fine by agate morter. All specimens were measured on the Shimadzu (Japan) UV-365 Spectrophotometer. This instrument utilizes an integrating sphere with a detector part. Two detector were used these measurements: a photomultiplies tube (200-800 nm) and lead sulfide detector (800-1800 nm). The spectral reflectance were recorded on X-Y plottar. In order to compare spectral features of the meteorite yet selected Xinjiang iron meteorite and igneous rocks.

Though contained mineral of chondrites were more simple than terrestrial rocks, but their relfectance spectrum were complicated. Figure 1 shown the reflectance spectrum of Jilin chondrite etc..

The sample (Ol) got back from olivine xenolith in basic rockmass. spectra absorption band centered near 1060 nm drift 90 nm than olivine absorption centered. The spectra have abroad asymmatric absorption feature. The feldspar produce a weak absorption feature near 1300 nm. A maximum near 1460 nm caused by orthopyroxene. The visible and near-infrared (420-800 nm) displays a broad strong reflectance band at 500 and 600 nm due to Fe^{2+} and Fe^{3+}. The spectrum showed absorption edge was steep. This spectra showed that the sample mainly is olivine, but containing number of orthopyroxene and a few feldspar.

The spectra of Xinjiang iron meteorite is consistent with that of Ni-Fe metals. The infrared reflectance is featureless and a inclination line. The near-ultraviolet absorption edge is range 200-430 nm. It has been noted, e.g. Gaffey (3), the infrared reflectance of iron meteorite decreases with increasing nickel content. All the spectra of iron meteorite are featureless, but differ in the slope of their reflectance cures in the infrared as a function of nickel content. The inclination line vary in slope from 30 degree (metal iron) to negative 11 degree (metal nickel).

H GROUP CHONDRITES Excepling Laocheng Zhen, Jilin, Zaoyang and Xinyang chondrites displays a broad shallow absorption band. Specially Zaoyang chon-

drite showed strikingly. Absorption centered at 980 nm result from Fe^{2+} d-d transition both olivine and orthopyroxene. Near-infrared of pyroxene near 1400 nm influenred distinctness. Becaus of Ni-Fe metal influence, near-infrared spectra approached to horizon. For Xinyang and Zaoyang chondrites near-ultraviolet absorption edge were steep, but Jilin chondrite possibly contained more Fe^{2+} to make for absorption edge drift toward infrared. Two weak absorption near 500 nm and between 320 and 340 nm due to Fe^{3+}. The spectra of Laocheng Zhen different from Jilin chondrite and that in the range of 400-1200 nm wavelength were lower reflectance (10%), following slowly increase with wavelength. The spectral shape approximated Qingzhan enstatite chondrite, but reflectance higher above 1400nm.

L GROUP CHONDRITES The spectral reflectance curves for Quangrao and Suizhou L-group chondrites had similar H-group chondrites. Because of olivine rice more than H-group appeared olivine absorption feature and minimum near 1000 nm. Absorption strong of Suizhou chondrite more high than Guangrao were explained the former high-metamorphic grade.

E GROUP CHONDRITES Qingzhen enstatite chondrite was very uneqilibrium high iron enstatite chondrite. It consisted of enstatite and iron sulphide, metal-rice. The spectra was featureless with a variable reddish slope in the visible and very alowly increasing infrared reflectance. An approach to a line started from about 600 nm. The center of very weak band was shown near 980 nm, probably cause by pyroxene. The near-infrared reflectance had similar that of ataxite.

The spectral reflectance of ordinary chondrites characterized by resemblance. In order of H-L-LL relation concentration of olivine and Fe^{2+} content successively increase (ol/py =1.2, 1.6, 1.6; Fe^{2+}/Mg^{2+} =0.17, 0.2, 0.24) depened absorption valley and band center moved toward LL group. However, Fe^{o}/Fe_t ratio increased by LL-L-H-E order and to decrease near infrared reflectance toward smooth curve. In petrology type go up one grade within each group, thermal metamorphic level more and more higly, composition of olivine and pyroxene more well-distributed, the orthopyroxene transformation to clinopyroxene. So, their reflectance of Laocheng Zhen chondrite showed unusual. The curve as if Laocheng Zhen chondrite possibly provided with more high petrological type. Even probable approach to E-group.

The near-ultraviolet, visibl and near-infrared reflectance strength for igneous rocks were strong than that of meteorites. The reflectance of acid igneous rocks, basic and ultrabasic rocks vary from featureless to display absorption band features of olivine and pyroxene. Most cosmochemiste were long eagerly looking foward to find out traces of the meteorites from terrestrial rocks. In this way, parent rocks of basic and ultrabasic rocks came from H-group chondrites which were principle material of the Earth formation (4).

REFERENCES: (1) Adams,J.B. and Filice,A.L. 1967 J.G.R. 72,5705; Wagner,J.K. et.al. 1987 Icarus 69, 14-28; Glass,B.P. 1982 "Introduction to Planetary" Cambridge Univ. Press. (2) Glass,B.P. 1982 (3)Gaffey,M.J. 1976 J.G.R. 81,905 (4) Lin Wenzhu 1985 Chinese J. Space Sci. Vol. 4, No. 4,338

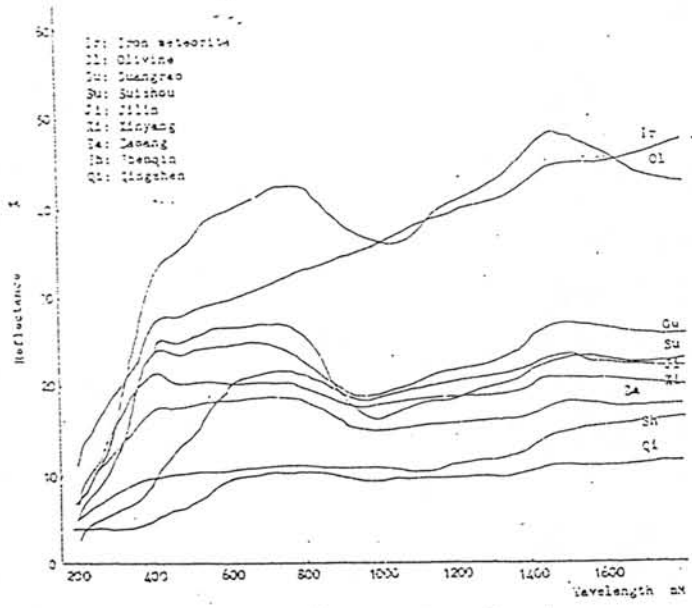

Fig. 1, Reflectance spectra of meteoritic powders

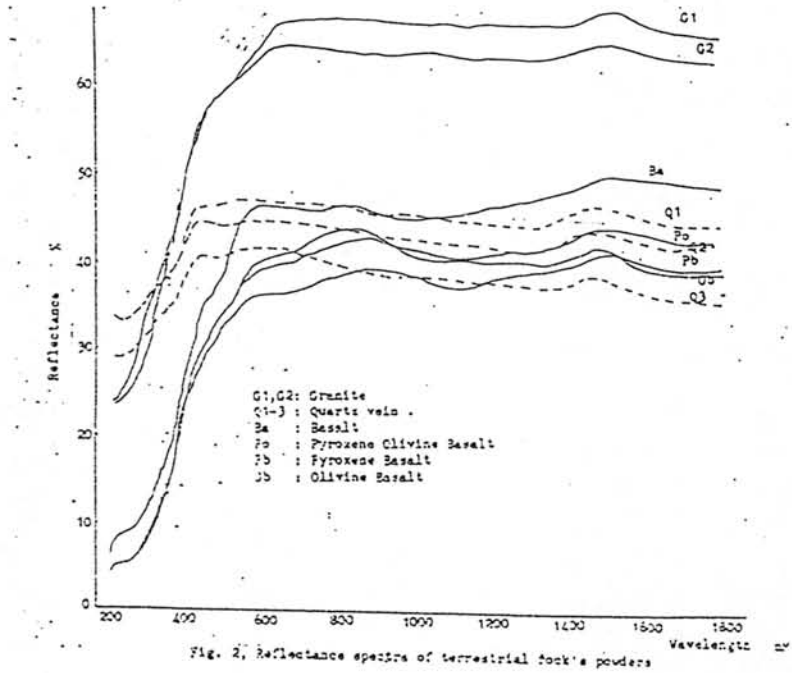

Fig. 2, Reflectance spectra of terrestrial rock's powders

Another thought on the origin of diamonds in meteorites: 'A radiation crystallization model'

by

Minoru Ozima

Geophysical Institute, University of Tokyo

On the basis of our recent experimental results on a carbonado, an aggregate of diamond microcrystals, we suggest that high energy particle bombardment which is likely to occur in the case of supernova explosion might have transformed carbonaceous matters to microdiamonds.